Spring 2016

Scale-up investigation and hydrodynamics study of gas-solid fluidized bed reactor using advanced non-invasive measurement techniques

Abdelsalam Efhaima

Department: Chemical and Biochemical Engineering

SCALE-UP INVESTIGATION AND HYDRODYNAMICS STUDY OF GAS-SOLID FLUIDIZED BED REACTOR USING ADVANCED NON-INVASIVE MEASUREMENT TECHNIQUES

by

ABDELSALAM EFHAIMA

A DISSERTATION

Presented to the Faculty of the Graduate School of the

MISSOURI UNIVERSITY OF SCIENCE AND TECHNOLOGY

In Partial Fulfillment of the Requirements for the Degree

DOCTOR OF PHILOSOPHY

in

CHEMICAL ENGINEERING

2016

Approved

Muthanna H. Al Dahhan, Advisor
Douglas Ludlow
Joontaek Park
Xinhua Liang
Shoaib Usman

PUBLICATION DISSERTATION OPTION

This dissertation has been formatted per Missouri University of Science and Technology specifications. It consists of the following articles that have been submitted for publication as follows:

PAPER I pages 18-76. Validation of new the scale-up methodology for gas-solid fluidized beds using advanced non-invasive measurement techniques (CT and RPT). It has been submitted to powder technology Journal.

PAPER II pages 77-142. Assessment of scale-up dimensionless groups methodology of gas-solid fluidized beds using advanced non-invasive measurement techniques (CT and RPT). It has been submitted to the Canadian Journal of Chemical Engineering.

PAPER III pages 143-170. Local time averaged gas holdup in gas-solid fluidized bed Study by non-invasive measurement technique. It has been published in International Journal of Industrial Chemistry.

PAPER IV pages 171-209. Bed diameter effect on the hydrodynamics of gas-solid fluidized beds via radioactive particle tracking (RPT) technique. It has been submitted to the Canadian Journal of Chemical Engineering.

ABSTRACT

This research focuses on validating our newly developed mechanistic scale-up methodology for hydrodynamics similarity of gas-solid fluidized bed reactors (FBRs) by implementing our advanced non-invasive measurement techniques which are gamma ray computed tomography (CT) and radioactive particle tracking (RPT) that measure local hydrodynamic parameters. Experiments were carried out in two fluidized beds of 14 cm and 44 cm in diameter using air as the gas phase and particles of different materials. Since in these reactors the gas dynamic dictates the bed hydrodynamics, the new mechanistic scale-up methodology is based on maintaining similar or closer time averaged radial profiles of gas holdups at a height within the bed in two different gas-solid fluidized beds in order to achieve local and global similarity of dimensionless hydrodynamic parameters. The findings validate the achievement of hydrodynamics similarity in local solids and gas holdups distribution obtained by CT technique and in three dimension local solids velocities, solids shear stresses, normal stresses, turbulent kinetic energy, and turbulent eddy diffusivities measured by RPT technique. Also in this work we found based on local hydrodynamic parameters obtained by using CT and RPT that the scale-up method of matching a set of dimensionless groups is invalid for hydrodynamics similarity and the proposed dimensionless groups are insufficient to capture the key phenomena in these reactors. In addition, we studied the effect of bed height and particles type, size, and density on gas holdup, particle velocity, and turbulent parameters measured by these advanced techniques.

ACKNOWLEDGMENTS

First of all praise belongs to God (ALLAH) for his kindness and so many blessings in my life.

Throughout my stay here at Missouri University of Science and Technology, several people have supported me both academically and personally and inspired me. I express gratitude from the depth of my heart to my advisor, Professor Muthanna H. Al - Dahhan, who gave me an opportunity to conduct research under his supervision. Dr. Al-Dahhan has continuously conveyed a passion for research work and excitement for teaching. Without his guidance and persistent help this thesis would not have been possible.

I would also like to acknowledge the members of my committee, namely, Dr. Douglas Ludlow, Dr. Joontaek Park, Dr. Xinhua Liang and Dr. Shoaib Usman, for taking interest in my work and examining my dissertation.

A special thanks to my friends and colleagues for their continued and untiring support during tough times.

I express a deep sense of appreciation to my parents, brothers and sisters for their support and encouragement throughout the years. Finally, thanks to my wife Rabeaa, and my kids (Reham, Hanan, Yahya, and Manal), who stood by my side during the ups and downs, for believing in me and for supporting my ideas and dreams. They were always the breath of fresh air that sailed me through my long PhD Journey.

TABLE OF CONTENTS

LIST OF ILLUSTRATIONS

Page

PAPER III

PAPER IV

LIST OF TABLES

Page

PAPER I

PAPER II

PAPER III

PAPER IV

NOMENCLATURE

Symbol	Description
D_C	Column diameter
CT	Computed tomography technique
RPT	Radioactive particle tracking
D_P	Particle diameter
L	Column height
H	Bed height
FBR	Fluidized bed reactor
U	Superficial gas velocity, cm/s
U_{mf}	Minimum fluidization velocity, cm/s
v_s	Particle velocity, m/s
g	Gravity
P	Pressure
Fr	Froude number
Ref	Gas Reynolds number
Res	Particle Reynolds number
ρ_g	Gas density, kg/m^3
ρ_s	Solid density, kg/m^3
g	Gravitational constant, m/s^2
TKE	Turbulent kinetic energy, cm^2/s^2
τ_{zz}	The axial normal stress, cm^2/s^2
τ_{rz}	The shear stress, cm^2/s^2

D_{zz}	The particle axial eddy diffusivity, cm^2/s^2
D_{rr}	The particle radial eddy diffusivity, cm^2/s^2
P	Bed pressure, N/m^2
ΔP	Overall pressure drop, N/m^2

1. INTRODUCTION

Multiphase flow reactors are critically important in industrial applications across many sectors of the economy. Conventional industries as varied as petroleum refining, petrochemical, chemical, mineral processing, pharmaceutical, energy and power, as well as the new economy industries such as bio-medical and nanotechnology, all have multiphase reactors and contactors at the heart of their respective processes, Rüdisüli et al. [1].

Gas-solid fluidized bed reactors as one of the multiphase reactors are widely used in commodity and specialty chemicals industry and in petroleum, roasting, drying, coating, combustion, gasification, catalytic cracking, gas adsorption, and gas phase polymerization processes, and many others, Dubrawski et al [2]. Fluidized bed reactors (FBRs) have many advantages over other gas-solid reactors, including their simple construction, favorable heat and mass transfer, excellent gas-solid mixing and contacting, low cost of maintenance and operation, low pressure drop, excellent heat and mass transfer, excellent contact between the solid particles and the gas phase as well as between particles and the wall, an approximately uniform temperature distribution, the ability to fluidize many particle types of different densities and sizes. Despite their advantages, gas-solid fluidized reactors have disadvantages that affect their industrial applications such as back maxing, complex interactions among phases, and difficult to scale-up.

Fluidized bed (FB) technology started in the early 1920s, when Fritz Winkler patented a FB for gasification of lignite in Germany, Winkler, (1923). Winkler was the first one to study this reactor in detail and built a commercial FB plant in the 1930s. By

the early 1940s, Germany had developed and commercialized FBs for coal gasification and metal refining processes, Tavoulareas, [3].

During World War II, FB technology was also developed in the United States by the petroleum industry for oil feedstock catalytic cracking, Chaouki et al. [4]. Although FB development has not been limited to combustion applications, in the early 1960s, FB combustion technology began to be used in the United Kingdom (UK) and China to burn poor-quality solid fuels. In the 1970s, research focused on improving FB combustion technology to reduce SO2 and NOx emissions without requiring post-combustion treatment of the flue gas.

In general, in its simplest form, a fluidized bed reactor (FBR) is a type of reactor that can be used to carry out a variety of multiphase chemical reactions. In this type of reactor shown in Figure 1.1, a gas is passed through a granular solids material (usually catalysts) at high enough velocities to suspend the solids and cause it to behave as though it were a fluid. The fluidized bed reactor is typically supported by a porous plate, known as a distributor. The gas is then forced through the distributor up through the solids material. In packed reactors with lower gas velocities, the solids remain in place as the gas passes through the voids in the bed. As the gas velocity is increased, the reactor will reach a stage where the force of the gas on the solids is enough to balance the weight of the solids material. This stage is known as incipient fluidization, and occurs at this minimum fluidization velocity. Once this minimum velocity is surpassed, the contents of the reactor bed begin to expand and swirl around a similar manner to what would occur in an agitated tank or boiling pot of water. The reactor is now a fluidized bed and depending

on the operating conditions and properties of solid phase various flow regimes can be observed in such reactor.

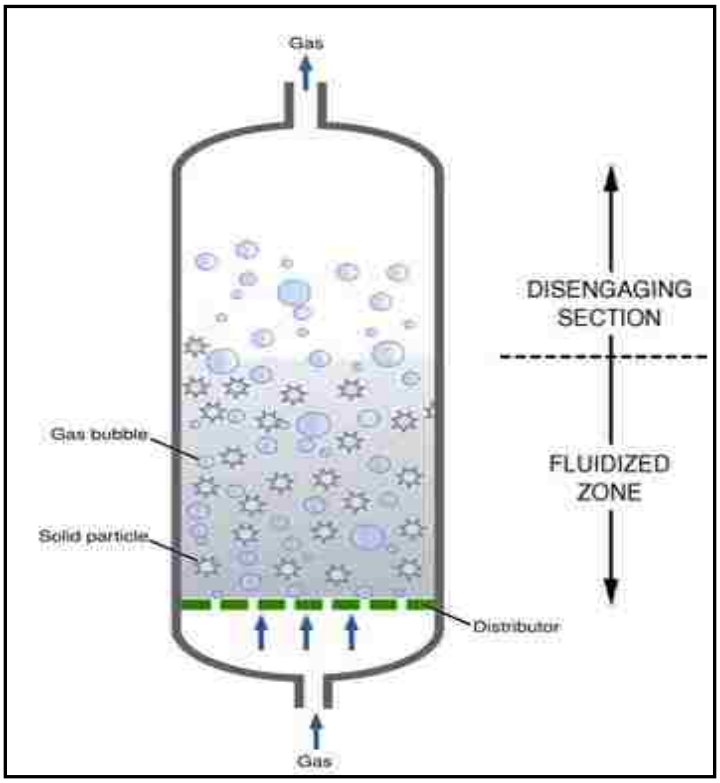

Figure 1.1 Schematic diagram of a fluidized bed reactor

Although research involving gas-solid fluidized reactors has progressed in the last decade, many important features of these reactors are still not well understood and need to be further explored, such as gas and solids distributions, solids recirculation velocities and turbulent parameters. Knowledge of these parameters is important for a proper understanding of their hydrodynamics, design, scale-up and performance predictions of fluidized bed reactors. In addition, proper measurements of these parameters provide

benchmark data for the evaluation and validation of computational fluid dynamics (CFD) models.

1.1. RESEARCH MOTIVATION

Gas-solid fluidized bed reactors are extensively used in various industrial processes that take place in large-scale operations, such as mineral, chemical, petrochemical, pharmaceutical, drying, combustion, gasification, catalytic cracking, calcinations processes, and many others Dubrawski et al. [2].

Gas-solid fluidized bed reactors are highly scale-dependent, and therefore it is difficult to predict the hydrodynamics of large industrial-scale reactors based on the information of smaller scales. Therefore, proper scaling-up from laboratory to industrial scales is still challenging task due to back mixing and the complex interactions of the gas-solid and solid-solid phases, Rüdisüli et al. [1].

When scaling up fluidized bed reactors the behavior of large-scale fluidized beds usually differ significantly from the lab-scale behavior. One of the problems of fluidized bed scaling-up is the inherent scale dependence of many of the essential operating and design parameters. That is, if one parameter is changed (e.g. bed diameter) most of the other parameters (e.g. gas velocity) will not change concordantly. This discordance will ultimately result in significantly different hydrodynamics and transports in the scaled fluidized bed. This is evident since fluidized beds are operated in many different regimes (bubbling, turbulent, fast fluidization, etc.) and with many different particle types. One discouraging problem during the process of scaling-up gas-solid fluidized beds is the decrease in the reactor performance. Such encountered problem could be caused by poor solid mixing, undesirable gas flow patterns, physical operating problems, etc. Rüdisüli et

al. [1]. Hence, attaining hydrodynamics similarity is essential and the key for any scale-up methodology.

Therefore, the scaling-up of the gas-solid fluidized beds has been the subject of a number of investigations in the last few decades. The open literature reports that, attempts have been made to develop scale-up methodologies in order to achieve hydrodynamics similarity when the size and the conditions of the fluidized beds change, Al-Dahhan et al. [5].

1.2. SCALE-UP METHODOLOGIES

In the literature, many approaches have been proposed for the scale-up of fluidized bed reactors to achieve the hydrodynamics similarity. These are: (1) new mechanistic scale-up methodology which is based on maintaining similar or closer time averaged radial profiles of gas holdups in two different gas-solid fluidized beds to achieve local and global hydrodynamics similarity, (2) matching selected dimensionless groups, (3) matching chaotic parameters. Hydrodynamics similarity could be expressed in similarity or in close in magnitude of the absolute values of the hydrodynamic parameters (e.g., holdups) or the dimensionless values of the hydrodynamic parameters.

1.2.1. The Scale-Up of Fluidized Beds Based on the New Mechanistic Methodology. The new mechanistic scale-up methodology for hydrodynamics similarity of gas-solid fluidized beds has been proposed in Professor Al-Dhahran's laboratory Al-Dahhan et al. [5]. It is based on maintaining similar or closer time averaged radial profiles of gas holdups in a height within the bed in two different gas-solid fluidized beds to achieve local and global similarity of dimensionless hydrodynamic parameters, since the gas dynamic dictates the hydrodynamics in these beds.

Al-Dahhan et al. [5] and Zaid, [6], evaluated and validated this new mechanistic scale-up methodology in two fluidized beds with diameters of 6 and 18 inch by implementing sophisticated optical fiber probes that measured at selected radial positions the point-wise local up-flow solids velocity and a parameter related to the solids concentration.

1.2.2. The Scale-Up of Fluidized Beds Based on Dimensionless Groups. The open literature reports that, attempts have been made to develop scale-up methodology based on matching governing dimensionless groups based on non-dimensionalizing the continuity and momentum equations for the gas and solids phases along with their boundary conditions in order to achieve the hydrodynamic similarity when the size and the conditions of the fluidized beds change, Al-Dahhan et al. [5].

Romero and Johanson [7] were among the earliest researchers who used this approach to obtain the scaling relationships. They suggested four non-dimensional groups to characterize the quality of fluidization, which are the Froude number, the Reynolds number, (both the Froude number and the Reynolds number are based on the minimum fluidization velocity), the ratio of solid-to-fluid density, and the ratio of bed height at minimum fluidization velocity to the bed diameter. The experimental verification showed that, this set is inadequate.

Glicksman [8] proposed a set of dimensionless groups for scaling up gas-solid fluidized beds based on non-dimensionalizing the continuity and momentum equations for the gas and solids phases along with their boundary conditions. Several assumptions and simplifications were taken into consideration, such as incompressible fluid and

neglecting the inter-particle forces other than the mechanical forces due to collisions. With these assumptions the following set of dimensionless groups is obtained:

$\frac{u_0{}^2}{gL}$, $\frac{\rho_s}{\rho_g}$, $\frac{BL}{\rho_s u_0}$, $\frac{L_1}{L_2}$, $\frac{P_0}{\rho_s u_0{}^2}$. It is important to mention that the reactor configuration remains the same for both the large and small scales. The bed height-to-bed diameter ratio and the ratios of other geometric bed dimensions are expressed in the $\frac{L_1}{L_2}$ term. The $\frac{BL}{\rho_s u_0}$ term, representing the fluid-to-particle drag coefficient which is related to the Ergun equation (low gas velocities, dense bed). When the Ergun equation is non-dimensionalized, it is shown that this term depends on the Reynolds number and $\frac{L}{d_p}$. By substituting these two dimensionless groups into the last set of dimensionless groups, the following set of dimensionless groups emerges, which is called the full set of scaling law: $\frac{u_0{}^2}{gL}$, $\frac{\rho_s}{\rho_g}$, $\frac{\rho_g u_0 d_p}{\mu}$, $\frac{L_1}{L_2}$, $\frac{L}{d_p}$, ϕ and the particle size distribution.

Horio et al. [9] proposed a set of scaling-up relationships based on attaining similarities in bubbles behavior. These relationships are: $\frac{u_0 - u_{mf}}{\sqrt{gD}}$ and $\frac{u_{mf}}{\sqrt{gD}}$, where u_{mf} is the minimum fluidization velocity. Rearranging these groups gives the condition for geometrically similar bubble coalescence as $u_0 - u_{mf} = \sqrt{m}\ (u_0 - u_{mf})^0$ and the condition for geometrically similar flow field around a bubble and for similar bubble splitting as $u_{mf} = \sqrt{m}\ u_{mf}{}^0$, where (m) represents the geometrical similarity of the two beds ((m) here is the ratio of the bed diameter of the two beds which is also equal to the ratios of the bed height, orifice diameter, and pitch dimension of the two beds). Horio et al. [9] used three geometrically similar bubbling fluidized beds of diameters 0.04, 0.1, and 0.24 m to verify their proposed scaling relationships. The solid-to-gas density ratio

was not varied in the experiments although it was not one of the proposed scaling parameters. Video analysis of the bubble eruptions at the beds' surface was used to determine the cross-sectional average bubble diameter, bubble diameter distribution, and radial distribution of the superficial bubble velocity. Similarity was achieved in these hydrodynamic parameters when the above groups and density of solids to gas ratio, and the ratio of superficial to minimum fluidization velocities were matched.

Glicksman [10] proposed a viscous limit set of scaling relationships. It is similar to the full set of scaling relationships that proposed by Glicksman [8], but with a simplification of the Ergun equation for the viscosity dominated system. The viscous limit was set for dense fluidized beds, at low gas velocities, as $\frac{\rho_g u_0 d_p}{\mu} < 4$. In this region, the viscous forces dominant over the inter-particle forces. Due to the negligible inter-particle forces, the requirements for scaling are less stringent. The Ergun equation can then be limited to its first term, which expresses the drag resulting from viscous forces. In this case the $\frac{BL}{\rho_s u_0}$ is proportional to $\frac{{u_0}^2}{gL}$ and $\frac{u_0}{u_{mf}}$. This results in a lower number of dimensionless groups that have to be matched for scaling-up: $\frac{{u_0}^2}{gL}$, $\frac{u_0}{u_{mf}}$, $\frac{L_1}{L_2}$, ϕ and the particle size distribution.

Glicksman et al. [11] found that, matching all of the dimensionless groups proposed by Glicksman [8], [10] could be difficult. Hence, Glicksman et al. [11] suggested simplified a set of dimensionless groups to match to attain hydrodynamics similarity. These are: $\frac{{u_0}^2}{gL}$, $\frac{\rho_s}{\rho_g}$, $\frac{u_0}{u_{mf}}$, $\frac{L_1}{L_2}$, $\frac{L}{d_p}$, ϕ and the particle size distribution. This approach has been validated by measuring the global parameters such as pressure drop cross the bed, pressure signal at the wall, overall solids holdup, and overall gas holdup.

1.2.3. The Scale-Up of Fluidized Bed Based on Chaotic Analysis. Design and scale-up of gas-solid fluidized beds remain difficult and time or cost intensive. The hydrodynamics behavior of gas-solid fluidized bed reactors is very complicated due to the complex interactions of the gas-solid and solid-solid phases. A more detailed understanding of the hydrodynamics is therefore required. The fact that fluidized beds are nonlinear systems and may exhibit a strongly chaotic behavior makes it difficult to be both scaled up and controlled during operation. Due to this non-linearity, these systems are sensitive to small changes in initial conditions and, therefore, characterized by a limited ability to predict their evolution with time, Van den Bleek et al. [12].

In the literature, fluidized bed hydrodynamics are usually studied using time-averaged quantities, such as the average bubble diameter, average rise velocity, average bed expansion, and the average local bed voidage. Although it is widely recognized that the time dependent behavior is an essential characteristic feature of the fluidized bed and important for its performance, this approach neglects the time dependent dynamical behavior. Traditionally, time series of fluctuations of pressure or voidage are analyzed using statistical (e.g. mean, standard deviation) or spectral (e.g. fourier transform, autocorrelation) analysis. Implicitly, these analysis techniques assume that the oscillations can be described by a linear summation of random variations, or by a linear addition of different periodic waves, Kage et al., [13].

Stringer [14] was the first to suggest that the irregular periodic behavior of fluidized bed's dynamics is due to the fact that it is a non-linear, chaotic system. For this reason, it seems appropriate to analyze time-dependent fluidized bed data with specific techniques that take account of the periodicity and non-linearity of the dynamics. This is what is

called chaos analysis, which offers new and useful quantitative tools to characterize the non-linear dynamic behavior of fluidized beds.

Chaotic system is usually characterized by its fractal structure and by its sensitivity to initial conditions. Chaos analysis can be applied for quantitative comparison: not only between various operating conditions (in the same or different beds), or between two scaled beds to assess dynamic similarity, but also between experiments and dynamic model simulations. Moreover, differences between dynamic fluidization regimes and their transitions can also be quantitatively identified, Nedeltchev et al. [15].

As earlier mentioned in the scale-up methodology based on dimensionless groups, several dimensionless parameters derived from the governing equations of dynamics should be kept constant to achieve the dynamic similarity between the scaled beds. However, because of the complexity of fluidized bed hydrodynamics, the scaling rules sometimes fail. In such cases, geometric similarity does not ensure the hydrodynamics similarity needed to preserve, for instance, heat and conversion similarities, consequently, new balances have to be taken into account during the scale-up process, Briongos and Guardiola [16].

Chaotic time-series analysis is a powerful tool to facilitate dimensionless scaling of fluidized beds. It applied to assess quantitively the hydrodynamic similarity between scaled fluidized beds. Moreover, by chaotic analysis of experimental time-series, an indication will be obtained about the number of the significant degrees of freedom that are related to the number of relevant dimensionless similarity groups, Van den Stappen et al. [17].

Earlier experimental work demonstrated the chaotic characteristics from pressure fluctuation data, and showed that these varied with operating conditions and position in the bed Daw et al. [18]; Fuller et al. [19]; Hay et al. [20]; Van den Bleek and Schouten [21].

Van den Bleek and Schouten [21] proposed the chaos scale-up methodology which based on the hypothesis that, beside the laws of conservation of mass, energy and momentum in dimensionless groups scaling methodology of fluidized bed reactors the law of conservation of information should be also taken into accounts. The basic idea of the chaos scale-up methodology is that, the rate of information loss (or the degree of disorder) should be kept similar when scaling up a fluidized bed from the small scale to the large scale in order to ensure hydrodynamics similarity between two beds. Therefore to properly scale-up of fluidized beds the rate of information change s (or the degree of disorder) in both systems should be the same.

Two main characteristics chaos invariants are attractor and kolmogorove entropy (KE). The attractor is a fingerprint of the system and reflects its hydrodynamics state. It is the set of positions in state space at a given set of process conditions, along which the system evolves in time in the stationary situation, which is a measure for the overall complexity or the number of freedom of the system. The kolmogorove entropy (KE) is a direct measure of the chaos level (unpredictability) that determines the rate of loss of information in the system (expressed in bits of information per unit of time), and which quantifies the limited predictability of chaotic systems and represents the degree of disorder. In general, kolmogorov entropy is large for very irregular dynamic behavior (like pressure fluctuations in turbulent gas flow), while it is small in case of more regular,

periodic-like, lower dimensional behavior (like in slugging beds). The limiting values for kolmogorov entropy are infinity for complete random systems (infinite information loss), and zero for completely periodic systems (in which no information is lost during evolution of the system, because next states can be completely and accurately predicted from previous ones). A practical maximum-likelihood method to estimate kolmogorov entropy from measured time series has been reported by Schouten et al, [22].

Both attractor and kolmogorov entropy can be calculated from a time series of only one characteristic variable of the system, in the case of multiphase reactors often the pressure is used because it is easily measurable.

Schouten et al. [23] studied scale-up of the hydrodynamics behavior of gas-solid bubbling fluidized bed reactors where Glicksman et al. [11] similarity rules were analyzed using chaos analysis. The degree of chaos is quantified by the kolmogorov entropy (KE), which is a measure of the rate of loss of information in the system. Pressure fluctuation time series have been used to calculate (KE). They proposed that the rate of information loss should be kept similar when scaling up bubbling fluidized bed reactors. A set of Geldart-B and D particle system used as bed material for a range of bed diameters (from 0.1 m ID up to 0.8 m ID), an empirical correlation is derived that relates kolmogorov entropy to main bubbling bed design parameters such as fluidization conditions (superficial gas velocity, bed height), particle properties (minimum fluidization velocity), and bed size (diameter). They illustrated by some numerical examples how this correlation might be used in scaling up bubbling fluidized reactors, such that the entropy has some desired value at a give bed diameter K α $1/\sqrt{m}$, where the scaling factor (m) is the ratio of the bed diameters of the large and small bed.

Briongos and Guardiola [16] presented a new method of scaling hydrodynamics data obtained from a 2D gas-solid fluidized bed and establishing links between 2D and 3D geometries. They showed that the proposed methodology may also useful for verifying 3D-3D dynamic scaling. According to the chaos scale-up methodology proposed by Van den Bleek and Schouten [21] the information balance should be taken into account. They showed that, there is a need to consider the information generation rate between two scaled fluidized beds using the information group ($\frac{K\, d_P}{U_0}$) thus to achieve hydrodynamic similarity between the scaled beds. The information flow on a normalized time scale ($\frac{K\, d_P}{U_0}$) should be kept constant during the scale-up process. The Fluidized beds of different geometry (2D, 3D) performing under the bubbling regime were operated at different bed height and bed aspect ratios by fluidizing several particle groups belonging to Geldart group B and D. The complexity shown by these systems is measured as the Kolmogorov entropy (KE). They observed that the fact that this methodology is based on the deterministic chaos theory makes it suitable for studying non-linear dynamics, rather than using the more common frequency and time domain analysis.

Accordingly, there is a need to assess in more detail the scaling methods (new methodology and scale-up base on dimensionless groups) by implementing advanced non-invasive measurement techniques which can provide in 2D and 3D detailed local hydrodynamics parameters which is the focus of this research. We have implemented gamma ray computed tomography (CT) technique for measuring time averaged cross-sectional distributions and radial profiles of gas and solids holdups at different axial levels and RPT technique for measuring in three dimensions (3D) solids velocity field and turbulence parameters (Reynolds stress, normal stresses, turbulent kinetic energy,

turbulent eddy diffusivities, etc.). In addition, in this research the effects of various operating and design variables on the above mentioned hydrodynamic parameters have been addressed. This work also provides valuable data to benchmark computational fluid dynamics (CFD) models.

1.3. RESEARCH OBJECTIVES

The main objective of this work is to assess the scale-up methodologies based on detailed local hydrodynamics of gas-solid fluidized bed reactors (FBRs) using advanced non-invasive measurement techniques (CT and RPT). This can be achieved by performing the following tasks:

I. Assessing the new mechanistic scale-up methodology for hydrodynamics similarity of gas-solid fluidized beds that has been proposed in our laboratory which is based on maintaining similar or closer time averaged radial profiles of gas holdups in two different gas-solid fluidized beds to achieve local and global similarity of dimensionless hydrodynamic parameters, since the gas dynamic dictates the hydrodynamics in these beds.

II. Evaluating and demonstrating the non-validity of the literature reported scale-up methodology based on matching the dimensionless groups as scaling parameters to achieve hydrodynamic similarity by measuring the local hydrodynamics parameters using set of operating conditions that fulfilled the matching and not matching dimensionless groups proposed by Glicksman et al. [11].

III. Investigating the effect of reactor size along with selected operating conditions at various axial bed heights on solid holdup and particle velocity, turbulence parameters (Reynolds stresses, turbulent kinetic energy, turbulent eddy diffusivities, etc.), using

advanced non-invasive measurement techniques: gamma ray computed tomography (CT) to measure the time averaged cross-sectional distributions and radial profiles of gas and solids holdups at different axial levels, and the non-invasive radioactive particle tracking (RPT) to measure in three dimensions (3D) the local particle velocity field and turbulence parameters (Reynolds stresses, normal stress, turbulent kinetic energy, turbulent eddy diffusivities, etc.).

1.4. DISSERTATION ORGANIZATION

Thesis is structured in the following manner:

- Section 1. Introduction and motivation which provide a brief literature review relevant to the work done in this dissertation, the available scale-up methodologies and the objectives of this study.
- PAPER I. Validation of the new scale-up methodology for gas-solid fluidized beds using advanced non-invasive measurement techniques (CT and RPT).
- PAPER II. Assessment of scale-up dimensionless groups methodology of gas-solid fluidized beds using advanced and non-invasive measurement techniques (CT and RPT).
- PAPER III. Local time-averaged gas holdup in fluidized bed reactor using gamma ray computed tomography technique (CT).
- PAPER IV. Bed diameter effects on the hydrodynamics of gas-solid fluidized beds via radioactive particle tracking technique.
- Section 2. Presents conclusions and recommendations for future work on fluidized beds.

REFERENCES

[1] Rüdisüli, R., Tilman, J. Schildhauer, Serge M.A. Biollaz J. Ruud van Ommen. Scale-up of bubbling fluidized bed reactors - A review. Powder Technology , 217, pp. 21-38, 2012

[2] Dubrawski, K., Tebianian, S.,Bi, H.T.,Chaouki,J.,Ellis,N.,Gerspacher,R.,Jafari,R., Kantzas, A.,Lim,C.,Patience,G.S.,Pugsley,T.,Qi,M.Z.,Zhu,J.X.,Grace,J.R. Traveling column for comparison of invasive and non-invasive fluidization voidage measurement techniques.PowderTechnol.235, pp. 203–220, 2013.

[3] Tavoulareas, E S. 1991. "Fluidized Bed Combustion Technology." Annual Review of Energy and the Environment 16 (1) (November): 25-57. doi:10.1146/annurev.eg. 16.110191.000325.

[4] Mosfoufi N., Chaouki J. Flow Structure of Solids in Gas-Solid Fluidized Bed, Chemical Engineering Science. 59, pp. 4217, 2004.

[5] Al-Dahhan, M.H., Shreekanta, A., Faraj, Z., Neven, A., Thaar, A. 2014. Scale-up and on-line monitoring of gas-solid system using advanced and non-invasive measurement techniques, Symphos 2013, 2nd International Symposium on Innovation and Technology in the Phosphate Industry, 2014.

[6] Zaid, F. Gas-solid fluidized bed reactors: scale-up, flow regimes identification and hydrodynamics, PhD, thesis, Missouri University of Science & Technology, Rolla, 2013.

[7] Romero, J. B., Johanson, L. N. Factors affecting fluidized bed quality. Chemical Engineering Progress, Symposium Series, 58(38), pp. 28–32, 1962.

[8] Glicksman, L. R. Scaling Relationships for Fluidized Beds. Chemical Engineering Science 39, pp. 1373-1379, 1984.

[9] Horio, M., Akira, N., A., Yoshitaka, S., Iwao, M. A new similarity rule for fuidized bed scale-up. A.I.Ch.E. Journal 32, pp. 1466–1482, 1986.

[10] Glicksman, L. R. Scaling Relationships for Fluidized Beds. Chemical Engineering Science, 43, pp. 1419-1421, 1988.

[11] Glicksman, L. R., Hyre, M. and Woloshun, K. Simplified Scaling Relationships for Fluidized Beds. Powder Technology, 77, pp. 177-199, 1993.

[12] Van den, C. M., Coppens, M. O., Scouten, J.C. Application of chaos analysis to multiphase reactors, Chem. Eng. Sci. 57, pp. 4763-4778, 2002.

[13] Kage, H., Iwasaki, N., Yamaguchi, H., Matsuno, Y. Frequency Analysis of pressure Fluctuation in Fluidized bed Plenum. J. Chem. Eng. Japan, 24, pp. 76-81, 1991.

[14] Stringer, J., 1989, Proc. 10 th Int. Conf. on Fluidized Bed Combustion, Vol. 1, pp. 265-272, (1989).

[15] Nedeltchev, S., Aradhya., Zaid, F. Flow regime identification in three multiphase reactors based on kolmogorov entropys derived from gauge pressure fluctuations, Journal of Chem Eng of Japan, 45, pp. 757-764, 2012.

[16] Briongos, J. V., Guardiola, J. New Methodology for scaling Hydrodynamic Data from a 2D – Fluidized bed. Chem. Eng. Sci. 60 (18), pp. 5151-5163, 2005.

[17] Van der Stappen, M.L.M., Scouten, J.C., Van den Bleek.C.M. Deterministic chaos analysis of the dynamical behavior of slugging and bubbling fluidized beds. Int.Conf. on Fluidized Bed Combustion, pp. 129-140, 1993.

[18] Daw, C.S., Lawkins, W.F., Downing, D.J., Clapp., N.E. Phys. Rev. A, 41,1179.(1990).

[19] Fuller, T.A., Flynn, T.J., Daw, C.S., Halow. J.S. 1993. Proc.12th Int. Conf. on Fluidized Bed Combustion, vol. 1, pp. 141, (1993).

[20] Hay, J.M., Nelson, B.H., Briens, C.L., Bergougnou, M.A. 1995. Chem. Eng. Sci. , 50, pp. 373, (1995)

[21] Van den Bleek, C. M., Schouten, J.C. Deterministic Chaos: A New Tool in Fluidized Bed Design and Operation, Chem. Eng. Sci. 53, pp. 75-87, 1993.

[22] Schouten, J.C., Takens, F., Van den Bleek, C. M. Maximum-Likeli-hood Estimation of the Entropy of an Attractor , Phys. Rev. E Stat. Phys. Plasmas Fluids Relate. Interdiscip. Topics, 49, pp.126-129 .1994.

[23] Schouten, J.C., Van der Stappen, M.L.M., Van den Bleek, C. M. Scale-up of chaotic fluidized bed hydrodynamics, Chem. Eng. Sci. 51,No.10, pp. 1991-2000, (1996).

PAPER

I. VALIDATION OF THE NEW MECHANISTIC SCALE-UP METHODOLOGY FOR GAS-SOLID FLUIDIZED BEDS USING ADVANCED NON-INVASIVE MEASUREMENT TECHNIQUES (CT AND RPT)

Abdelsalam Efhaima and Muthanna H. Al Dahhan

Department of Chemical and Biochemical Engineering, Missouri University of Science and Technology 1101 North State Street. 110 Bertelsmeyer Hall Rolla, MO 65409 USA. ayed67@mst.edu

ABSTRACT

This study focuses on validating the new mechanistic scale-up methodology for hydrodynamics similarity of gas-solid fluidized bed reactors that has been developed in our laboratory. It is based on maintaining similar or closer time averaged radial profiles of gas holdups in two different gas-solid fluidized beds to achieve local and global similarity of the dimensionless hydrodynamic parameters. This is because the gas dynamic dictates the hydrodynamics of these beds. The new scale-up methodology has been successfully validated by assessing for the first time the local hydrodynamic parameters such as time averaged cross-sectional distributions and radial profiles of gas and solids holdups at different axial levels measured by gamma ray computed tomography (CT) technique and particles velocity field and turbulent parameters (Reynolds stress, normal stresses, turbulent kinetic energy, and turbulent eddy diffusivities) measured by radioactive particle tracking (RPT) technique. The experimental results showed that achieving similarity in the radial profiles of the gas

holdup in the geometrically similar beds is essential for ensuring closer or similar local and global hydrodynamics similarity. As the differences increase in terms of magnitude and trend in the gas holdup radial profiles between two beds, the differences increase in the detailed hydrodynamics.

Keywords: Fluidized beds hydrodynamics, new mechanistic scale-up methodology, gamma ray computed tomography (CT), radioactive particle tracking (RPT).

1. INTRODUCTION

Gas-Solid fluidized bed reactors are widely used in commodity and specialty chemicals industry and in petroleum, roasting, drying, coating, combustion, gasification, catalytic cracking, gas adsorption, and gas phase polymerization processes. Fluidized beds reactors (FBRs) have many advantages over other gas-solid reactors, including their simple construction, low operating and maintenance costs, low pressure drop, good heat and mass transfer, excellent contact between the solid particles and the gas phase as well as between particles and the wall, an approximately uniform temperature distribution, the ability to fluidize many particle types of varying sizes, the ability to continuously withdraw product and introduce new reactants into the bed, and the ability to operate at a continuous process state.

Although fluidized bed reactors are relatively simple in mechanical construction, their hydrodynamics behavior is not well understood due to complex interaction among the gas and solids phases. Without such proper understanding of their hydrodynamics it is hard to improve the beds performance, to overcome the operational problems and to achieve a proper scale-up or scale-down methodology. This makes it difficult to predict and understand the hydrodynamics of large industrial-scale reactors.

Therefore, the scale-up of gas-solid fluidized beds has been the subject of a number of investigations in the last few decades. The literature is replete with numerous dimensional and non-dimensional parameters, which have been proposed to characterize the scale-up and the hydrodynamics of the fluidized beds.

Glicksman et al. [1] found that, matching all of the dimensionless groups proposed by Glicksman [2,3] could be difficult and Hence, they suggested simplified set

of dimensionless groups to be matched to attain hydrodynamics similarity. These are: $\frac{u_0{}^2}{gL}$, $\frac{\rho_s}{\rho_g}$, $\frac{u_0}{u_{mf}}$, $\frac{L_1}{L_2}$, $\frac{L}{d_p}$, ϕ and the particle size distribution. Foscolo et al. [4] derived a set of dimensionless groups by including the Archimedes number, density ratio, and geometry ratios, where the Archimedes number can be derived from the Reynolds and Froude numbers and the density ratio. These groups are compatible with those suggested by Glicksman [2] and Horio et al. [5]. In all these studies, the proposed dimensionless groups were validated for hydrodynamics similarity by measuring some global hydrodynamic parameters such as pressure drop, pressure signal measured at the wall, and overall solids or gas holdups. Stein et al. [6] experimentally evaluated the Glicksman et al. [1] set of scale-up dimensionless groups using non-invasive positron emission particle tracking (PEPT) technique. They measured the vertical solids motion and particle cycle frequency. Three cylindrical beds (70, 141, and 240 mm inside diameter) equipped with multiple orifice-type distributors were used. It was shown that for geometrically similar beds, the pair of Froude numbers based on the minimum fluidized velocity (Umf/(g* Dc)^0.5) was sufficient for similarity of these measured parameters.

Knowlton et al. [7] and Rüdisüli et al. [8] reported that interparticle forces, particle-particle interactions, wall effects, different Geldart particle types, and different flow regimes have not been accounted for in the dimensionless groups suggested for scaling-up of gas-solid fluidized beds, since they cannot be characterized adequately.

Van Ommen et al. [9] used computational fluid dynamics (CFD) to assess the validity of the dimensionless groups for scaling up fluidized beds using the simplified set of Glicksman et al. [1] the full set of Glicksman [2] and the full set of Glicksman [2] extended with a diamensionless pressure group. They used two gas-solid fluidized beds

of 30 and 15 cm diameter. The comparison of the time cycle distribution of the normalized pressure and voidage signals of the two scales of fluidized beds were used. Both kolmogorove-smirnov test and attractors were implemented to analyze these signals for comparison. The kolmogorove-smirnov test is a standard statistical test to judge whether or not two probability density functions show a significant difference. The attractor is defined as a multi-dimensional distribution of delay vectors containing successive pressure values and hence it represents consecutive states of the dynamics systems as finger print. They found that matching these sets of dimensionless groups did not lead to complete similarity in the hydrodynamics in terms of the pressure and voidage data of the studied two scales of fluidized beds. However, they found that the simplified set of dimensionless groups, Glicksman et al.[1] gave better comparison of the quantities mentioned above between the two scales compared to the other sets of dimensionless groups mentioned above.

Sanderson et al. [10] applied 3D discreet element method (DEM) to assess the full set of dimensionless groups with two 3-D fluidized beds. They found a moderate agreement.

Rüdisüli et al. [8] reviewed the scale-up methodologies of fluidized beds reported in the literature. They discussed issues and difficulties associated with the dimensionless groups based approach for gas-solid fluidized beds, such as bed physical properties (bubble size, viscosity) have not been considered in dimensionless groups.

Furthermore, it has been found that it is difficult to experimentally implementing the theoretically calculated the matching dimensionless groups and the bed and particle properties for scale-up based on a lab-scale fluidized bed. For example it is not easy to

find the proper particles in terms of sphericity, size distribution and density to match the related dimensionless groups Rüdisüli et al. [8]. Due to the complexity of the fluidized bed and its heterogeneous mixture of solids and gas phases with a behavior liquid-like, matching dimensionless laws often fail to capture the hydrodynamic similarity and to represent reactive fluidized beds where the performance of the bed is linked to the interaction of kinetics, hydrodynamics, and transport of mass and heat. Therefore, Rüdisüli et al. [8] reported that even with all these short comings the approach of dimensionless groups is still considered due to the lack of alternative that does not rely on dimensionless groups.

Furthermore, the literature shows that, the reported scale-up methodologies in general and the matching dimensionless groups in particular for fluidized beds have been assessed and validated by measuring only the global parameters such as overall gas or solids holdups, pressure drop and pressure signals measured at the wall, etc. Although if two different beds have similar overall hydrodynamic parameters, the existence of different local gas holdup radial profiles possibly leads to different flow patterns and mixing intensities, Al-Dahhan et al.[11]. Accordingly, in our group Zaid [12] measured at selected radial positions point-wise local parameters of up-ward solids velocity and a parameter related to solids concentration to evaluate the validity of the scale-up methodology based on matching the dimensionless groups of the simplified set of Glicksman et al. [1] in two fluidized beds with diameters of 0.14 and 0.44 m. Two types of particles of glass beads and copper particles were used as the beds material to achieve matching these dimensionless groups. A sophisticated fiber optical probe was used to measure these parameters. It has been demonstrated experimentally that the similarity

was not attained in the measured point upward solids velocity and quantity that represents the solid concentration for the studied fluidized beds when all of the dimensionless groups were matched. Efhaima and Al-Dahhan, [13] further evaluated this methodology by implementing advanced non-invasive gamma ray computed tomography (CT) to measure the local time averaged cross-sectional distribution and the radial profiles of the solids and gas holdups, and radioactive particle tracking (RPT) technique to measure in three dimensions (3D) local solids velocity components, Reynolds stresses, turbulent kinetic energy, and eddy diffusivities. Two fluidized beds with diameters of 0.14 and 0.44 m were employed using sets of operating conditions that fulfilled the matching and not matching of the dimensionless groups suggested by Glicksman et al. [1]. The experimental results revealed non-similarity in the measured local hydrodynamics when the dimensionless groups were matched in two beds of different sizes. In addition they confirmed that, measuring global parameters (overall holdups and pressure drop, and pressure signal, etc.) is inadequate to assess the scale-up methodology of fluidized beds. These findings are consistent of those reported by Van Ommen et al. [9] using CFD simulations and the analyses and remarks reported by Rüdisüli et al. [8].

Accordingly to overcome what Rüdisüli et al. [8] reported that there is no alternative to the scaling-up with a set of dimensionless groups, we have proposed the following new mechanistic methodology for hydrodynamics similarity of fluidized beds. Since in these types of multiphase reactors the gas phase dictates the hydrodynamics of the reactor, by maintaining similar or closer time averaged radial profiles of gas holdups in two different gas-solid fluidized beds with geometrical similarity, the global and local

similarities of the dimensionless hydrodynamic parameters can be attained (Al-Dahhan et al. [11], Zaid, [12].

Al-Dahhan et al. [11] and Zaid, [12] evaluated and validated this new mechanistic scale-up methodology by implementing sophisticated fiber optical probes that measured at selected radial positions the point-wise local up-flow solids velocity and a parameter related to the solids concentration. Hence, in this work we have evaluated and further validated our new mechanistic scale-up methodology by implementing gamma ray computed tomography (CT) technique for measuring time-averaged cross-sectional distribution and radial profiles of solids and gas holdups along the bed height, and radioactive particle tracking (RPT) technique for measuring in three dimensions (3D) dimensionless solids velocity and its components, flow pattern and the dimensionless turbulent parameters such as normal stresses, shear stresses, turbulent kinetic energy, and eddy diffusivities.

2. EXPERIMENTAL WORK

2.1 EXPERIMENTAL SET-UP

The gamma ray computed tomography (CT) and radioactive particle tracking (RPT) experiments were performed in two fluidized beds of different diameters of 0.14 m and 0.44 m with similar geometries. The columns were constructed from Plexiglas and the plenums were constructed from aluminum. A schematic diagram of the used beds is illustrated in Figure 2.1. The 0.14 m column was 1.68 m high connected from the top with an upper section that had a larger diameter of 0.42 m and was 0.84 m high to disengage the solid particles from the flowing gas by reducing the superficial gas velocity and hence the terminal velocity of the solids. The gas phase was introduced through a sparger tube in the plenum and then through a distributor mounted between the column and the plenum. The gas distributor was made of a porous polyethylene sheet and had a pore size of 40 μm. The sparger tube was plugged at one end, and had 14 holes, all facing downward with respect to the column. The 0.44 m diameter fluidized bed very closely resembled the 0.14 m fluidized bed. The shape of the upper section was similar, but it had a diameter of 0.88 m and was 0.95 m high. The distributor design was similar to that used with the 0.14 m diameter fluidized bed. The plenum also consisted of a sparger tube, which had 20 holes, all facing downward with respect to the column. Both columns were electrically grounded to minimize electrostatic effects. Compressed air supplied from an industrial compressor, that can deliver compressed air of 735 CFM capacity at pressures up to 200 Psig, was used in this work. Two rotameters (Omega® Engineering, Inc.) with different flow ranges were connected in parallel to cover a wide range of flow rates (160 to 3200 SCFH). The CT scans were acquired at H/D = 0.286, 0.64 and 1.7 above the gas

distributor for the 0.14 m diameter column, and at about equivalent H/D levels of H/D = 0.286, 0.88 and 1.6 above the gas distributor for 0.44 m diameter bed. RPT technique was implemented on the bed height of H/D = 0.1 - 2.2 above the gas distributor for the 0.14 m diameter column and of H/D = 0.05 – 2.5above the gas distributor for 0.44 cm diameter column as illustrated in Figure 2.1.

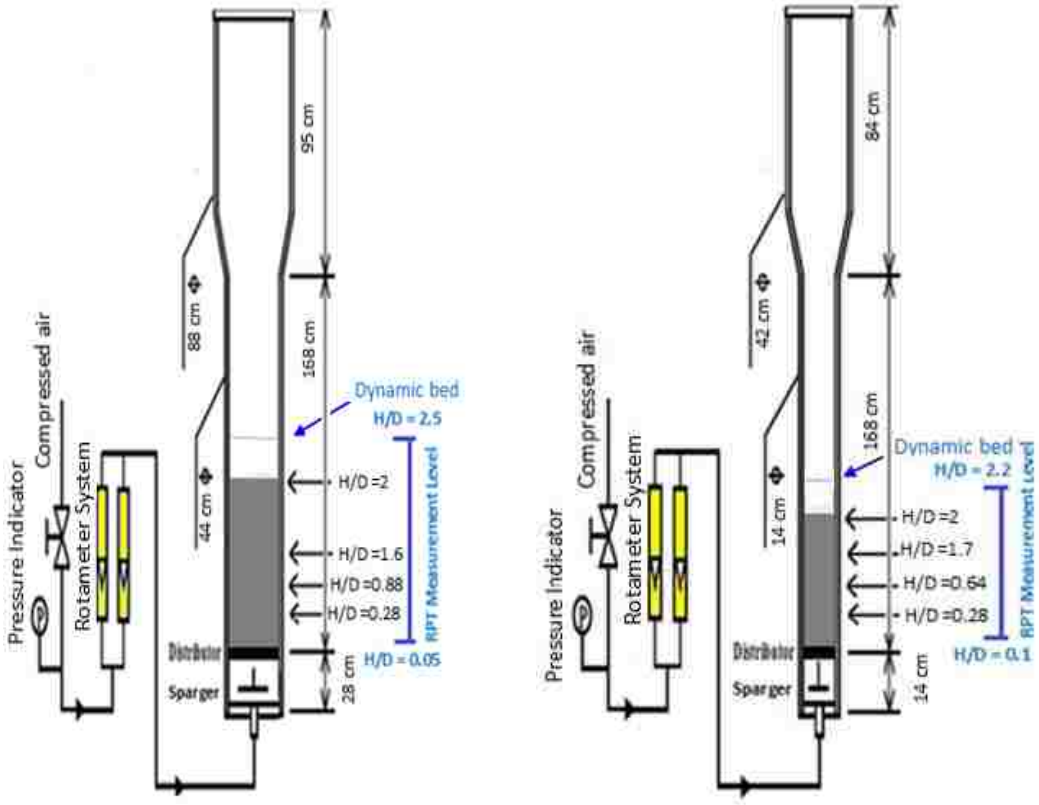

Figure 2.1 Schematic diagram of 0.44 m and 0.14 m cold–flow fluidized bed reactors with measurement levels for CT and RP

As mentioned earlier, the simplified set of dimensionless groups of Glicksman et al. [1] includes dimensionless gas velocity with respect to the minimum fluidization velocity (U_0/U_{mf}). Also, Horio et al. [5] used U_{mf} as part of their dimensionless groups.

Stein et al. [6] found that matching Froude number based on minimum fluidized velocities (U_{mf}) is the key for the similarity in their measured parameters of vertical solids motion and particle cycle frequency. Hence, the minimum fluidization velocity (U_{mf}) was used to convert the solids velocities and turbulent parameters into dimensionless quantities. Therefore**,** in this work the (U_{mf}) was measured by measuring the pressure drop along the bed of particles as a function of the gas velocity. U_{mf} refers to velocity at which the bed stars fluidization and below this velocity the bed is not fluidized. The values of U_{mf} for the 0.14 bed diameter using glass beads of 70 μm was 0.08 m/s, and for the 0.44 bed diameter using glass beads of 210 μm mean particle size was 0.10 m/s, Efhaima and Al-Dahhan, [13]

2.2. EXPERIMENTAL CONDITIONS

It is essential to identify the experimental conditions that can provide similar and non-similar radial profiles of the gas holdup in the used beds, in order to properly assess the new mechanistic scale-up methodology of gas-solid fluidized bed. The experimental conditions used by Al-Dahhan et al. [11] and Zaid, [12] have been implemented in this study. These sets of the experimental conditions are listed in Table 2.1.

A 0.44 m diameter bed has been used as the base (reference) condition (Case 1). The condition used by Glicksman et al. [1]. Al-Dahhan et al. [11] and Zaid [12] identified the experimental conditions in 0.14 m diameter bed that provided closer or similar radial profiles of gas holdup with respect to the Case 1 (reference case). They used optical fiber probe and computational fluid dynamic (CFD) as an enabling tool to search for these conditions. These conditions have been used in our work and we call them for

abbreviation “similarity conditions” designated as Case 2 in Table 2.1. For the conditions that provide in 0.14 m diameter bed non-similar radial profile of gas holdup with respect to the Case 1, the conditions used by Glicksman et al. [1] in 0.14 m in diameter bed were selected. We call these conditions as “non-similarity conditions” designated as Case 3 in Table 2.1.

We have performed the CT and RPT experiments on all these conditions mentioned above and listed in Table 2.1 (similarity and non-similarity in gas hold-up radial profiles conditions).

Table 2.1 Conditions for similar and non-similar gas holdup radial profiles for validating the new scale-up methodology

Condition	**Reference Case Case 1**	**Conditions for Similar ($\varepsilon_{g(r)}$) Case 2**	**Conditions for No-similar ($\varepsilon_{g(r)}$) Case 3**
Dc (m)	0.44	0.14	0.14
Particle Type	Glass Bead	Glass Bead	Glass Bead
L (m)	4.877	4.775	4.775
H (m)	0.88	0.28	0.28
T (K)	298	298	298
P (Kpa)	101	101	101
dp (μ m)	210	70	70
ρs (kg/(m^3))	2500	2500	2500
ρf (kg/(m^3))	1.21	1.21	1.21
μ (kg·s m–2)	1.81E-05	1.81E-05	1.81E-05
Ug (m/s)	0.36	0.25	0.20
U_{mf} (m/s)	0.10	0.08	0.08
Φ (sphericity)	0.95	0.95	0.95
Dc/dp	2095.24	2000	2000
H/Dc	2	2	2
ρs/ρf	2066.12	2066.12	2066.12
U/Umf	3.42	3.12	2.50
Fr=(U^2)/g* H	0.015	0.0145	0.0145
Fr=(U^2)/g* Dc	0.03	0.045	0.029

The goal here is to further validate based on detailed local hydrodynamic parameters that, if one maintains similar or closer radial profiles of gas holdups the hydrodynamics of the two systems in terms of dimensionless hydrodynamics parameters will be the same or closer. Such a similarity in the hydrodynamics of the systems is the ultimate goal of any scale-up methodology to attain with lesser uncertainty the desired conversion and process performance.

3. MEASUREMENT TECHNIQUES

3.1. COMPUTED TOMOGRAPHY (CT) TECHNIQUE

Gamma ray computed tomography (CT) technique has been extensively implemented on various multiphase flow systems in our Multiphase Reactors Engineering and Application Laboratory (mReal) at the Chemical and Biochemical Engineering Department, Missouri University of Science and Technology (Missouri S&T). The gamma ray computed tomography (CT) technique comprises of Cs-137 sealed source and a set of 15 NaI scintillation detectors. This technique is a part of the dual source and energy (Cs-137 and Cobalt Co-60) gamma ray computed tomography (DSCT) technique, which was developed by Varma [14] with the help of the team from the Oak Ridge National Laboratory (ORNL) sponsored by the Department of Energy (DOE). In this work, CT experiments were performed under two-phase conditions, gas and solids, and hence a single sealed source (Cs-137) and its 15 NaI scintillation detectors located opposite to the (Cs-137) sealed source have been used to measure in a non-invasive manner the time-averaged cross-sectional phase holdups distributions and their radial profiles at the operating conditions previously outlined in Table 2.1. As shown in Figure 3.1 the array of detectors and the source are built on a rotary plate to move together in 360° around the object to be scanned, providing 197 views in each scan and 21 projections in each view. The plate can be moved up and down by stepper motor along the bed height to scan the bed at different axial positions. Each detector consists of a 2-inch cylindrical NaI crystal, a photomultiplier (MP), and electronics. Each of these detectors was collimated with a lead collimator with an open aperture. Two sizes of collimators were used in this work. Since in 0.44 m diameter bed high attenuation was

encountered, large aperture size was used in order to collect enough counts. Collimators that have approximately an open aperture of 2 mm × 2 mm were used with 0.14 m diameter column, while those that have approximately an open aperture of 2 mm × 5 mm were used with 0.44 m diameter column. However, in this case the special resolution was reduced to the size of 2 mm × 5 mm for 0.44 m diameter column. The CT scan sampling rate was 60 samples at 10 Hz, which took approximately 7.2 seconds to finish a 50 projection and 8.25 hours to complete a full scan by 360° rotation of the Cesium (CS-137) source and detectors around the column.

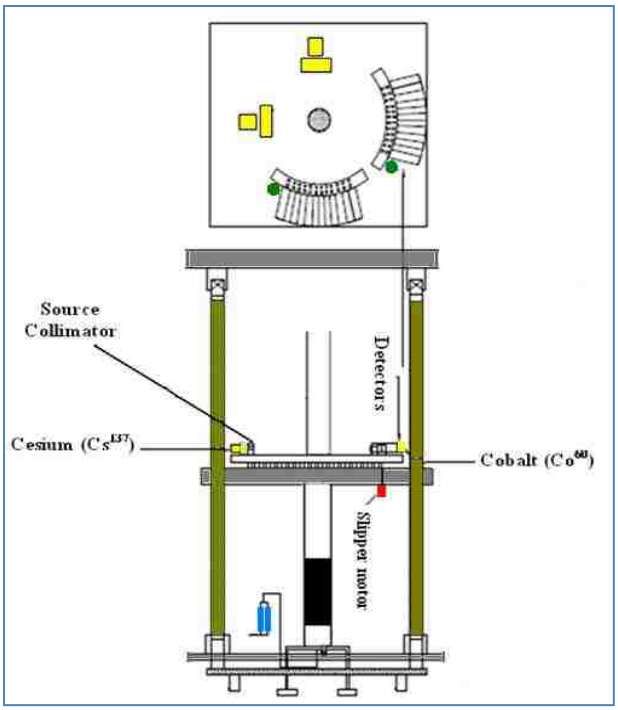

Figure 3.1 Schematic diagram of dual-source computed tomography technique

The set of scans performed consists of 1) Scanning the column empty as reference CT scan, 2) Scanning the column filled with solids (glass beads) as packed bed to estimate the attenuation coefficient of the solids phase in each pixel, and 3) Scanning the

column at the desired condition of gas-solid fluidization**.** The CT scans were acquired at H/D = 0.28, 0.64, and 1.7 above the gas distributor for the 0.14 m diameter column, and at about equivalent levels, which were at H/D = 0.28, 0.88, and 1.6 above the gas distributor for 0.44 m diameter bed as shown in Figure 3.1.

Alternating Minimization (AM) algorithm and programs developed by varma et al. [15] have been used to process gamma ray computed tomography data to obtain holdups distribution. The cross-section of the bed is divided into 80 × 80 square pixels. More detailed on both the hardware and the software used in this technique and the related post-data processing have been described by (Varma et al. [15]; Varma et al. [16]; Bhusarapu, [17]; Bhusarapu et al. [18]; Fadah [19]; Efhaima and Al-Dahhan [13].

3.2 RADIOACTIVE PARTICLE TRACKING (RPT) TECHNIQUE

The RPT is a powerful technique for mapping the Lagrangian trajectory of a particular phase in a given system by tracking a single tracer radioactive particle. One of the two advanced radioactive particle tracking (RPT) technique that were built in our Multiphase Reactors Engineering and Application Laboratory (mReal) at the Chemical and Biochemical Engineering Department, Missouri University of Science and Technology (Missouri S&T) has been used in this work. This setup included a fully automatic calibration device (r, z, and θ) and a single processing and data acquisition system. Twenty-eight NaI scintillation detectors were used and positioned between H/D = 0.1 - 2.2 above the gas distributor for 0.14 m column and between H/D = 0.05 - 2.5 above the gas distributor for 0.44 m column as shown in Figure 2.1. The detectors were held on four vertical supports at equal distances around the column. Each support had 7 detectors

placed at different axial levels. Each detector consisted of a cylindrical NaI crystal (2 in x 2 in), a photomultiplier and electronics. A single radioactive tracer particle was introduced into the fluidized bed. In this study a 600 micron diameter irradiated Cobalt-60 particle with an activity of about 500μCi was used. Cobalt has a high density of 8.9 g/cm^3. Hence, the 600 μm diameter irradiated cobalt-60 particle was encapsulated with a gap of air in an aluminum ball with a 1 mm outer diameter to achieve the same density as the solids used (glass beads density of 2.5 gcm^{-3} density). This composite single radioactive tracer particle was used to track the solids of 210 and 70 μ in the studied fluidized beds. It is noteworthy that larger tracer particle with similar density of the solid particles of the fluidized bed should be able to track with fidelity the smaller particles sizes in fluidized bed. This is because the particles in the gas-solid fluidized bed usually do not move as single isolated particles but they do as a cluster (Tebianian et al. [20]; Mostoufi et al. [21]; Mostoufi et al. [22]). Each single particle is attached to a solid aggregate in the dense bed and moves with it until the solid aggregate breaks-up. The particle then enters another solid ensemble and continues its movement with the new ensemble. It is not necessary then to use a tracer particle of size that matches the size of experimental particles. Mostoufi et al. [21] and Mostoufi et al. [22] showed that all studied parameters were affected by the superficial gas velocity, and were independent of the size of the tracer. Tebianian et al. [20] used in RPT experiments scandium as tracer particle with size and density different from that solid particle used as their tracer diameter was 400 μm which was 4-times greater than the particle size of 107 μm, but with the same density. In our experiment a total of 28 NaI scintillation detectors were positioned around the column. These detectors were held on four vertical supports at

equal distances around the column. Each support had 7 detectors placed at different axial levels. Each level had 2 detectors that were staggered with the other levels by 45^0. Figure 3.2 shows a schematic diagram of the detectors distribution around the bed. RPT experiments typically consist of the following two steps: 1) the RPT calibration (static location of the tracer particle by the use of the calibration device under the desired experimental conditions), and 2) the RPT experiment (where the tracer particle is freely moving with the solids). During in-situ calibration, the detectors were calibrated by placing the tracer particle by the automated calibration device and moving it through the bed at several hundred known locations where each NaI scintillation detector records intensity counts that depend on the distance between the radioactive tracer particle and the detector for each calibration location and the materials in between.

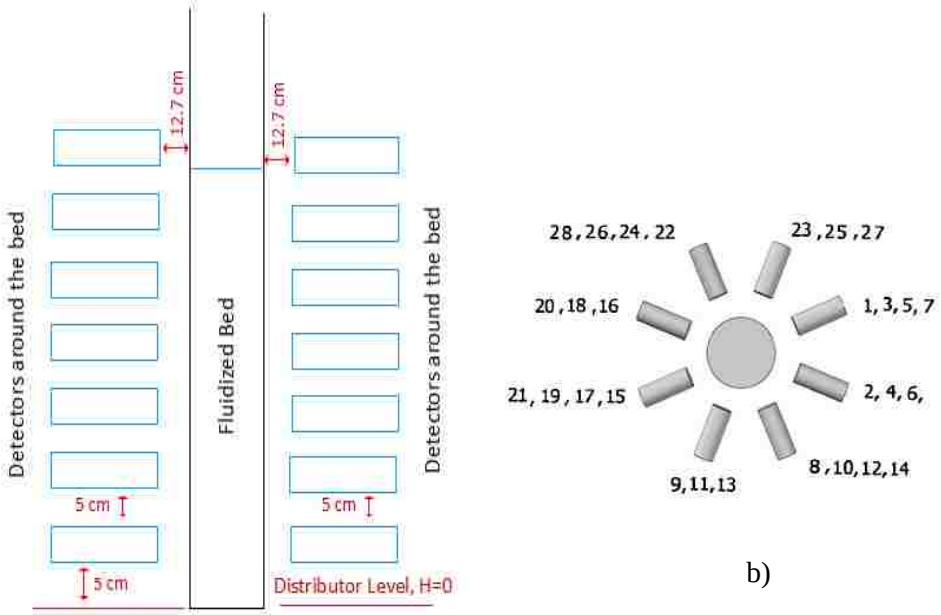

a) b)

Figure 3.2a) - Detectors Arrangement around the bed, and b)- Side view of the detectors distribution around the bed

From the calibration step, a count-distance map can be obtained for each detector, which will be used in a subsequent step to obtain the location of the tracer particle during the RPT experiment where the radioactive particle moves freely inside the reactor to track the solids phase motion. The experiments were conducted using a data acquisition frequency of 50 Hz for 8 hours, and during this time, the radiation emitted by the radioactive tracer particle was recorded by the detectors. The data obtained from the calibration and actual experiments can be used to reconstruct the lagrangian trajectory of the tracer radioactive particle. A cross correlation based search method Bhusarapu, [17] and Bhusarapu et al. [18] was used to reconstruct the tracer particle position. This method is a two steps approach in which cross-correlation based search algorithm utilizing the calibration data is used to approximately locate the tracer particle position and a semi-empirical mechanistic model is fitted to the calibration data to relate the counts recorded to the position of emitting tracer particle. This semi-empirical mechanistic model takes into account the geometry as well as the attenuating medium in between the particle and the detector. It is used to generate computed points of counts versus locations of high resolution around the approximate location identified by the first step of cross-correlation with the help of the calibration data. Then again cross-correlation based search is applied on the computed points of counts versus locations to identify the tracer particle location where then the Lagrangian trajectory of the tracer particle is obtained. More detailed can be found in Bhusarapu, [17] and Bhusarapu et al. [18]. By processing the lagrangian trajectory where the distance travelled by the tracer particle during the recorded sampling time provides the instantaneous solids velocities from which the time average solids velocity can be estimated. The difference between

the instantaneous solids velocities and the time average solids velocities yields the fluctuation velocities which allow estimation of the turbulent parameters (Reynolds stress, normal stresses, turbulent kinetic energy, turbulent eddy diffusivities, etc.). In order to obtain the time-averaged hydrodynamic parameters as a function of the position, the columns 0.14 m (6 inch) and 0.44 m(18 inch) were first divided into sampling compartments of certain dimensions that provide equal compartments volume, depending on the column diameter and the height of expanded solid when is in operation. To obtain reliable estimates of the turbulent parameters, the instantaneous particle position data obtained from RPT experiments must be filtered in order to extract only the coherent part of the signal by eliminating the white noise. The discrete wavelet transformation threshold de-noising filtration analysis proposed by Degaleesan [23] and Degaleesan et al. [24] was used in this work. Table 2 summaries how these velocity and turbulent parameters are estimated Roy [25] and Upadhyay [26].

Table 3.1 hydrodynamic parameters estimated for each compartment (i,j,k) from rpt reconstruction lagrangian trajectory.

Instantaneous Velocity (cm/s)	$u_{z,i-1/2} = \frac{z_i - z_{i-1}}{\Delta t}$ $u_{r,i-1/2} = \frac{r_i - r_{i-1}}{\Delta t}$ $u_{\theta,i-1/2} = \frac{(\theta_i - \theta_{i-1})}{\Delta t} \ \frac{(r_i + r_{i+1})}{\Delta t}$
Time-averaged velocities (cm/s)	$\overline{u}_{p(i,j,k)} = \frac{1}{N_v} \sum_{i=1}^{N_v} u_{p(i,j,k),i}$ p = z, r,θ
fluctuating velocity (cm/s)	$u'_{p(i,j,k)} = u_{p(i,j,k)} - \overline{u}_{p(i,j,k)}$
Azimuthally averaged velocity (cm/s)	$\overline{u}_{(i,k)} = \frac{1}{N_\theta \, \tilde{N}_{v(i,k)}} \sum_{j=1}^{N_\theta} \overline{u}_{(i,j,k)} \quad N_{v(i,j,k)}$
Stresses (cm^2/s^2)	$\tau_{pq} = \overline{u'_p u'_q}(i,j,k) = \frac{1}{N_v} \sum_{n=1}^{N_v} u'_p(i,j,k),n \, u'_q(i,j,k),n$
Turbulent Kinetic Energy (cm^2/s^2)	$K = \frac{1}{2}(\overline{u'^2_r} + \overline{u'^2_z} + \overline{u'^2_\theta})$
Normal radial eddy diffusivity (cm^2/s^2)	$D_{rr}(t) = \frac{1}{2}\frac{d}{dt}\overline{Y_r^2(t)} = \int_0^t u'_r(t) \, . \, u'_r(t') \, . dt'$
Normal axial eddy diffusivity (cm^2/s^2)	$D_{zz}(t) = \frac{1}{2}\frac{d}{dt}\overline{Y_z^2(t)} = \int_0^t \left[\left[\overline{u'_z(t) \, . \, u'_z(t')} + \overline{\left.\frac{du_z}{dr}\right\|_{Y_{r(t')}}} \, . \left(\int_0^{t'} u'_z(t) \, . \, u'_r(t'') \, dt'' \right) \right] . dt' \right]$

4. RESULTS AND DISCUSSION

The statistical differences in the measured hydrodynamic parameters profiles (gas holdups, particles velocity, and turbulent parameters) between the conditions outlined in Table 2.1 are represented in terms of the percentage average absolute relative difference (AARD) of all the measured local points and the percentage absolute relative difference (ARD) of each individual measured local point as follows

$$AARD = \frac{1}{N}\sum_{1}^{N}\left[\frac{x(r)-y(r)}{x(r)}\right] \times 100 \quad (1)$$

$$ARD = \left[\frac{x(r)-y(r)}{x(r)}\right] \times 100 \quad (2)$$

Where, x and y the measured hydrodynamic parameters at the radial and cross-sectional locations for the cases outlined in Table 1 and (N) is the total number of the local data points. The reproducibility of the experiments is one of the most important factors to consider before taking any measurements. To check the reproducibility CT measurements were repeated in 0.14 m diameter column with glass beads-gas system three times under identical operating conditions. The time averaged gas holdup values were almost identical with few differences were accepted, they were within 4.5% error Efhaima and Al-Dahhan, [27]. Also the RPT experiments were repeated three times under identical operating conditions Efhaima and Al-Dahhan, [28]. The bars shown in the figures represent the standard deviation around the mean wherever they are presented.

4.1 CONDITION FOR SIMILAR RADIAL PROFILES OF GAS HOLDUP ($\boldsymbol{\varepsilon_{g(r)}}$)

In this section we discuss the analysis of the local parameters for the two fluidized beds (0.14 m and 0.44 m) using the conditions that provide similar radial

profiles of gas holdup, (Case 1 and Case 2) outlined in Table 2.1 which validate the new mechanistic scale-up methodology. We start with the CT results to confirm the similarity of the radial profiles of gas holdup for Case 1 and Case 2 obtained by optical fiber probe, Zaid, [12]. It is clear that the gas holdup radial profiles were very close or similar for both cases as shown in Figure 4.1 which confirms the result of the optical fiber probe used by Zaid, [12]. The percentage Average Absolute Relative Difference (AARD) in H/D of 0.88 was 3.3%. The percentage Absolute Relative Difference (ARD) was 3.96% at the center (r/R= 0); 3.84% at (r/R = 0.2) away from the center; 3.78%; at (r/R= 0.4); 3.14% at (r/R= 0.6); 2.92% at (r/R= 0.8); 2.12% at r/R= 1 (close to the wall).

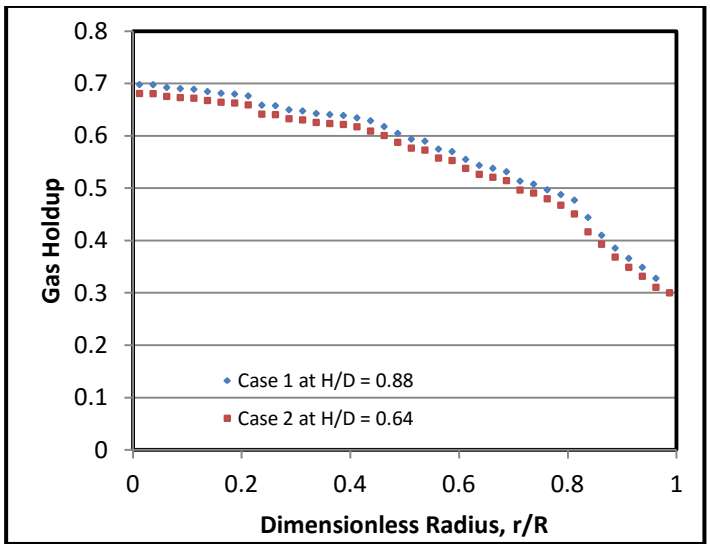

Figure 4.1 Time average gas holdup radial profiles as function of radial position for Case (1) (at H/D = 0.88) and Case (2) (at H/D = 0.64) by (CT) technique

4.1.1. Cross-Section Distributions of Solids Holdup. Figure 4.2 demonstrates the time averaged cross-sectional distribution of solids holdup for Cases 1 and 2,

outlined in Table 2.1 at three levels measured by the computed tomography (CT) technique.

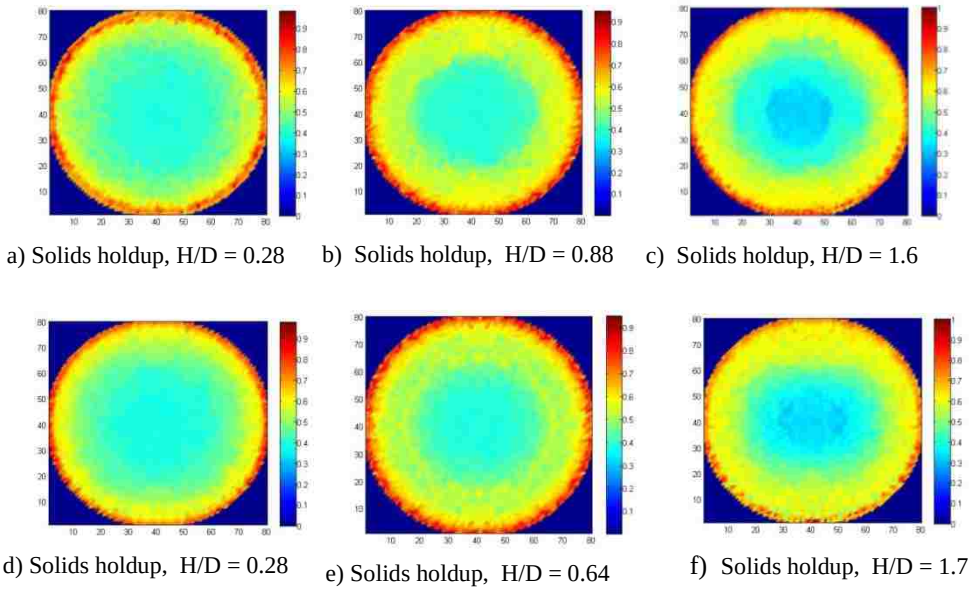

a) Solids holdup, H/D = 0.28 b) Solids holdup, H/D = 0.88 c) Solids holdup, H/D = 1.6

d) Solids holdup, H/D = 0.28 e) Solids holdup, H/D = 0.64 f) Solids holdup, H/D = 1.7

Figure 4.2 Cross-sectional distribution of solids holdup (a,b,c) for Case 1 (0.44 m), and (d,e,f) for Case 2 (0.14 m) at different dimensionless axial positions

The figure illustrates the similarity in local solids holdup cross-sectional distribution along the bed height between Case 1 (reference case) and Case 2. Since the time averaged solids distributions show axisymetry, the similarity can be further demonstrated by the radial profiles as discussed in the following section.

4.1.2. Time-Averaged Solids and Gas Holdup Radial Profiles. The azimuthally averaged radial profiles of the solids holdups obtained from the time averaged cross-sectional distribution at the conditions of similar radial profiles of gas holdup (Case 1 and Case 2) at different H/D measurement levels are shown in Figure 4.3. It is clear that the solids holdup radial profiles were very close or similar for both cases at

all levels when the radial profiles of gas holdup are similar at a level within the bed. This confirms the validity of the new mechanistic scale-up methodology.

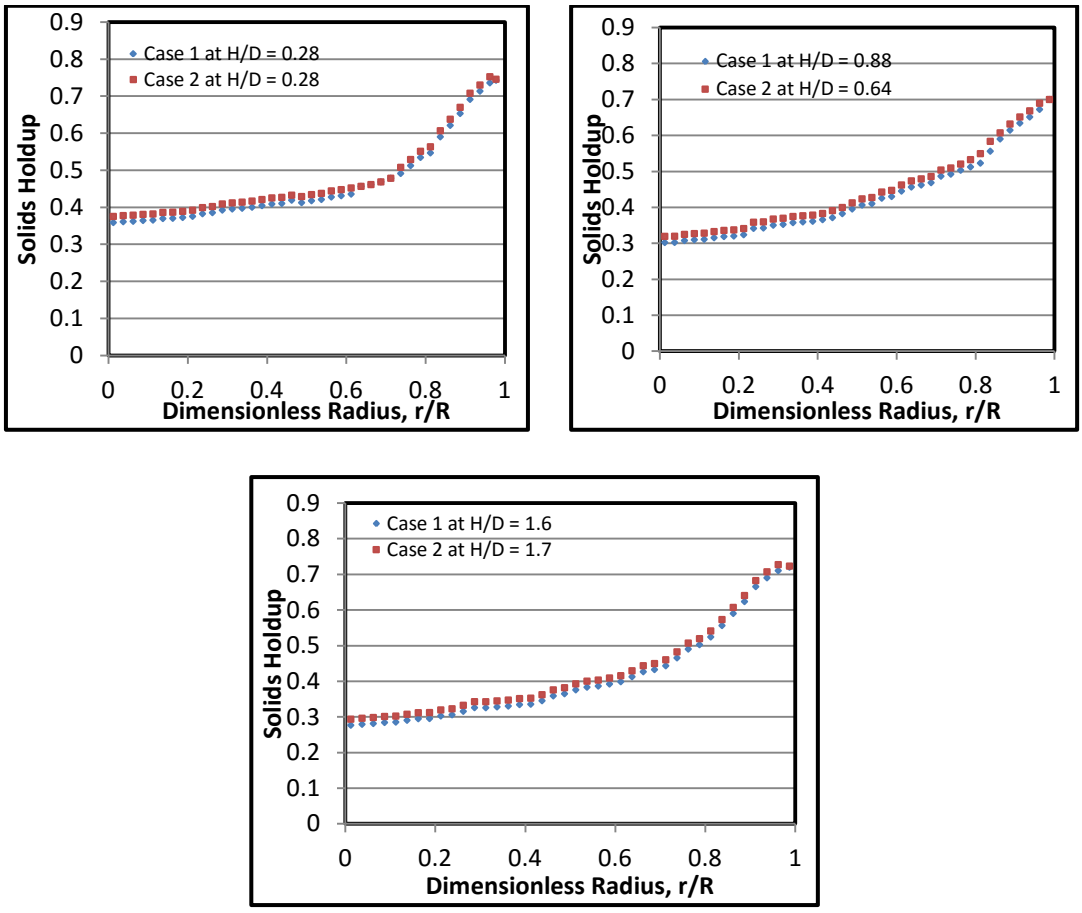

Figure 4.3 Time average solids holdup radial profiles as a function of the dimensionless radial position for Case (1) and Case (2) at different axial levels by (CT) technique

The percentage Average Absolute Relative Difference (AARD) was 3.1% at (H/D = 1.7); and the percentage Absolute Relative Difference (ARD) was 3.93% at the centre (r/R= 0); 3.76% at (r/R = 0.2) away from the centre; 3.63%; at (r/R= 0.4); 2.86% at (r/R= 0.6); 2.1% at (r/R= 0.8); 2.3% at r/R= 1 (close to the wall).

Not much change took place when the H/D changed from 1.7 to 0.88. The percentage Average Absolute Relative Difference (AARD) in H/D of 0.88 was 3.85%, and the percentage Absolute Relative Difference (ARD) was 3.84% at the centre (r/R= 0); 4.28% at (r/R = 0.2) away from the centre; 4.18%; at (r/R= 0.4); 3.93% at (r/R= 0.6); 3.64% at (r/R= 0.8); 3.23% at r/R= 1 (close to the wall).

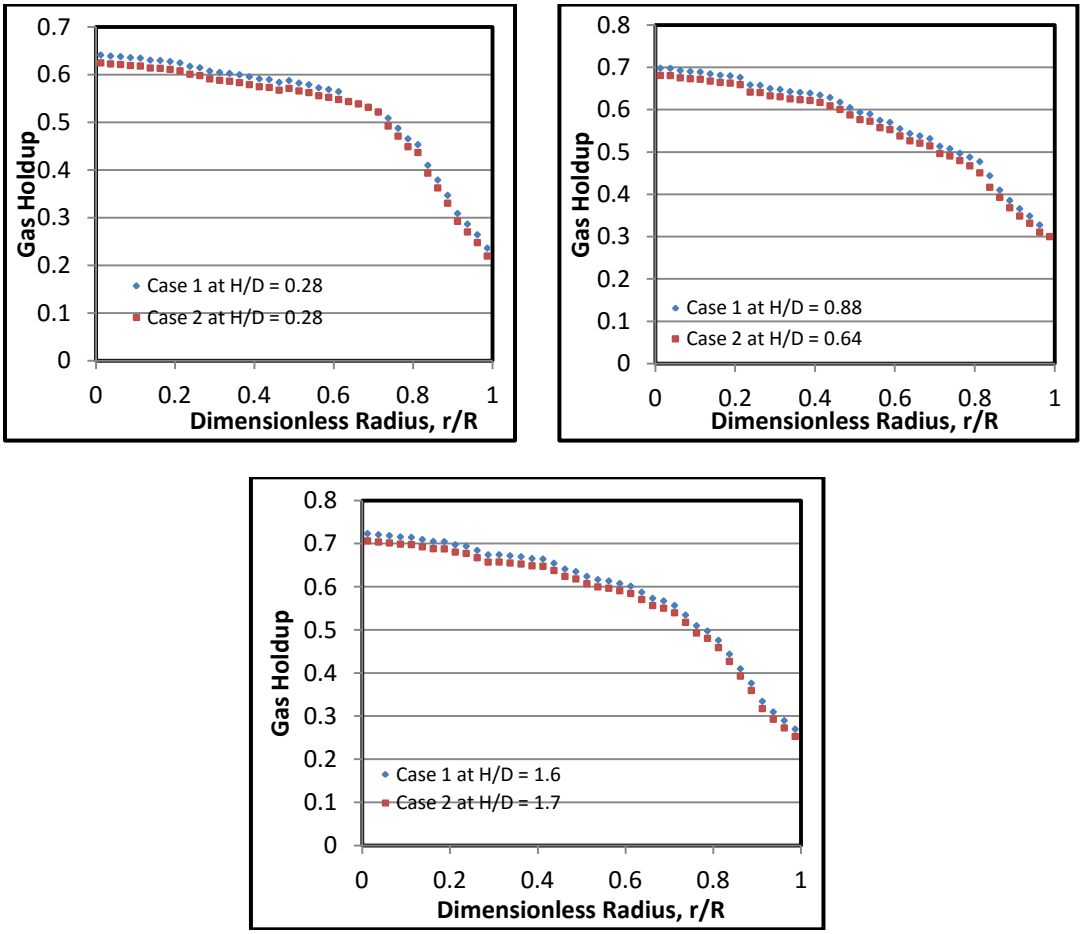

Figure 4.4 Time average gas holdup radial profiles as a function of the dimensionless radial position for Case (1) and Case (2) at different axial levels by (CT) technique

Also, at H/D= 0.28, which is close to or at the sparger region matching was able to be attained as the percentage Average Absolute Relative Difference (AARD) in this dimensionless height was 3.1%.

Since 1- solids holdup = gas holdup also similarities in gas holdup has been achieved at all levels in addition to the H/D = 0.88 and 0.64 as shown in Figure 4.4.

Same trends of the variation of gas holdup with the height of the bed obtained compared to those of solids holdup. Figure 4.5 shows the radial variation of the percentage Absolute Relative Difference (ARD) in solids holdup radial profiles between Case 1 at (H/D = 0.88) and 2 at (H/D = 0.64). Similar ranges of (ARD) were found for all the other levels

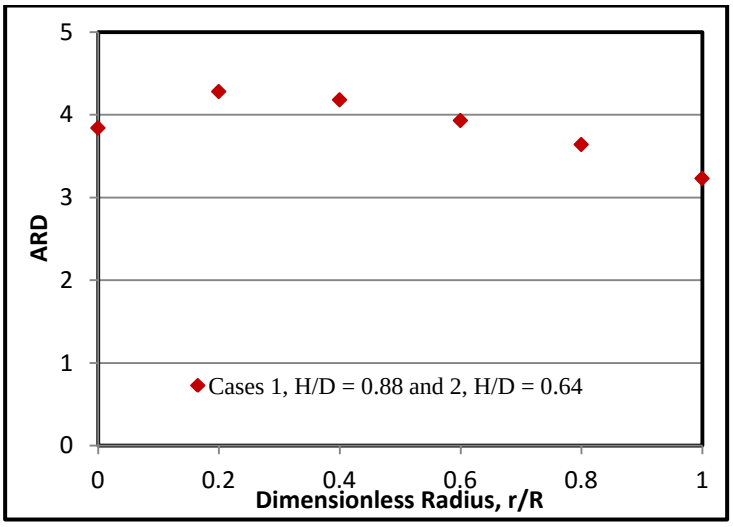

Figure 4.5 The radial variation of ARD in solids holdup radial profiles between Case (1) and Case (2) at H/D = 0.88

4.1.3. Time-Averaged Particle Velocities. The proper design and scale-up of gas-solid fluidized beds depends upon the quality of the description of the particles movement inside the bed, Rüdisüli et al. [8]. The non-invasive Radioactive Particle

Tracking (RPT) technique measures the 3-D local particle velocity components. In this section the time and azimuthally averaged radial profiles of the particle velocities (axial, radial and azimuthal) have been calculated from RPT data at different axial levels where CT scans are performed. Also the azimuthally and axially averaged particle velocities have been calculated along the measured axial height indicated in Figure 2.1. In order to obtain the time averaged particle velocities as a function of the position the column was divided into equal volume sampling compartments as previously mentioned. The time averaged particle velocities were calculated by averaging the instantaneous particle velocities (axial, radial and azimuthal) for a give compartment (i,j,k) according to Table 3.1. The time averaged particle velocities at three CT axial locations and overall axially averaged (i.e. along the axially RPT measure height) are presented in this work. The three levels are at H/D = 0.286, 0.64 and 1.7 above the gas distributor for the 0.14 m diameter column, and at about equivalent H/D levels of H/D = 0.286, 0.88 and 1.6 above the gas distributor for 0.44 m diameter bed. The overall axially averaged profiles are obtained by averaging axially the instantaneous particle velocities (axial, radial and azimuthal) for a give compartment (i,j,k) over the measured bed height along all the axial bed compartments.

4.1.3.1. Axial particle velocity radial profiles. The comparison of the time and azimuthally averaged axial particle velocity radial profiles for the similarity conditions (Case 1 and 2) are shown in Figure 4.6. The results show that, the axial velocity of glass beads particle is positive at the center region of the column, and negative near the wall, which shows that the solids are going upward within the center region of the column (r/R = 0 – 0.62) while coming downward near the wall region (r/R $\geq$ 0.63). This finding is

consistent with the previous study of Mostoufi and Chaouki [29]. They used RPT to investigate the circulation patterns in two different sizes bubbling fluidized beds of 0.19 m and 0.292 m with glass beads of 700 μm diameter were used as the bed material. They found that, the transition from up- to down- flow was at approximately (r/R = 0.63). The percentage Average Absolute Relative Difference (AARD) in Figure 4.6 was 17.3%, 18.2%, 20.3% at H/D = 0.28, 0.88, 1.7, respectively and was 18.6% for the overall axially averaged axial particle velocity. The difference in the absolute local values of particle velocity between the reference case (case 1) and the case of similar radial profile of gas holdup (case 2) is high. This is because the gas phase is the driving force in the fluidized bed and thus dictates the bed hydrodynamics. Bubbles and voids derive the solids circulation in the fluidized beds, Hamed et al. [30]. Hence, bubble size and bubble rise velocity are among the most important parameters in the design and scale-up of gas-solid fluidized bed reactors, Rüdisüli et al. [8]. The bubbles size, the bubble frequency, and the bubble rise velocity are all strongly influenced by the bed size. In the small size reactor, the bubble size would reach the bed diameter and slugging would occur depending on the gas velocity. Hence, in smaller beds bubbles move in the form of slugs, Verma et al .[31]. While in sufficient large beds, slugging will not occur and the fluidization in the large-scale will be drastically different from the small-scale reactor (Rüdisüli et al. [8], Bangyou et al. [32]). The maximum stable bubble diameter is in the order of 15 to 30 cm. Slugging starts if the bubble size is about 2/3 of the bed diameter (Rüdisüli et al. [8]). In the large commercial reactors, bubbles could grow continuously and proportionally to their rise velocity Knowlton et al. [7]. This is confirmed in Figure 4.4 where the gas holdup increases with the bed height particularly at the centre region of the bed. Bubbles

in a large diameter column are large and tend to rise faster than bubbles in a smaller diameter column due to the restraining effects of the column walls and also due to the strong slugging effect in the small diameter column Hamed et al. [30]. These differences in the bubble behavior directly affect the contacting between gas and solids. The solids in a larger bed are mostly carried through the wakes of the bubbles (Verma et al .[31]. Furthermore, the gas holdups as per Figure 4.4 are larger in the centre region of the column as compared to the wall region which drives the circulation of the particles in the bed causing higher center line axial particle velocity. As the bed height increases the gas holdup increases and hence the axial particle velocity increases. Therefore, the magnitude of solids velocity is higher in larger bed (0.44 m); the upward solids velocity of glass beads in the large column (0.44 m) is higher than the upward axial velocity of glass beads in the small column (0.14 m). The finding is consistent with previous study of Verma et al. [31]. They investigated hydrodynamics differences between three- dimensional fluidized beds of diameter 0.10, 0.15, 0.30, 0.60, and 1.0 m. They concluded that the bubble size generally increases with increasing bed diameter. They emphasized that, a significant difference in the bubble size caused increasing particle velocity in large diameter. Solid circulation, gas flow, and solid-gas contacting patterns in large column are different from those in small scale column (Rüdisüli et al. [8]). The particle velocities also increase with an increase in the gas velocity. These findings are consistent with the previous studies (Wang et al. [33]; Tebianian et al. [20]; Laverman et al. [34]; Mostoufi and Chaouki. [29]). In addition, the reference case (0.44 m) has a higher drag force on the particles compared to the case of similar radial profile of gas holdup, case 2, (0.14 m), which has lower drag force acting on the particles this is because the momentum from the

gas phase is imparted to the solids phase. The imparted momentum from the gas phase is transferred to the mean particles velocity and its fluctuations.

Furthermore, for the same reasons outlined above and due the growing bubbles size with the height of the bed, Figure 4.6 shows that the particle axial velocities increase with the height of the bed in the upward and downward regions. This is consistent with the increase of gas holdups with the bed height as shown in Figure 4.4.

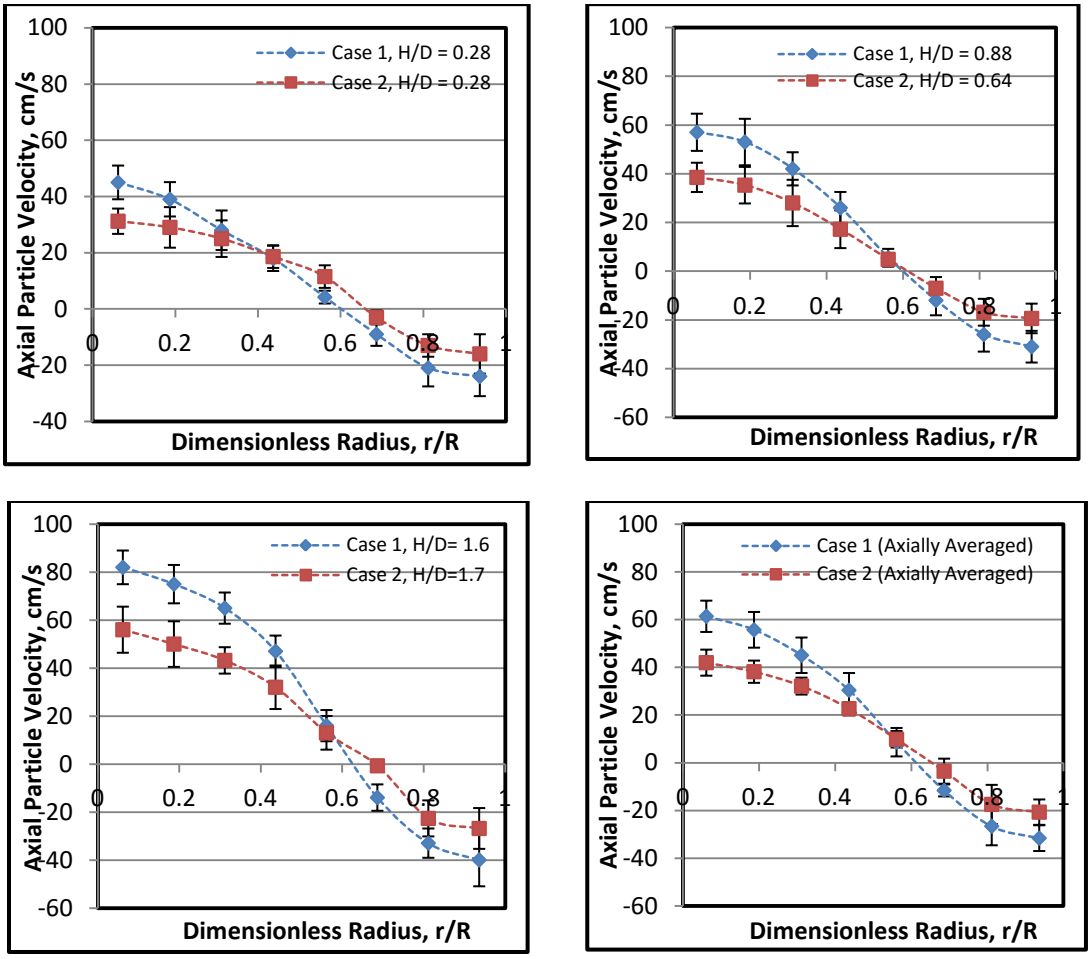

Figure 4.6 Time and azimuthally averaged and overall axially averaged particle velocity radial profiles for the similarity conditions (Case 1 and Case 2) (dot lines represent the trend)

To have a common basis for comparison between various sizes of beds the axial particle velocity in both fluidized beds has been non-dimensionalized by dividing the velocity values by the minimum fluidization velocity (U_{mf}). U_{mf} for the 0.14 bed diameter was 0.08 m/s and for the 0.44 bed diameter was 0.10 m/s. Figure 4.7 shows the compared dimensionless radial profiles of particle velocity for the conditions of similar radial profiles of gas holdup (Case 1 and Case 2). The percentage average absolute relative difference (AARD) between Case 1 and Case 2 are 4.7%, 4.3%, 3.8% at H/D = 0.28, 0.88, 1.7 respectively and was 4.2% for the overall axially averaged velocity

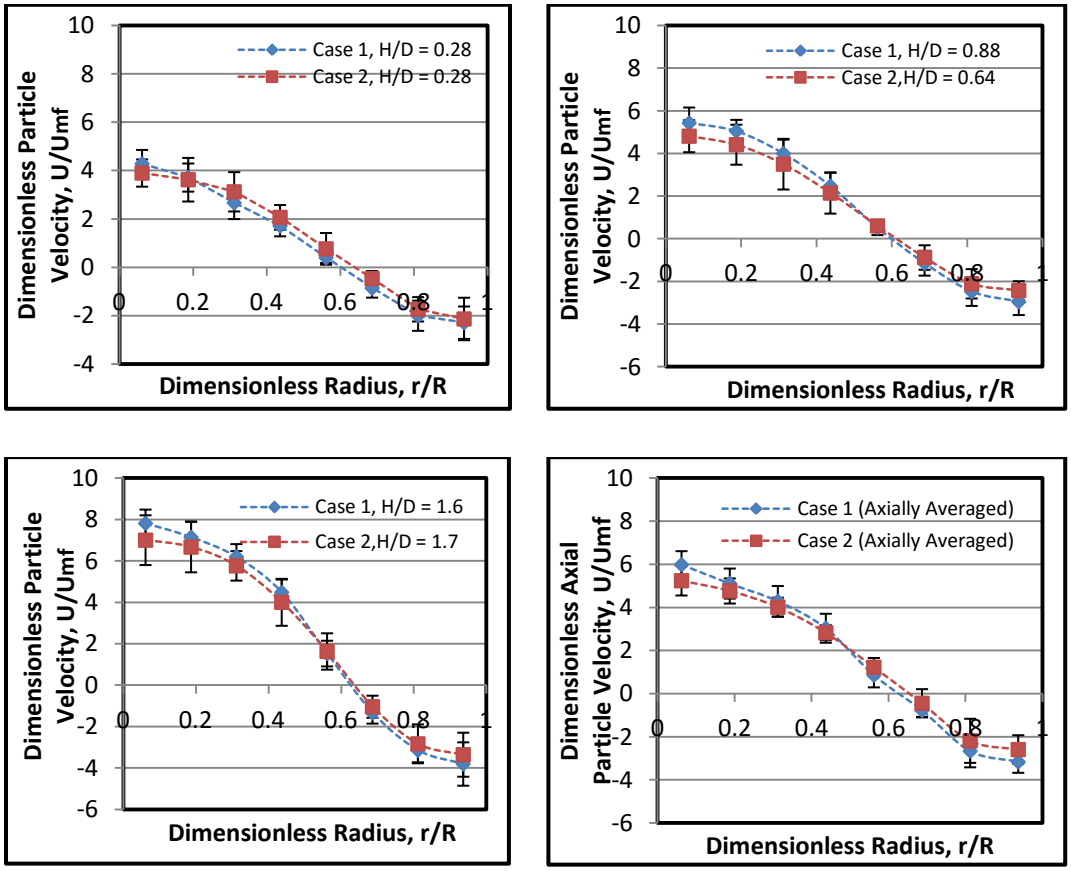

Figure 4.7 Dimensionless time and azimuthally averaged and overall axially averaged particle velocity radial profiles for the similarity conditions (Case 1 and Case 2) (dot lines represent the trend)

Also Figure 4.7 demonstrates that the dimensionless axial particle velocities in upward and downward regions increase with the increase height of the bed due to the causes discussed earlier. Figure 4.8 shows the radial variation of the percentage Absolute Relative Difference (ARD) of the dimensionless axial particle velocity profiles between Case 1 and 2 at different axial positions above the distributor.

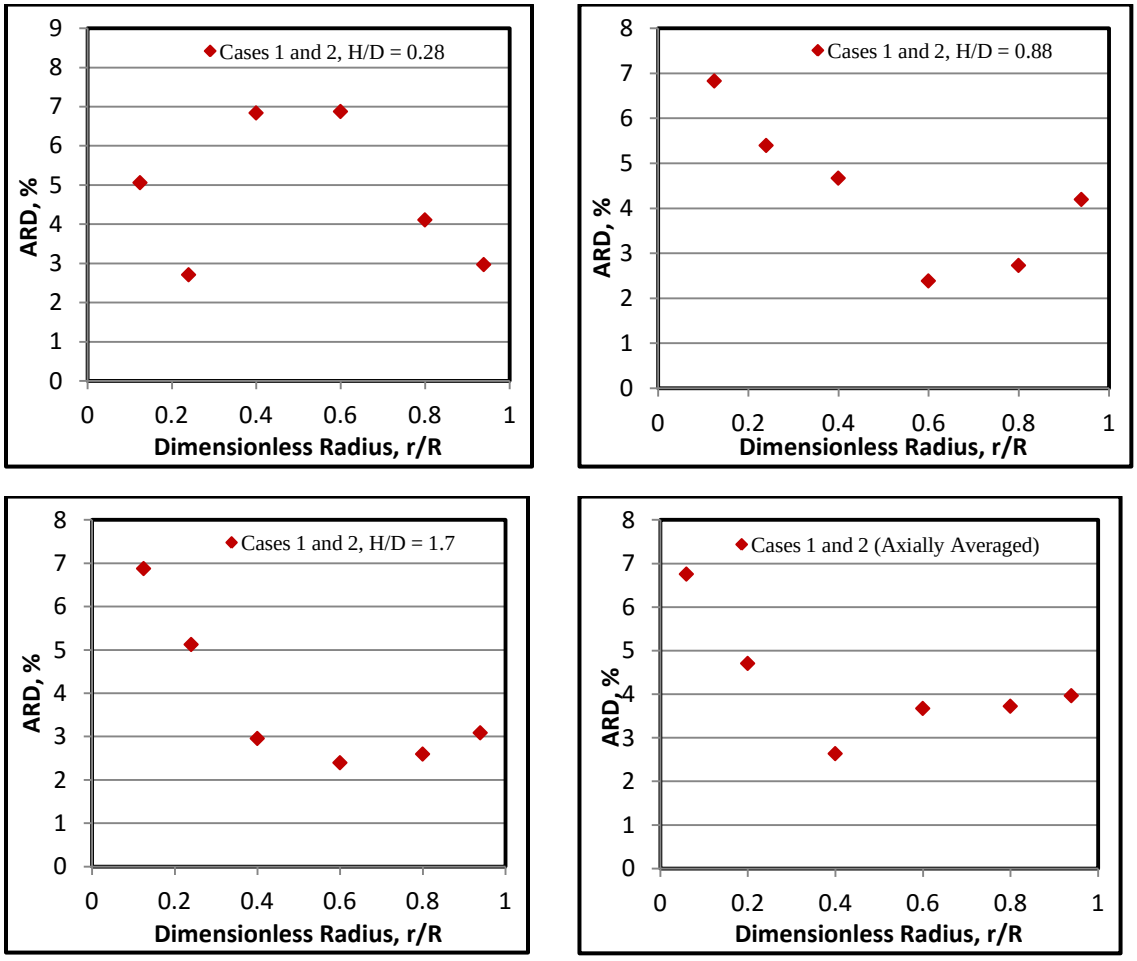

Figure 4.8 The radial variation of ARD in dimensionless axial particle velocity radial profiles between (Case1 and Case 2)

It is obvious that, when the gas holdup radial profiles are close or similar in two different sizes the dimensionless axial particle velocity get closer to each other. This is an important finding for estimating the local axial particle velocities in a larger diameter bed if they are known in a smaller bed and if the minimum fluidization velocities are known. This can be done by matching the values of dimensionless axial particle velocities to the larger column and then by use the minimum fluidization velocity (U_{mf}) the local axial particle velocities can be obtained.

4.1.3.2. Radial particle velocity radial profiles. The time and azimuthally averaged radial particle velocity radial profiles of the conditions of similar radial profiles of gas holdups, Case 1 and Case 2 at three axial levels also investigated in this study. The radial particle velocity radial profiles of the overall axially averaged and at only one axial level above the distributor are depicted in Figure 4.9. The rest of the results represents similar trend. Both the positive and negative values of the radial particle velocity correspond to the outward and inward motion of solids, respectively. Obviously, the time averaged radial velocity of the particles is small compared to the axial particle velocity. In fact, the radial particle velocity is at least an order of magnitude smaller than the axial particle velocity. Therefore, axial particle velocity can be considered the dominant effective velocity field of the bed. The maximum value is less than 2 cm/s as shown in Figure 4.9. This finding is consistent with the previous study of Mostoufi and Chaouki, [29]. The radial particle velocity radial profiles show similar trend. Differences in the magnitude of the radial particle velocity profiles for the conditions of similarity in radial profiles of gas holdup (Case 1 and 2) have been observed. The percentage average absolute relative difference (AARD) is 19.6%, 16.4% at (H/D = 0.88 and 0.64) and for

the overall axially averaged radial particle velocity respectively. The profile trend show maximum range of radial particle velocity within the range of r/R= (0.2 – 0.4) while the velocities is lower in the center and wall regions of the bed. This trend will reflect on the profile of the shear stresses in particular

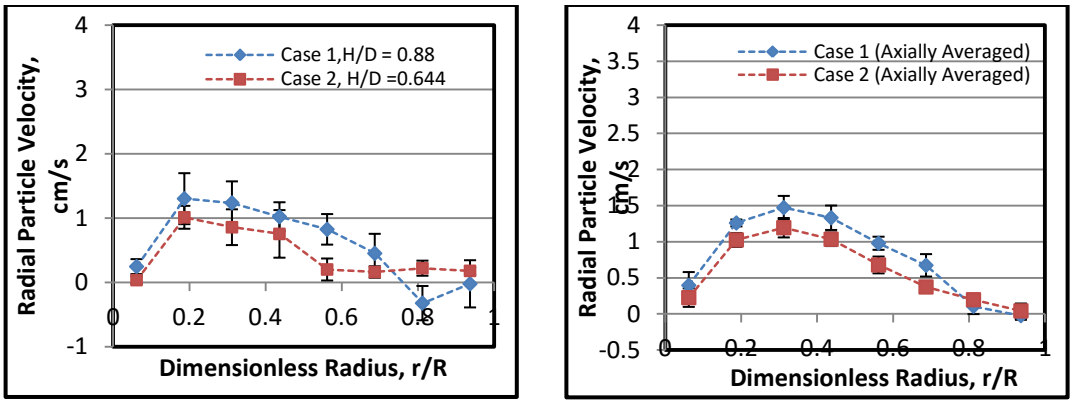

Figure 4.9 Time and azimuthally averaged and overall axially averaged radial particle velocity radial profiles for the similarity conditions (Case 1 and Case 2) (dot lines represent the trend)

Figure 4.10 illustrates the compared dimensionless radial particle velocity radial profiles for the conditions of similar radial profiles of gas holdup (Case 1 and Case 2). The radial profiles showed similar trend and closer to each other. The percentage average absolute relative difference (AARD) is 13.2% at H/D = 0.88 and 0.64 and is 8.2% for overall axially averaged particle velocity respectively. Also the profile of the dimensionless radial particle velocity shows maximum range between r/R = (0.2 – 0.4) and lower magnitude at the center and wall regions.

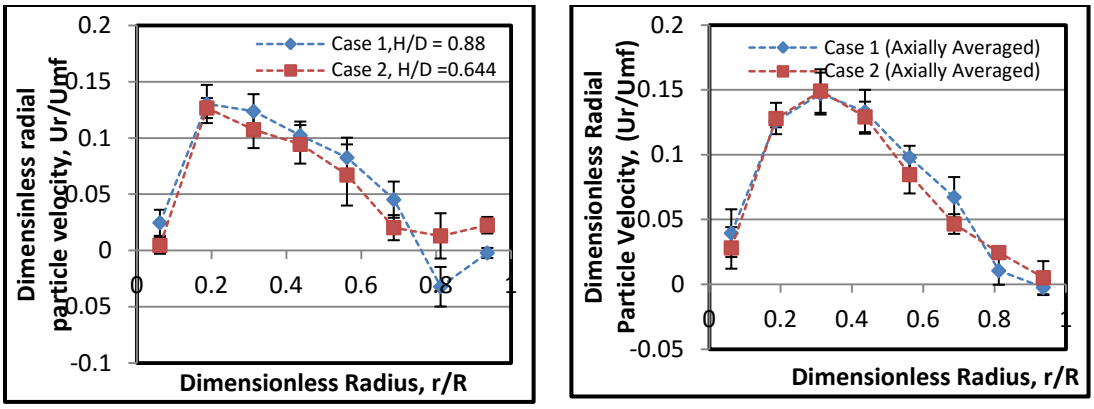

Figure 4.10 Dimensionless time and azimuthally averaged and overall axially averaged radial particle velocity radial profiles for the similarity conditions (Case 1 and Case 2) (dot lines represent the trend)

4.1.3.3. Azimuthal particle velocity radial profiles. Figure 4.11 shows the compared radial profiles of aximuthal particle velocity in both fluidized beds of Case 1 and Case 2. The azimuthal particle velocity radial profiles showed similar trend. The percentage average absolute relative difference (AARD) is 20.3% at H/D = 0.88 and 0.64 and is 9.3% for the overall axially averaged azimuthal particle velocity respectively.

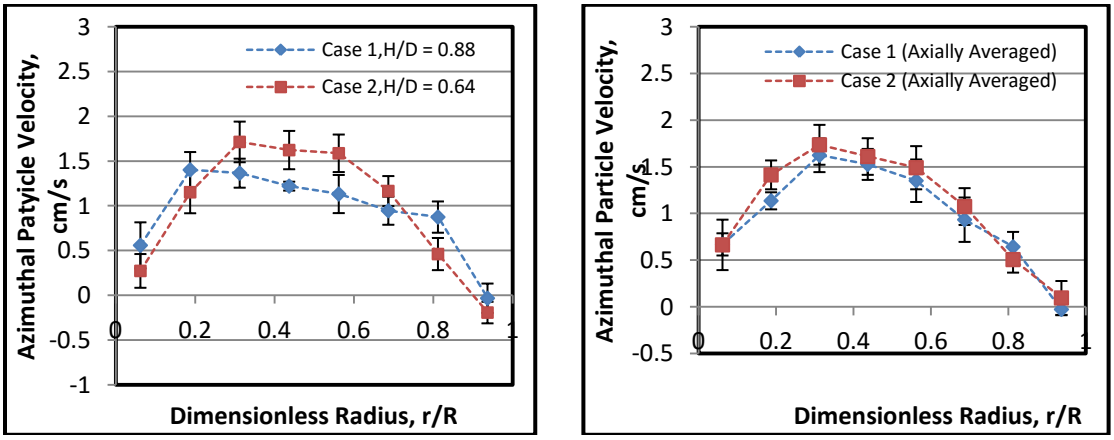

Figure 4.11 Time and azimuthally averaged and overall axially averaged azimuthal particles velocity radial profiles for the similarity conditions (Case 1 and Case 2) (dot lines represent the trend)

Similar findings have been obtained for the dimensionless azimuthal particle velocities and their radial profiles as shown in Figure 4.12. The percentage average absolute relative difference (AARD) is 14.2%, at H/D = 0.88 and 0.64 and is 11.6% for the overall axially averaged respectively.

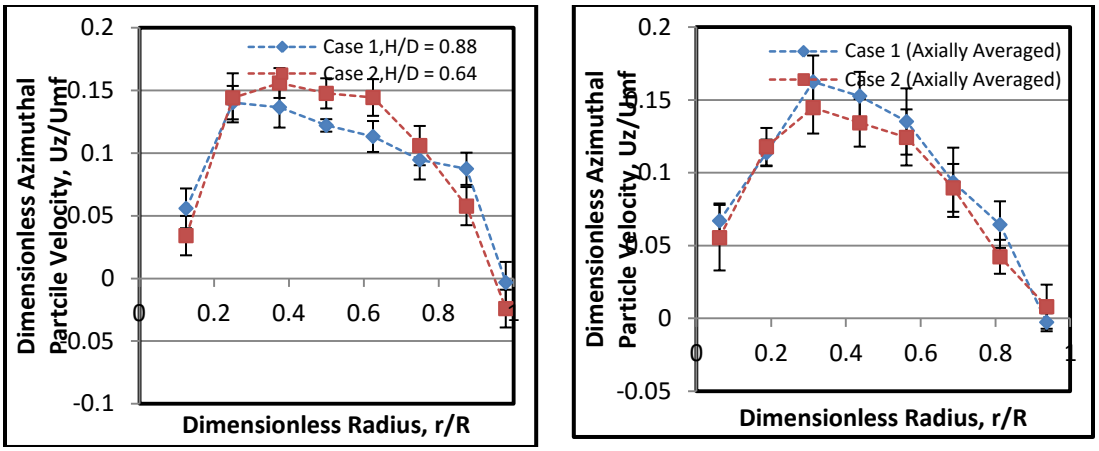

Figure 4.12 Dimensionless time and azimuthally averaged and overall axially averaged azimuthal particles velocity radial profiles for the similarity conditions (Case 1 and Case 2) (Dot lines represent the trend)

4.1.4. Turbulent Parameters. Additional assessment and investigation are required to further validate the new methodology of scale-up for hydrodynamic similarity of fluidized beds. The RPT technique makes it possible to evaluate all the turbulent parameters of the particles. Time averaged solids turbulent parameters (Shear stress, normal stress, turbulent kinetic energy, and eddy diffusivities) are directly calculated from the fluctuation velocities obtained from the difference between the instantaneous and the time averaged particle velocities as pre Table 3.1. In this section the radial profiles of the overall axially averaged and two axial levels above the distributor are presented where the results of the other levels provide same trends.

4.1.4.1. Shear stress radial profiles. Shear stresses are defined in Table 3.1. The time and azimuthally averaged particle shear stress of τ_{rz} for the condition of similar radial profiles of gas holdup, (Case 1 and Case 2) at two axial levels and for overall axially averaged τ_{rz} are compared in Figure 4.13.

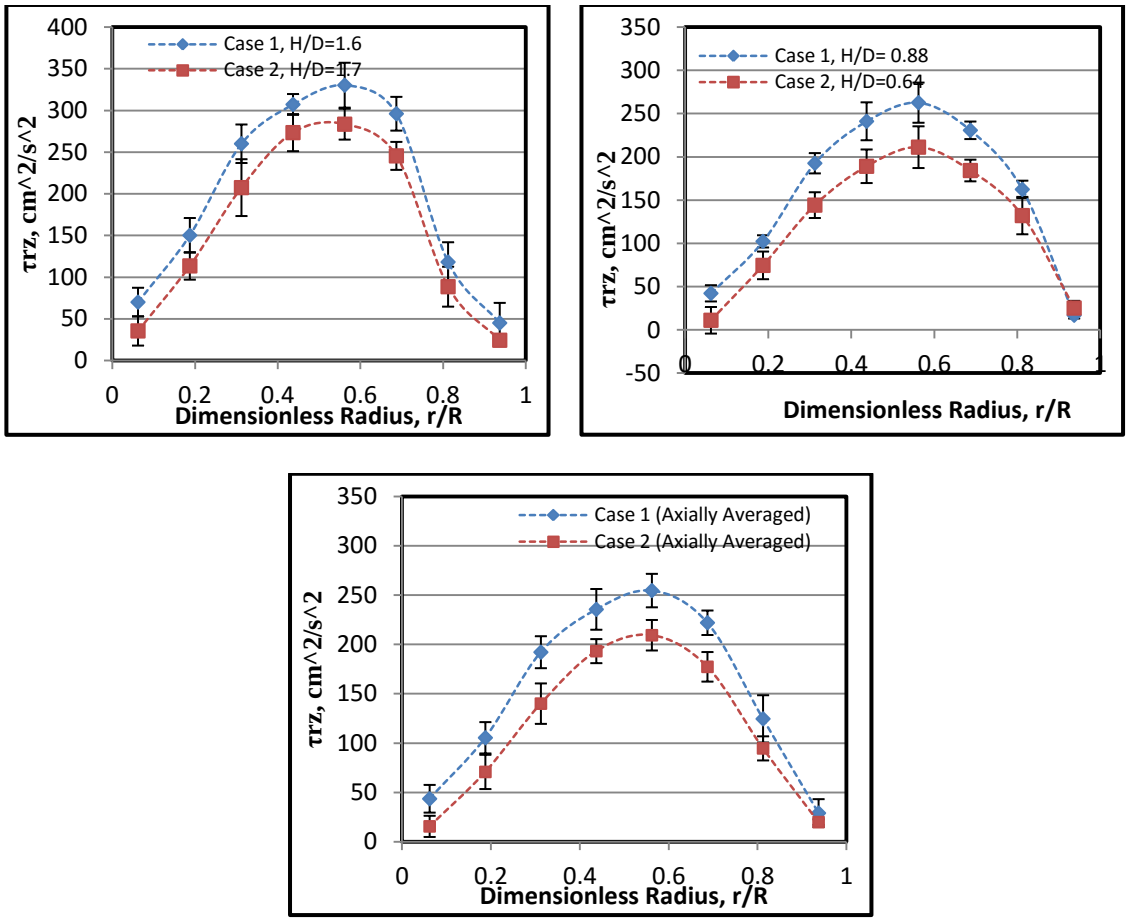

Figure 4.13 Time and azimuthally averaged and overall axially averaged shear stress (τrz) radial profiles for similarity conditions (Case 1 and Case 2) (dot lines represent the trend)

The other components of shear stresses represent the same trend and comparison and hence they are not reported here. The shear stress τ_{rz} profiles showed the same trend for both different sizes but their magnitudes are different, with the maximum values of τ_{rz}

occur within the range of r/R = 0.4 - 0.63 and lower values at the centre and wall regions of the bed. The trend of the τ_{rz} reflects the trend obtained for radial particle velocity (Figure 4.9). It is higher for Case 1 which is consistent with the particle velocity trends. Also Figure 4.13 demonstrates that the shear stress τ_{rz} increases with the increase height of the bed in two different size fluidized beds. The percentage Average Absolute Relative Difference (AARD) is 27.86% at H/D = 1.6 and 1.7, and is 29.2%, at H/D = 0.88 and 0.64 and is 28.7% for the overall axially averaged radial particle τ_{rz} .

The radial profiles of shear stress τ_{rz} in fluidized beds, case 1 and case 2 have been non-dimensionalized by dividing them by the square of the minimum fluidization velocity. Figure 4.14 depicts the compared radial profiles of dimensionless shear stress τ_{rz} for the conditions of similar radial profiles of gas holdup, Case 1 and Case 2. It is clear that the dimensionless shear stress increases with the increase height of the bed in two different size fluidized beds. Also the comparison shows that the profiles get closer to each other except at the maximum region. The percentage average absolute relative difference (AARD) for the radial profiles of dimensionless shear stress τ_{rz} between Case 1 and Case 2 is 14.23% at H/D = 1.6 and 1.7 and is 16.5% at H/D = 0.88 and 0.64 and is 19.5% for the overall axially averaged τ_{rz}.

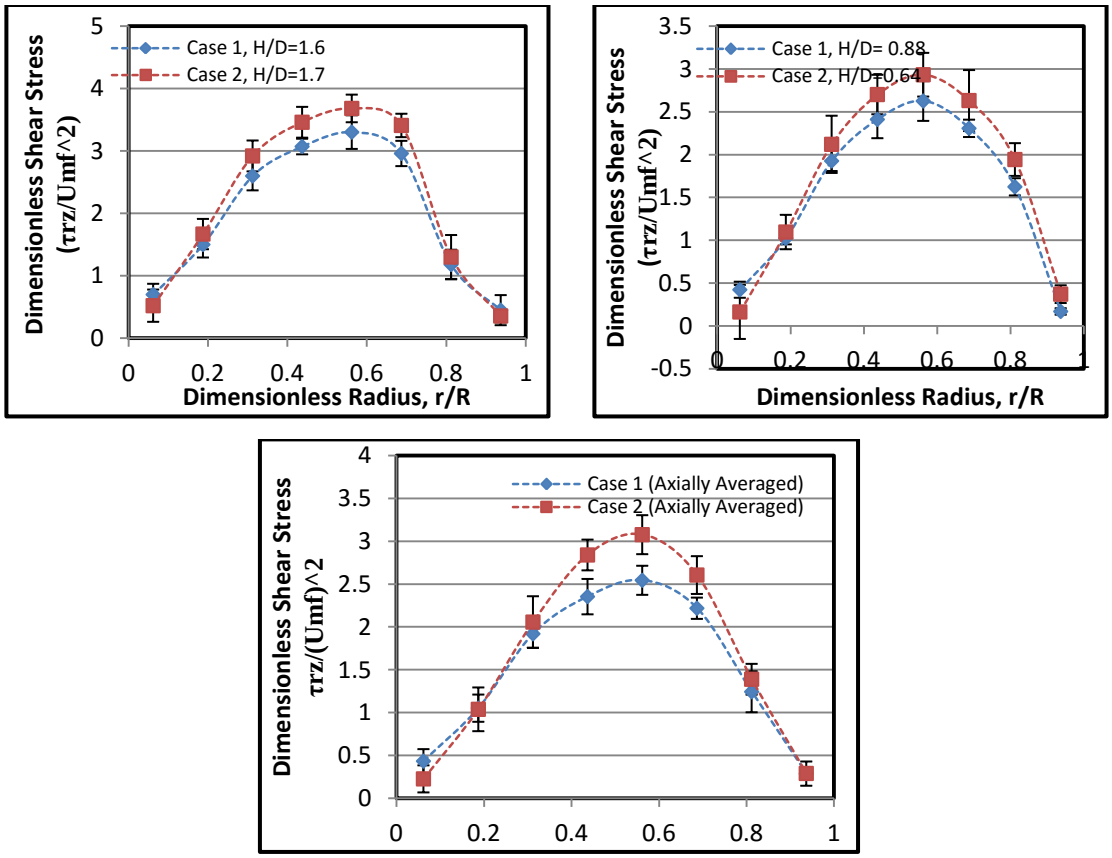

Figure 4.14 Dimensionless time and azimuthally averaged and overall axially averaged shear stress (τrz) radial profiles for similarity conditions (Case 1 and Case 2) (dot lines represent the trend)

4.1.4.2 Axial normal stress radial profiles. The measurements have shown that in both column sizes the axial normal stress is higher than the shear stress. The finding is consistent with the previous study of Moslemian et al. [35]. They measured turbulent parameters in 0.19 m gas-solid fluidized bed by utilizing radioactive particle tracking (RPT) technique. Also the finding agrees with Mostoufi and Chaouki [21, 22]. The axial normal stresses τ_{zz} for the conditions of similar radial profiles of gas holdup Case 1 and Case 2 are compared in Figure 4.15. The other normal stresses (τ_{rr} and $\tau_{\Theta\Theta}$) demonstrate the same trend and hence they are not reported here. Figure 4.15 demonstrates that the axial normal stress τ_{zz} increase with the increase height of the bed in two different size

fluidized beds. The profiles showed the same trend for both cases, with the higher values within the center region of the column and lower values close to the wall. However, the magnitudes of these profiles differ. The percentage Average Absolute Relative Difference (AARD) is 37.4% at H/D = 1.6 and 1.7 and is 33.7% at H/D = 0.88 and 0.64 and is 36.8% for the overall axially averaged τ_{zz}.

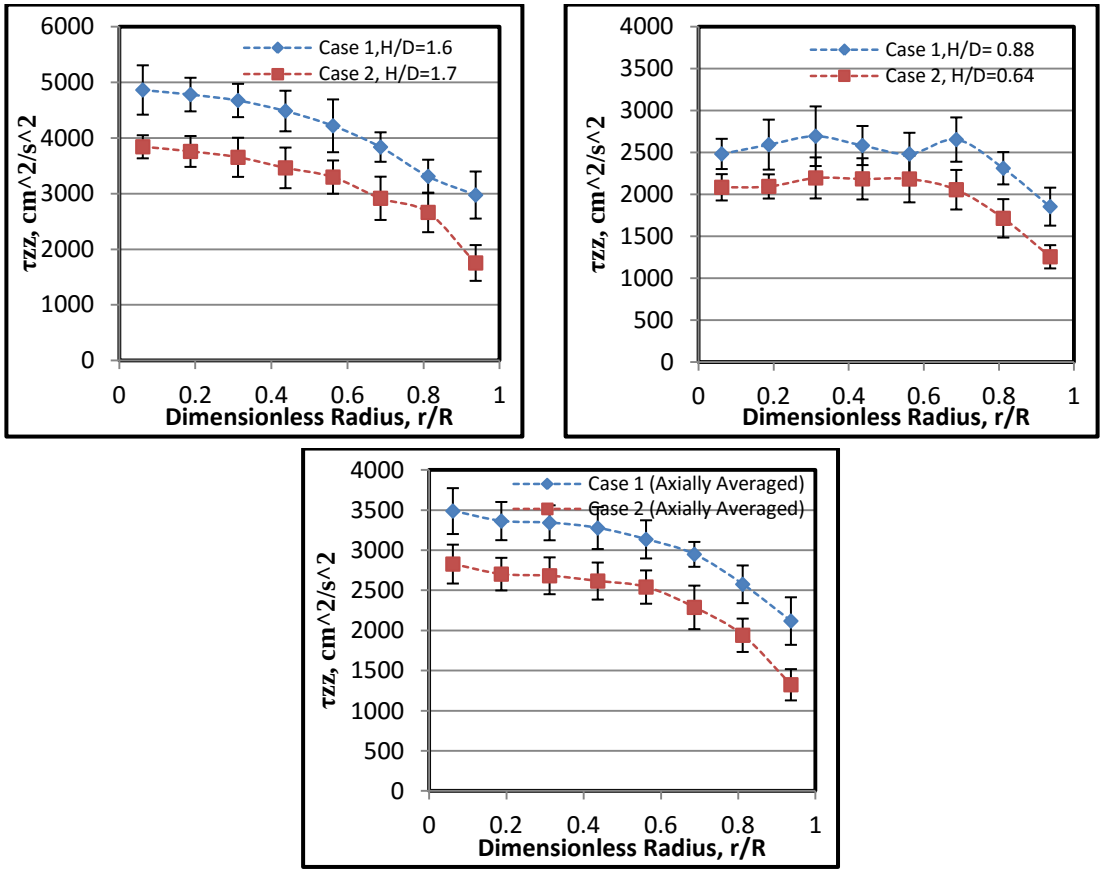

Figure 4.15 Time and azimuthally averaged and overall axially averaged normal stress (τzz) radial profiles for similarity conditions (Case 1 and Case 2) (dot lines represent the trend)

The radial profiles of axial normal stress τ_{zz} in both fluidized beds of case 1 and case 2 are non-dimensionalized by dividing them by square of the minimum fluidization velocity. Figure 4.16 shows the compared radial profiles of dimensionless axial normal

stress τ_{zz} for the condition of similar radial profiles of gas holdup, Case 1 and Case 2. It is clear that the dimensionless axial normal stress increase with the increase height of the bed in two different size fluidized beds. Also the comparison show that the profiles get closer and the percentage average absolute relative difference (AARD) is 18.37% at H/D = 1.6 and 1.7 and is 26.67% at H/D = 0.88 and 0.64 and is 19.34% for the overall axially averaged τ_{zz}.

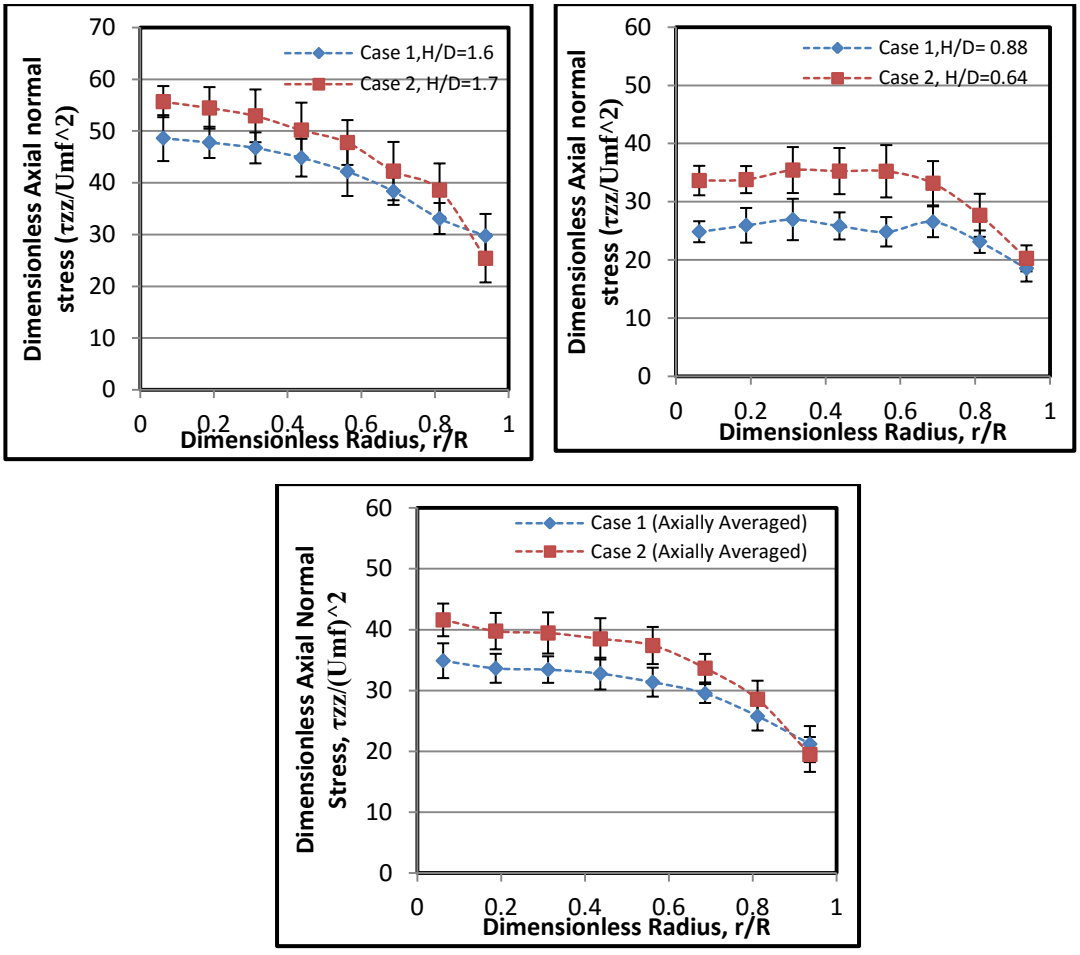

Figure 4.16 Dimensionless time and azimuthally averaged and overall axially averaged normal stress (τzz) radial profiles for similarity conditions (Case 1 and Case 2) (dot lines represent the trend)

4.1.4.3 Turbulent kinetic energy (TKE) radial profiles. The mixing intensity at the conditions of similar radial profiles of gas holdup (Case 1 and Case 2) is expressed in terms of the turbulent kinetic energy (TKE). The time averaged turbulent kinetic energy is directly calculated from the fluctuations of the particle velocity. The turbulent kinetic energy (TKE) is defined $K = \frac{1}{2}(\overline{u'^2_r} + \overline{u'^2_z} + \overline{u'^2_\theta})$ as noted in Table 3.1. Figure 4.17 compares the radial distribution of TKE for the conditions of similar radial profiles of gas holdup, Case 1 and Case 2. The profiles showed the same trend for both cases with higher magnitude in the large column. The trend follows the trend of axial particle velocity where the fluctuations in the axial particle velocity dominate the estimation of turbulent kinetic energy (TKE). Turbulent kinetic energy (TKE) in two sizes is larger in the center region of the column and decrease towards the column wall. Also Figure 4.17 demonstrates that the TKE increases with the increase height of the bed in two different size fluidized beds. Turbulent kinetic energy (TKE) is directly related to the motion of the particles, the gas holdup distribution, and the bubbles velocity and structure. An increase in particle velocity makes the system increasingly more turbulent which is reflected in an increased turbulent kinetic energy. The kinetic energy of glass beads particles is enhanced in large column with an increase in particle velocity. The percentage AARD in TKE between two cases Case1 and Case 2 is found to be 36.4% at H/D = 1.6 and 1.7and is 32.4% at H/D = 0.88 and 0.64 and is 34.3% for the overall axially averaged TKE.

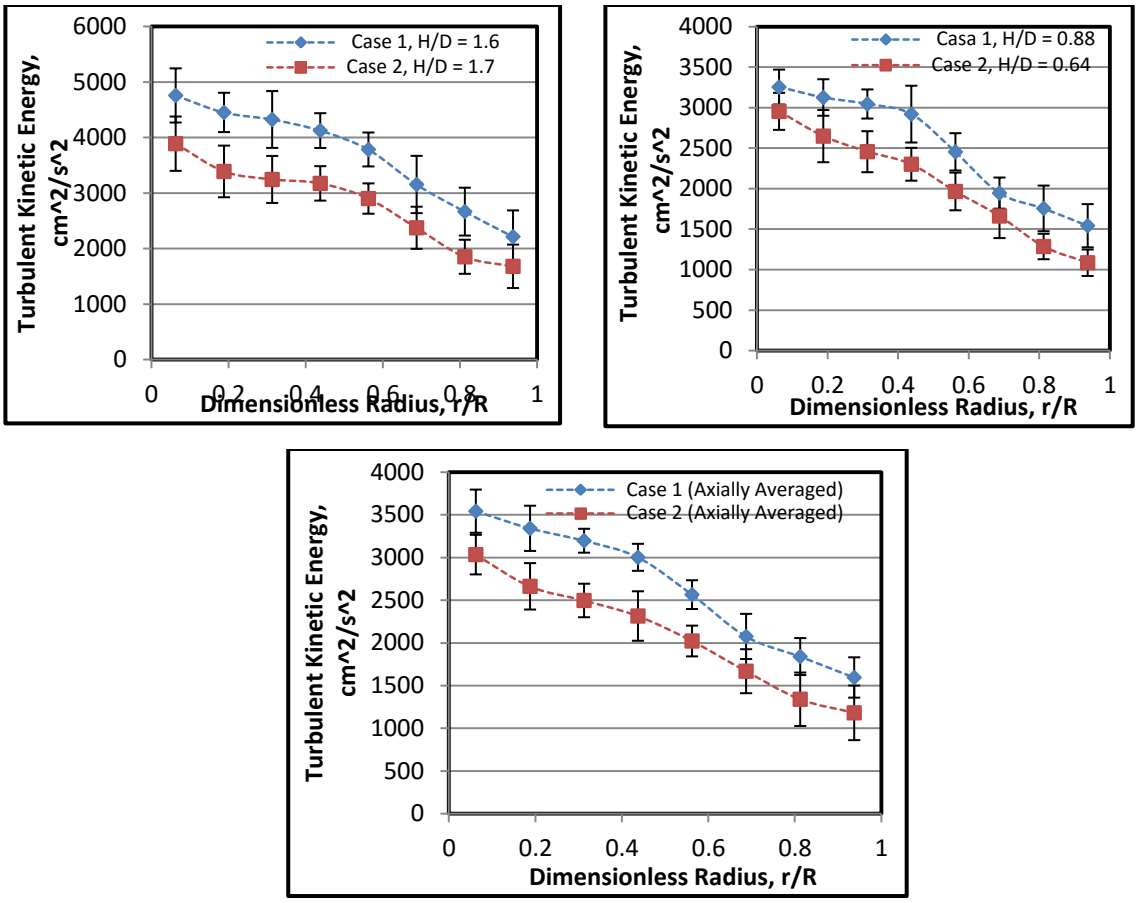

Figure 4.17 Time and azimuthally averaged and overall axially averaged turbulent kinetic energy (TKE) radial profiles for similarity conditions (Case 1 and Case 2) (dot lines represent the trend)

The radial profiles of turbulent kinetic energy in both fluidized beds (Case 1 and Case 2) have been also non-dimensionalized by dividing them by the square of the minimum fluidization velocity. Figure 4.18 shows the comparison of the radial profiles of dimensionless turbulent kinetic energy for the conditions of similar radial profiles of gas holdup, Case 1 and Case 2. Figure 4.18 demonstrates that the dimensionless turbulent kinetic energy increases with the increase height of the bed in two different size fluidized beds. The profiles of Cases 1 and 2 get closer with the percentage average

absolute relative difference (AARD) is 15.7% at H/D = 1.6 and 1.7 and is 28.7% at H/D = 0.88 and 0.64 and is 14.65% for the overall axially averaged TKE

.

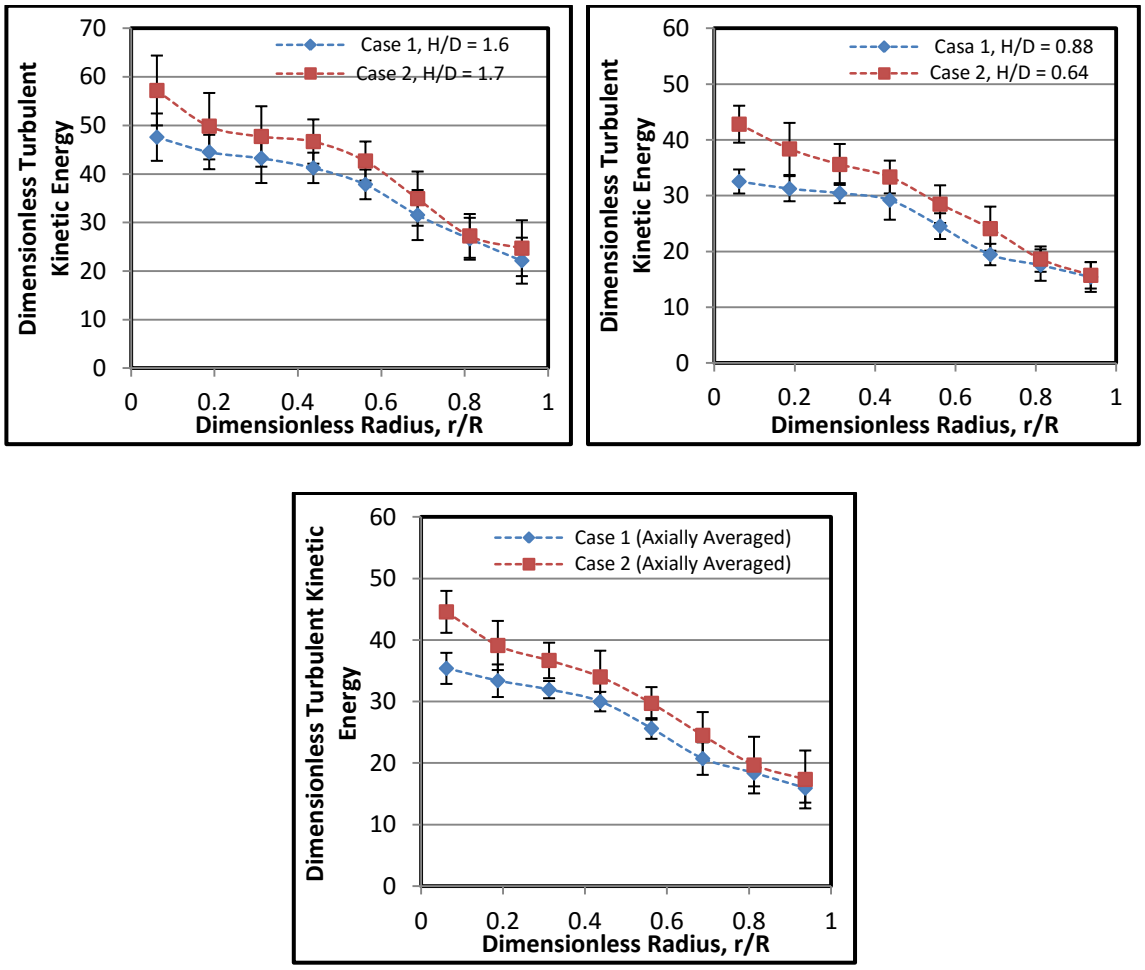

Figure 4.18 Dimensionless Time and azimuthally averaged and overall axially averaged (TKE) radial profiles for similarity conditions (Case 1 and Case 2) (dot lines represent the trend)

4.1.4.4. Axial and radial eddy diffusivities radial profiles. It has been reported and shown that the solids mixing are driven by two principal mechanisms: 1) convective mixing due to the gross circulation of solids, and 2) dispersive mixing due to solids turbulent motion (Mostoufi and Chaouki [21, 22]. The former mechanism controls the global solids mixing in the gas-solid fluidized bed and the latter mechanism dictates the

local solids mixing (Mostoufi and Chaouki, [21]). Axial and radial diffusivities are reflected by the solid mixing and diffusion of particles in the bed. As a result, high mass and heat transfer rate are achieved by rapid mixing of solids and solids diffusion. In this work we measured the axial and radial diffusivities of particles for two different fluidized beds using radioactive particle tracking (RPT) technique. The measured fluctuation velocities and the formulas reported by Efhaima and Al-Dahhan, [13]; Roy [25]; Upadhyay, [26] and listed in Table 2 were used to estimate the axial and radial diffusivities. Bubbles and voids structures are the keys for solids circulation in the fluidized beds. Shape, size and frequency of the bubbles influence the diffusivity of the solids, Hamed et al, [30].

Since the bubbles/voids are larger within the center region of the bed as compared to that in the region near the wall as shown by CT results (Figure 4.4) (Tebianian et al .[20]) and the particles velocity is also larger in the centre region of the bed as compared to that in the region near the wall. The values of the turbulent eddy diffusivity are expected to follow the same trend particle velocity. An increase in the superficial gas velocity increases the bubble velocity and bubble frequency. Therefore, both axial and radial diffusivities are increased accordingly. In addition, diffusivities in both directions are higher in the large column. This is consistent with the data reported by Mostoufi and Chaouki [21]. Both axial and radial eddy diffusivities as a function of the radial position for the conditions of similar radial profiles of gas holdup (Case 1 and Case 2) have been measured and presented in Figures 4.19 and 4.20. It is seen that diffusivities in both directions and in both sizes columns are higher in the large column finding consistent with previous studies (Hamed et al. [30]; Mostoufi and Chaouki, [21]). It could be

attributed to a higher turbulent and bubbles velocity at large column. Also Figures 4.19 and 4.20 demonstrate that the diffusivities in both directions increase with the increase height of the bed in two different size fluidized beds. The radial diffusivity is an order of magnitude smaller than that of the axial diffusivity. The percentage average absolute relative difference (AARD) for the radial profiles of axial eddy diffusivity between the two fluidized beds (Case 1 and 2), is 38.2% at H/D = 1.6 and 1.7 and is 32.7% at H/D = 0.88 and 0.64 and is 28.65% for the overall axially averaged D_{zz}.

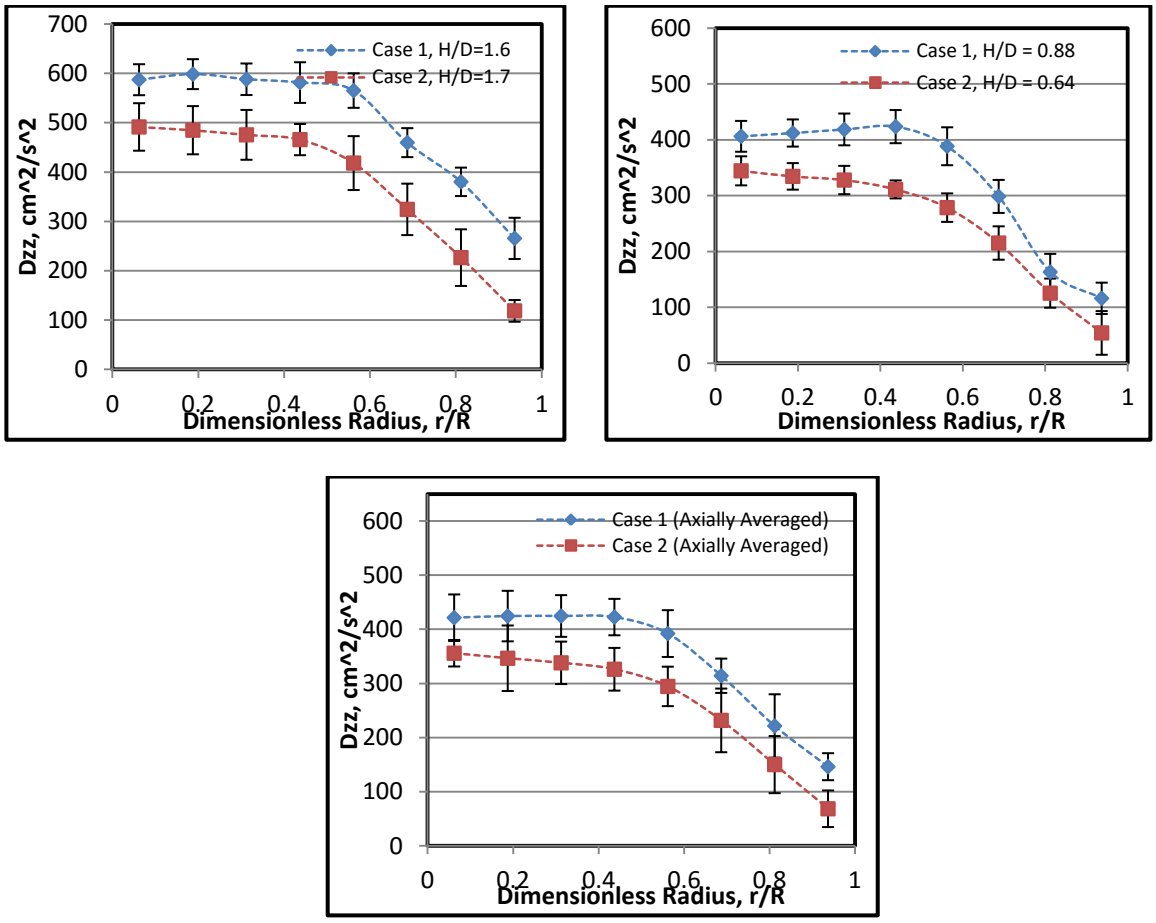

Figure 4.19 Time and azimuthally averaged and overall axially averaged axial eddy diffusivity radial profiles for similarity conditions (Case 1 and Case 2) (dot lines represent the trend)

The percentage average absolute relative difference (AARD) for the radial profiles of radial eddy diffusivity, for the conditions of similar radial profiles of gas holdup, Case 1 and Case 2 as shown in Figure 4.20 is 37.3% at H/D = 1.6 and 1.7 and is 42.3% at H/D = 0.88 and 0.64 and is 39.8% for the overall axially averaged Drr.

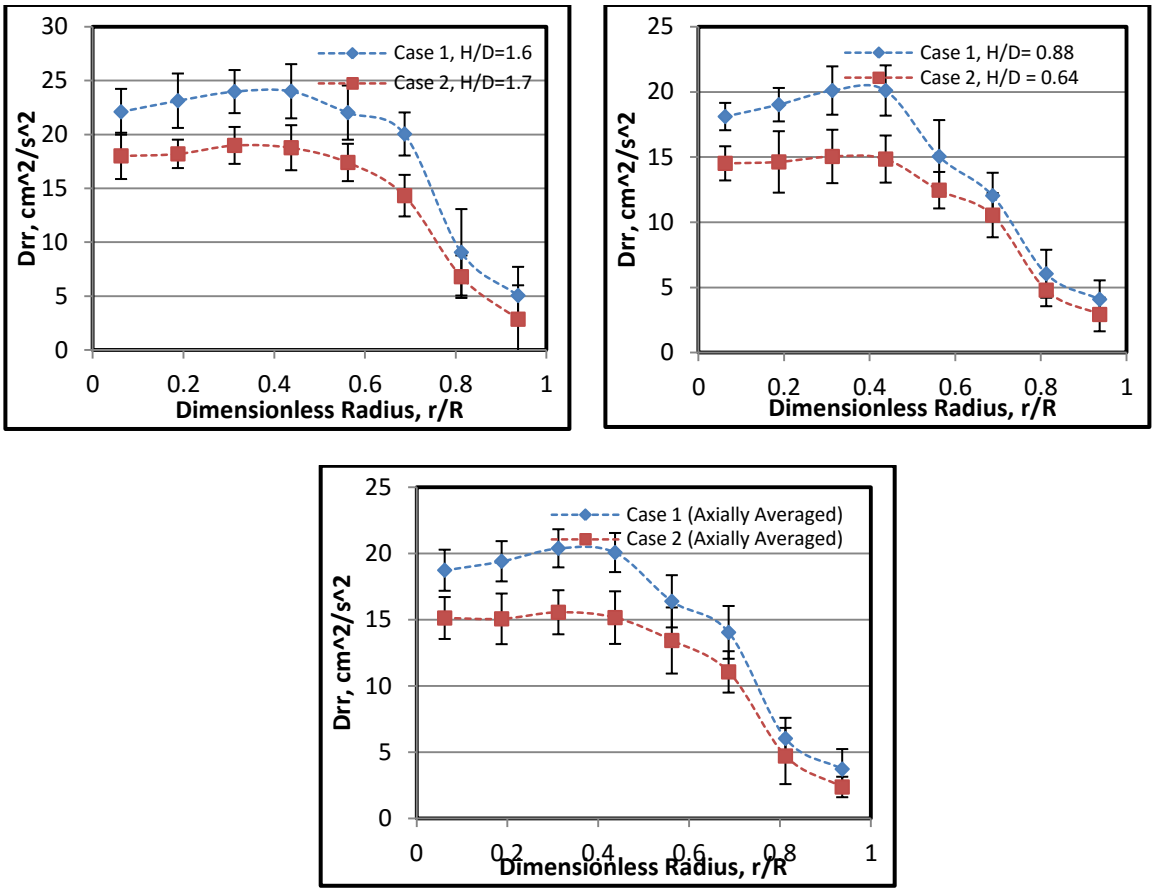

Figure 4.20 Time and azimuthally averaged and overall axially averaged radial eddy diffusivity radial profiles for similarity conditions (Case 1 and Case 2) (dot lines represent the trend)

The radial profiles of axial and radial diffusivity for the conditions of similar radial profiles of gas holdup, Case 1 and Case 2 have been also non-dimensionalized by dividing them by the square of the minimum fluidization velocity. Figure 4.21 shows the compared radial profiles of the dimensionless axial eddy diffusivity, while Figure 4.22

presents the compared radial profiles of the dimensionless radial eddy diffusivity for the conditions of similar radial profiles of gas holdup, Case 1 and Case 2. Figures 4.21 and 4.22 demonstrate that the dimensionless eddy diffusivities in both directions increase with the increase height of the bed in two different size fluidized beds. It is obvious that the profiles get closer as depicted by the reduction in the AARD.

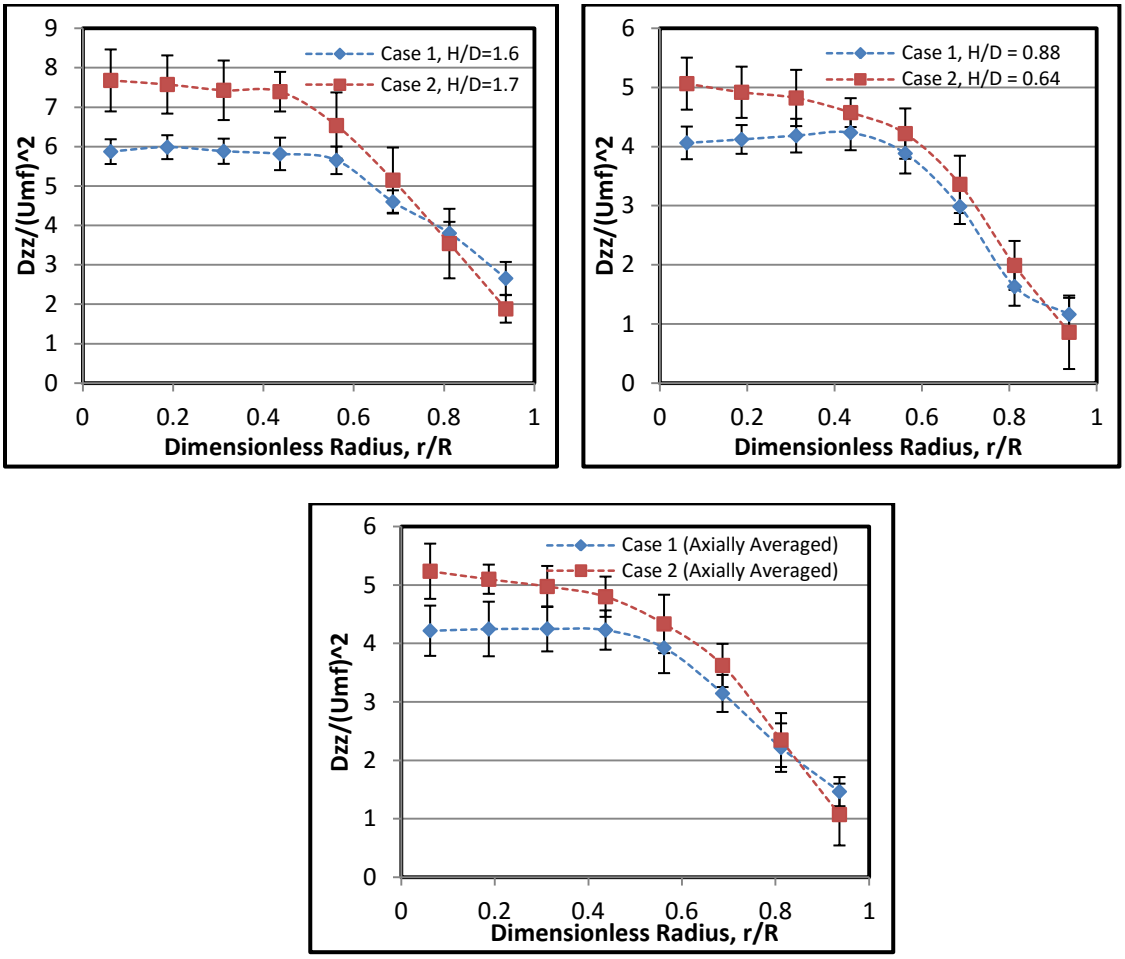

Figure 4.21 Dimensionless time and azimuthally averaged and overall axially averaged axial eddy diffusivity radial profiles for similarity conditions (Case 1 and Case 2) (dot lines represent the trend)

The percentage average absolute relative difference (AARD) for the radial profiles of dimensionless axial eddy diffusivity for the conditions of similar radial

profiles of gas holdup, Case 1 and Case 2 is 22.6% at H/D = 1.6 and 1.7 and is 18.8% at H/D = 0.88 and 0.64 and is 20.7% for the overall axially averaged one. For the dimensionless radial eddy diffusivity the percentage average absolute relative difference (AARD) between two scaled fluidized beds, Case 1 and Case 2 is 20.3% at H/D = 1.6 and 1.7 and is 17.6% at H/D = 0.88 and 0.64 and is 18.4% for the overall axially averaged ones.

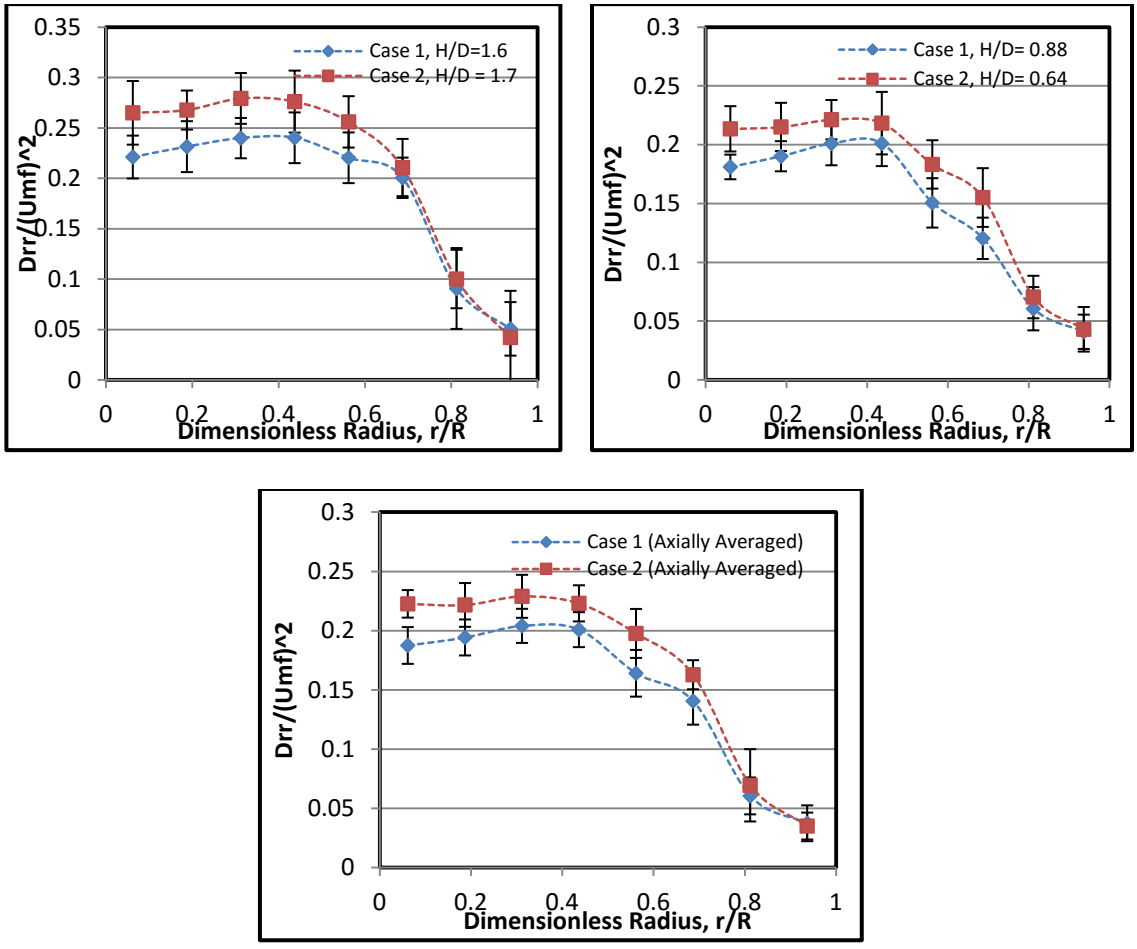

Figure 4.22 Dimensionless time and azimuthally averaged and overall axially averaged radial eddy diffusivity radial profiles for similarity conditions (Case 1 and Case 2) (dot lines represent the trend)

4.2. CONDITIONS FOR NON-SIMILARITY IN RADIAL PROFILES OF GAS HOLDUP.

The focus is to show that if the difference in radial profiles of gas holdup increases, the differences in velocities and turbulent parameters also increase relatively to the magnitude of the difference. Time averaged gas holdup radial profiles for the conditions of non-similar radial profiles of gas holdup Case 1 and Case 3 as outlined in Table 2.1, have been measured by using gamma ray computed tomography (CT) technique at different H/D ratios. Figure 4.23 shows the comparison of the time average gas holdup radial profiles at different axial levels.

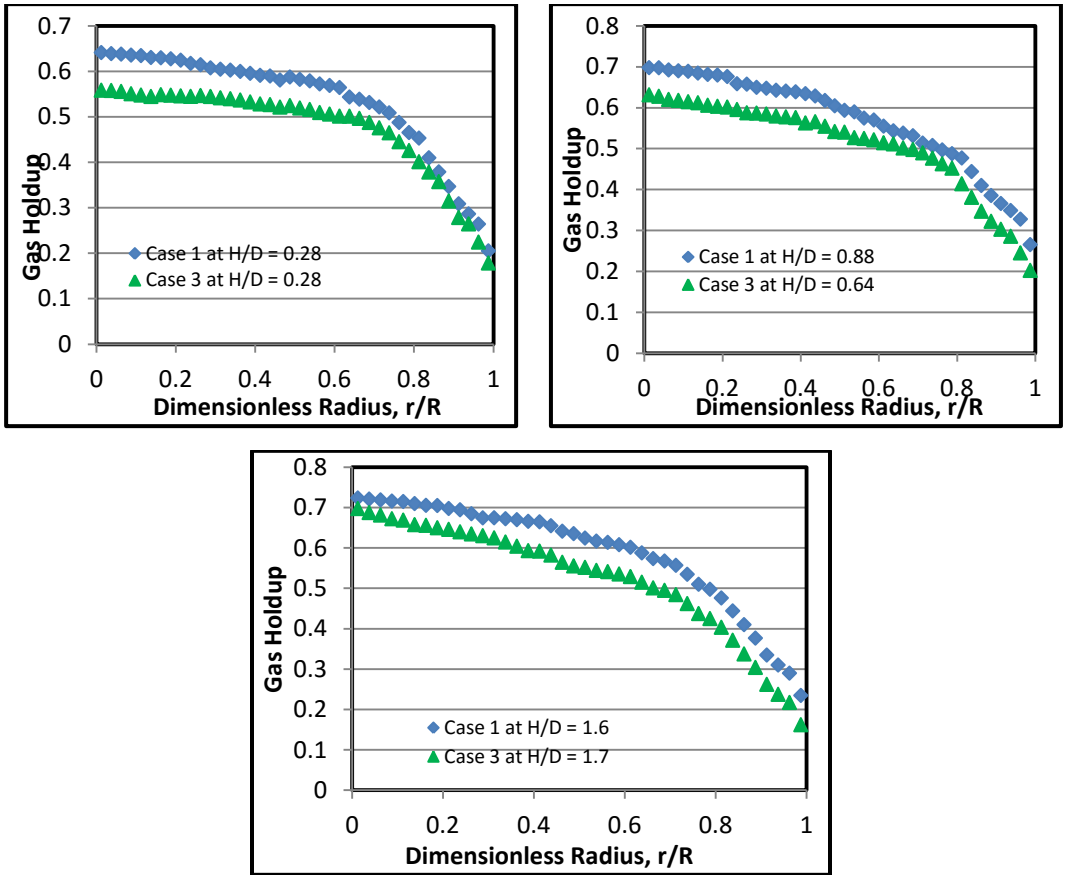

Figure 4.23 Time averaged gas holdups radial profiles as function of radial position at different dimensionless axial levels above the distributor for Case (1) and Case (3) measured by (CT) technique

The percentage Average Absolute Relative Difference (AARD) was 12.8%, 14%, and 13%, at H/D equal to 0.28, 0.64, and 1.7 respectively.

The time and azimuthally averaged and the overall axially averaged the particles velocities (axial, radial, and azimuthal) radial profiles at different H/D measurement levels for the condition of non-similar radial profiles of gas holdup, Case 1 and Case 3 have been measured by using radioactive particle tracking (RPT) technique. Figure 4.24 shows only the radial profiles of particle velocities for the overall axially averaged. The particle velocities (axial, radial, and azimuthal) at different levels have been reported in Efhaim and Al-Dahhan [13].

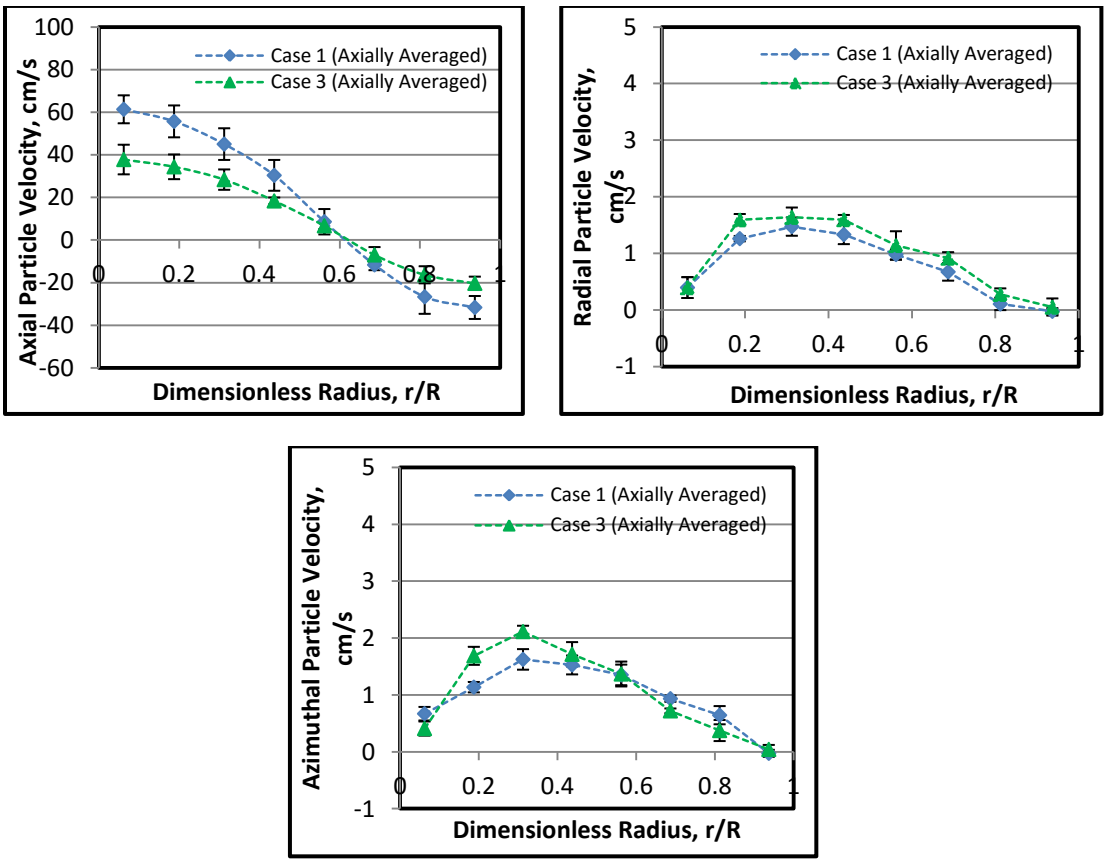

Figure 4.24 The overall axially averaged particle velocity radial profiles for the non-similarity conditions (Case 1 and Case 3) (dot lines represent the trend)

It is found that the velocity profiles in the two beds are different. The percentage average absolute relative difference (AARD) between Case 1 and Case 3 is 20.3% in axial particle velocity, 15.3% in radial particle velocity, and 17.5% in azimuthal particle velocity as shown in Figure 4.24.

In this work also the particle turbulent parameters for the conditions of non-similar radial profiles of gas holdup, Case 1 and Case 3 have been compared only for the overall axially averaged as shown in Figure 4.25. The percentage Average Absolute Relative Difference (AARD) is 42.3% in shear stress τ_{rz} and is 48.2% in axial normal stress τ_{zz}, and 45.4% in TKE, and is 38.5% in axial eddy diffusivity Dzz, and is 47.85% in radial eddy diffusivity Drr

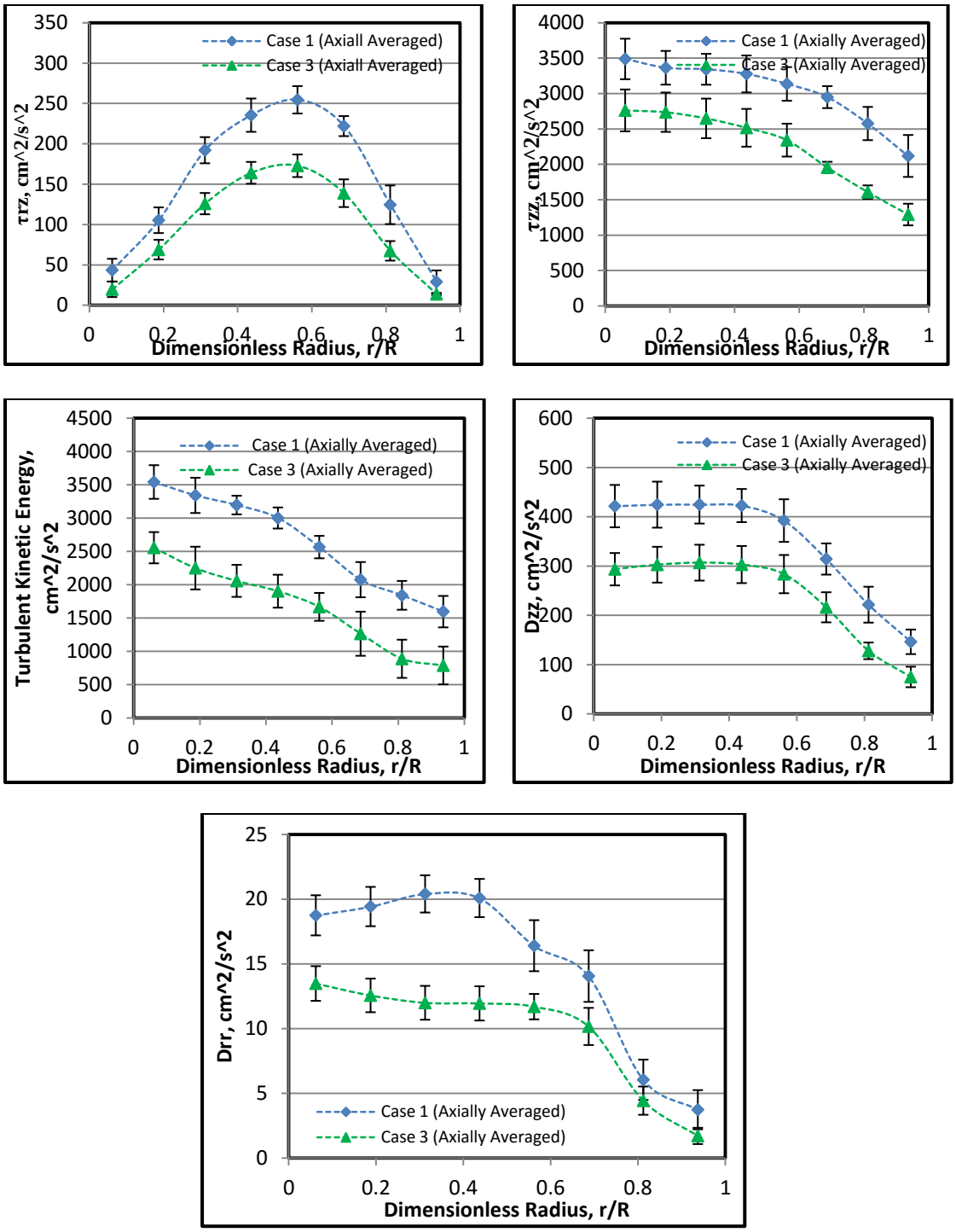

Figure 4.25 The overall axially averaged turbulent parameters radial profiles for the non-similarity conditions (Case 1 and Case 3) (dot lines represent the trend)

5. REMARKS

In this work we have successfully validated the new mechanistic scale-up methodology for hydrodynamics similarity of gas-solid fluidized beds which has been proposed in our Multiphase Reactors Engineering and Applications Laboratory (mReal) by assessing for the first time the local hydrodynamic parameters. Two fluidized bed with diameters of 0.44 and 0.14 m were employed. Advanced non-invasive measurement techniques of gamma ray computed tomography technique (CT) and radioactive particle tracking (RPT) were utilized in this work. The experimental results showed that achieving similarity in the radial profiles of the gas holdup in the geometrically similar beds is essential for ensuring closer or similar hydrodynamics similarity. In addition as the differences increase in the gas holdup radial profiles between two beds, the differences increase in the detailed local and global hydrodynamic similarities. As the bed height increases gas holdup increase due to the growth of gas bubbles with the bed height. This yield increase in the particle velocities and hence in the turbulent parameters with the bed height, with the increase in superficial gas velocity, the magnitude of the hydrodynamic parameters increases. This finding confirms that the dynamics of the gas phase dictate the hydrodynamics of the bed. It is noteworthy that the obtained data in this work are valuable for benchmarking computational fluid dynamics (CFD) simulations and closure. The particle velocities and turbulent parameters at different levels have been reported in Efhaim and Al-Dahhan [13]

ACKNOWLEDGMENT

The authors wish to acknowledge the Libyan Ministry of Education for sponsoring the primary author's study within the Chemical and Biochemical Engineering Department at Missouri University of Science and Technology. Also the primary author would like to acknowledge the use of the gamma ray, radioactive particle tracking techniques, experimental facilities set-up and materials that were used in this work and funded by professor Al-Dahhan's research fund.

REFERENCES

[1] Glicksman, L. R., Hyre, M. and Woloshun, K. Simplified Scaling Relationships for Fluidized Beds. Powder Technology,77, pp. 177-199, 1993

[2] Glicksman, L. R., Scaling Relationships for Fluidized Beds. Chemical Engineering Science, 39, 1373-1379 (1984)

[3] Glicksman, L. R., Scaling Relationships for Fluidised Beds. Chemical Engineering Science, 43, 1419-1421 (1988)

[4] Foscolo, P.U., Di Felice, R., Gibilaro, L.G., Piston, L., Piccolo.V. 1990. Scaling relationships for fluidization: The generalized particle bed model. Chemical Engineering Science, 45, pp. 1647-1651, 1990

[5] Horio, M., Nonaka, A., Sawa, Y., & Muchi, I. (1986). A New Similarity Rule for Fluidized Bed Scale-up. AIChE Journal, 32, 1466–1482.

[6] Stein M., Y.L. Ding, J.P.K. Seville, , Experimental verification of the scaling relationships for bubbling gas-fluidized beds using the PEPT technique, Chemical Engineering Science 57 (2002) 3649–3658.

[7] Knowlton, T.M., Karri, S.B.R., Issangya, A., Scale Up of Fluidized-Bed Hydrodynamics. Powder Technology, Vol. 150, No. 2, 72-77 (2005)

[8] Rüdisüli, R., Tilman, J. Schildhauer, Serge M.A. Biollaz J. Ruud van Ommen. Scale-up of bubbling fluidized bed reactors - A review. Powder Technology , 217, pp. 21-38, 2012

[9] Van Ommen JR, Teuling M, Nijenhuis J, Van Wachem BGM., Computational Validation of the Scaling Rules for Fluidized Beds. Powder Technology. 163(1-2):32-40 (2006)

[10] Sanderson. J, Rhodes. M.J, Wand.X.S, Lim.K.S, in:12 th Int.Conf. on Fluidization, 2007.

[11] Al-Dahhan, M.H., Shreekanta, A., Faraj, Z., Neven, A., Thaar, A. 2014. Scale-up and on-line monitoring of gas-solid system using advanced and non-invasive measurement techniques, Symphos 2013, 2nd International Symposium on Innovation and Technology in the Phosphate Industry, 2014.

[12] F. Zaid, gas-solid fluidized bed reactors: scale-up, flow regimes identification and hydrodynamics, PhD, thesis, Missouri University of Science & Technology, Rolla, 2013.

[13] Efhaima. A., H. Al-Dahhan, Assessment of Scale-up Dimensionless Groups Methodology of Gas-Solid Fluidized beds using Advanced Non-Invasive Measurement Technique (CT and RPT)

[14] Varma R. Characterization of anaerobic bioreactors for bioenergy generation using a novel tomography technique. Thesis, PhD, Washington University in St. Louis, Saint Louis, Mo, USA. 2008.

[15] Varma R, Bhusarapu S, O'Sullivan, JA, Al-Dahhan, M.H. A comparison of alternating minimization and expectation maximization algorithms for single source gamma ray tomography. Measurement Science & Technology, Vol 19(1), pp. 1-13, 2007

[16] Varma R, Bhusarapu S, O'Sullivan JA, Al-Dahhan MH. A comparison of alternating minimization and expectation maximization algorithms for single source gamma ray tomography. Measurement Science & Technology, Vol 19(1):015506, 14pp, 2008.

[17] Bhusarapu, SB. Solids flow mapping in gas-solids risers. D.Sc. Thesis. Department of Chemical Engineering, Washington University, St. Louis, 2005

[18] Bhusarapu S, Al-Dahhan MH, Dudukovic MP. Solids Flow Mapping in a Gas-Solid Riser: Mean Holdup and Velocity Fields. Powder Technology, Vol 163, (1-2), pp. 98-123 (2006)

[19] A. Fadha. Experimental Investigation of The Pebble Bed Structure By Using Gamma Ray Tomography, master thesis, Missouri University of Science & Technology, Rolla, 2014

[20] Tebianian S., Dubrawski K., Ellis N., Cocco R., D.J. Parker., Chaouki J., Investigation of particle velocity in FCC gas-fluidized beds based on different measurement techniques, Chemical Engineering Science 127(2015) 310–322

[21] Mostoufi, N., Chaouki, J. Local solid mixing in gas–solid fluidized beds, Powder Technology 114, pp. 23–31, 2001

[22] Mosfoufi N., Chaouki J. Flow Structure of Solids in Gas-Solid Fluidized Bed, Chemical Engineering Science. 59, pp. 4217, 2004

[23] Degaleesan, S. 1997. Turbulence and liquid mixing in bubble columns. Thesis, PhD, Washington University, Saint Louis, Missouri, USA, 1997

[24] Degaleesan, S., Dudukovic, MP, Pan, Y. Application of wavelet filtering to the radioactive particle tracking technique. Flow Measurement and Instrumentation, 13(1-2), PP. 31- 43, 2002.

[25] Roy, S. Quantification of Two-phase Flow in Liquid-solid Risers, PhD, Thesis,PhD, Washington University in St. Louis, Saint Louis, MO, USA, 2000

[26] Upadhyay, R., Roy. S. Investigation of hydrodynamics of binary fluidized beds via radioactive particle tracking and dual-source densitometry, The Canadian journal of chemical Eng. Vol. 88, 2010

[27] Efhaima. A., H. Al-Dahhan, Local time-averaged gas holdup in fluidized bed reactor using gamma ray computed tomography technique (CT), Int J Ind Chem (2015) Volum.6:143-152

[28] Efhaima. A., H. Al-Dahhan, Bed diameter effect on the hydrodynamics of Gas-Solid Fluidized Bed via Radioactive Particle Tracking (RPT) Technique

[29] N. Mosfoufi and J. Chaouki, on The Axial Movement of Solids in Gas-Solid Fluidized Beds. I ChemE, Vol 78, Part A, (2000)

[30] Bashiri H., Ramin R., Rahmat S., Chaouki J., Effect of Bed Diameter on the Hydrodynamics of Gas-solid Fludized beds, Iran. J. Chem.Eng. Vol.29, No.3 (2010)

[31] Verma. V,Padding. J.T, Deen.N.G, Kuipers. J.A.M, Barthel. F, Bieberle. M. Bubble dynamics in a 3-D gas-solid fluidized bed using ultrafast electron beam X-ray tomography and two-fluid model. AICHE Journal, V.60. pp, 1632:1644

[32] Bangyou W., Guang Yu., Bellehumeur C., Kantzas A., Dynamic flow behavior measurements in gas-solid fluidized beds using different non-intrusive techniques and polyethylene powder. Flow measurement and instrumentation, 18 pp. 197-203 (2007)

[33] Wang, Q., Zhnag, K., Yang, K., Jiang, J. Particle velocity in a Dense Gas-Solid Fluidized Bed. Inter. J. of Chemical Reactor Eng, 2008.

[34] Laverman, J.A ., Fan, X., Ingram, A., van Sint Annaland, M, Parker DJ, Seville, J.P.K, Kuipers, J.A.M. Expermental study on the influence of bed material on the scaling of solids circulation patterns in 3D bubbling gas-solid fluidized beds of glass and polyethylene using positron emission particle tracking . Power Technol, 224, pp. 297-305, 2012

[35] D. Moslemian, M.M. Chen, B.T. Chao, Experimental and numerical investigation of solids mixing in a gas fluidized bed, Part. Sci. Technol. 7 (1989) 335-355.

II. ASSESSMENT OF SCALE-UP DIMENSIONLESS GROUPS METHODOLOGY OF GAS-SOLID FLUIDIZED BEDS USING ADVANCED NON-INVASIVE MEASUREMENT TECHNIQUES (CT AND RPT)

Abdelsalam Efhaima and Muthanna H. Al Dahhan

Department of Chemical and Biochemical Engineering, Missouri University of Science and Technology, 1101 North State Street. 110 Bertelsmeyer Hall, Rolla, MO 65409,USA, ayed67@mst.edu

ABSTRACT

In this work we assessed the literature reported scale-up methodology based on matching dimensionless groups by measuring the local hydrodynamic parameters using non-invasive gamma ray computed tomography (CT) and radioactive particle tracking (RPT) techniques. Two scales of fluidized beds with diameters of 0.14 and 0.44 m were employed using sets of operating conditions that fulfilled the matching and not matching dimensionless groups proposed by Glicksman et al. [1]. The gamma ray computed tomography (CT) technique measures time averaged cross-sectional distributions and radial profiles of gas and solids holdups at different axial levels. Radioactive particle tracking (RPT) technique measures the particles velocity field and turbulence parameters (Reynolds stress, normal stresses, turbulent kinetic energy, and turbulent eddy diffusivities, etc.). The experimental results revealed non-similarity in the local hydrodynamics (solids and gas holdups, solids velocity field, and turbulence parameters) when all related dimensionless groups were matched in two beds of different sizes. This finding confirms that global parameters (overall holdups and pressure drop, etc.)

inadequate to assess the scale-up methodology. Our work indicates that the current dimensionless groups insufficient to achieve the hydrodynamics similarity of fluidized beds.

Keywords: Scale-up, dimensionless groups, fluidized bed hydrodynamics, computed tomography, RPT.

1. INTRODUCTION

Fluidization is a process in which solid particles become suspended and fluidized at a high enough gas velocity (higher than the minimum fluidization velocity). Gas-solid fluidized bed reactors are extensively used in various industrial processes, such as mineral, chemical, petrochemical, pharmaceutical, drying, combustion, gasification, catalytic cracking, calcinations processes, and many others, Dubrawski et al. [2]. This is because these reactors offer many advantages, including favorable heat and mass transfer, excellent gas-solid mixing and contacting, low pressure drop, approximately uniform and controllable temperature distributions, and the ability to fluidize many particle types of different densities and sizes (Geldart groups). Despite their advantages, gas-solid fluidized reactors have disadvantages that affect their industrial applications.

Gas-solid fluidized bed reactors are highly scale-dependent, and therefore it is difficult to predict the hydrodynamics of large industrial-scale reactors, based on the information of smaller scales. Therefore, proper scaling-up from laboratory to industrial scales is still challenging due to back mixing and the complex interactions of the gas-solid and solid-solid phases, Rüdisüli et al. [3]. When scaling up fluidized bed reactors, the behavior of large-scale fluidized beds usually differs significantly from the lab-scale behavior. One of the problems of fluidized bed scaling-up is the inherent scale dependence of many of the essential operating and design parameters. That is, if one parameter is changed (e.g., bed diameter) most of the other parameters (e.g., gas velocity) will not change concordantly. This discordance will ultimately result in significantly different hydrodynamics and transports in the scaled up fluidized bed. This is evident since fluidized beds are operated in many different regimes (bubbling, turbulent, fast

fluidization, etc.) and with many different particle types. One discouraging problem during the process of scaling-up gas-solid fluidized beds is the decrease in reactor performance. Such encountered problem could be caused by poor solid mixing, undesirable gas flow patterns, physical operating problems, etc. Rüdisüli et al. [3]. Hence, attaining hydrodynamics similarity is essential and the key for any scale-up methodology.

Therefore, the scaling-up of gas-solid fluidized beds has been the subject of a number of investigations in the last few decades. The open literature reports that, attempts have been made to develop scale-up methodology based on matching governing dimensionless groups for gas-solid fluidized beds in order to achieve hydrodynamic similarity when the size and the conditions of the fluidized beds change (Al-Dahhan et al. [4]. Romero and Johanson [5] were among the earliest researchers who used this approach to obtain the scaling relationships. They suggested four non-dimensional groups to characterize the quality of fluidization, which are the Froude number, the Reynolds number, (both the Froude number and the Reynolds number are based on the minimum fluidization velocity), the ratio of solid-to-fluid density, and the ratio of bed height at minimum fluidization velocity to the bed diameter. The experimental verification showed that, this set is inadequate. Broadhurst and Becker [6] used the Buckingham Pi theorem, which tries to express the dependence of one parameter (e.g. U_{mf}) as a function of the relevant independent parameters (e.g., bed density, particle size, bed voidage, etc.), to derive a list of non-dimensional groups similar to that of Romero and Johanson [5] except that the superficial gas velocity was used in place of the minimum fluidization velocity. Glicksman [7] proposed a set of dimensionless groups for scaling up gas-solid fluidized beds based on non-dimensionalizing the continuity and momentum equations for the gas

and solids phases along with their boundary conditions. Several assumptions and simplifications were taken into consideration, such as incompressible fluid and neglecting the inter-particle forces other than the mechanical forces due to collisions. With these assumptions the following set of dimensionless groups is obtained:

$\frac{u_0^2}{gL}$, $\frac{\rho_s}{\rho_g}$, $\frac{BL}{\rho_s u_0}$, $\frac{L_1}{L_2}$, $\frac{P_0}{\rho_s {u_0}^2}$. It is important to mention that the reactor configuration remains the same for both the large and small scales. The bed height-to-bed diameter ratio and the ratios of other geometric bed dimensions are expressed in the $\frac{L_1}{L_2}$ term. The $\frac{BL}{\rho_s u_0}$ term, representing the fluid-to-particle drag coefficient which is related to the Ergun equation (low gas velocities, dense bed). When the Ergun equation is non-dimensionalized, it is shown that this term depends on the Reynolds number and $\frac{L}{d_p}$. By substituting these two dimensionless groups into the last set of dimensionless groups, the following set of dimensionless groups emerges, which is called the full set of scaling: $\frac{u_0^2}{gL}$, $\frac{\rho_s}{\rho_g}$, $\frac{\rho_g u_0 d_p}{\mu}$, $\frac{L_1}{L_2}$, $\frac{L}{d_p}$, ϕ and the particle size distribution.

Fitzgerald et al. [8] were among the first to evaluate the full set of dimensionless groups which proposed by Glicksman [7], by measuring global parameters. Using pressure fluctuation measurements, they compared the hydrodynamics of two scaled gas-solid fluidized beds: an atmospheric fluidized bed combustor and a quarter-scale cold model. In one bed, cork particles were fluidized with air and in the other bed sand particles were used. The fast Fourier transform of the pressure fluctuations was used to determine the average frequency of the fluctuations, which should be related to the bubble frequencies. In addition they used pressure fluctuation measurements to derive the auto-correlation function (ACF). The ratio of average frequencies for the two beds, and

the amplitude of the autocorrelation function were in fair agreement. Similar results for the dimensionless groups were obtained between the two beds.

Nicastro and Glicksman [9] experimentally verified the proposed set of dimensionless groups for scaling-up gas-solid fluidized beds, which proposed by Glicksman [7] with a fluidized bed combustor having a 0.61 m diameter and 4.4 m height. The validation tests were carried out on an atmospheric gas-solid fluidized bed combustor operated at 1050 K and its scale model which operated at ambient temperature. The global parameters measurements of the minimum fluidization velocity and pressure fluctuations caused by the bubbles were used to evaluate the method which showed good agreement in the fluid dynamic characteristics. Nicastro and Glicksman [9] also compared time-resolved differential pressure measurements to retrieve the power spectral density (PSD) and the probability density function (PDF). Good agreement was also obtained between the spectral content and the probability density distribution of the differential pressure fluctuations. Although the solid/gas density ratio could not be matched exactly, a good agreement among the studded scales was obtained. Moreover, the experimental results that were based on measuring global parameters improperly indicated that, the dimensionless groups proposed by Glicksman [7] can be used to construct a fluidized bed that will exhibit similar fluid dynamics behavior. However, all these conclusions were made based on the measurement and assessment of the global parameters.

Newby and Kearns [10] applied high-speed camera and pressure fluctuations to validate the set of dimensionless groups proposed by Glicksman [7]. Two cold gas-solid fluidized beds were used. The larger bed was fluidized with 200 μm glass powders using

ambient air. The second bed, which was one half the scale of the first, used pressurized air to fluidize 100 μm of steel powders. Newby and Kearns [10] found good agreement with the dimensionless bubble frequencies of the high-speed vedio and reasonable agreement between the dimensionless amplitudes of the pressure fluctuation.

Glicksman [11] proposed a viscous limit set of scaling relationships. It is similar to the full set of scaling relationships that proposed by Glicksman [7], but with a simplification of the Ergun equation for the viscosity dominated system. The viscous limit was set for dense fluidized beds, at low gas velocities, as $\frac{\rho_g u_0 d_p}{\mu} < 4$. In this region, the viscous forces dominant over the inter-particle forces. Due to the negligible inter-particle forces, the requirements for scaling are less stringent. The Ergun equation can then be limited to its first term, which expresses the drag resulting from viscous forces. In this case the $\frac{BL}{\rho_s u_0}$ is proportional to $\frac{{u_0}^2}{gL}$ and $\frac{u_0}{u_{mf}}$. This results in a lower number of dimensionless groups that have to be matched for scaling-up: $\frac{{u_0}^2}{gL}$, $\frac{u_0}{u_{mf}}$, $\frac{L_1}{L_2}$, ϕ and the particle size distribution.

Knowlton et al. [12] considered the validity of the viscous limit set of scaling-up that was proposed by Glicksman [11] at elevated pressures and temperatures. The non-dimensional dominant frequency and amplitude of the pressure drop fluctuations were used as the basis of the comparison. Knowlton et al. [12] concluded that when the set of dimensionless groups is employed, similarity is achieved. Moreover, they postulated that if the particles' Reynolds number is 30 or less, the gas-to-solid density ratio does not have to be matched to obtain similarity. However, their assessment was based on the global parameter of pressure drop fluctuations measured at the wall.

Horio et al. [13], proposed a set of scaling-up relationships based on attaining similarities in bubbles behavior. These relationships are: $\frac{u_0-u_{mf}}{\sqrt{gD}}$ and $\frac{u_{mf}}{\sqrt{gD}}$, where u_{mf} is the minimum fluidization velocity. Rearranging these groups gives the condition for geometrically similar bubble coalescence as $u_0 - u_{mf} = \sqrt{m}\ (u_0 - u_{mf})^0$ and the condition for geometrically similar flow field around a bubble and for similar bubble splitting as $u_{mf} = \sqrt{m}\ {u_{mf}}^0$, where (m) represents the geometrical similarity of the two beds ((m) here is the ratio of the bed diameter of the two beds which is also equal to the ratios of the bed height, orifice diameter, and pitch dimension of the two beds). Horio et al. [13] used three geometrically similar bubbling fluidized beds of diameters 0.04, 0.1, and 0.24 m to verify their proposed scaling relationships. The solid-to-gas density ratio was not varied in the experiments although it was not one of the proposed scaling parameters. Video analysis of the bubble eruptions at the beds' surface was used to determine the cross-sectional average bubble diameter, bubble diameter distribution, and radial distribution of the superficial bubble velocity. Similarity was achieved in these hydrodynamic parameters when the above groups and density of solid to gas ratio, and the ratio of superficial to minimum fluidization velocities were matched.

Van Ommen et al. [14] validated the scaling relationships proposed by Horio et al. [13]. Three geometrically similar fluidized beds with diameters of 0.03, 0.146, and 1.56 m were used. Experiments were conducted using 1 to 4 times the minimum fluidization velocity. Pressure fluctuations were measured at three bed heights: H/D = 0.20, 0.46, and 0.77. Traditional validation tools which are based on global parameters were used including the average pressure and the average cycle frequency as well as the

probability density function (PDF) and power spectral density (PSD). Van Ommen et al. [14] concluded that the traditional validation tools indicated the similarity.

Foscolo et al. [15] derived a set of dimensionless groups by including the Archimedes number, density ratio, and geometry ratios, where the Archimedes number can be derived from the Reynolds and Froude numbers and the density ratio. These groups are compatible with those obtained by Glicksman [7] and Horio et al. [13].

Glicksman et al. [1] found that, matching all of the dimensionless groups proposed by Glicksman [7,11] could be difficult. Hence, Glicksman et al. [1] suggested simplified a set of dimensionless groups to match to attain hydrodynamics similarity. These are: $\frac{u_0{}^2}{gL}$, $\frac{\rho_s}{\rho_g}$, $\frac{u_0}{u_{mf}}$, $\frac{L_1}{L_2}$, $\frac{L}{d_p}$, ϕ and the particle size distribution.

Stein et al. [16] experimentally evaluated the proposed set of scaling-up dimensionless groups that were proposed by Glicksman et al. [1]. They validated the proposed set from the viewpoint of the solids phase. The non-invasive positron emission particle tracking (PEPT) technique was used to follow the particle motion. They measured the vertical solids motion and particle cycle frequency. Three cylindrical beds (70, 141, and 240 mm ID) equipped with multiple orifice-type distributors were tested. It was shown that for geometrically similar beds, the pair of Froude numbers based on the minimum fluidized velocity was sufficient for similarity. In addition, the experimental results showed that the gas-to-particle density ratio had little effect on the bed scaling. The simplified set of scaling-up dimensionless groups proposed by Glicksman et al. [1] does not apply to the slugging regime.

Zaid, [17], assessed the dimensionless groups based on a simplified set proposed by Glicksman et al. [1] in two scaled fluidized beds with diameters of 14 and 44 cm

where two types of particles glass beads and copper particles were used as the beds material. A sophisticated fiber optical probe was used to measure the point measurements of up-flow particle velocity and a parameter related to solids hold-up at selected radial positions. It has been demonstrated experimentally that there was non-similarity in the local hydrodynamics for fluidized beds when all of the dimensionless groups were matched.

In a summary, the literature shows that scale-up methodology based on matching dimensionless groups was reported by Glicksman [7, 11], Glicksmanet et al. [1], Horio et al. [13], Horio et al. [18], Bonniol et al. [19], and others. They all suggested matching selected dimensionless groups based on the governing equations to keep the hydrodynamics similarity when scaling-up fluidized beds. Each of the abovementioned research measured the global parameters to evaluate their proposed approach. However, they did not evaluate the detailed local parameters for assessing the adequacy of the dimensionless group-based scale-up methodology. It is worth mentioning that such similarity based on global parameters is not surprising. Although these systems have similar overall gas holdup, the existence of different gas holdup radial profiles possibly leads to different flow patterns and mixing intensities, Al-Dahhan et al. [4].

Accordingly, there is a need to assess and evaluate in more detail this scale-up methodology approach that is based on matching dimensionless groups by implementing advanced measurement techniques which can provide in 2D and 3D detailed local parameters. In this case the local hydrodynamics similarity means that either the magnitudes of the dimensionless representation or the absolute values of the bed hydrodynamic parameters (Holdups, velocity, turbulent parameters, etc.) are close to each

other. Therefore, the focus of our work is to evaluate the scale-up dimensionless groups based methodology of Glicksman et al. [1] for local hydrodynamics similarity using gamma ray computed tomography (CT) and radioactive particle tracking (RPT) techniques.

2. EXPERIMENTAL SET-UP

In this work, we implemented the following advanced non-invasive techniques: Gamma ray computed tomography (CT) technique for measuring cross-sectional distribution and radial profiles of solids and gas holdups along the bed height and radioactive particle tracking (RPT) technique for measuring in 3D solids velocity and its components, flow pattern and turbulent parameters such as normal stresses, shear stresses, turbulent kinetic energy, etc. Two fluidized beds were used of 6-inch (0.14 m) and 18-inch (0.44 m) in diameter. The fluidized bed columns were constructed from Plexiglas and consisted of column and plenum. A schematic diagram of the beds used in this work is illustrated in Figure 3.1. The 0.14 m column was 1.68 m high connected from the top with an upper section that had a larger diameter of 0.42 m and was 0.84 m high to disengage the solid particles from the flowing gas by reducing the superficial gas velocity of the gas phase. The plenum was located at the bottom, which consisted of a sparger tube. The gas phase was introduced through a distributor at the bottom after passing through the sparger. The gas distributor was made of a porous polyethylene sheet and had a pore size of 40 μm. The sparger was plugged at one end, and had 14 holes, all facing downward with respect to the column. The 0.44 m diameter fluidized bed very closely resembled the 0.14 m fluidized bed. The shape of the upper section was similar, but it had a diameter of 0.88 m and was 0.95 m high. The distributor design was similar to that used with the 0.14 m diameter fluidized bed. The plenum also consisted of a sparger tube, which had 20 holes, all facing downward with respect to the column. Both columns were electrically grounded to minimize electrostatic effects. Compressed air supplied from an industrial compressor, that can deliver compressed air of 735 CFM capacity at pressures

up to 200 Psig, was used in this work. Two rotameters (Omega® Engineering, Inc.) with different scales were connected in parallel to cover a wide range of flow rates (160 to 3200 SCFH). The CT scans were acquired at H/D = 0.286, 0.64 and 1.7 above the gas distributor for the 0.14 m diameter column, and at equivalent levels, which are at H/D = 0.286, 0.88 and 1.6 above the gas distributor for 0.44 m diameter bed. RPR technique was implemented on the bed height of H/D = 0.1 - 2.2 above the gas distributor for the 0.14 m diameter column and of H/D = 0.05 - 2.5 above the gas distributor for 0.44 cm diameter column as illustrated in Figure 3.1.

3. EXPERIMENTAL CONDITIONS

Glicksman et al. [1] suggested matching selected dimensionless groups when scaling- up a fluidized bed to maintain the hydrodynamics similarity. A summary of the scaling test conditions used for matching and mismatching dimensionless groups as scaling parameters is provided in Table 3.1. Case 1 lists the conditions used in the 0.44 m diameter column with glass beads of 210 μm mean diameter as a reference case. The same particle used in Case 1, with a mean particle diameter of 70 μm, was employed in Case 2, in the 0.14 m diameter bed to provide matching dimensionless groups. Case 3 used glass beads of 210 μm mean diameter, in a 0.14 m diameter bed to provide mismatching dimensionless groups of $\frac{D_c}{d_p}$ and $\frac{u_0}{u_{mf}}$. The absolute relative difference (ARD) between the dimensionless groups was compared between Cases 1 and 2, and between Cases 1 and 3. ARDs between the dimensionless groups for Cases 1 and 2 are as the following: $\frac{{u_0}^2}{g\,H} = 3.33\%$, $\frac{u_0}{u_{mf}} = 2.6\%$, $\frac{H}{D_c} = 0\%$, $\frac{\rho_s}{\rho_g} = 0\%$, $\frac{D_c}{d_p} = 4.55\%$, and $\varphi = 0\%$; these values of the absolute relative difference are acceptable because they are less than 5%. Case 2 was designed to study the validity of the dimensionless groups as scaling parameters that proposed by Glicksman et al. (1993). ARDs between the dimensionless groups for Cases 1 and 3 are as follows: $\frac{{u_0}^2}{g\,H} = 3.33\%$, $\frac{u_0}{u_{mf}} = 60\%$, $\frac{H}{D_c} = 0\%$, $\frac{\rho_s}{\rho_g} = 0\%$, $\frac{D_c}{d_p} = 68\%$, and $\varphi = 0\%$. The values of the ARDs are mismatched for $\frac{D_c}{d_p}$ and $\frac{u_0}{u_{mf}}$. The values of U_{mf} reported in Table 3.1 were measured by an absolute pressure transducer and the results were compared with the prediction of the empirical correlation of Miller and Logwinuk ,Suksankraisorn et al. [20] (see Table 5.2).

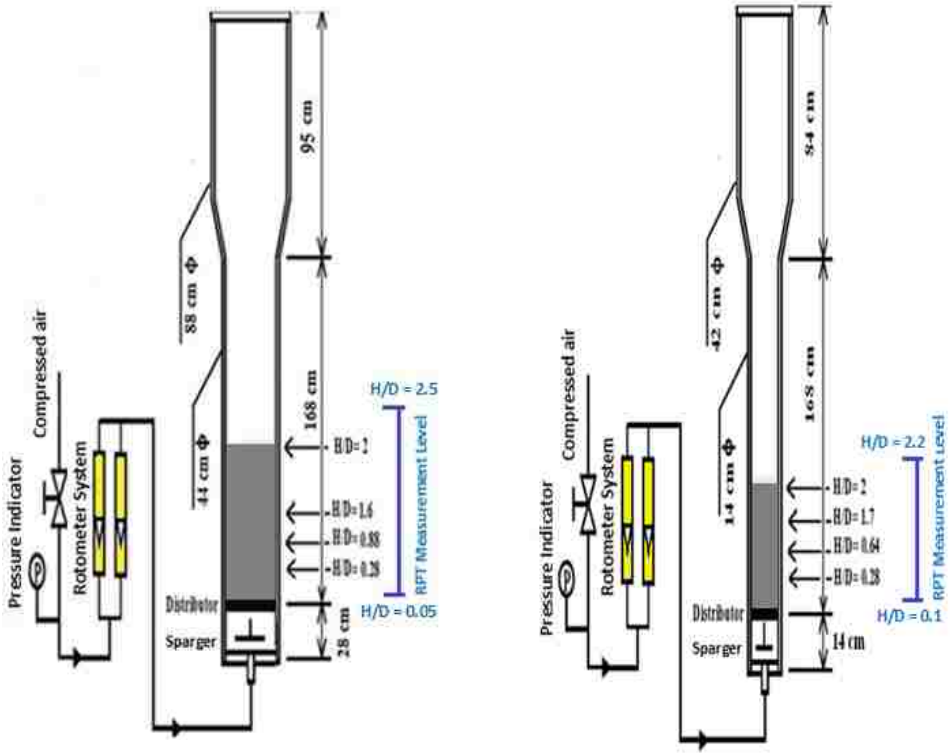

Figure 3.1 Schematic diagram of 0.44 m and 0.14 m cold–flow fluidized bed reactors with measurement levels for CT and RPT.

Table 3.1 conditions for matching and mismatching of the related dimensionless groups based on glicksman et al.[1]

Condition/ Cases	**Case1 (Reference)**	**Case 2 (match)**	**Case 3 (mismatch)**
Dc (m)	0.44	0.14	0.14
Particle Type	Glass Bead	Glass Bead	Glass Bead
L (m)	4.877	4.775	4.775
H (m)	0.88	0.28	0.28
T (K)	298	298	298
P (Kpa)	101	101	101
dp (μ m)	210	70	210
ρs (kg/(m^3))	2500	2500	2500
ρf (kg/(m^3))	1.21	1.21	1.21
μ (kg·s m–2)	1.81E-05	1.81E-05	1.81E-05
Ug (m/s)	0.36	0.20	0.20
U_{mf} (m/s)	0.10	0.08	0.12
φ	0.95	0.95	0.95
Dc/dp	2095.24	2000	666.7
H/Dc	2	2	2
ρs/ρf	2066.12	2066.12	2066.12
U/Umf	3.42	3.33	1.667
Fr=(U^2)/g* H	0.015	0.0145	0.0145
U/(g* Dc)^0.5	0.1732	0.1706	0.1706
Fr=(U^2)/g* Dc	0.03	0.029	0.029

4. MEASUREMENT TECHNIQUES

4.1 GAMMA RAY COMPUTED TOMOGRAPHY (CT) TECHNIQUE

The gamma ray computed tomography (CT) technique that has been used in this work comprises of Cs-137 sealed source and a set of 15 NaI scintillation detectors. This technique is a part of the dual source and energy (Cs-137 and Cobalt Co-60) gamma ray computed tomography (CT) technique, which was developed by Varma [21] with the help of the team from the Oak Ridge National Laboratory (ORNL) sponsored by the Department of Energy (DOE). It is currently available in the professor Al-Dahhan's multiphase reactors engineering and application laboratory (mReal) at the Missouri University of Science and Technology (Missouri S&T). In this work, CT experiments were performed under two-phase conditions, gas and solids, and hence a single sealed source (Cs-137) and its related 15 NaI scintillation detectors located opposite to the (Cs-137) sealed source has been used to measure in a non-invasive manner the time-averaged cross-sectional phase holdups distributions and their radial profiles at the operating conditions previously outlined in Table 3.1. As shown in Figure 4.1 the sources and detectors are built on a rotary plate to move together in 360° around the studied bed, providing 197 views in each scan and 21 projections in each view. The entire assembly could be moved up and down by stepper motor along the bed height to scan the bed at different axial positions. Each detector consists of a 2-inch cylindrical NaI crystal, a photomultiplier and electronics. Each of these detectors was collimated with a lead collimator with an open aperture. Two sizes of collimators were used in this work. Collimators that have approximately an open aperture of 2 mm × 2 mm were used with 0.14 m diameter column, while those that have approximately an open aperture of 2 mm

× 5 mm were used with 0.44 m diameter column. Since in 0.44 m diameter bed high attenuation was encountered, large aperture size was used in order to collect enough counts. However, in this case the spatial resolution was reduced to the size of 2 mm × 5 mm

Figure 4.1 The photo of the single CT Setup with a 0.14 m fluidized bed reactor

The CT scan sampling rate was 60 samples at 10 Hz, which took approximately 7.2 seconds to finish a 50 projection and 8.25 hours to complete a full scan by 360° rotation of the Cesium (CS-137) source and detectors around the column. The set of scans performed consisted of: 1) Scanning the column empty as a reference CT scan, 2) Scanning the column filled with solids (glass beads) as a packed bed to estimate the attenuation coefficient of the solids phase in each pixel, and 3) Scanning the column at

the desired conditions of gas-solid fluidization. The CT scans were acquired at H/D = 0.28, 0.64 and 1.7 above the gas distributor for the 0.14 m diameter column, and at equivalent levels, which were at H/D = 0.28, 0.88 and 1.6 above the gas distributor for 0.44 m diameter bed as shown in Figure 3.1.

Alternating Minimization (AM) algorithm and programs developed by varma et al. [22] have been used to process gamma ray computed tomography data to obtain holdups distribution. The cross-section of the bed is divided into 80 × 80 square pixels. More detailed on both the hardware and the software used in this technique and the related post-data processing have been described by (Varma et al., [22]; Varma, [21]; Bhusarapu, [23]; Bhusarapu et al., [24]; Fadah, [25]). The measured time averaged cross-sectional distribution of gas and solids holdups have been used to estimate the radial profiles of the holdups at the designated axial levels mentioned above.

4.2. RADIOACTIVE PARTICLE TRACKING (RPT) TECHNIQUE

The radioactive particle tracking (RPT) technique is an advanced non-invasive measurement technique that is based on the principle of tracking the motion of a single tracer radioactive particle as a marker of the solids phase. The new RPT setup was built in our Multiphase Reactors Engineering and Application Laboratory (mReal) at the Chemical and Biochemical Engineering Department, Missouri University of Science and Technology (Missouri S&T). Details of the principle of RPT used in this study can be found elsewhere (Bhusarapu, [23]; Bhusarapu et al., [24]; Al-Mesfer, [26]). This setup included a fully automatic calibration device (r, z, and θ) and a processing and data acquisition system. For the gas-solid fluidized bed study the high velocities and high

attenuation, gave rise to many implementation issues. These include the following: 1) selecting the radioactive particle, 2) devising a method for the detector calibration, 3) selecting a safe procedure for the introduction and recovery of the radioactive tracer, and 4) selecting a post-processing method for the data. A single radioactive particle (cobalt-60) with an activity of approximately 500 μCi and a 600 μm diameter was irradiated in the nuclear reactor at the University of Missouri Research Reactor Center in Columbia, Missouri. Cobalt-60 has a half-life of 5.28 years and presents two photo-peaks, one at 1.18 MeV and one at 1.34 MeV. Cobalt-60 has a high density 8.9 gcm^{-3}. The 600 μm diameter irradiated cobalt-60 particle was encapsulated with a gap of air in an aluminum ball with a 1 mm outer diameter to achieve the same density as the solids used (glass beads of 2.5 gcm^{-3} density). This composite single radioactive tracer particle was used to track the solids of 210 and 70 μm in the studied fluidized beds. It is noteworthy that larger tracer particle with similar density of the solid particles of the fluidized bed should be able to track with confidence the smaller particles sizes in fluidized bed. This is because the particles in the gas-solid fluidized bed usually do not move as single isolated particles but they do as a cluster (Tebianian et al., [27]; Mostoufi et al., [28]; Mostoufi et al., [29]). Each single particle is attached to a solid aggregate in the dense bed and moves with it until the solid aggregate breaks-up. The particle then enters another solid ensemble and continues its movement with the new ensemble. It is not necessary then to use a tracer particle of size that matches the size of experimental particles, Mostoufi et al., [28]; Mostoufi et al., [29] showed that all studied parameters were affected by the superficial gas velocity, and were independent of the size of the tracer. Tebianian et al. [27] used in RPT experiments scandium as tracer particle with size and density different

from that solid particle used, tracer diameter was 400 μm, which was 4-times greater than particle size (107 μm) but with the same density. In our experiment a total of 28 NaI scintillation detectors were positioned around the column. These detectors were held on four vertical supports at equal distances around the column. Each support had 7 detectors placed at different axial levels. Each level has 2 detectors that are staggered with the other levels by 45^0. Figure 4.2 shows a photograph of the configuration. Each detector consisted of a cylindrical NaI crystal (2 in x 2 in), a photomultiplier and electronics. RPT experiments typically consist of the following two steps: 1) the RPT calibration (static experiment under experimental conditions), and 2) the RPT experiment (dynamic experiment). During in-situ calibration, the detectors were calibrated by placing the tracer particle manually by the automated calibration device and manipulating it through the bed, at several hundred known locations, and each NaI scintillation detector records intensity counts, which depend upon the distance between the radioactive tracer particle and the detector for each calibration location and the materials in between. From the calibration step, a count-distance map can be obtained, which will be used in a subsequent step to obtain the location of the tracer particle. During the experimental run (dynamic experiment), the radioactive particle moves freely inside the reactor to track the solids phase motion. The experiments were conducted using a data acquisition frequency of 50 Hz for 8 hours, and during this time, the radiation emitted by the radioactive tracer particle was recorded by the detectors. The data obtained from the calibration and actual experiments can be used to reconstruct the lagrangian trajectory of the tracer radioactive particle. A cross correlation based search method (Bhusarapu, [23]; Bhusarapu et al., [24]) was used to reconstruct the tracer particle position. This method is

a two steps approach in which cross-correlation based search algorithm utilizing the calibration data is used to approximately locate the tracer particle position and a semi-empirical mechanistic model is fitted to the calibration data to relate the counts recorded to the position of emitting tracer particle.

a)

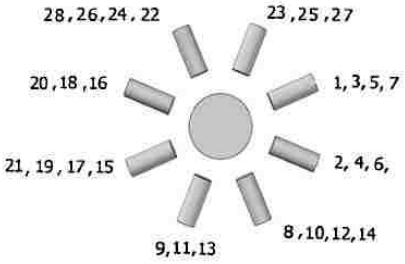

b)

Figure 4.2 a) Photograph of radioactive particle tracking (RPT) set-up and b) Top view of the detectors distribution for RPT Technique

This mechanistic model takes into account the geometry as well as the attenuating medium in between the particle and the detector. It is used to generate computed points of counts versus locations of high resolution around the approximate location identified by the first step of cross-correlation with the help of the calibration data. Then again cross-

correlation based search is applied on the computed points of counts versus locations to identify the tracer particle location where then the Lagrangian trajectory of the tracer particle is obtained. More detailed can be found in (Bhusarapu, [23]; Bhusarapu et al., [24]). By processing the lagrangian trajectory where the distance travelled by the tracer particle during the recorded sampling time provides the instantaneous solids velocities from which the time average solids velocity can be estimated. The difference between the instantaneous solids velocities and the time average solids velocities yields the fluctuation velocities which allow estimation of the turbulent parameters (Reynolds stress, normal stresses, turbulent kinetic energy, turbulent eddy diffusivities, etc.). To obtain reliable estimates of the turbulent parameters, the instantaneous particle position data obtained from RPT experiments must be filtered in order to extract only the coherent part of the signal by eliminating the white noise. The discrete wavelet transformation threshold de-noising filtration analysis proposed by Degaleesan [30] and Degaleesan et al., [31] was used in this work. Table 4.1 summaries how these parameters are estimated (Roy, [32]: Upadhyay, [33]).

Table 4.1 hydrodynamic parameters estimated for each compartment (i,j,k) from rpt reconstruction lagrangian trajectory.

Instantaneous Velocity (cm/s)	$u_{z,i-1/2} = \frac{z_i - z_{i-1}}{\Delta t}$ $u_{r,i-1/2} = \frac{r_i - r_{i-1}}{\Delta t}$ $u_{\theta,i-1/2} = \frac{(\theta_i - \theta_{i-1})}{\Delta t} \ \frac{(r_i + r_{i+1})}{\Delta t}$
Time-averaged velocities (cm/s)	$\overline{u}_{p(i,j,k)} = \frac{1}{N_v} \sum_{i=1}^{N_v} u_{p(i,j,k),i} \quad p = z, r, \theta$
fluctuating velocity (cm/s)	$u'_{p(i,j,k)} = u_{p(i,j,k)} - \overline{u}_{p(i,j,k)}$
Azimuthally averaged velocity cm/s	$\overline{u}_{(i,k)} = \frac{1}{N_\theta \, \breve{N}_{v(i,k)}} \sum_{j=1}^{N_\theta} \overline{u}_{(i,j,k)} \quad N_{v(i,j,k)}$
Stresses (cm^2/s^2)	$\tau_{pq} = \overline{u'_p u'_q}(i,j,k)$ $= \frac{1}{N_v} \sum_{n=1}^{N_v} u'_p(i,j,k),n \, u'_q(i,j,k),n$
Turbulent kinetic Energy (cm^2/s^2)	$K = \frac{1}{2}(\overline{u'^2_r} + \overline{u'^2_z} + \overline{u'^2_\theta})$
Normal radial eddy diffusivity (cm^2/s^2)	$D_{rr}(t) = \frac{1}{2}\frac{d}{dt}\overline{Y_r^2(t)} = \int_0^t u'_r(t) \, . \, u'_r(t') \, . dt'$

5. RESULTS AND DISCUSSION

The similarity in the local hydrodynamic parameters was assessed for the cases mentioned in Table 4.1. The gas and solids holdups and their radial profiles measured by CT are discussed first. The discussion on the solids velocity field and turbulent parameters (Reynolds stress, normal stresses, turbulent kinetic energy, and turbulent eddy diffusivities) obtained from RPT experiments are followed. The statistical difference between a hydrodynamic parameter profiles (gas and solids holdups, particle velocity field, and turbulent parameters) shown in this work are represented in terms of the average absolute relative difference (AARD) and absolute relative difference (ARD) as follows:

$$AARD = \frac{1}{N}\sum_{1}^{N}\left[\frac{x(r)-y(r)}{x(r)}\right] \quad (1)$$

$$ARD = \left[\frac{x(r)-y(r)}{x(r)}\right] \quad (2)$$

Where, x and y can either be gas, or solids holdup, particle velocity, or any turbulence parameters at corresponding radial locations for the cases of comparison in Table 3.1, and (N) is the corresponding total number of data points. The bars shown in the figures represent the standard deviation around the mean.

5.1 CROSS- SECTIONAL DISTRIBUTION OF GAS AND SOLIDS HOLDUPS

The presented results in this section of the gas and solids holdups distribution provide also valuable insight into the complexity of the hydrodynamics of gas-solid fluidized beds. Gas and solids holdups are important hydrodynamic parameters. The computed tomography (CT) technique was used to quantitatively measure the cross-

sectional distribution of the phases, gas and solids for all cases outlined in Table 3.1 at different axial locations. Figure 5.1 demonstrates the cross-sectional distribution of gas phase holdup for all cases outlined in Table 3.1. The color variation indicates the change in the gas holdup magnitude value. Red color indicates higher gas holdup values, while the blue color indicates lower values. In general, it can be observed that gas holdup is higher in the center and lower near the wall regions.

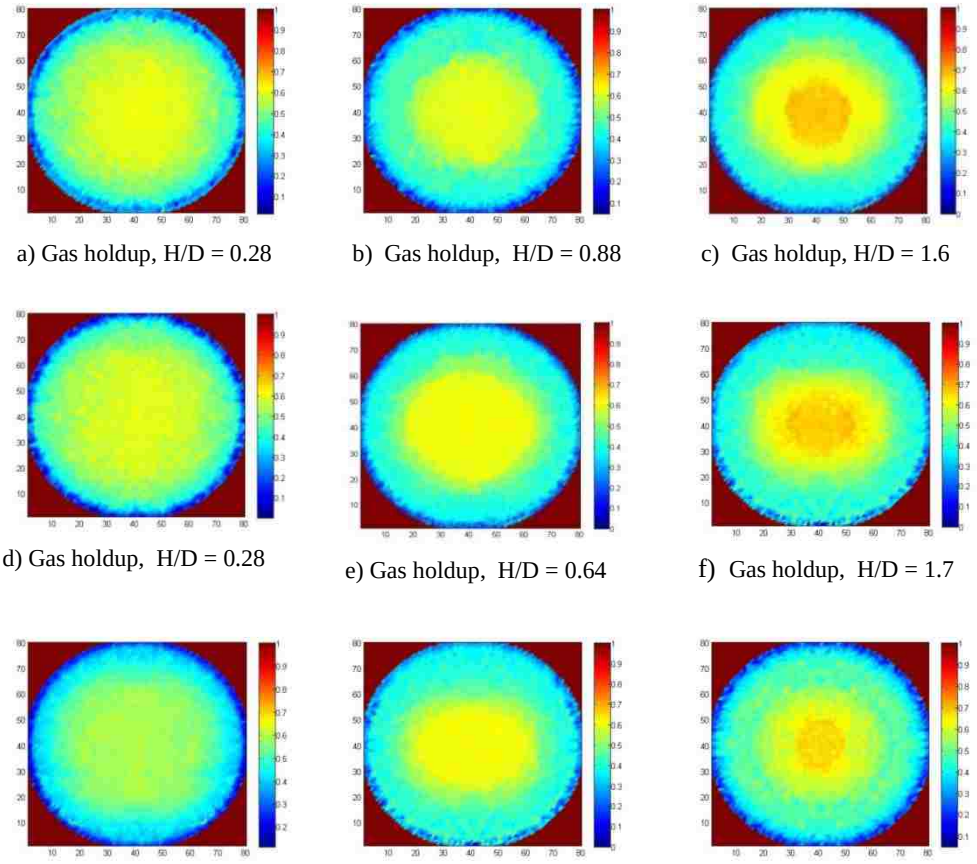

a) Gas holdup, H/D = 0.28 b) Gas holdup, H/D = 0.88 c) Gas holdup, H/D = 1.6

d) Gas holdup, H/D = 0.28 e) Gas holdup, H/D = 0.64 f) Gas holdup, H/D = 1.7

g) Gas holdup, H/D = 0.286 h) Gas holdup, H/D = 0.64 i) Gas holdup, H/D = 1.7

Figure 5.1 Cross-sectional distribution of gas holdup (a,b,c) for Case 1 (0.44 m), (d,e,f) for Case 2 (0.14 m), and (g,h,i) for Case 3 (0.14 m) fluidized beds at different axial position above the distributor.

Figure 5.2 demonstrates the cross-sectional distribution of solids holdup for all cases outlined in Table 3.1. Same findings were obtained for solids holdup distribution and the comparison among the cases.

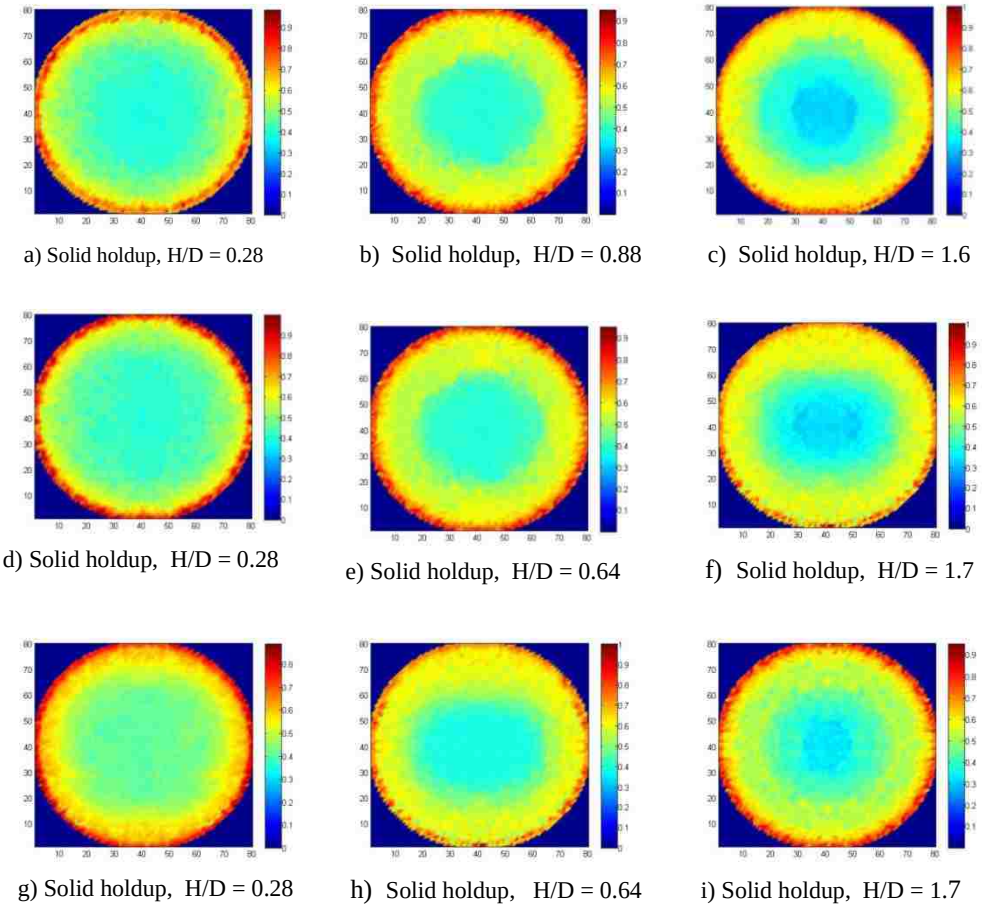

a) Solid holdup, H/D = 0.28 b) Solid holdup, H/D = 0.88 c) Solid holdup, H/D = 1.6

d) Solid holdup, H/D = 0.28 e) Solid holdup, H/D = 0.64 f) Solid holdup, H/D = 1.7

g) Solid holdup, H/D = 0.28 h) Solid holdup, H/D = 0.64 i) Solid holdup, H/D = 1.7

Figure 5.2 Cross-sectional distribution of solids holdup (a,b,c) for Case 1 (0.44 m), (d,e,f) for Case 2 (0.14 m), and (g,h,i) for Case 3 (0.14 m), fluidized beds at different axial position above the distributor.

Figure 5.3 displays the probability density (distribution) functions (PDF) of the gas holdup values in the imaging pixels of 80 × 80 pixels as shown in Figure 4. Such gas holdup distribution PDF characterizes the gas holdup variation values in the pixels of the cross-section at different axial positions. The PDF depends on the superficial gas

velocity, particle size, fluidization regime, and the bed geometry. The corresponding mean, variance and standard deviation (Std) of these pdfs as they listed in Figure 5.3 used to assess the hydrodynamics similarity between cases outlined in Table 3.1. The results show that, there were some differences in comparison of these values of the mean, variance and Standard deviation between the cases outlined in Table 3.1.

Table 5.1 summarizes the percentage deviations between case 1 and case 2, and also the percentage deviations between case 1 and case 3 for Figure 5.3 related to the mean, Standard deviation, and variance. Same results were obtained for the solids holdup pdf since the solids holdup is equal to (1 - gas holdup) in each pixel. It has been observed that the gas-solid interaction is different in the two cases (case 1 and 2), and also in between case 1 and case 3. The non-similarity between Case 1 and case 2 is obvious. Same findings have been reported by Rüdisüli et al., [3] where they reported that this methodology of matching dimensionless groups would be applied with great caution due to the negligence of many key parameters such as wall effects, effects of slugging, and the chaotic behavior of the fluidized bed.

Table 5.1 Comparison Of The Deviation Between The Cases Outlined In Table 1 Based On Cross – Sectional Gas Holdup

	H/D	Deviation between Case 1 and 2 (%)	Deviation between Case 1 and 3 (%)
Mean	0.286	10.52	16.7
	0.644	10	15.78
	1.7	9.3	11.9
St. Deviation	0.286	13	13
	0.644	9.1	20
	1.7	18.18	30
Variance	0.286	30	30
	0.644	16.67	40
	1.7	33.3	45.45

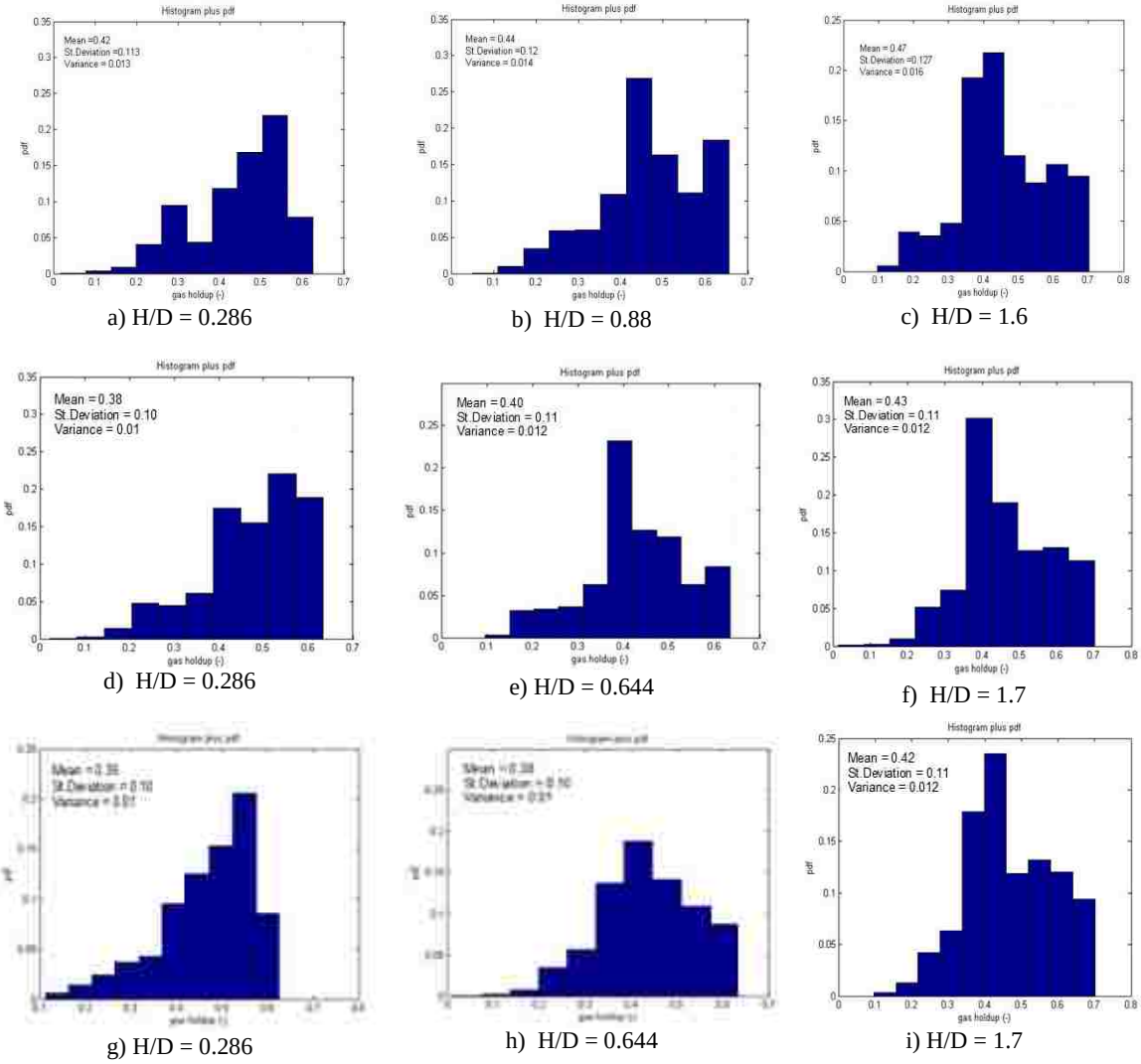

a) H/D = 0.286 b) H/D = 0.88 c) H/D = 1.6

d) H/D = 0.286 e) H/D = 0.644 f) H/D = 1.7

g) H/D = 0.286 h) H/D = 0.644 i) H/D = 1.7

Figure 5.3 Probability Density Function (PDF) of the values of Gas Holdup in the Pixel Cells (a,b,c) for Case (1) and (d,e,f) for Case (2), and (g,h,i) for Case (3) at different axial positions above the distributor

5.2. TIME-AVERAGED GAS AND SOLIDS HOLDUP RADIAL PROFILES.

Figure 5.4 (a,b,c) shows the comparison of the azimuthally averaged radial profiles of the gas and solids holdups obtained from the cross-sectional distribution of these holdups (Figures 5.1 and 5.2) for the cases outlined in Table 3.1 at different axial locations. The results show that, there is a deviation in the local gas and solids holdups radial profiles when all dimensionless groups were matched (case 1 and case 2). The

variation in the gas and solids holdup radial profiles between the two beds of case 1 and 2 have been observed at all three levels of the measurements (H/D = 0.286, 0.644, and 1.7). The Average Absolute Relative Difference (AARD) was 12.8% at H/D = 0.286, which is the sparger region. Figure 5.4 a(1), a(2) represents gas and solids holdup at H/D = 0.286. The Absolute Relative Difference (ARD) for these cases (Case 1 and 2) was 21.32% at the centre (r/R= 0); 19.16% at (r/R= 0.2) away from the center; 16.72% at (r/R= 0.4); 12.85% at (r/R= 0.6); 3.89% at (r/R= 0.8); and was 2.81% at r/R = 1 (close to the wall). The percentage difference at the lower level (H/D = 0.286) is because of the higher chaotic nature caused by the gas phase near the inlet region. The Average Absolute Relative Difference (AARD) was 14% at H/D = 0.644. The Absolute Relative Difference (ARD) for these cases (Case 1 and 2) was 18.76% at the center (r/R= 0); 18.89% at (r/R= 0.2) away from the centre; 17.85% at (r/R= 0.4); 9.86% at (r/R= 0.6); 6.87% at (r/R= 0.8); and was 10.76% at r/R= 1 (close to the wall). Not much change took place when the H/D changed from 0.286 to 0.644 as shown in Figure 5.4 b(1), b(2). The Average Absolute Relative Difference (AARD) was 13% (H/D = 1.7) Figure 6 C(1), C(2). The Absolute Relative Difference (ARD) was 4.56% at the center (r/R= 0); 13.8% at (r/R= 0.2) away from the center; 17.78% at (r/R= 0.4); 17.8% at (r/R= 0.6); 11.6% at (r/R= 0.8); and was 10.8% at r/R= 1.

Gas holdup for Case 3 at all axial levels was noticeable lower than in Cases 1 and 2. This presumably because the Dc/dp and U/U_{mf} ratios were much lower. Figure 5.4 a(1), a(2), shows that there was a clear difference in gas and solid holdups radial profiles between Cases 1 and 3, where the Average Absolute Relative Difference (AARD) was around 22% at H/D = 0.286. Also for these cases (Case 1 and 3) the Absolute Relative

Difference (ARD) was 31.76% at the centre (r/R= 0); 29.83% at (r/R= 0.2) away from the center; 28.28% at (r/R= 0.4); 24.31% at (r/R= 0.6); 9.92% at (r/R= 0.8); and was 7.87% at (r/R= 1) (close to the wall). The Average Absolute Relative Difference (AARD) between these cases (Case 1 and 3) was 13% at H/D = 0.644, Figure 5.4 b(1), b(2). The Absolute Relative Difference (ARD) was 22.67% at the center (r/R= 0); 21.95% at (r/R= 0.2) away from the center 19.63% at (r/R= 0.4); 16.73% at (r/R= 0.6); 11.32% at (r/R= 0.8); and was 12.32% at r/R= 1.

The Average Absolute Relative Difference (AARD) was 14% at H/D =1.7, Figure 7 C(1), C(2). The Absolute Relative Difference (ARD) was 12.63% at the center (r/R= 0); 16.12% at (r/R= 0.2) away from the center, 21.32% at (r/R= 0.4); 21.35% at (r/R= 0.6); 15.39% at (r/R= 0.8); and was 12.36% at r/R= 1 (close to the wall).

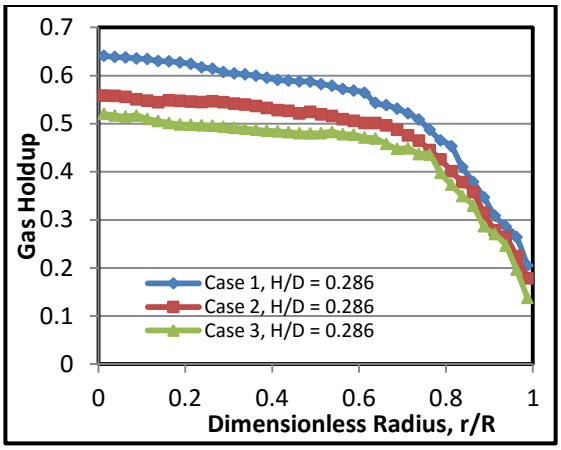

a(1)

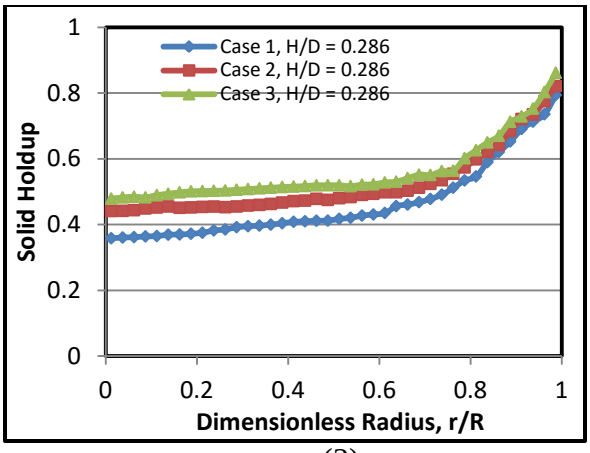

a(2)

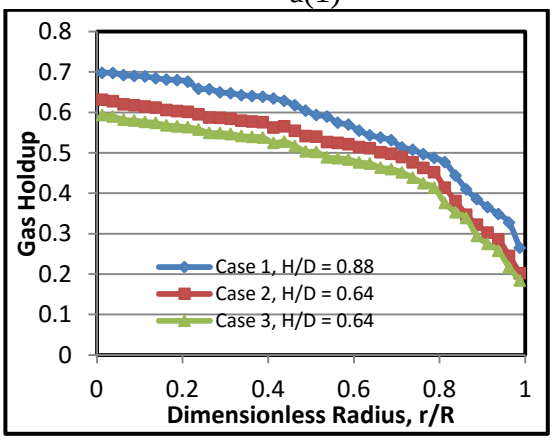

b(1)

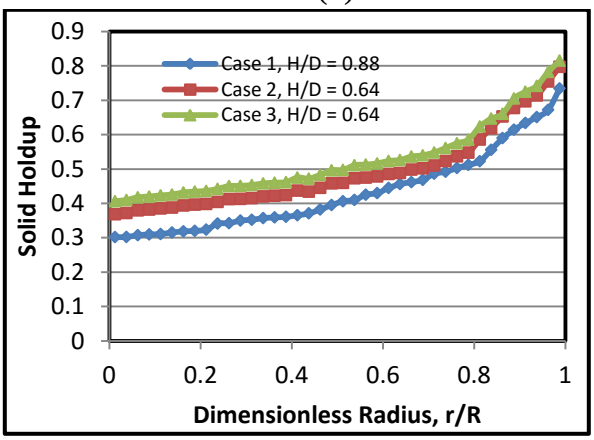

b(2)

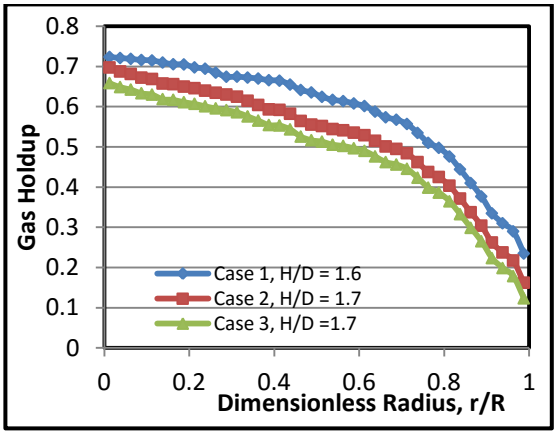

c(1)

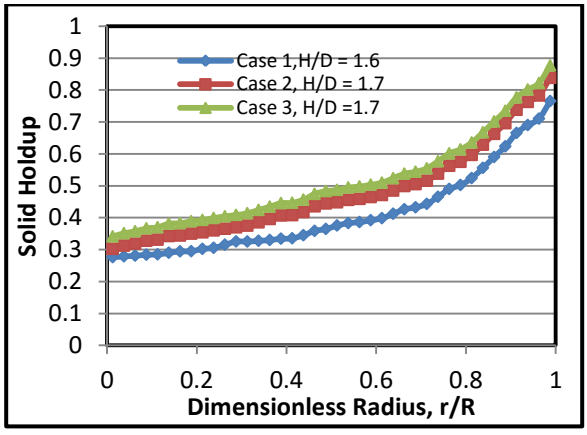

c(2)

Figure 5.4 Time average gas and solids holdup as a function of the dimensionless radial position at different axial levels above the distributor for all cases outlined in Table 1

The differences in the gas and solids holdups radial profiles can be attributed to the fact that these dimensionless groups may not completely account for the entire bed

hydrodynamics. Figure 5.5 shows the radial variation of an Absolute Relative Difference (ARD) in gas and solid holdups radial profiles between Case 1 and 2 and also between Case 1 and 3 at different axial positions above the distributor.

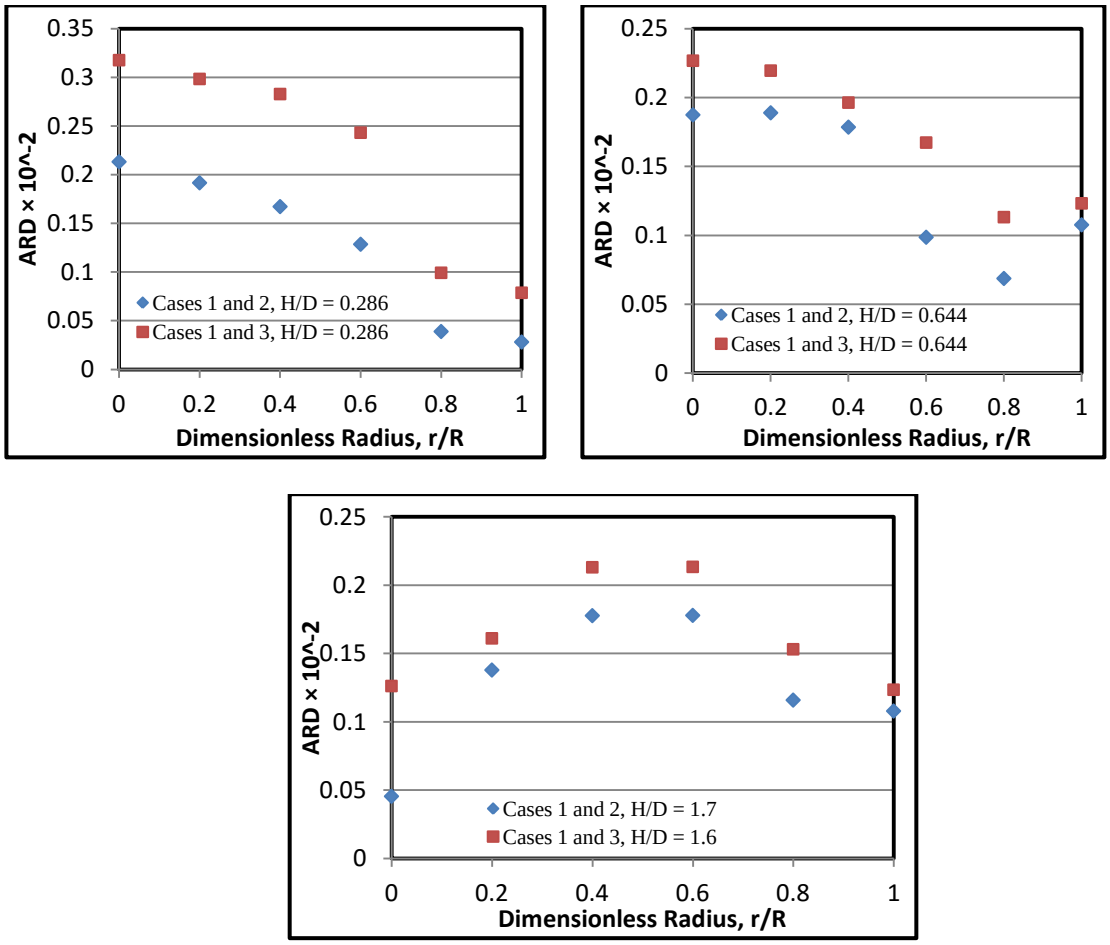

Figure 5.5 The radial variation of ARD in gas/solid holdups radial profiles between Case1 and 2, and between Case1 and 3 at different axial positions above the distributor

5.3. TIME-AVERAGED PARTICLE VELOCITIES

5.3.1. Axial Particle Velocity Radial Profiles. The solids velocity profiles for the conditions of the beds listed in Table 3.1 are measured using non-invasive radioactive

particle tracking (RPT) technique at the different axial levels (H/D = 0.286, 0.644 and 1.7) for 0.14 m column, while (H/D = 0.286, 0.88 and 1.6) for 0.44 m column. The results show that, the axial velocity of glass beads particle is positive at the center region of the column, and negative near the wall, which shows that the solids are going up from the center region of the column (r/R = 0 – 0.62) while coming down near the wall region (r/R ≥ 0.63). This finding is consistent with previous studies (Wang et al., [34]; Laverman et al., [35]; Bhusarapu et al., [24]; Mostoufi and Chaouki, [36]; Tebianian et al., [27]).

There are several earlier studies of solids motion in fluidized beds using different measurement techniques. Tebianian et al., [27] studied experimentally the particles velocity in FCC gas-solid fluidized beds. They implemented four different measurement techniques (Radioactive Particle Tracking, positron emission particle tracking, optical fiber probes and borescopic high-speed particle image velocimetry). Tebianian et al., [27], used in RPT experiments scandium as tracer particle with size and density different from that solid particle used, tracer diameter was 400 μm, which was 4-times greater than particle size (107 μm). Tebianian et al., [27] conclude that, radial profiles provided by each of the four techniques show upward solid velocity at the center of the column due to the solid movement induced by the wakes and drift caused by rising voids, accompanied by corresponding downward velocities near the wall.

As discussed in last section there was some deviation between gas and solids holdups radial profiles for case1 and case 2 (Figure 5.4). The deviation in gas and solids holdups radial profiles could be attributed to the differences in solids axial velocities. Figure 5.6 demonstrates the azimuthally averaged axial solids velocity profiles for those two cases 1 and 2. It is found that the velocity profiles in the two beds are different at all

H/D axial positions. The average absolute relative difference (AARD) was 21.6%, 17.8%, 22.2% at H/D = 0.28, 0.88, 1.7 respectively. The bars shown in the figures represent the standard deviation around the mean as mentioned early.

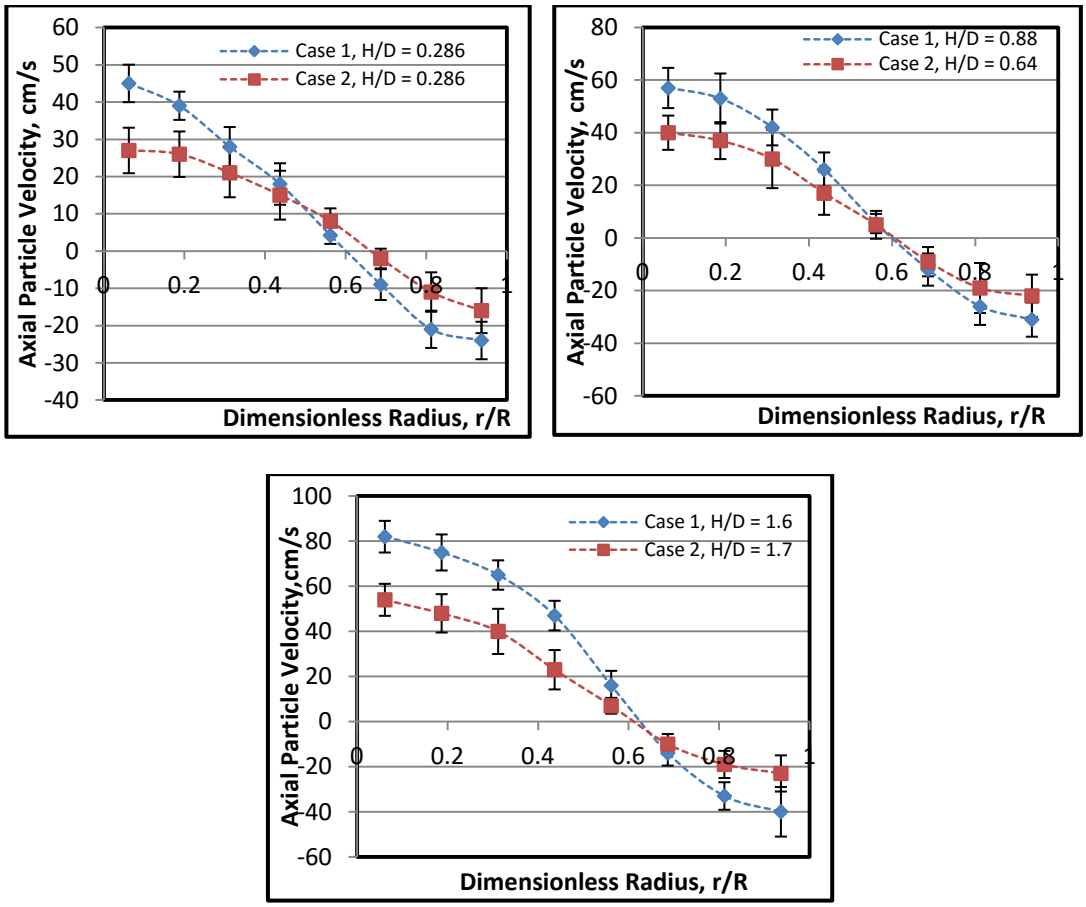

Figure 5.6 Time and azimuthally averaged axial particle velocity radial profiles at different H/D ratios for two different bed sizes Case1 and Case 2, (dot lines represent the trend)

Figure 5.7 shows the axial particle velocity profiles in both fluidized beds Case 1 and Case 3. The comparisons of radial profiles of the axial particle velocities in both fluidized beds at different axial positions show that, the profiles were not similar. The

average absolute relative difference (AARD) between Case 1 and Case 3, at H/D= 0.286 was 30.4%, at H/D= 0.644 was 13.32%, and at H/D = 1.7 was 37.4%.

Figure 5.8 shows the radial variation of an ARD between Case1 and Case 2 and also the radial variation between Case1 and Case 3 at different axial positions above the distributor.

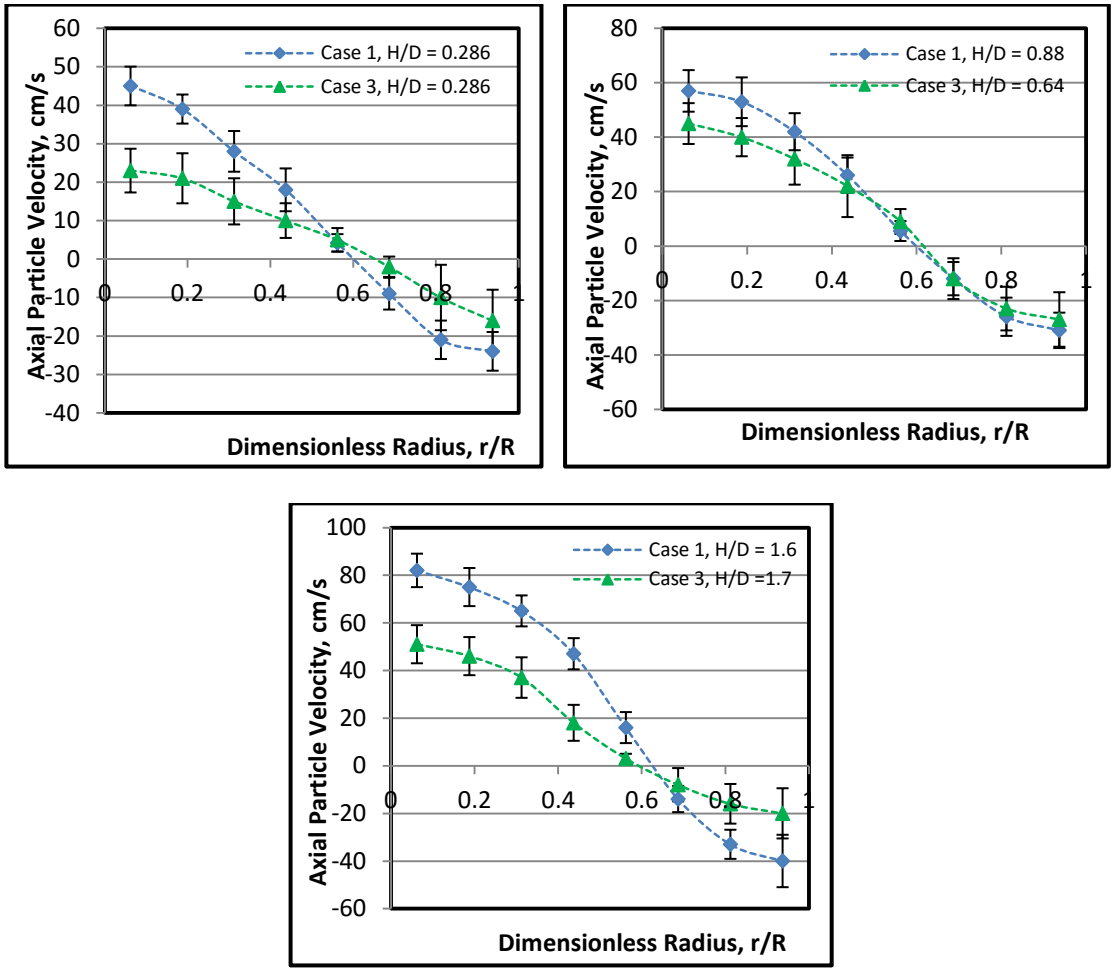

Figure 5.7 Time and azimuthally averaged axial particle velocity radial profiles at different H/D ratios for two different bed sizes Case1 and Case 3 (dot lines represent the trend)

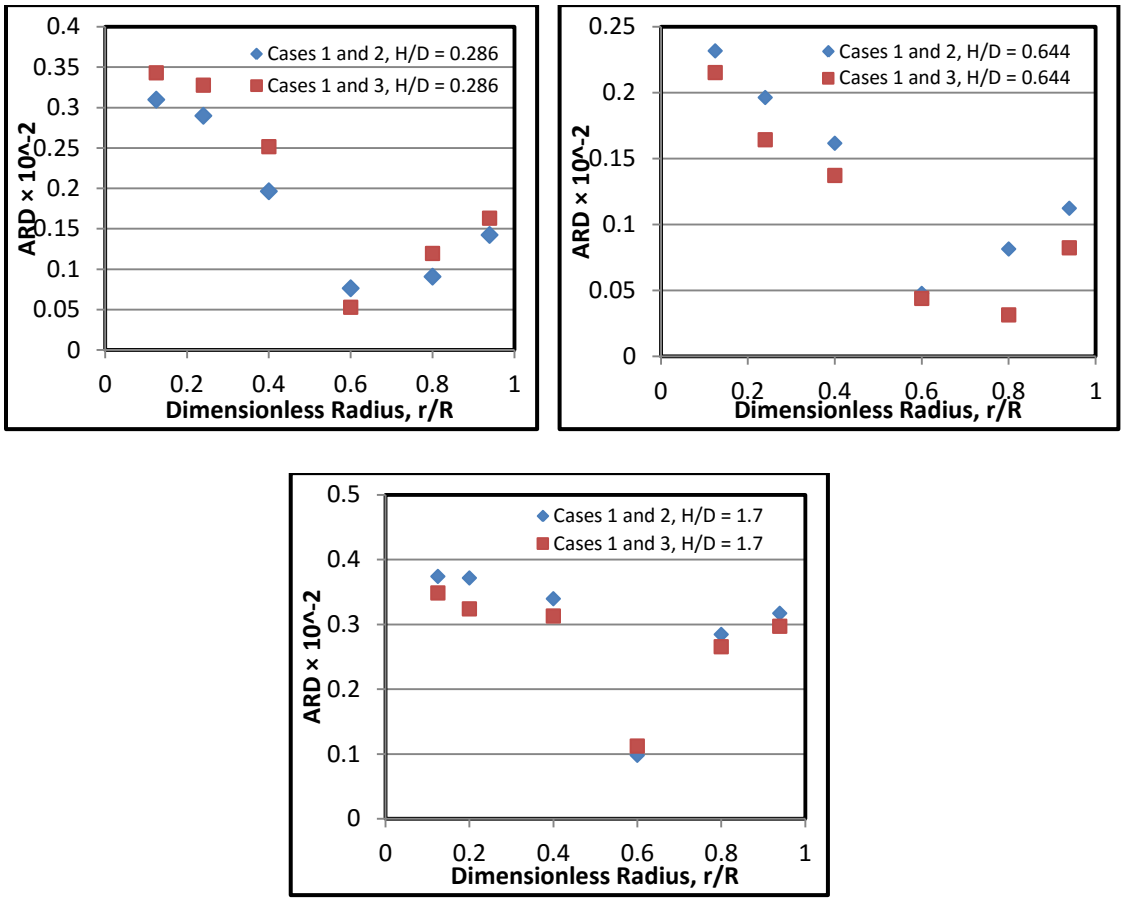

Figure 5.8 The radial variation of ARD in axial velocity profiles between Case1 and 2, and between Case1 and 3 at different axial positions above the distributor

Figure 5.9 shows the velocity 2D vector plots for case 1 and case 2. One-cell recirculation pattern in a time averaged sense was observed for the glass beads in two beds of case 1 and case 2 with clear differences in the vortex configurations. This behavior can be interpreted in terms of bubble behavior. There is a concentration of bubbles close to the center of the bed giving rise to high upward solids velocities in that region, (positive axial velocity) in the central region of the column. While at the positions close to the wall, where the bubbles are absent, the solids move toward the distributor resulting in downward solids velocities in that region. Down-flow (negative axial velocity) in the annular region near the column wall. The behavior of the solids and

bubbles displayed in this work is in a good agreement with the results obtained in the literature (Bashiri et al., [37]; Laverman et al., [35]; Tebianian et al., [27]. The comparison of the vortex of solids circulation in two beds, Case 1 and Case 2, shows that, as the bed diameter is increased, the solids move with higher velocity due to the increase in bubble size and bubble rise velocity. The vortex of solids circulation gets enlarged and horizontally elongated as the bed size is increased in Case 2. In the small bed size case1 the vortex was small due to wall effects. In addition it seems not well developed flow and solids circulation as compared to the larger bed 0.44 m diameter.

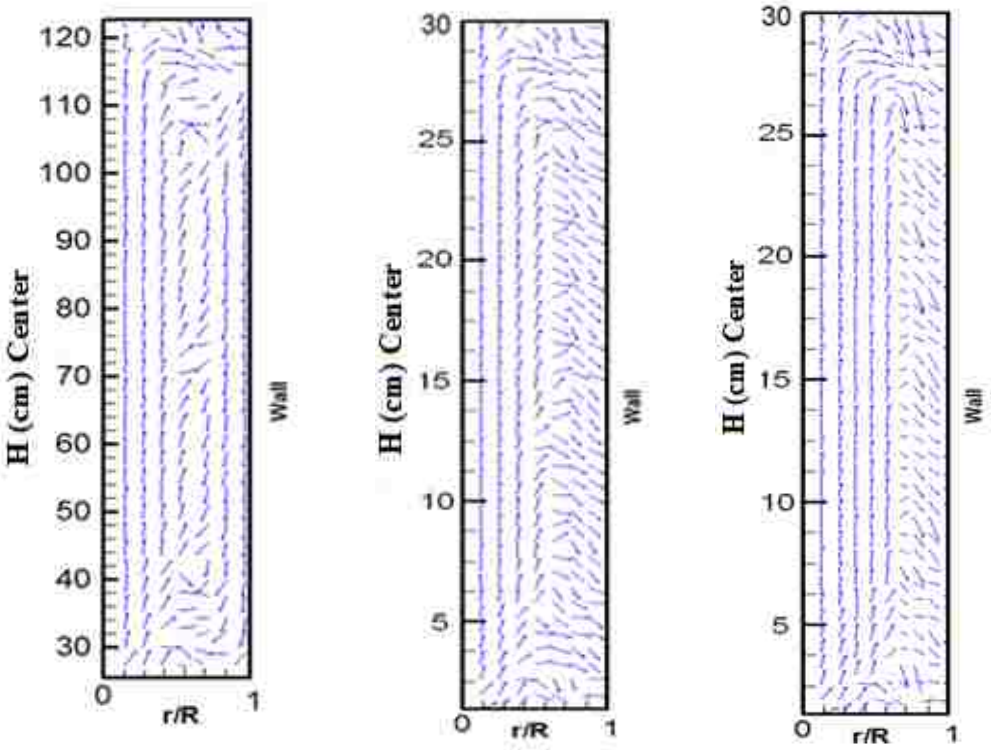

Case 1 **Case 2** **Case 3**

Figure 5.9 Azimuthally and time-averaged velocity vector plot in the r-z plane for Case 1 and Case 2, the arrows represent the direction of the velocity and the length represents the magnitude

To have a common basis for comparison and to examine if the axial velocity profiles and magnitudes get closer in the two beds, the radial profiles of the axial particles velocity in both fluidized beds (case 1 case 2, and case 3) were non-dimensionalized by dividing them by the minimum fluidization velocity (U_{mf}). Minimum fluidization velocity refers to the velocity at which the bed starts fluidization, and below this velocity the bed is not fluidized. It was measured experimentally by the pressure drop through a bed of particles as a function of the superficial gas velocity. The minimum fluidization velocity (U_{mf}) in both beds was compared with the predictions of the correlation available in the literature Miller and Logwinuk, Suksankraisorn et al., [20] the values of U_{mf} for the 0.14 m bed diameter using glass beads with 70 µm and 210 µm were 0.08 m/s and 0.12 m/s, respectively, and for the 0.44 m bed diameter using glass beads with 210 µm mean particle size was 0.10 m/s. Table 5.2 shows the comparison of U_{mf} measured experimentally and that predicted by correlations. It was found that the comparison of the values in Table 5.2 is in a good agreement.

Table 5.2 Comparison between experimental values and correlation predictions of U_{mf}.

Diameter of fluidized bed	Particle type	Particle size	Experimental Values	Correlation prediction of Miller and Logwinuk
0.14 m	Glass beads	210 µm	0.12 m/s	0.117 m/s
0.14 m	Glass beads	70 µm	0.08 m/s	0.093 m/s
0.44 m	Glass beads	210 µm	0.10 m/s	0.089 m/s

The data graphed in Figure 5.10 reveals that the profiles were not similar. Thus, dimensionalizing with respect to minimum fluidization velocity does not help in producing close axial particle velocity profiles and confirmed the dissimilarity between the hydrodynamic of the two fluidized beds, (case1 and case 2). The average absolute relative difference (AARD) was 12.2% at H/D equal 0.286, and was 10.5% at H/D = 0.644 and at level H/D = 1.7 (AARD) between Cases 1 and 2 was 15.82%.

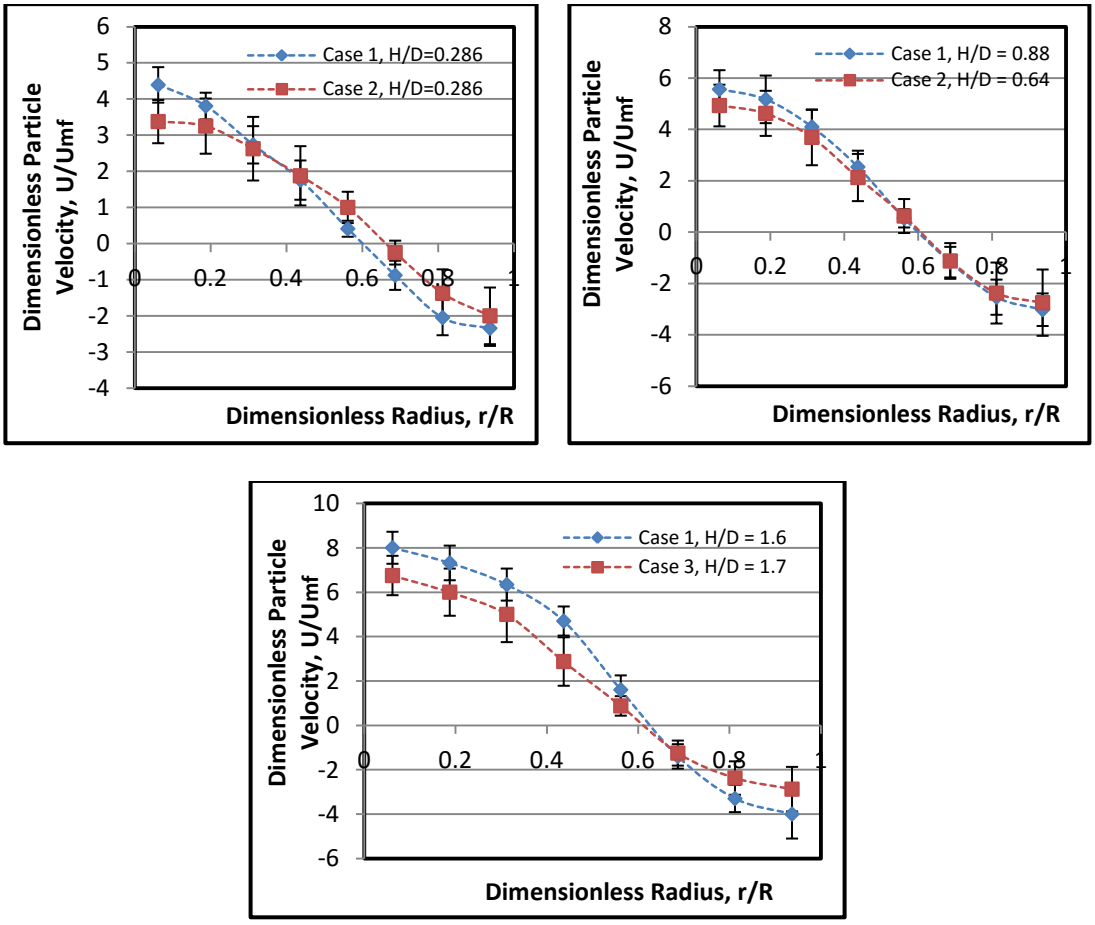

Figure 5.10 Dimensionless time and azimuthally averaged axial particle velocity radial profiles at different H/D ratios for two different bed sizes Case1 and Case 2, (dot lines represent the trend)

Figure 5.11 shows the radial profiles of dimensionless axial particle velocity in both fluidized beds Case 1 and Case 3. The comparisons of radial profiles of the dimensionless axial particle velocity in both fluidized beds at different axial positions show that the profiles were not similar. The average absolute relative difference (AARD) between Case 1 and Case 3, at H/D= 0.286 was 28.8%, at H/D= 0.644 was 12.3%, and at H/D = 1.7 was 34.52%. The bars shown in the figures represent the standard deviation around the mean as mentioned early.

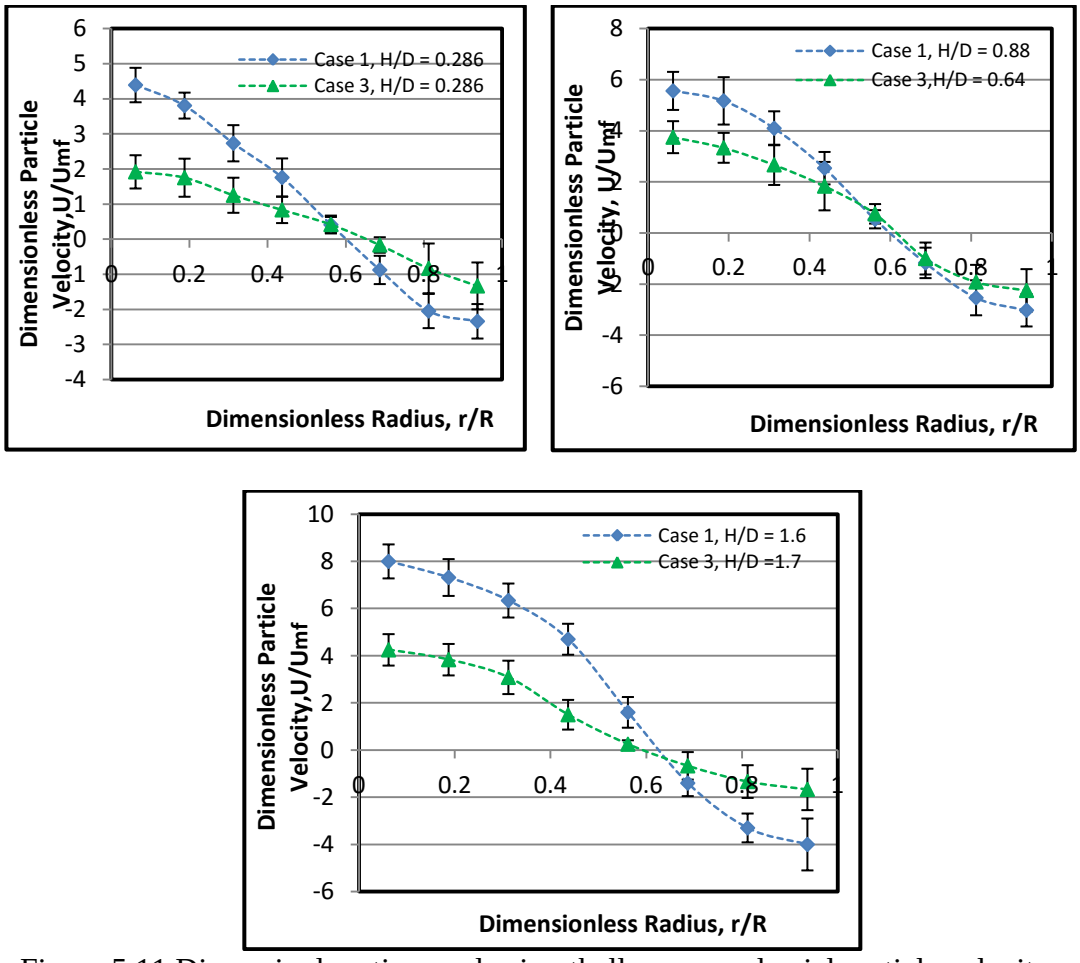

Figure 5.11 Dimensionless time and azimuthally averaged axial particle velocity radial profiles at different H/D ratios for Case 1 and Case 3 fluidized beds, (dot lines represent the trend)

Figure 5.12 shows the radial variation of an ARD between case1 and case 2, and also between case1 and case 3, based on dimensionless particle velocity at different axial positions.

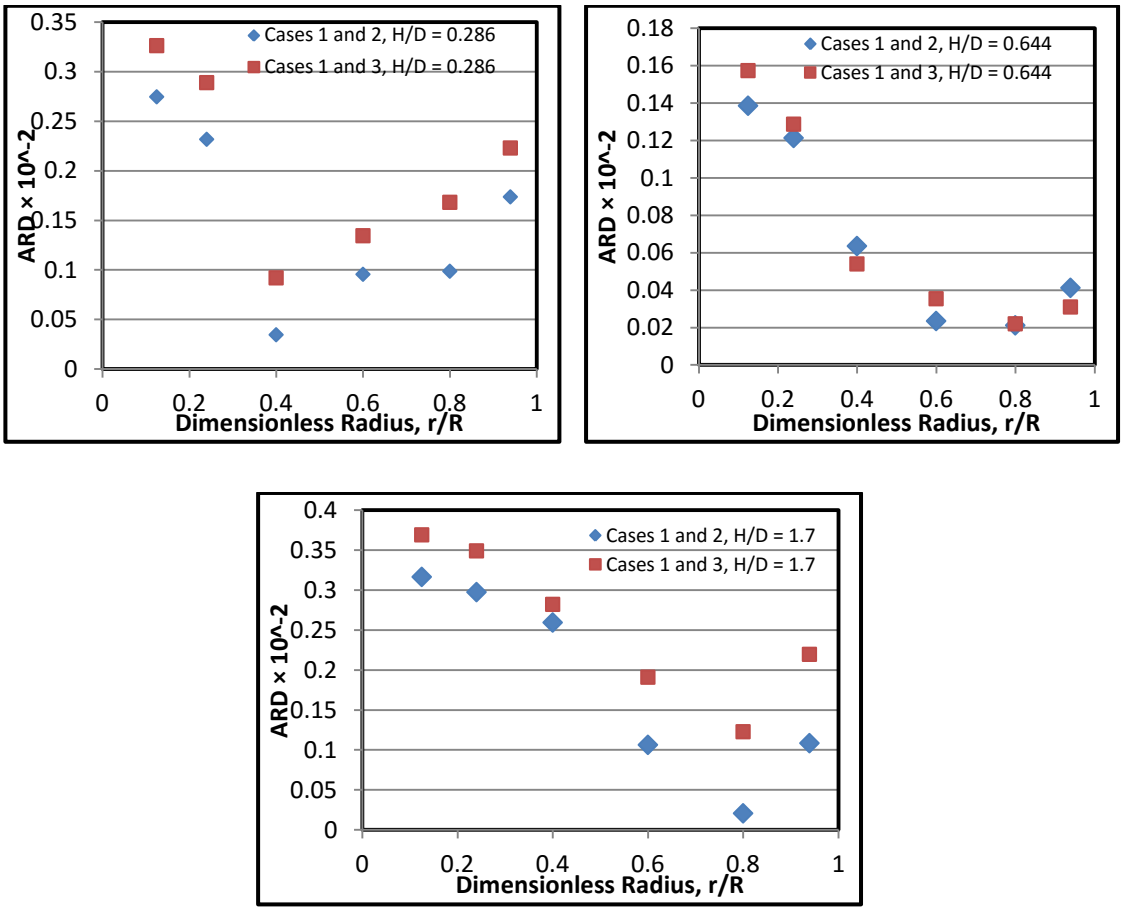

Figure 5.12 The radial variation of ARD in dimensionless axial particles velocity profiles between Case 1 and 2 and between Case 1 and 3 at different axial positions above the distributor

5.3.2. Radial Particle Velocity Radial Profiles. The radial profiles of the radial velocity of the fluidized beds also investigated in this study, and are depicted in Figure 5.13 and 5.14. Both the positive and negative values of the radial velocity correspond to the outward and inward motion of solids, respectively. The time averaged radial velocities of solids were very small compared to the corresponding axial velocities,

which is really to be expected since there is no solids motion in the radial direction. Deviations in the radial velocity profiles for the compared fluidized beds, case1 and case 2 have been observed at all the three levels of measurements. The average absolute relative difference (AARD) for the radial velocity profiles between the two fluidized beds was 18.67%, 21.2%, and 14.68% at H/D = 0.286, 0.644, and1.7 respectively.

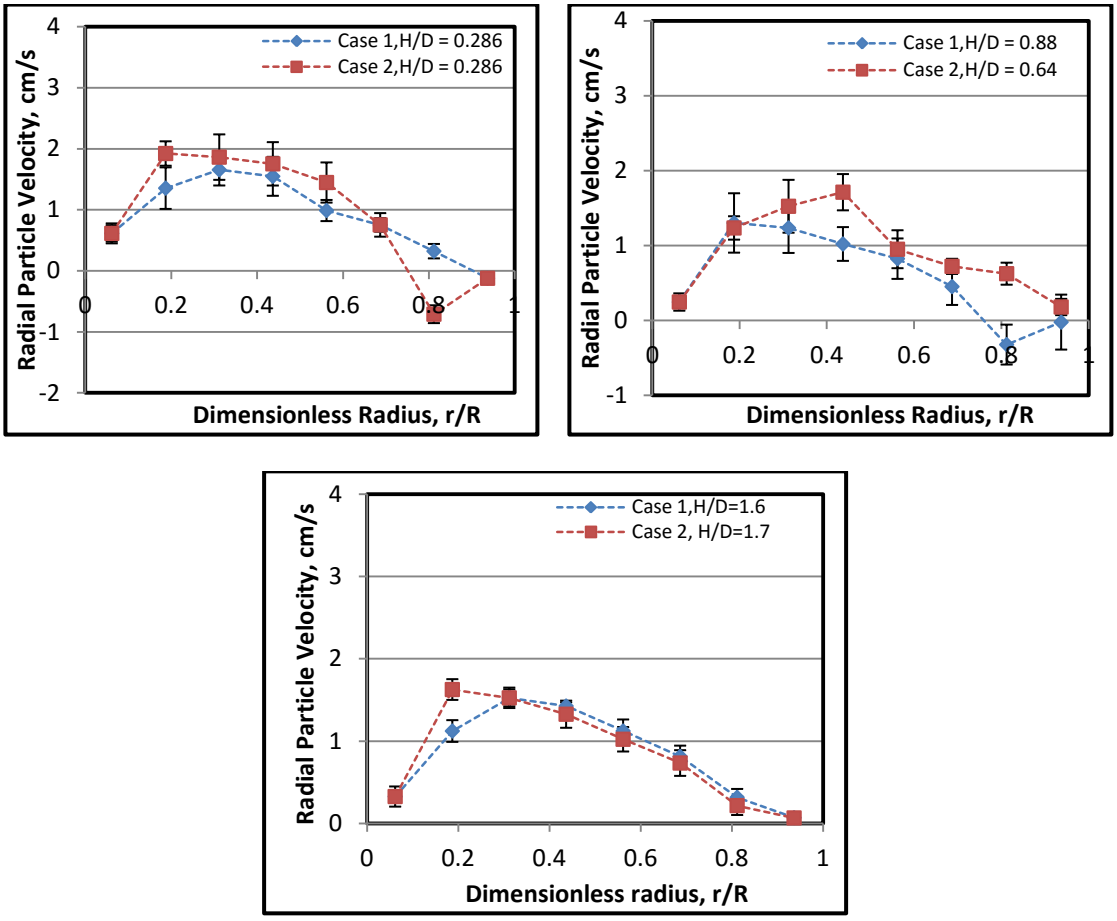

Figure 5.13 Time and azimuthally averaged radial particle velocity radial profiles for Case 1 (0.44 m) and Case 2 (0.14 m) at different axial positions above the distributor (dot lines represent the trend)

Figure 5.14 shows the deviations in the radial velocity profiles between case 1 and case 3 at all the three levels of measurements. The average absolute relative

difference (AARD) for the radial velocity profiles between the two fluidized beds was 31.6%, 13.2%, and 21.68% at H/D = 0.286, 0.644, and1.7 respectively.

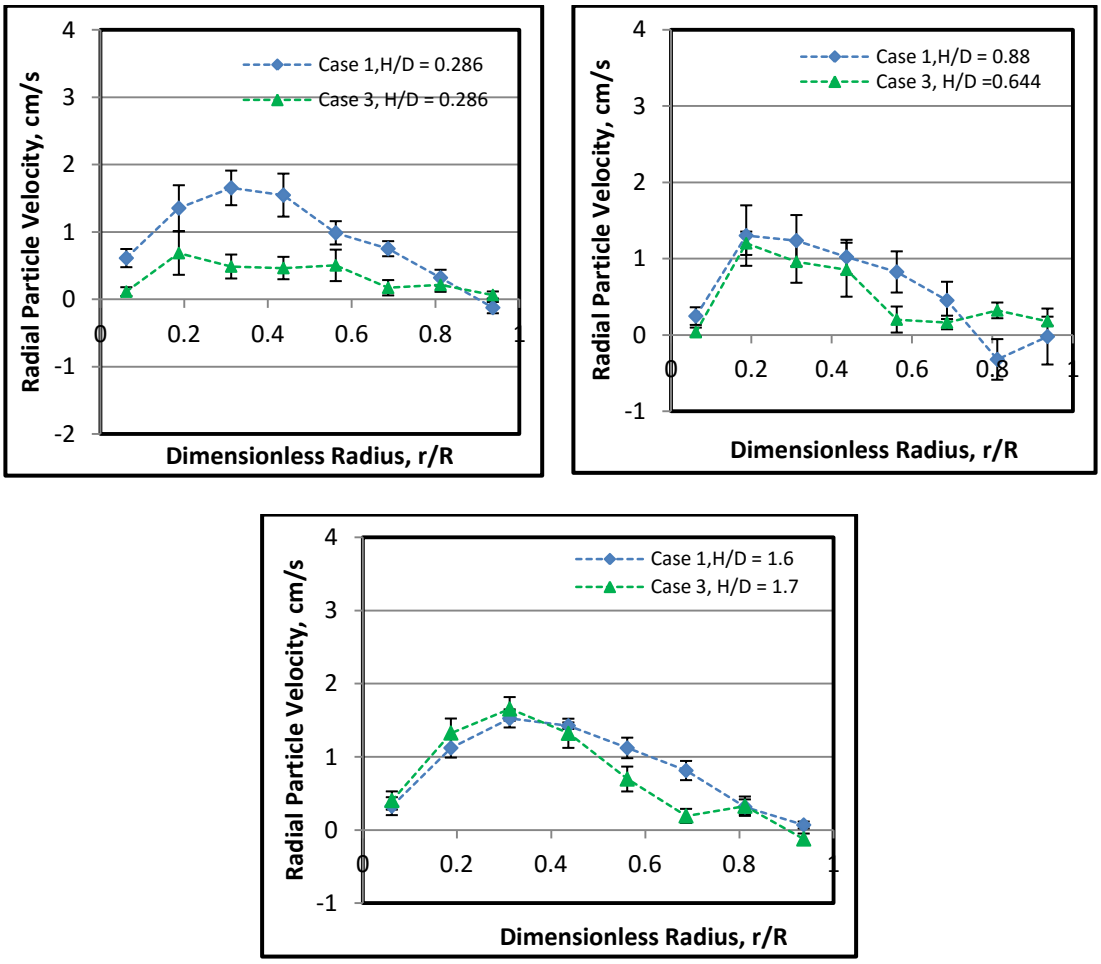

Figure 5.14 Time and azimuthally averaged radial particle velocity radial profiles for Case 1 (0.44 m) and Case 3 (0.14 m) at different axial positions above the distributor, (dot lines represent the trend)

Figure 5.15 shows the radial variation of an ARD between case1 and case 2, and also between case1 and case 3, based on radial particle velocity at different axial positions.

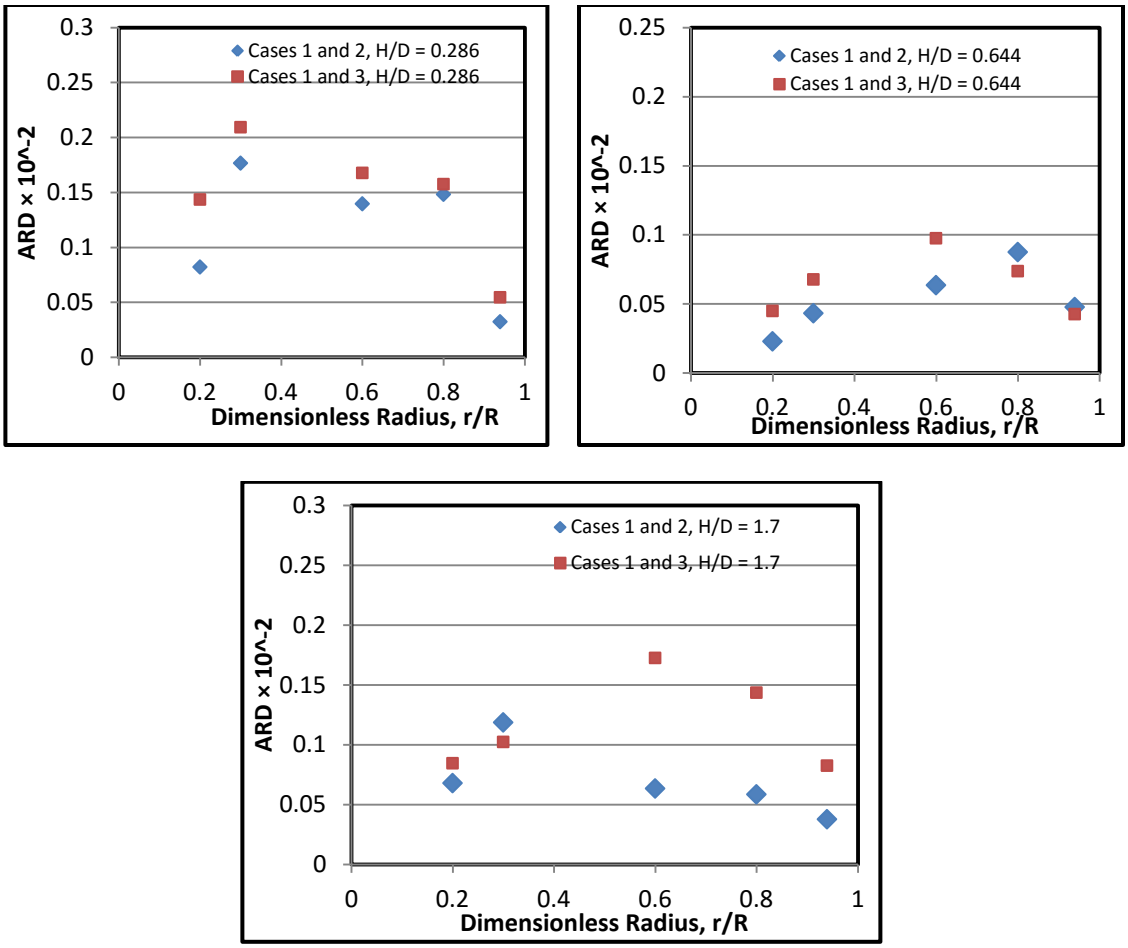

Figure 5.15 The radial variation of ARD in radial particles velocity profiles between Case 1 and 2 and between Case 1 and 3 at different axial positions above the distributor

5.3.3. Azimuthal Particle Velocity Radial Profiles. Figure 5.16 shows the compared radial profiles of azimuthal particle velocity in both fluidized beds of Case 1 and Case 2. The comparisons of radial profiles of the azimuthal particle velocities in both fluidized beds at different axial positions show that the profiles were not similar. The average absolute relative difference (AARD) between Case 1 and Case 2, at H/D= 0.286 was 21.5%, at H/D= 0.64 was 26.3%, and at H/D = 1.7 was 17.6%.

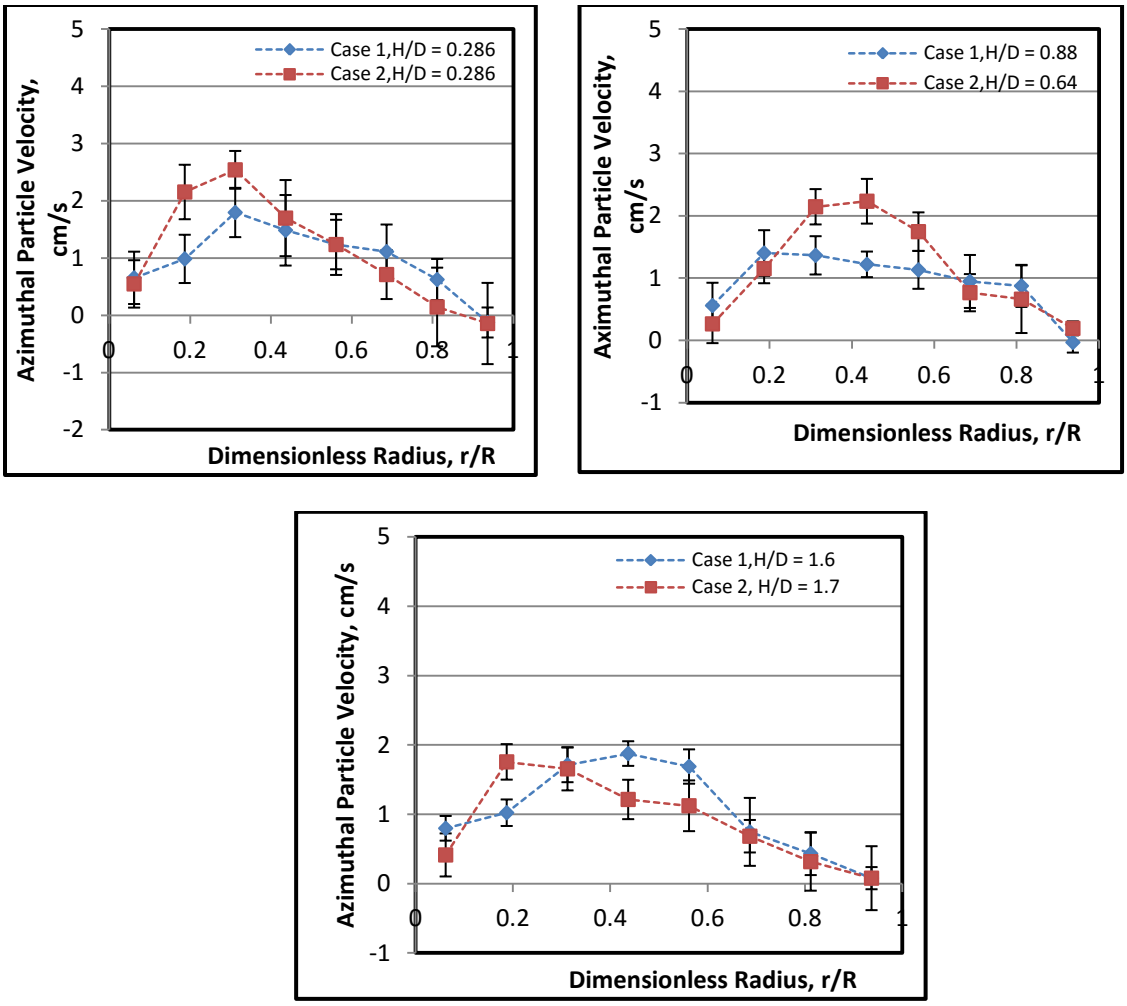

Figure 5.16 Time and azimuthally averaged azimuthal particle velocity radial profiles at different H/D ratio for Case 1 (0.44 m) and Case 2 (0.14 m) (dot lines represent the trend)

5.4. TURBULENT PARAMETERS

Additional investigation and further assessment is required to draw conclusion on the applicability of dimensionless groups for the hydrodynamics similarity of fluidized beds.

5.4.1. Reynolds' Stress (Shear Stress) Radial Profiles. The particle shear stress for two different fluidized bed sizes Case 1, (0.44 m) and Case 2, (0.14 m) were compared in Figure 5.17. The shear stress profiles showed the same trend for both cases,

with the maximum values of shear stress occurred close to inversion point (Axial particle velocity is zero), which could be due to the change of the flow dynamics from upward to downward, while the minimum value for both cases occurred at the center and the wall of the column, but their magnitudes were different. The Average Absolute Relative Difference (AARD) at (H/D = 1.7) was 52%, at H/D= 0.64 was 40.2% and at H/D = 0.289 was 56.1%.

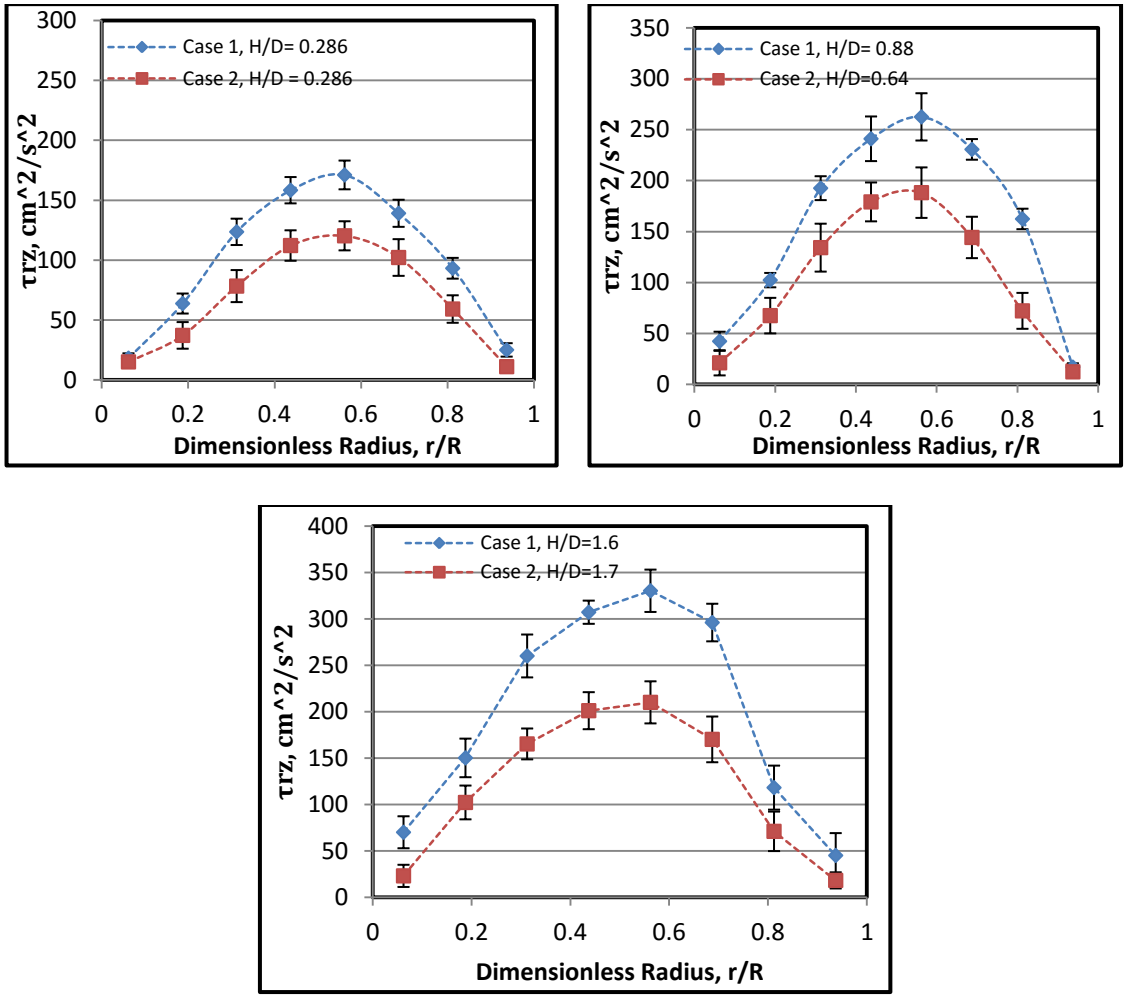

Figure 5.17 Time and azimuthally averaged shear stress radial profiles at different H/D ratios for Case 1 (0.44 m) and Case 2 (0.14 m) fluidized bed (dot lines represent the trend)

The radial profiles of shear stress in both fluidized beds of case 1 and case 2 are also non-dimensionalized by dividing them by the square of the minimum fluidization velocity. Figure 5.18 depicts the compared radial profiles of dimensionless shear stress in both fluidized beds, Case 1 and Case 2. The comparison at different axial positions above the distributor shows that there was a percentage of deviation between two profiles. The average absolute relative difference (AARD) for the radial profiles of dimensionless shear stress between Case 1 and Case 2, at H/D= 0.286 was 39.64%, at H/D= 0.64 was 38.1% and at H/D = 1.7 was 45.7%.

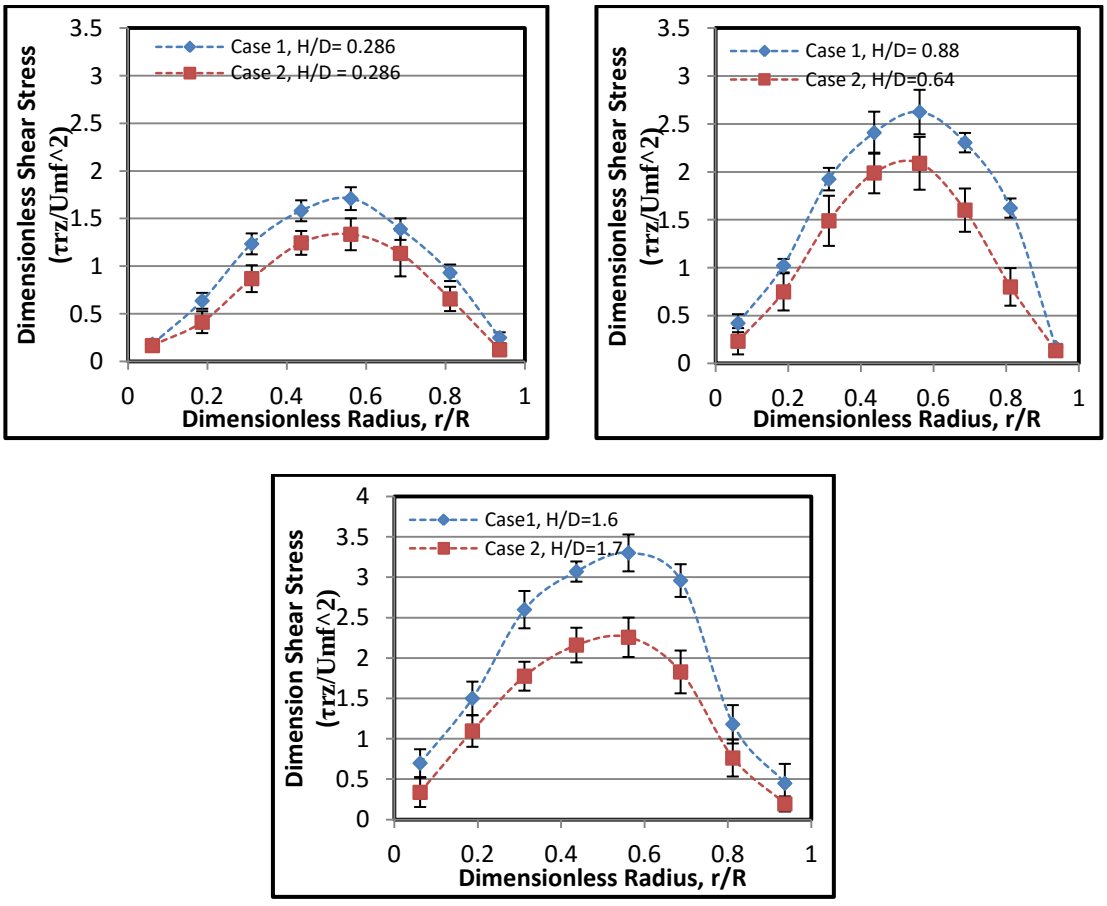

Figure 5.18 Dimensionless time and azimuthally averaged shear stress radial profiles at different H/D ratios for Case 1 (0.44 m) and Case 2 (0.14 m) fluidized bed

5.4.2. Axial Normal Stress Radial Profiles. The axial normal stress for two different fluidized bed sizes Case 1 (0.44 m) and Case 2 (0.14 m) are compared in Figure 5.19. The profiles showed the same trend for both cases, with the maximum values close to the center of the column and low values close to the wall, but their magnitudes were different. The Average Absolute Relative Difference (AARD) at a fully developed region (H/D = 1.7) was 38.7%, at H/D= 0.64 was 37.3% and at H/D = 0.289 was 33.6%.

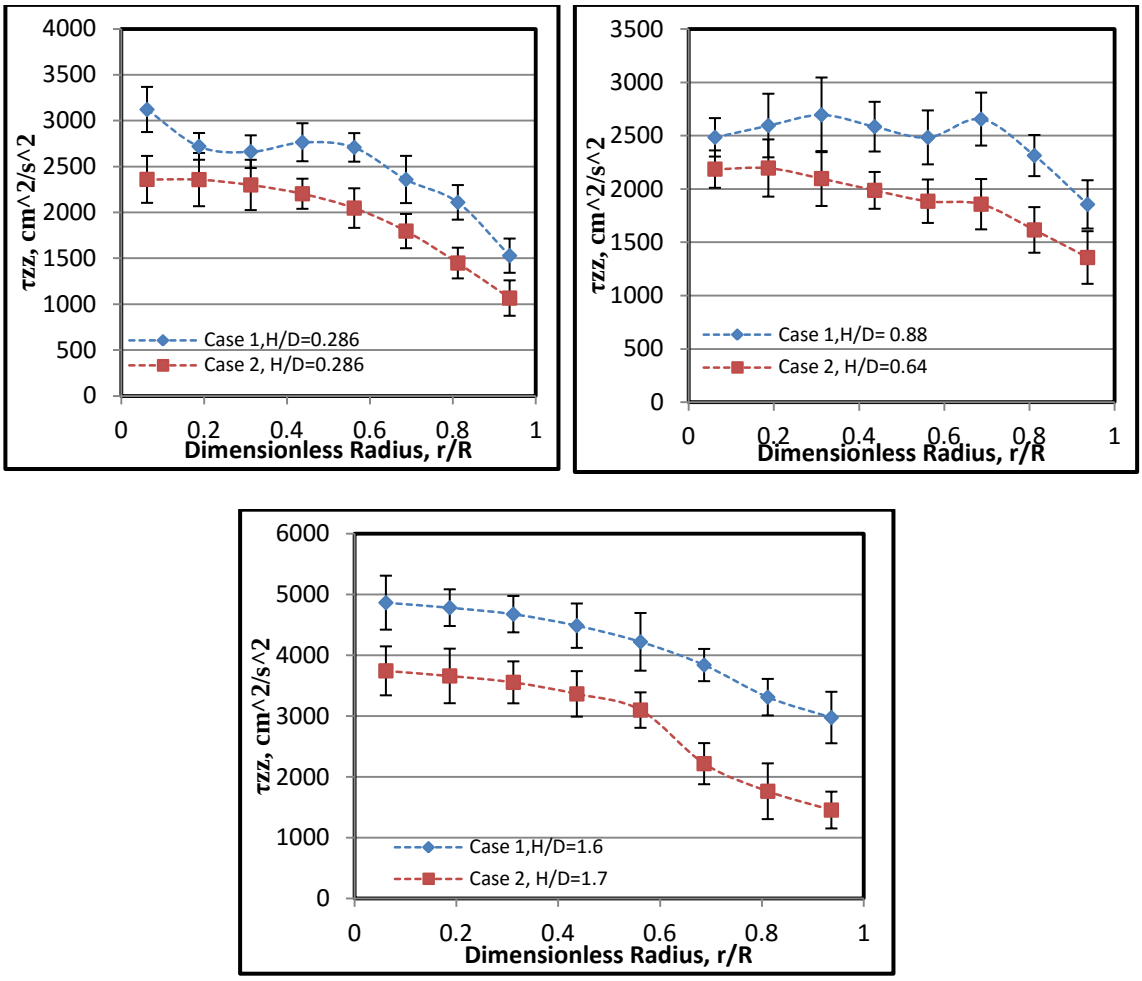

Figure 5.19 Time and azimuthally averaged axial normal stress radial profiles at different H/D ratios for Case 1 (0.44 m) and Case 2 (0.14 m) fluidized bed, (dot lines represent the trend)

The radial profiles of axial normal stress in both fluidized beds case 1 and case 2 are non-dimensionalized by dividing them by the square of the minimum fluidization velocity. Figure 5.20 shows the compared radial profiles of dimensionless axial normal stress in both fluidized beds Case 1 and Case 2. The comparison showed that the profiles are not similar. The average absolute relative difference (AARD) for the radial profiles of dimensionless axial normal stresses between Case 1 and Case 2, at H/D= 0.286 was 38.5%, at H/D= 0.64 was 36.9% and at H/D = 1.7 was 19.7%.

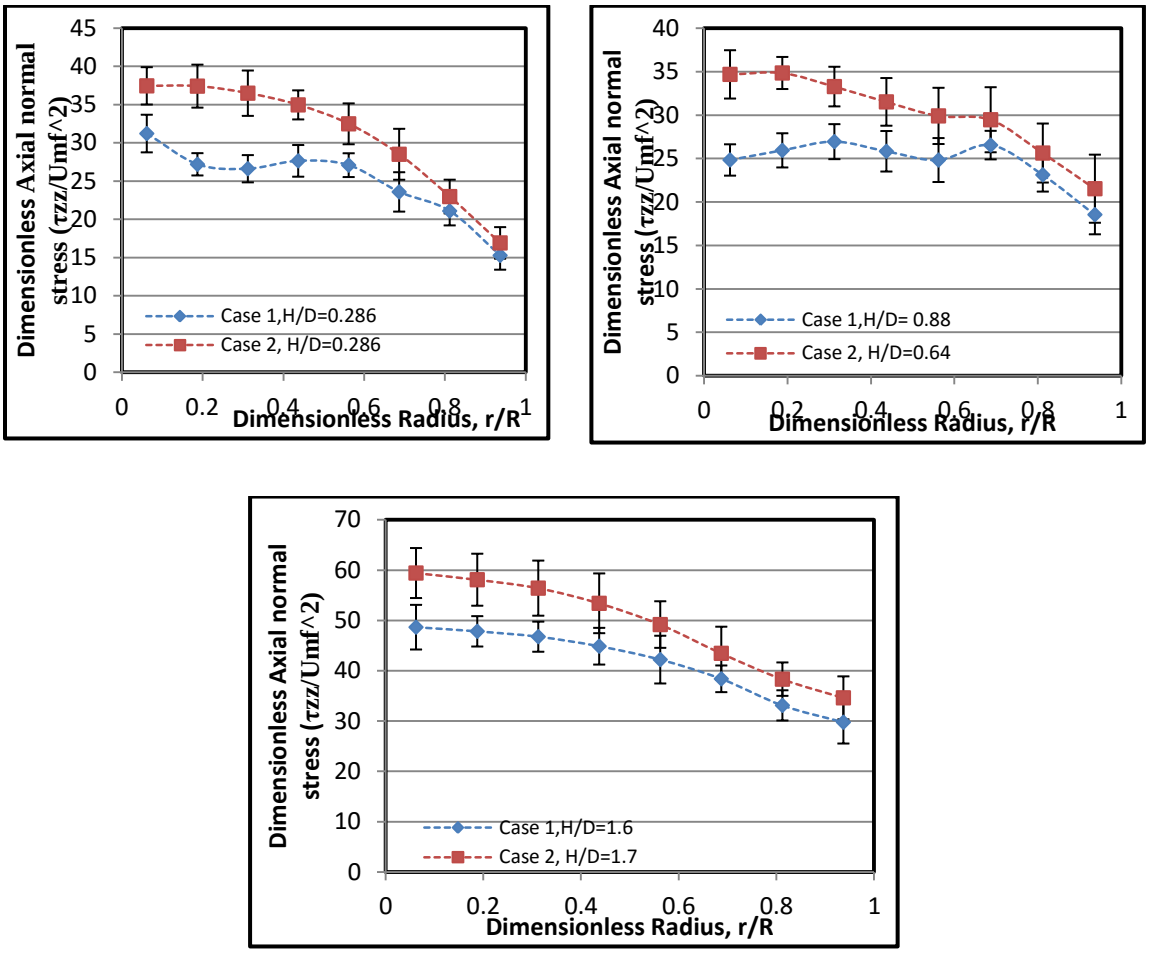

Figure 5.20 Dimensionless time and azimuthally averaged axial normal stress radial profiles at different H/D ratios for Case 1 (0.44 m) and Case 2 (0.14 m) fluidized bed, (dot lines represent the trend)

5.4.3. Turbulent Kinetic Energy (TKE) Radial Profiles. The radial profiles of turbulent kinetic energy (TKE), for Case 1 and Case 2 at different axial positions above the distributor were compared to evaluate how the mismatched gas holdup radial profiles affect mixing intensity. Figure 5.21 shows that, there was a significant quantitative and qualitative difference in their magnitudes. The average absolute relative difference (AARD) for the radial profiles of turbulent kinetic energy (TKE), between the two fluidized beds (case 1 and case 2) was 20.4%, 40.3%, and 47.8%, at H/D = 0.286, 0.644, and 1.7 respectively. The bars shown in the figures represent the standard deviation around the mean as mentioned early.

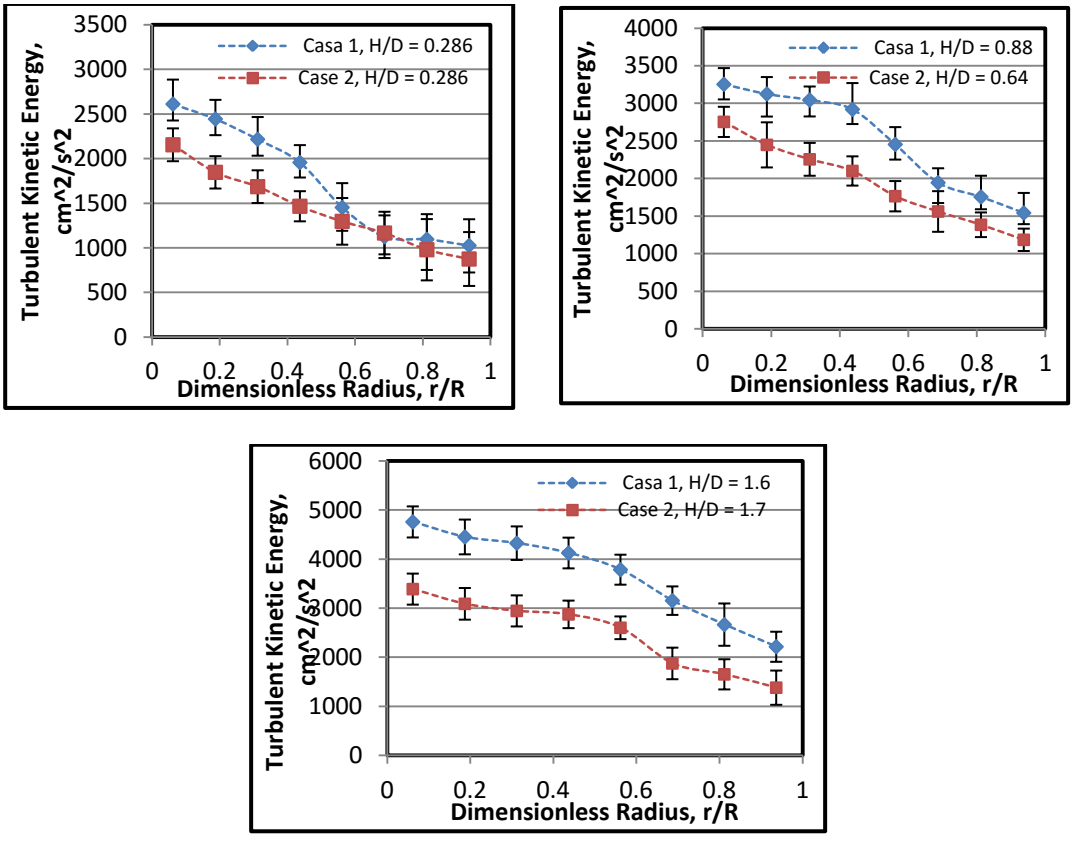

Figure 5.21 Time and azimuthally averaged turbulent kinetic energy radial profiles at different H/D ratios for Case 1 (0.44 m) and Case 2 (0.14 m) fluidized bed, (dot lines represent the trend)

Figure 5.22 shows the comparison of turbulent kinetic energy radial profiles for Case 1 and Case 3 at different axial positions above the distributor. There was a significant difference in their magnitudes. The average absolute relative difference (AARD) between the two fluidized beds (case 1 and case 3) was 12.63%, 43.76%, and 52.6%, at H/D = 0.286, 0.644, and 1.7 respectively.

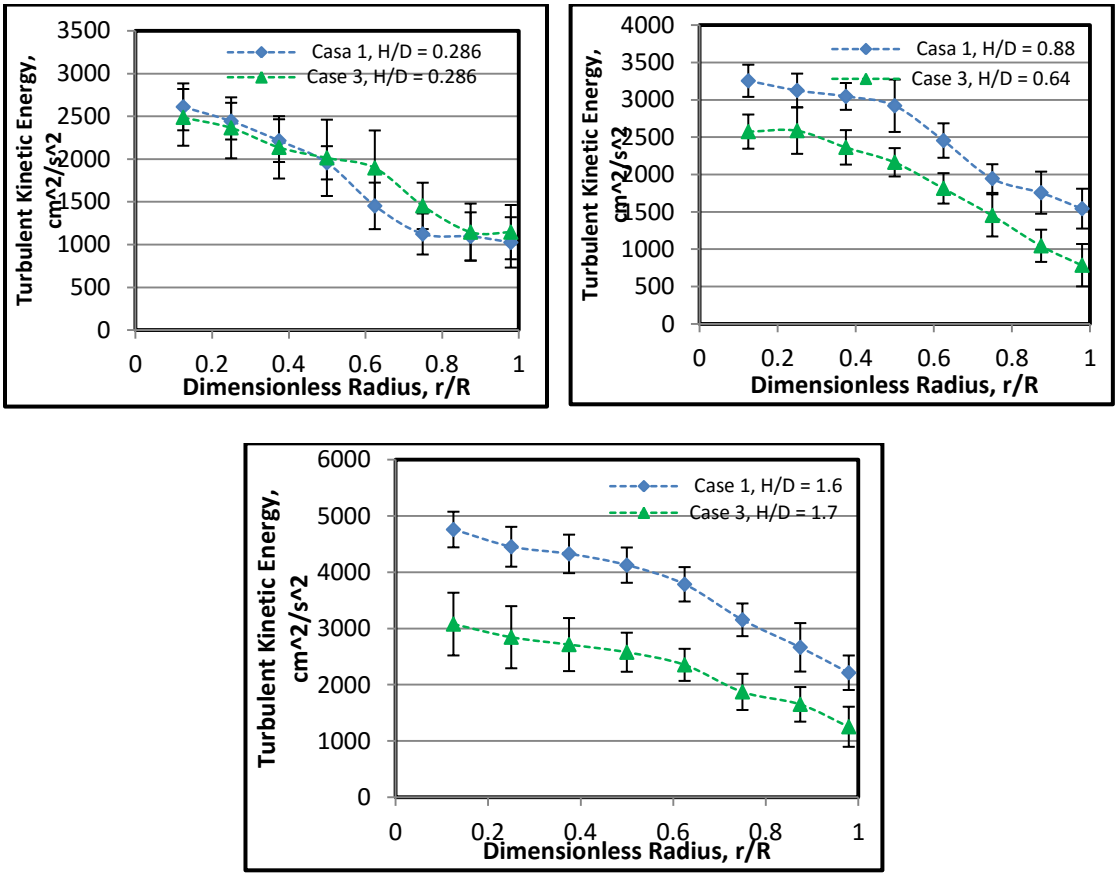

Figure 5.22 Time and azimuthally averaged turbulent kinetic energy radial profiles at different H/D ratios for Case 1 (0.44 m) and Case 3 (0.14 m) fluidized bed, (dot lines represent the trend)

Figure 5.23 shows the variation of ARD in turbulent kinetic energy profiles between Case1 and 2 and also between Case1 and 3 at different axial positions above the distributor.

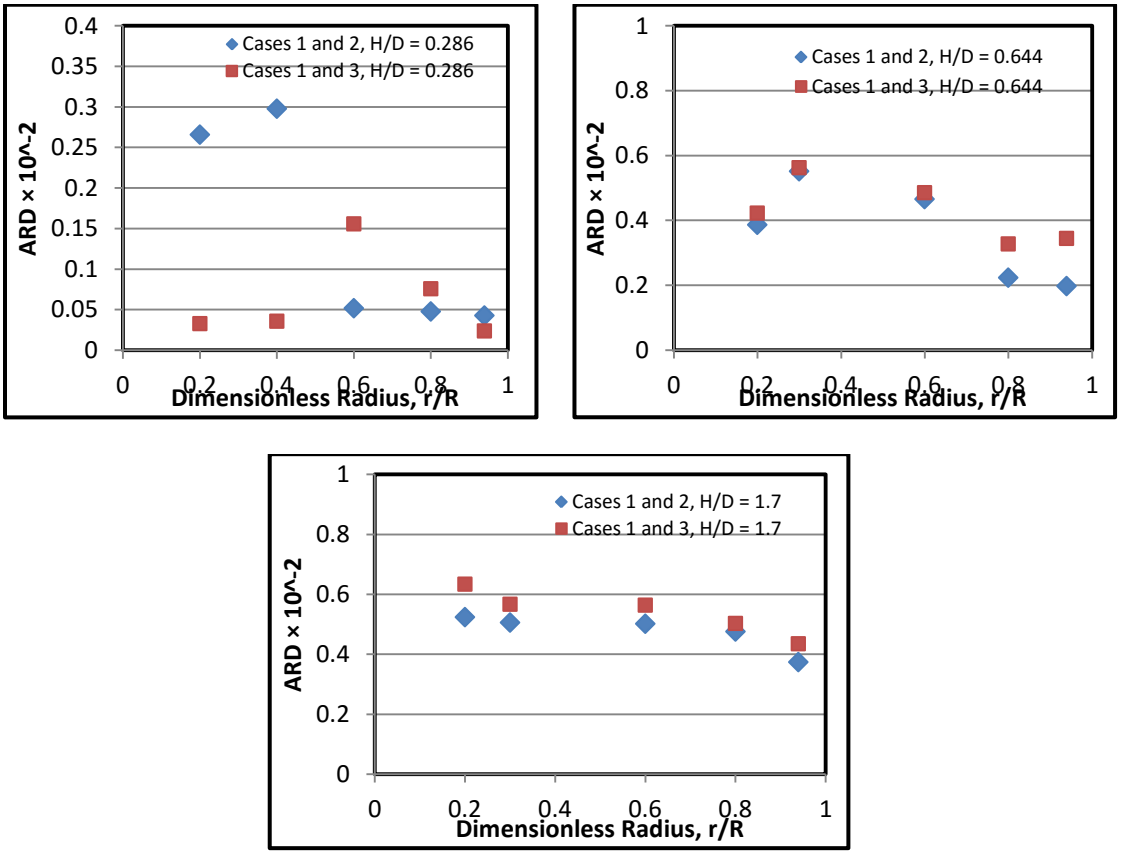

Figure 5.23 The radial variation of ARD in Turbulent kinetic Energy profiles between Case1 and 2 along the column diameter at different axial positions

The radial profiles of turbulent kinetic energy in both fluidized beds (Case 1 and Case 2) are non-dimensionalized by dividing them by the square of the minimum fluidization velocity. The comparison of the radial profiles of dimensionless turbulent kinetic energy in both fluidized beds Case 1 and Case 2 shows that the profiles are not similar. Figure 5.24 shows that, the average absolute relative difference (AARD) for the radial profiles at H/D= 0.286 was 18.4%, at H/D= 0.64 was 32.5% and at H/D = 1.7 was 30.7%

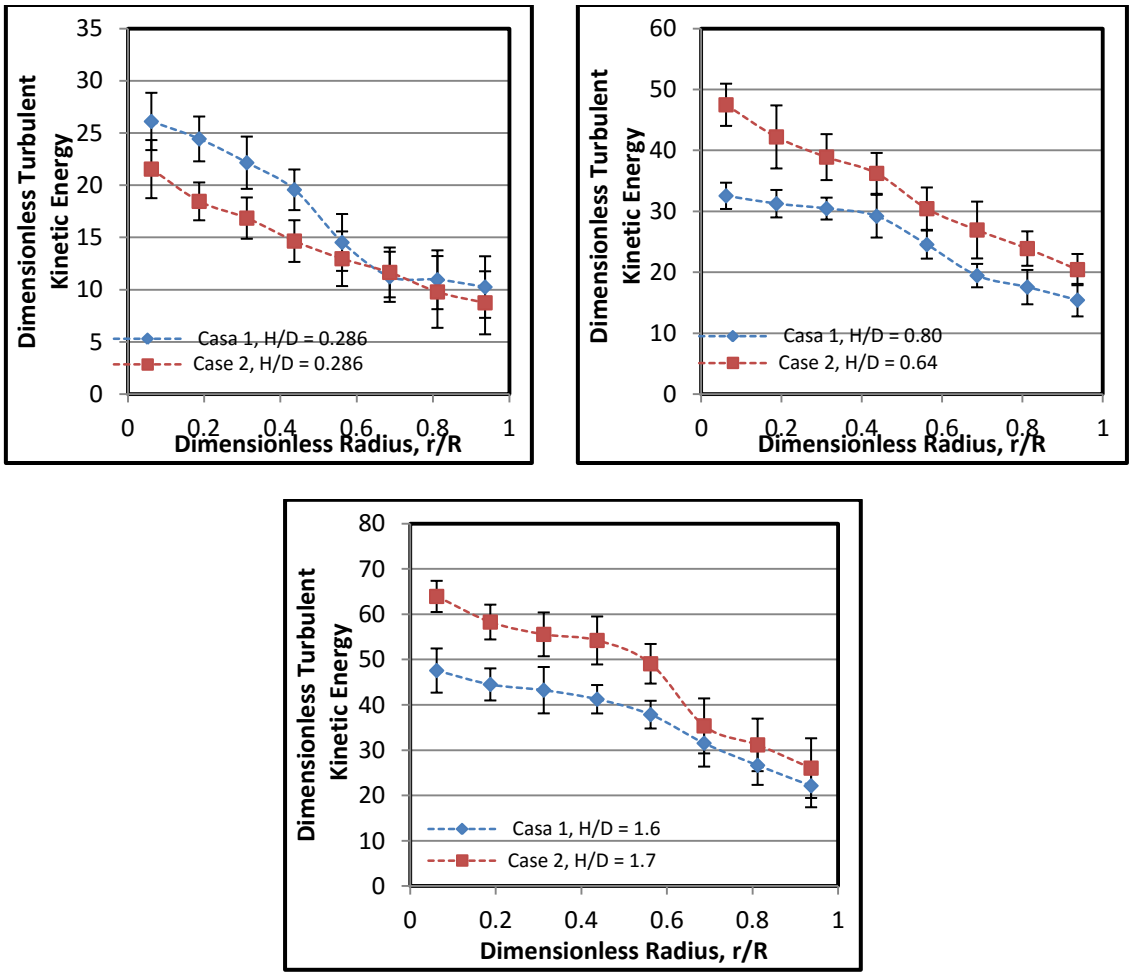

Figure 5.24 Dimensionless time and azimuthally averaged turbulent kinetic energy radial profiles at different H/D ratios for Case 1 (0.44 m) and Case 2 (0.14 m) fluidized beds, (dot lines represent the trend)

5.4.4. Axial and Radial Eddy Diffusivities Radial Profiles. The both axial and radial eddy diffusivities as a function of the radial position for Cases outlined in Table 3.1 at different axial positions above the distributor were measured by using a radioactive particle tracking (RPT) technique. There was a clear difference in axial and also in radial eddy diffusivity profiles between Case 1 and Case 2. Diffusivities in both directions (axially and radial) are higher in the large column (Case 1). Lower solids diffusivity in

smaller column (Case 2 and Case 3) can be attributed to the wall effect where restraining forces caused by the wall of the bed can be considered as an obstacles for mobility of particles, therefore, in the smaller column (Case 2 and 3) in which wall effects is more significant, particles would not be able to diffuse through the bed easily. This finding aligns with the results of previous studies conducted by Mostoufi and Chaouki [36]. They measured the diffusivity of the solids in a bubbling fluidized bed. Mostoufi and Chaouki [28] showed that the solids diffusivities increased with increasing superficial gas velocity and that the diffusivities are correlated with the axial solids velocity gradient.

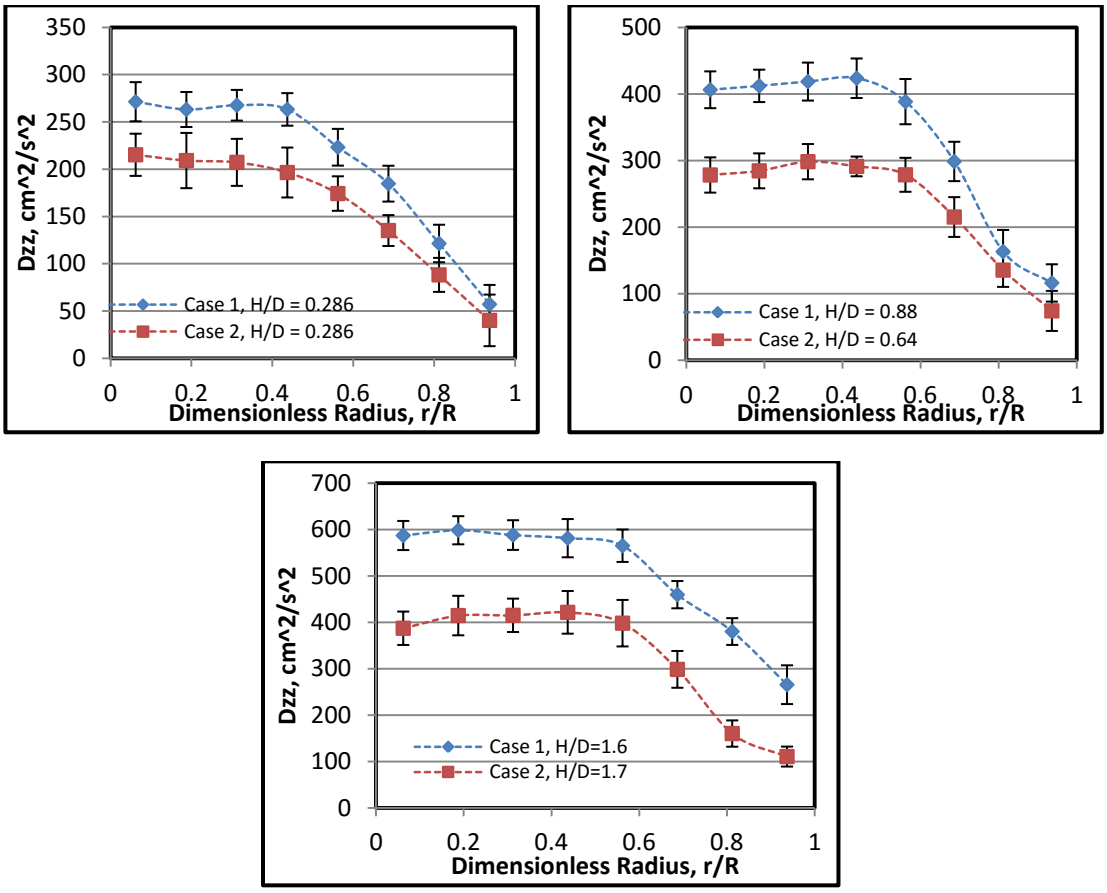

Figure 5.25 Time and azimuthally averaged axial eddy diffusivity radial profiles at different H/D ratios for Case 1 (0.44 m) and Case 2 (0.14 m) fluidized bed, (dot lines represent the trend)

The average absolute relative difference (AARD) for the radial profiles of axial eddy diffusivity between the two fluidized beds (Case 1 and 2), was 28.5%, 45.5%, and 49.58% at H/D = 0.286, 0.644, and 1.7 respectively as shown in Figure 5.25. The variation in the radial profiles of axial eddy diffusivity between the two beds of Case 1 and 3 have been observed at all three levels of the measurements. Figure 5.26 demonstrates axial eddy diffusivity for those two cases at the different axial levels. The average absolute relative difference (AARD) was 47.8%, 52.3%, and 57.6% at H/D = 0.286, 0.644, and 1.7 respectively.

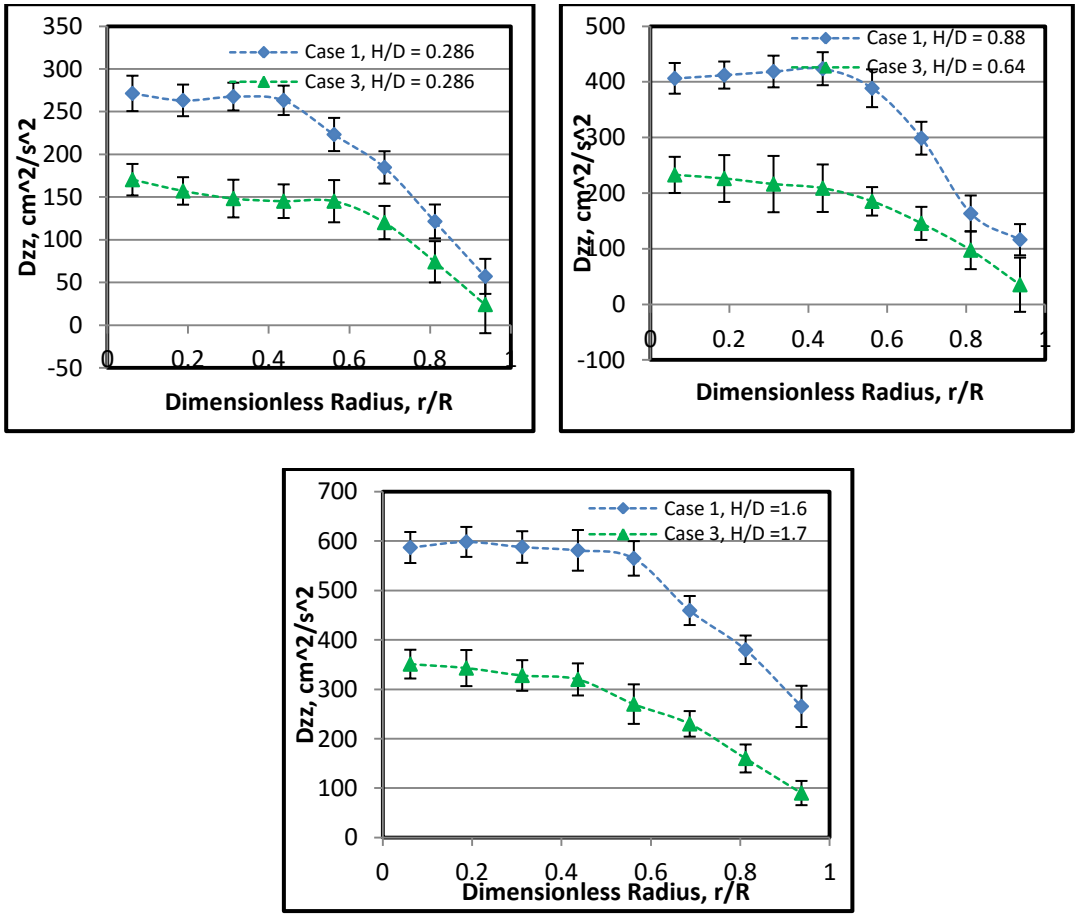

Figure 5.26 Time and azimuthally averaged axial eddy diffusivity radial profiles at different H/D ratios for Case 1 (0.44 m) and Case 3 (0.14 m) fluidized bed (dot lines represent the trend)

Figure 5.27 shows the variation of ARD in axial eddy diffusivity profiles between Case1 and 2 and also between Case1 and 3 at different axial positions above the distributor.

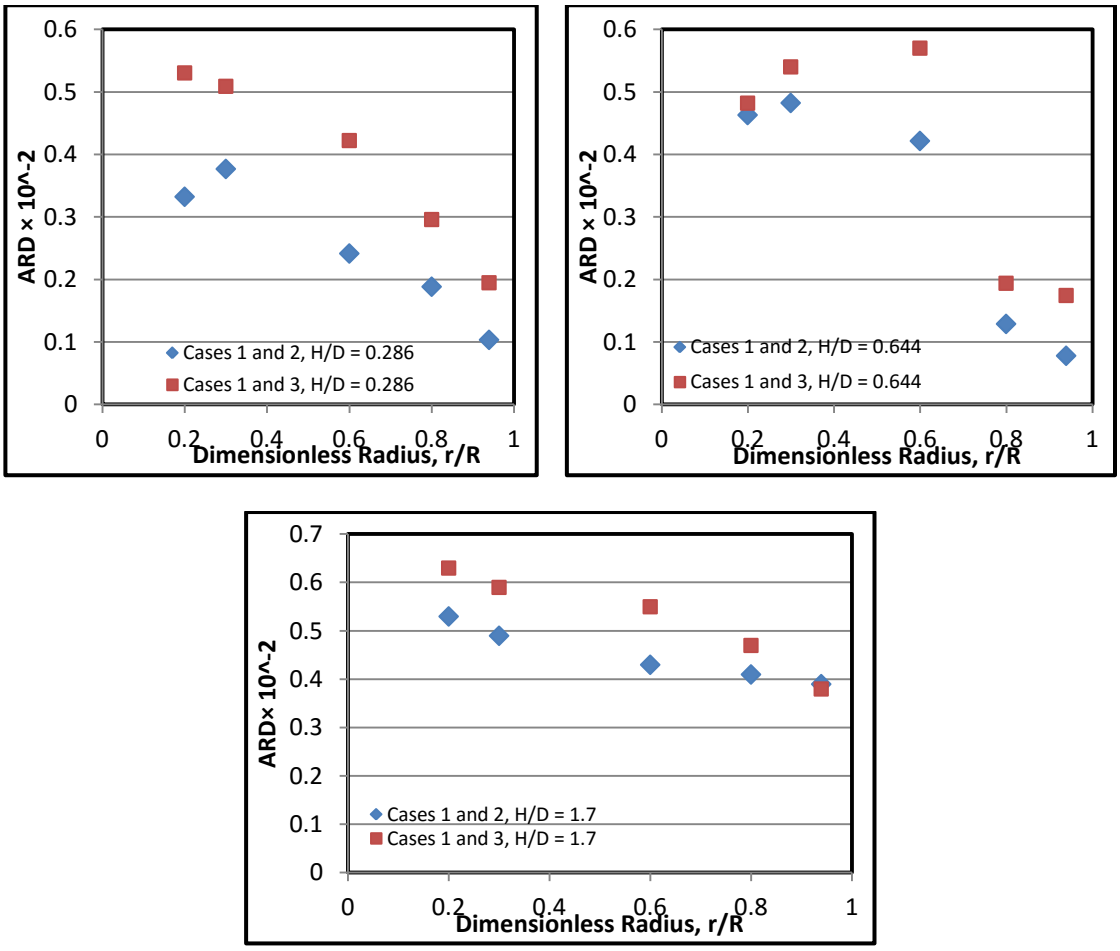

Figure 5.27 The radial variation of ARD in axial eddy diffusivity profiles between Case1 and 2, and between Case 1 and 3 at different axial positions above the distributor

The average absolute relative difference (AARD) for the radial profiles of radial eddy diffusivity, between Case 1 and Case 2 Figure 5.28 was 47.85%, 48.65%, and 42.5% at H/D = 0.286, 0.644, and 1.7 respectively.

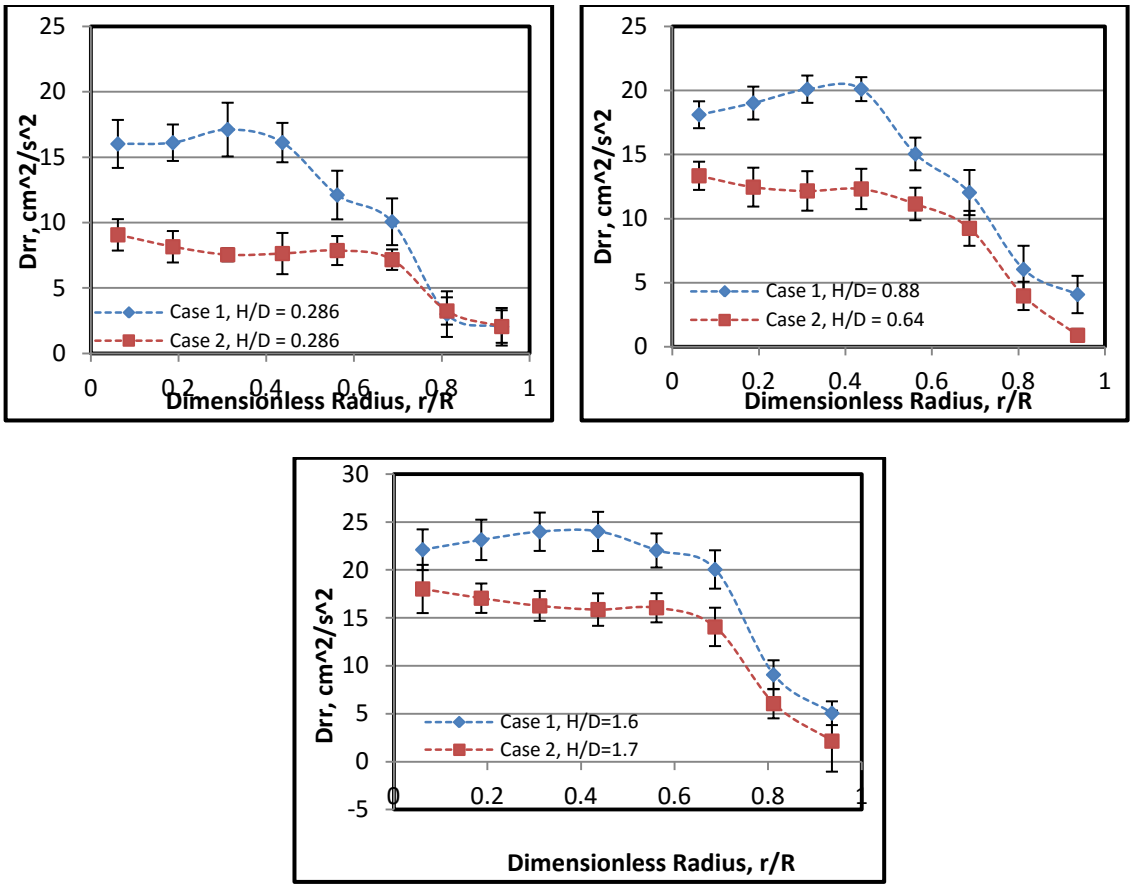

Figure 5.28 Time and azimuthally averaged radial eddy diffusivity radial profiles at different H/D ratios for Case 1 (0.44 m) and Case 2 (0.14 m) fluidized bed, (dot lines represent the trend)

The radial profiles of axial and radial diffusivity in both fluidized beds case 1 and case 2 are non-dimensionalized by dividing the by the square of the minimum fluidization velocity. Figure 5.29 shows the compared radial profiles of dimensionless axial diffusivity at difference axial positions above the distributor, while Figure 5.30 shows the compared radial profiles of dimensionless radial diffusivity in both fluidized beds Case (1) and Case (2). The comparison shows that the profiles are not similar. The average absolute relative difference (AARD) for the radial profiles of dimensionless axial diffusivity between Case 1 and Case 2, at H/D= 0.286 was 25.3%, at H/D= 0.64 was 28.9% and at H/D = 1.7 was 30.8%. And The average absolute relative difference

(AARD) for the radial profiles of dimensionless radial diffusivity between two scaled fluidized beds, Case 1 and Case 2, at H/D= 0.286 was 39.7%, at H/D= 0.64 was 35.7% and at H/D = 1.7 was 38.6%.

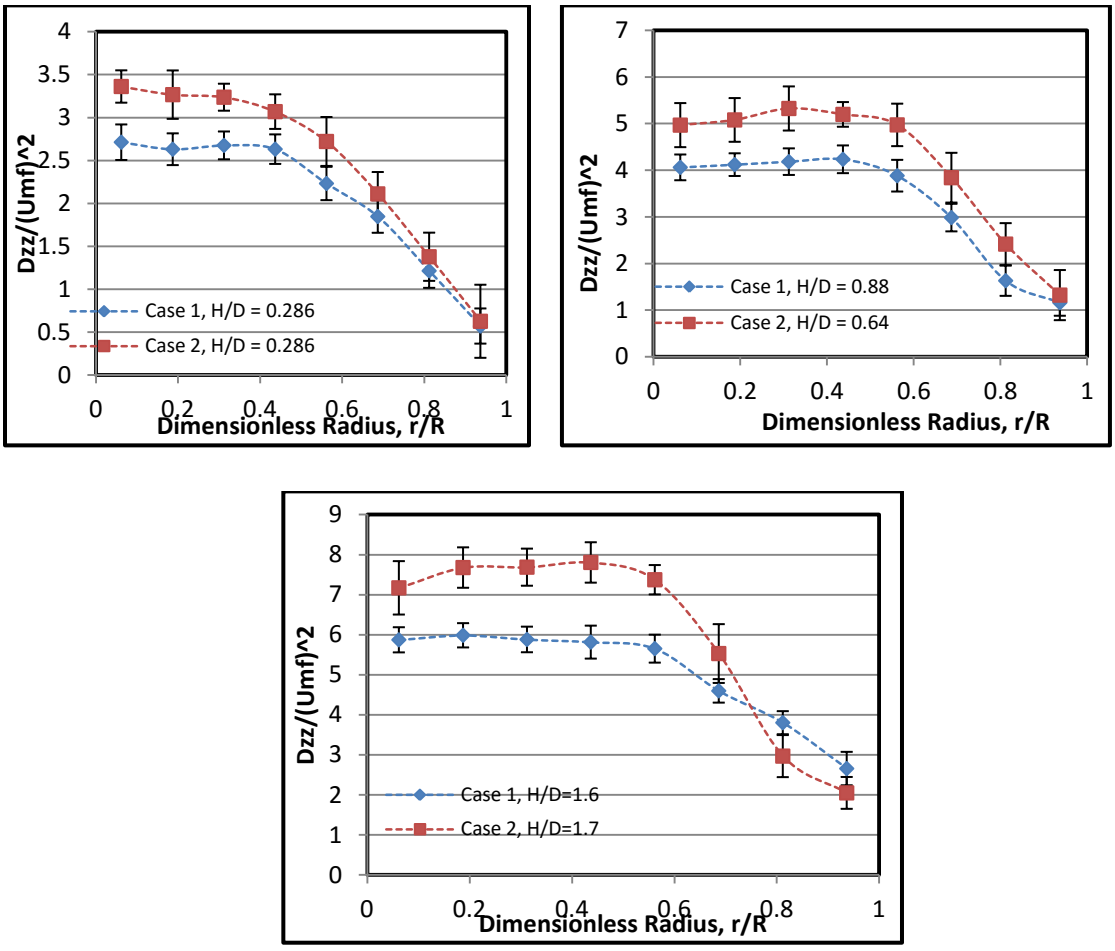

Figure 5.29 Dimensionless time and azimuthally averaged axial eddy diffusivity radial profiles at different H/D ratios Case 1 (0.44 m) and Case 2 (0.14 m) fluidized beds

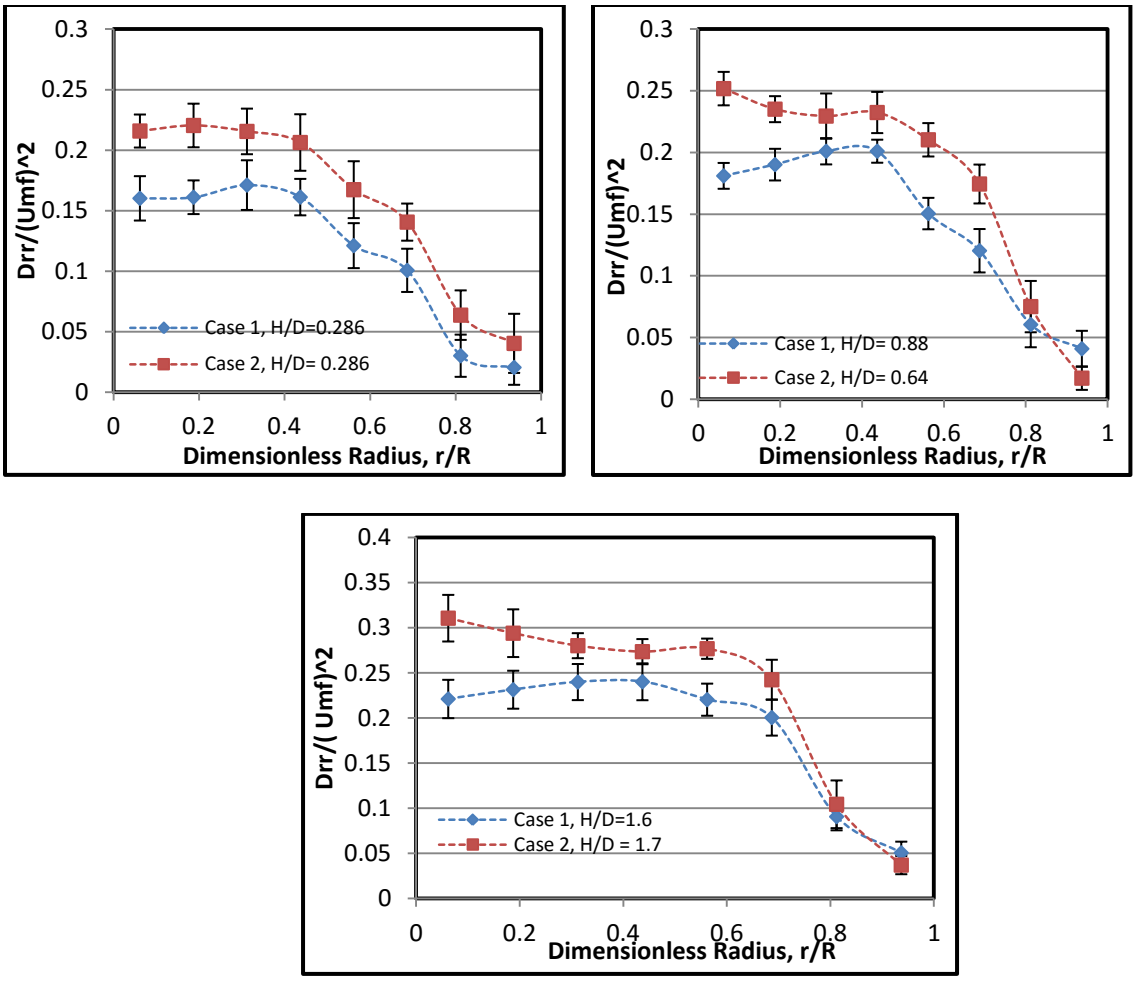

Figure 5.30 Dimensionless time and azimuthally averaged radial eddy diffusivity radial profiles at different H/D ratios for Case 1 (0.44 m) and Case 2 (0.14 m) fluidized bed, (dot lines represent the trend).

6. REMARKS

In this work we evaluated the scale-up of fluidized bed reactors based on matching dimensionless groups methodology that proposed by Glicksman et al., [1] by utilizing CT and RPT as advance non-invasive techniques, that provided detailed local hydrodynamic parameters. It was observed that the local hydrodynamics for the studied conditions of fluidized beds are not similar when the dimensionless groups of Glicksman et al., [1] are matched.

The variation shown in the local parameters, confirms that global parameters are not adequate to assess the scale-up methodology. The assessment of the conditions for matching dimensionless groups (Case 1and case 2), suggests that current dimensionless groups are insufficient to explain the complete hydrodynamics of the fluidized bed system. Therefore, the scale-up methodology of dimensional analysis for fluidized beds should be modified to establish a reliable scale-up methodology, not only considering the similarity in global hydrodynamics, but also considering the similarity in local hydrodynamics. However, adding more dimensionless groups to match in order to capture the needed similarity in hydrodynamics will make its implementation difficult since it is very hard in practice to match large number of dimensionless groups.

ACKNOWLEDGMENT

The authors wish to acknowledge the Libyan Ministry of Education for sponsoring the primary author's study within the Chemical and Biochemical Engineering Department at Missouri University of Science and Technology. Also the primary author would like to acknowledge the use of the gamma ray, radioactive particle tracking techniques, experimental facilities set-up and materials that were used in this work and funded by professor Al-Dahhan's research fund.

REFERENCES

[1] Glicksman, L. R., Hyre, M. and Woloshun, K. Simplified Scaling Relationships for Fluidized Beds. Powder Technology, 77, pp. 177-199, 1993.

[2] Dubrawski, K., Tebianian, S.,Bi, H.T.,Chaouki,J.,Ellis,N.,Gerspacher,R.,Jafari,R., Kantzas, A.,Lim,C.,Patience,G.S.,Pugsley,T.,Qi,M.Z.,Zhu,J.X.,Grace,J.R. Traveling column for comparison of invasive and non-invasive fluidization voidage measurement techniques.PowderTechnol.235, pp. 203–220, 2013.

[3] R., Tilman, J. Schildhauer, Serge M.A. Biollaz J. Ruud van Ommen. Scale-up of bubbling fluidized bed reactors - A review. Powder Technology , 217, pp. 21-38, 2012.

[4] Al-Dahhan, M.H., Shreekanta, A., Faraj, Z., Neven, A., Thaar, A. 2014. Scale-up and on-line monitoring of gas-solid system using advanced and non-invasive measurement techniques, Symphos 2013, 2nd International Symposium on Innovation and Technology in the Phosphate Industry, 2014.

[5] Romero, J. B., Johanson, L. N. Factors affecting fluidized bed quality. Chemical Engineering Progress, Symposium Series, 58(38), pp. 28–32, 1962.

[6] Broadhurst, T. E., Becker, H. A. The application of the theory of dimensions to fuidized beds. In Proc. Int. Symp. Ste. Chimie Indust., Toulouse, France, 1973.

[7] Glicksman, L. R. Scaling Relationships for Fluidized Beds. Chemical Engineering Science 39, pp. 1373-1379, 1984.

[8] Fitzgerald, T., Bushnell, D., Crane, S., Yeong-Cheng Shieh. Testing of cold scaled bed modeling for fluidized-bed combustors. Powders Technology 38, pp. 107-120, 1984.

[9] Nicastro, M.T., Glicksman, L.R. 1984. Experimental verification of scaling relationships for fluidized bed. Chemical Engineering Science 39, pp. 1381-1391, 1984.

[10] Newby, R.A., Keairns, D.L. 1986. Test of the scaling relationships for fluidized-bed dynamics, in fluidization, Engineering Foundation, New York, pp. 31-38, 1986.

[11] Glicksman, L. R. Scaling Relationships for Fluidized Beds. Chemical Engineering Science, 43, pp. 1419-1421, 1988.

[12] Knowlton, T.M., Karri, S.B.R., Issangya, A. Scale-up of Fluidized-Bed Hydrodynamics. Powder Technology, 150, No. 2, pp. 72-77, 2005.

[13] Horio, M., Akira, N., A., Yoshitaka, S., Iwao, M. A new similarity rule for fuidized bed scale-up. A.I.Ch.E. Journal 32, pp. 1466–1482, 1986.

[14] Van Ommen, J.R., Teuling, M., Nijenhuis, J., Van Wachem BGM. Computational validation of the Scaling Rules for Fluidized Beds. Powder Technology, 163(1-2), pp. 32-40, 2006.

[15] Foscolo, P.U., Di Felice, R., Gibilaro, L.G., Piston, L., Piccolo.V. 1990. Scaling relationships for fluidization: The generalized particle bed model. Chemical Engineering Science, 45, pp. 1647-1651, 1990.

[16] Stein, M., Ding, Y.L., Seville, J.P.K. Experimental verification of the scaling relationships for bubbling gas-fluidized beds using the PEPT technique, Chemical Engineering Science, 57, pp. 3649-3658, 2002.

[17] Zaid, F. Gas-solid fluidized bed reactors: scale-up, flow regimes identification and hydrodynamics, PhD, thesis, Missouri University of Science & Technology, Rolla, 2013.

[18] Horio, M., Ishii, H., Kobuki, Y., Yamanishi, N. A Sacling Law for circulating fluidized beds. Journal of Chemical Engineering of Japan, 22, pp. 587-592, 1989.

[19] Bonniol, F., Sierra, C., Occelli, R., Tadrist, L. Similarity in dense gas-solid fluidized bed, influence of the distributor and the air-plenum, Powder Technology 189, pp. 14-24, 2009.

[20] Suksankraisorn. K., Patumsawad. S., Fungtammasan. B. Prediction of minimum fluidization velocity from correlations: An observation. Asian J. Energy Environ, 2 issue 2, pp. 145-154, 2001.

[21] Varma R. Characterization of anaerobic bioreactors for bioenergy generation using a novel tomography technique. Thesis, PhD, Washington University in St. Louis, Saint Louis, Mo, USA. 2008.

[22] Varma R, Bhusarapu S, O'Sullivan, JA, Al-Dahhan, M.H. A comparison of alternating minimization and expectation maximization algorithms for single source gamma ray tomography. Measurement Science & Technology, Vol 19(1), pp. 1-13, 2007.

[23] Bhusarapu, S.B. Solids flow mapping in gas-solids risers. Thesis, PhD, Washington University, St. Louis, 2005.

[24] Bhusarapu S, Al-Dahhan M.H, Dudukovic M.P. 2006. Solids Flow Mapping in a Gas-Solid Riser: Mean Holdup and Velocity Fields. Powder Technology, 163, (1-2), 98-123.

[25] Fadha, A. Experimental Investigation of The Pebble Bed Structure by Using Gamma Ray Tomography, master thesis, Missouri University of Science & Technology, Rolla, 2014.

[26] Al-Mesfer, M. Effect of dense heat exchanging internals on the hydrodynamics of bubble column reactors using non-invasive measurement techniques. Thesis, PhD, Missouri University of Science & Technology, Rolla, 2013.

[27] Tebianian, S., Dubrawski, K., Ellis, N., Cocco, R., D.J. Parker., Chaouki, J. Investigation of particle velocity in FCC gas-fluidized beds based on different measurement techniques, Chemical Engineering Science, 127, PP. 310–322, 2015.

[28] Mostoufi, N., Chaouki, J. Local solid mixing in gas–solid fluidized beds, Powder Technology 114, pp. 23–31, 2001.

[29] Mosfoufi N., Chaouki J. Flow Structure of Solids in Gas-Solid Fluidized Bed, Chemical Engineering Science. 59, pp. 4217, 2004.

[30] Degaleesan, S. 1997. Turbulence and liquid mixing in bubble columns. Thesis, PhD, Washington University, Saint Louis, Missouri, USA, 1997.

[31] Degaleesan, S., Dudukovic, MP, Pan, Y. Application of wavelet filtering to the radioactive particle tracking technique. Flow Measurement and Instrumentation, 13(1-2), PP. 31- 43, 2002.

[32] Roy, S. Quantification of Two-phase Flow in Liquid-solid Risers, PhD, Thesis,PhD, Washington University in St. Louis, Saint Louis, MO, USA, 2000.

[33] Upadhyay, R., Roy. S. Investigation of hydrodynamics of binary fluidized beds via radioactive particle tracking and dual-source densitometry, The Canadian journal of chemical Eng. Vol. 88, 2010.

[34] Wang, Q., Zhnag, K., Yang, K., Jiang, J. Particle velocity in a Dense Gas-Solid Fluidized Bed. Inter. J. of Chemical Reactor Eng, 2008.

[35] Laverman, J.A ., Fan, X., Ingram, A., van Sint Annaland, M, Parker DJ, Seville, J.P.K, Kuipers, J.A.M. Expermental study on the influence of bed material on the scaling of solids circulation patterns in 3D bubbling gas-solid fluidized beds of glass and polyethylene using positron emission particle tracking . Power Technol, 224, pp. 297-305, 2012.

[36] Mosfoufi, N., Chaouki, J. On The Axial Movement of Solids in Gas-Solid Fluidized Beds. I ChemE, Vol 78, Part A, 2000.

[37] Bashiri H., Ramin R., Rahmat S., Chaouki J. Effect of Bed Diameter on the Hydrodynamics of Gas-solid Fludized beds, Iran. J. Chem.Eng. Vol.29, No.3, 2010.

III. LOCAL TIME-AVERAGED GAS HOLDUP IN FLUIDIZED BED REACTOR USING GAMMA RAY COMPUTED TOMOGRAPHY TECHNIQUE (CT)

Abdelsalam Efhaima and Muthanna H. Al Dahhan

Department of Chemical and Biochemical Engineering, Missouri University of Science and Technology, 1101 North State Street. 110 Bertelsmeyer Hall, Rolla, MO 65409,USA, ayed67@mst.edu

ABSTRACT

Many invasive and non-invasive techniques have been used to analyze the hydrodynamics of fluidized beds. In this study, the effect of superficial gas velocity and bed particle density on the hydodynamics of gas-solid fluidized beds was investigated by using a cylindrical plexiglas fluidized bed column, 14 cm in diameter. Air at room temperature was used as the fluidizing gas and two different Geldart type-B particles were used: glass beads and copper particles with material densities of 2.5 and 5.3 g/cm^3, respectively, with the same size particle, 210 μm. To measure the time-averaged cross-sectional gas and solid holdup distribution, gamma ray computed tomography (CT) used for the first time as a non-invasive technique instead of using x-rays (due to the height attenuation of the copper particles). The results show that gas hold-up increases by increasing the superficial gas velocity, decreasing the particle density increases the gas hold-up in the bed.

Keywords: Fluidized beds, hydrodynamics, Gamma ray Computed Tomography, Gas holdup, Solid holdup

1. INTRODUCTION

Contacting solid particles with gases is often a necessity in many industrial operations. The gas-solid fluidized bed reactor (FBR). is one of the most widely employed gas-solid reactors. Fluidized beds provide good mixing, height mass and heat transfer rates between gas and solid particles, low pressure drop, approximately uniform temperature distribution, and the ability to fluidize many particle types of different densities and sizes. Due to these advantages, fluidized bed reactors (FBRs) are extensively used in many industrial applications such as drying granular materials, cooling of fertilizers, coal combustion and gasification, chemical process, , gas phase polymerization and for various uses in the pharmaceutical and petroleum industries McCabe et al. [1].

Phosphate rock deposits vary in composition. To prepare the phosphate rock for making phosphoric acid, which is then utilized in subsequent reactions; (i.e., the manufacture of triple superphosphate and for other valuable products), it is necessary to beneficiate the phosphate rock by removing certain of the impurities. Very often, a substantial amount of limestone ($CaCO_3$) is associated with the phosphate rock, and a calcining operation is indicated to drive off the CO_2. One commercial method for the calcinations of phosphate rock employs a fluidized bed reactor. In this process, finely divided phosphate rock is dried in the first fluidized bed and then transported to a second fluidized bed, where calcinations take place. Drying is very important process, as effective moisture removal, defines the process efficiency and the subsequent unit operations. The drying process can be characterized as a gas-solid fluidized bed system.

The performance of these multiphase fluidized bed reactors greatly depends on their hydrodynamic properties, therefore understanding the hydrodynamics behavior of fluidized bed reactors is essential for their proper design, effectively scale-up, and efficient operation.

Although considerable research efforts have focused on the hydrodynamics of the fluidized bed, such as studying the shape and size of bubbles/void, the solid concentration, solid holdup distribution, gas holdup distribution at different gas velocities, and turbulence parameters (Reynolds stresses, normal stresses, turbulent kinetic energy, turbulent eddy diffusivities, etc), the lack of accurate, instantaneous, and simultaneous techniques for measurement along the bed cross-section prevents a precise description of the dynamic flow behavior in the fluidized bed.

In order to obtain deeper insight into a highly complex gas and solid flow system, detailed and accurate experimental works are obviously important. The hydrodynamic properties in a fluidized bed can be measured using invasive techniques, such as the capacitance probe and the optical fiber probe. These approaches cannot adequately monitor internal flow features. Also, since fluidization is a dynamic process, invasive monitoring methods can influence the internal flow, In addition, it is, difficult to measure the simultaneous flow variations across the bed with such tools. Instead, such measurements need to be carried out with non-invasive techniques, such as the pressure transducer and tomography techniques, e.g., electrical capacitance tomography (ECT), x-ray computed tomography, and γ-ray computed tomography (CT). Among various tomography techniques, the γ-ray computed tomography technique exhibits versatility for

practical usage for the imaging of multiphase flow systems and suitability for height attenuation particles, as well as for small and large vessels.

One of the earliest applications of computed tomography (CT) to two-phase flow was the study by Fincke et al. [2], they obtained density distributions for a horizontal air-water flow in a 3-inch diameter pipe. Nine detectors arranged in an arc were used and 21 views at 9 ° increments were obtained for a total of 189 data values. From this data they were able to obtain density maps corresponding to different flow regimes.

Seville et al. [3] used a single-source single-detector arrangement capable of translation and rotation about the test section. They obtained the voidage structure in the jet region of a fluidized bed. The total time for scanning one section was 6-7 hours.

Banholzer et al. [4], used a medical x-ray CT scanner to conduct a feasibility study on a model fluidized bed (43 mm ID and 150 mm long) under a range of experimental conditions. A spatial resolution of 1.5 mm and a density resolution of better than 30 kg m^3were achieved.

Grassler and Wirth [5], used X-ray computed tomography (CT) imaging to determine the solid concentration in a 0.19 m diameter circulation fluidized bed with 50-70μm glass beads as the bed material, they showed that the radial solid concentration exhibited a parabolic shape with a maximum concentration close to the wall of the reactor and a minimum concentration in the centre of the bed.

X- ray computed tomography (CT) imaging was used by Escudero et al. (2011) to determine bed height and material density effects on fluidized bed hydrodynamics in a 10.2 cm fluidized bed, using low-density materials. They used three different materials: Geldart-type-B particles (glass beads, ground walnut shell and ground corncob) with

material densities of 2.6, 1.3, and 1 g/cm^3, respectively. Results showed that decreasing the bed density increased the gas holdup in the bed.

Escudero et al. [6] also studied the profiles of solid holdup for low-density materials at various superficial gas velocities at specific H/D ratios and found that the solid holdup decreased by increasing the superficial gas velocity.

Zhu et al. [7] determined the solid volumetric fraction (1-εg) in gas-solid systems for bubbling and turbulent fluidization regimes. The turbulent regime showed that solid concentrations were not uniform in the axial or radial direction. In the bubbling regime, the non-uniformity increased as the superficial gas velocity increased.

Du et al. [8] measured the solid concentration for bubbling and turbulent fluidized beds. Results showed that at high superficial gas velocities, especially in the turbulent regime, the cross-section solids holdup exhibited a radially symmetric distribution, which this was not the case for the bubbling regime. At low superficial gas velocity in the bubbling regime, dispersed bubble produced a lower solid concentration (high solid holdup) in the center of the bed.

Mabrouk et al. [9] studied the axial and radial profiles of the solids holdup using an optical fiber probe and radioactive particle tracking (RPT) technique. The axial solid hold-up profiles obtained by an optical fiber needle probe and radioactive particle tracking technique show a quasi-linear profile.

2. EXPERIMENTAL SET-UP

A cold-flow fluidized bed was used in this study, with outside diameter 14 cm and a height of 168 cm. A schematic diagram of the setup used in this study is provided in Figure 2.1. The fluidized bed column was constructed from plexiglas and consisted of two pieces (column and cone) attached to a plenum base. Connected from the top with an upper section that had a diameter of 42 cm and was 84 cm tall, this upper section of the fluidized bed had a larger diameter to reduce the superficial gas velocity of the gas phase and thus enhance the solids separation. The column sat at the top of a stainless steel base. A porous polyethylene sheet with a pore size of 40 μm was employed as the gas distributor. The plenum was located at the bottom. The fluidized bed column was electrically grounded to minimize electrostatic effects. Air under ambient conditions was the fluidizing gas. The gas flow rate to the unit was controlled by rotameters.

Table 2.1 Summary of the bed materials and their properties

Material Properties	Glass beads	Copper Particles
Particle Diameter (μm)	210	210
Bed Height (H/D)	2	2
Particle Density (g/cm^3)	2.5	5.3
Minimum Fluidization velocity (cm/s)	12	20

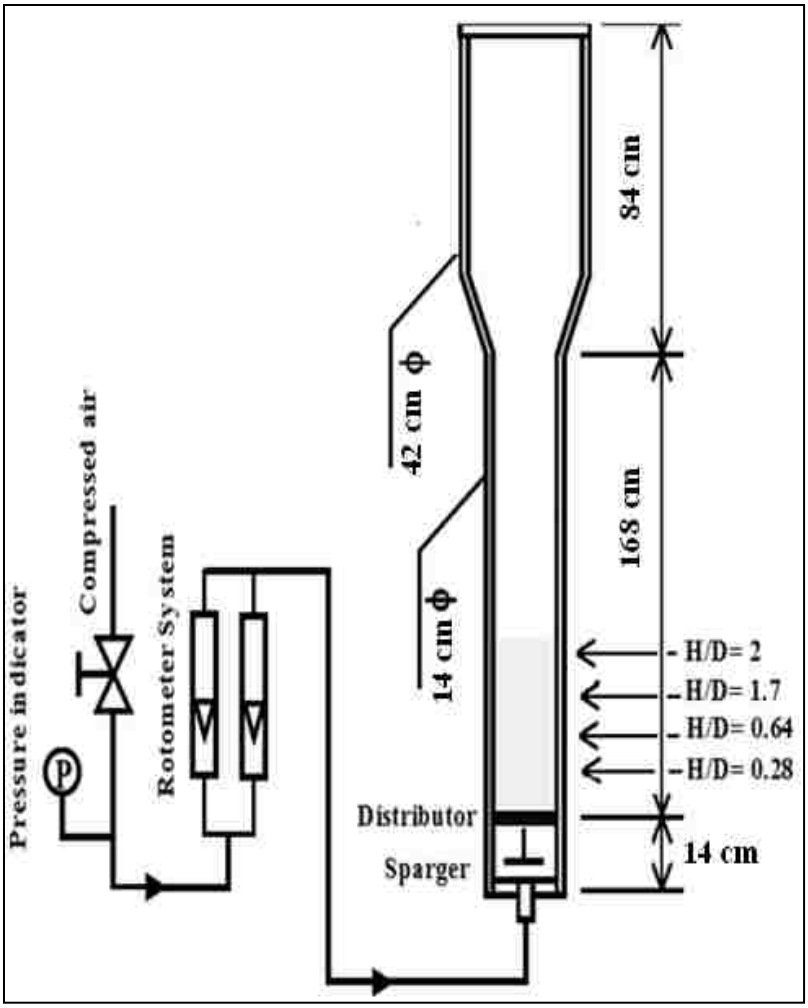

Figure 2.1 Schematic of the cold–flow fluidized bed reactor

3. MEASUREMENT TECHNIQUES

3.1 COMPUTED TOMOGRAPHY (CT)

3.1.1. CT Facility and Measurement Procedure. The dual source computed tomography (DSCT) scanner at Missouri University of Science and Technology which was developed by Varma [10] with support from the Department of Energy (DOE) was used in this work to determine the time-averaged cross-sectional variation of gas and solid holdups at the operating conditions previously outlined (see Table 2.1). The CT used in this study was based on a newer generation of double fan-beam scanning configuration. Details on both the hardware and the software used in this study have been described by (Varma and Al-Dahhan [11], Varma et al. [12]). A photograph of the CT facility used in this study is pictured in Figure 3.1

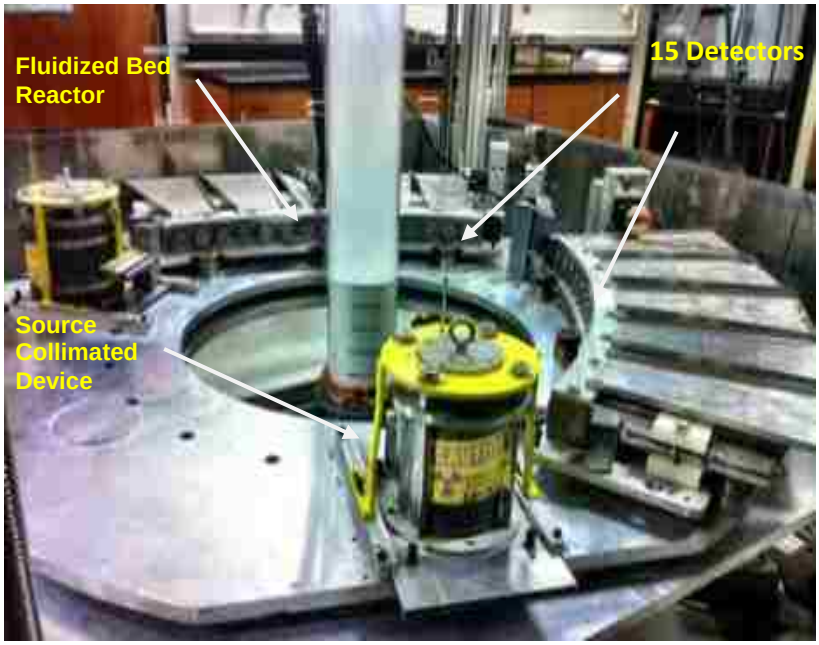

Figure 3.1 The CT with a 0.14m fluidized bed reactor used in this study.

The scanner's configuration consisted of two independent gamma ray sources, encapsulated Cesium (C-137) and Cobalt (Co-60), with initial strengths of (~250 mCi) and (50 mCi), respectively (dualsource CT), as well as two arrays of fifteen NaI scintillation detectors located opposite each source for imaging the phases. The sources and detectors are built on a rotary plate that moves them together 360° around the studied object, providing 197 views in each scan and 21 projections in each view. The entire assembly could be moved up and down along the column to scan the object at different axial positions (see Figure 3.2). Each detector consists of a cylindrical NaI crystal measuring 2" in both diameter and length, a photomultiplier and electronics.

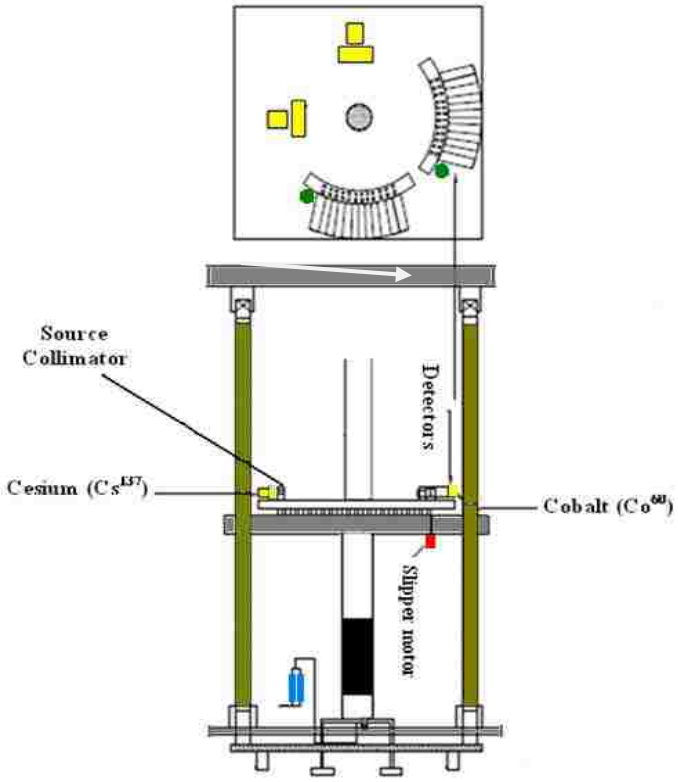

Figure 3.2 Schematic Diagram of Dual-Source CT Unit

Each of these detectors was collimated with a lead collimator. Collimators had approximately an open aperture 2 mm × 2. This aperture reduces the crystal's effective exposed area to a rectangular region and the counts received by the detectors are limited to what is incident on this aperture. CT scan sampling rate was 60 samples at 10 Hz, which took approximately 7.2 seconds to finish a 50 projection and 8.25 hours to finish a comprehensive scan.

3.1.2. Steps of Scanning. In this study, CT experiments were performed under a two-phase condition, (gas and solid). To measure the cross-sectional distribution of each phase, the Cesium (Cs-137) source was used to measure the phase holdup distribution. The fluidized bed column's cross-section was divided into n × m square pixels and the following CT scans were performed:

1-Scanning the column empty as reference CT scan.

2-Scanning the column filled with solids (glass beads)

3- Scanning the column at normal gas-solid operations at the desired conditions

The attenuations were measured along a number of beams paths through the column from different angles. Based on Beer Lambert's Law, the attenuation through the materials along the beam path is expressed as follows:

$$T = \frac{I}{I_0} = \exp(-\mu\rho l) \qquad (1)$$

Where (T) is the transmission ratio, (I_0) is the incident radiation, (I) is the detected radiation, (μ) is the mass attenuation coefficient, (ρ) is the medium density,(l) is the path length through the medium. The measured quantity ln (I/I_0) (called A, for simplicity) is equal to the integral sum of the attenuation through the material along the beam path.

$$A = \ln\frac{I}{I_0} = \mu\rho l \qquad (2)$$

To obtain statistically significant results and to reduce the effect of position, the CT scans were obtained by scanning 360 degrees around the column for a total scanning time of about eight hours, if the scanned cross-section is divided into pixels or cells and the medium is comprised of two materials (gas and solid), (μ_s) is mass attenuation coefficient for solid, (μ_g) is mass attenuation coefficient for gas, ρ is the medium density, (ρ_s) solid density, (ρ_g) gas density, and thickness (l_g), (l_s) for gas and solid phases respectively , the total attenuation

$$A = \rho_s\mu_s l_s + \rho_g\mu_g l_g \qquad (3)$$

Where $L_{ij} = l_{s,ij} + l_{g,ij}$, $l_{s,ij} = \mathcal{E}_{s,ij}L_{ij}$ and $l_{g,ij} = \mathcal{E}_{g,ij}L_{ij}$

Where, L_{ij} is the total length between the pixel along the gamma ray beam. $\mathcal{E}_{g,ij}$, $\mathcal{E}_{s,ij}$ are the holdups (volume fractions) for the gas and solid phases.

$$A = \left[\rho_s\mu_s\mathcal{E}_{s,ij} + \rho_g\mu_g\mathcal{E}_{g,ij}\right].L_{ij} \qquad (4)$$

The summation of the holdups is equal to unity (i.e. $\mathcal{E}_{g,ij} = 1 - \mathcal{E}_{s,ij}$)

$$A_{s-g,ij} = \left[\rho_s\mu_s\mathcal{E}_{s,ij} + \rho_g\mu_g(1 - \mathcal{E}_{s,ij})\right].L_{ij} \qquad (5)$$

Since $\rho_g << \rho_s$, the attenuation caused by the gas phase is negligible compared to the solids, and *L* is common for all *A*s. Hence, solids holdup for the line averaged measurement can be written as follows:

$$\mathcal{E}_{s,ij} = A_{s-g,ij}/L_{ij}\rho_s\mu_s \qquad (6)$$

$$A_{s-g,ij} = \rho_{s,ij}\mu_s \mathcal{E}_s L_{ij} \quad (7)$$

Finally, the gas holdup was determined using the expression

$$\mathcal{E}_{g,ij} = 1 - \left(\frac{A_{s-g,ij}}{L_{ij}\rho_s\mu_s}\right) \quad (8)$$

3.1.3. CT Reconstruction Algorithm. The reconstruction algorithm proposed and used by Varma and Al-Dahhan [11] 2007; Varma et al. [12] was implemented to reconstruct the cross-sectional distribution of relative attenuation in a two-phase system. Proposed an alternating minimization (AM) algorithm based on turning a maximum likelihood problem into a double minimization of I-divergence introduced by Csiszar et al. [13]. I-divergence is a measure of inconsistency between two functions, a(y) and b(y) Csiszar, [13], which is given as:

$$I(a\backslash\backslash b) = \sum_{y\epsilon Y} a(y) \ln\left[\frac{a(y)}{b(y)}\right]] - \sum_{y\epsilon Y}[a(y) - b(y)] \quad (9)$$

where Y is a finite dimensional space. The function a(y) is taken to be the measured data, while b(y) is taken to be a nonlinear model (Bhusarapu, [14]. Let q(y:μ) be defined based on Beer Lamert's law for the transmission of photons (Varma, [10] as follows:

$$q(y{:}\,\mu) = I_0(y) \exp[-\sum_{x\epsilon X} b(y/x)\mu(x)]] \quad (10)$$

Where I0(y) is the incident intensity, $b(y/x)$ is the length of projection y in pixel x, $q(y{:}\,\mu)$ represents the transmission of photons and is a function of the attenuation and b(y) represents a Poisson random number d(y). Equation (1) can be rewritten as

$$I(d\backslash\backslash q(y{:}\,\mu) = \sum_{y\epsilon Y} \left\{\mathrm{d(y)}\ln\left[\frac{d(y)}{q(y{:}\mu)}\right] - [d(y) - q(y{:}\,\mu)]\right\} \quad (11)$$

The algorithm minimizes the left term in Eq. (12) with respect to the attenuation (μ). More details and mathematical proofs regarding the AM algorithm are available

elsewhere (O'Sullivan and Benace, [15]; Bhusarapu, [14]). In this work, the AM algorithm was used to reconstruct images that represent attenuation of the gas-solid system. For local holdup/attenuation measurements using computed tomography (CT).

3.1.4. CT Validation. Before implementing the computed tomography (CT) technique. It is advisable to test the ability of the CT set-up to obtain the time averaged cross-sectional and radial profile of phase holdup distribution by using phantom which is designed to represent multiphase systems. The object represented in Figure 3.3(a) was made of perspex. The phantom consists of two sections. The inner section is a tube with 7.6 cm in diameter which is filled with air. The outer section was filled with water and has a diameter of 14 cm. The dimensions of the phases obtained by CT were well close to the phantom's dimensions with discrepancy of 0.92% (see Figure. 3.3(b)).

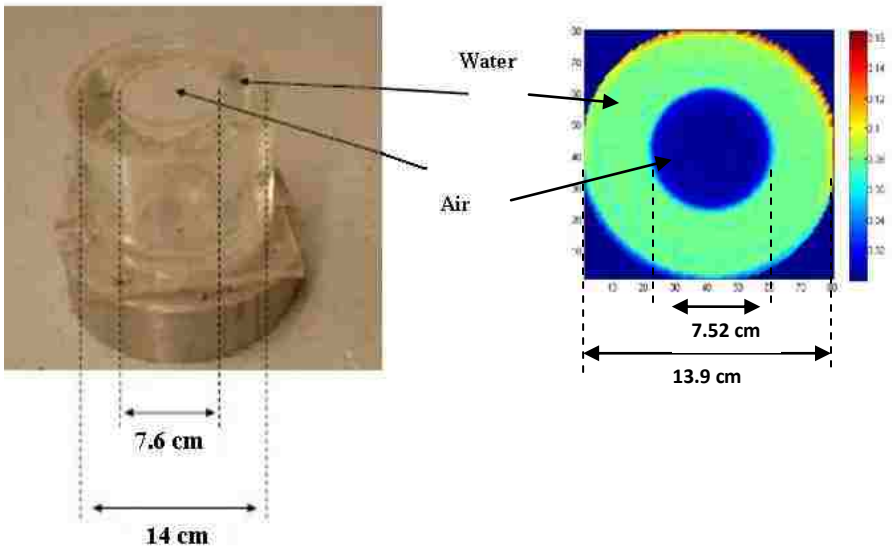

(a) (b)

Figure 3.3 (a) Picture of 14 cm phantom (perspex) used in the CT scan experiments with two phases: (air in the inner tube and water in the outer section), (b) The mass attenuation coefficient distribution for the two phases Phantom

4. RESULTS AND DISCUSSION

4.1. REPRODUCIBILITY OF CT MEASUREMENTS

All CT scans were acquired at one fixed axial position, H/D = 1.7. CT measurements were repeated in the 14 cm diameter column with the glass bead-gas system on two successive days to demonstrate the reproducibility (runs no. 1 and no. 2 in Figures 4.1 and 4.2). The time-averaged cross-sectional gas holdup distributions Figure 4.1 and the radial gas holdup profiles Figure 4.2 exhibit good reproducibility. Figure 4.1(a,b) exhibits similar cross-sectional gas holdup distributions to those obtained for runs no. 1 and no. 2; the results correspond to the superficial gas velocity of 25 cm/s and the axial location of H/D =1.7 (from the distributor). At most radial positions the radial gas holdup values were almost identical. The few differences were accepted because they were within ± 4.5% error.

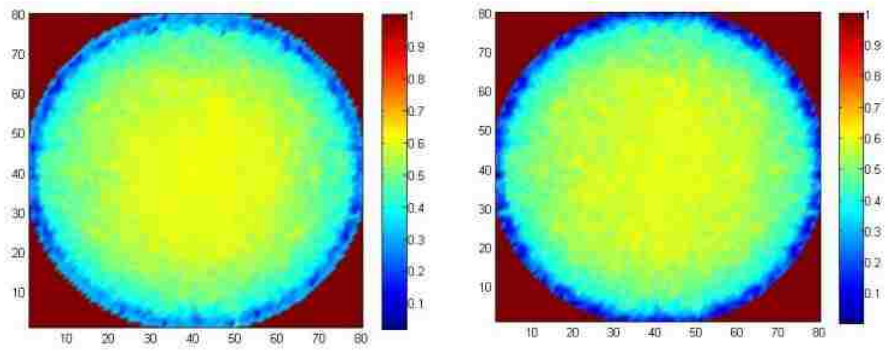

Figure 4.1 Distribution: glass beads-gas system, (a) run no. 1, and (b) run no.2.

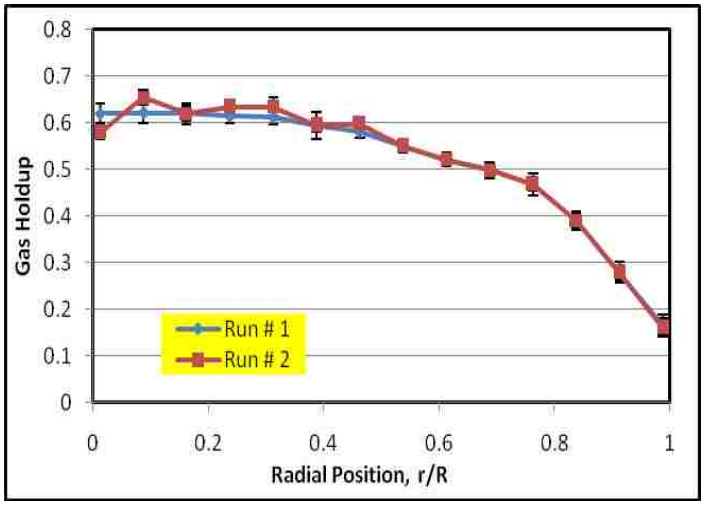

Figure 4.2 Reproducibility of CT measurements for radial gas holdup profiles: superficial gas velocity Ug = 25 cm/s; axial level H/D = 1.7, glass beads - gas system.

Overall gas holdup was measured at the same operating conditions using bed expansion as another independent technique to estimate the accuracy of the holdup data reported in this paper. It was found that the difference between the cross-sectional averaged holdup obtained by CT and the overall holdup by bed expansion was about 4.7 %.

4.2 CROSS-SECTIONAL AND RADIAL PROFILES OF PHASE HOLDUPS DISTRIBUTION

The reconstructed image, processed from data obtained through CT scans, provides the cross-sectional time-averaged gas and solid holdups distribution. The effect of the superficial gas velocity on both the time-averaged gas and solid holdups (gas holdup + solid holdup = 1), and radial profiles at different superficial gas velocities was investigated. Offering an idea of how gas and solid are distributed through the column (see Figure 4.3). The change in the gas and solid holdup magnitude values were indicated by the colour variation. Red indicates a higher gas holdup value while blue indicates a

lower value of gas holdup. In general it can be observed that, gas holdup is higher in the centre and lower near the wall. At lower superficial gas velocity, relatively uniform distribution of gas holdup can be observed.

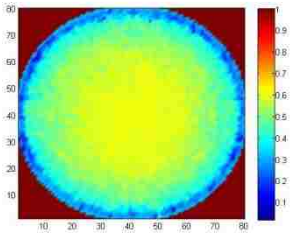

Gas holdup at Ug = 25 cm/s

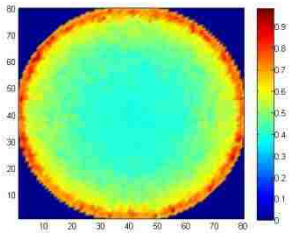

Solid holdup at Ug = 25 cm/s

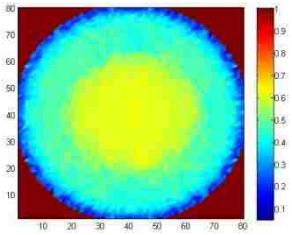

Gas holdup at Ug = 30 cm/s

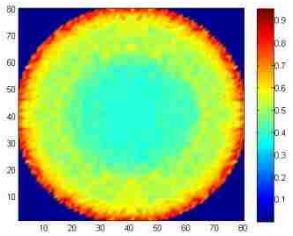

Solid holdup at Ug = 30 cm/s

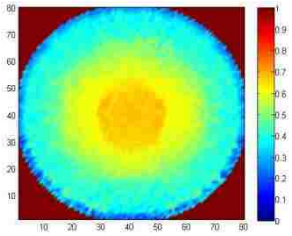

Gas holdup at Ug = 35 cm/s

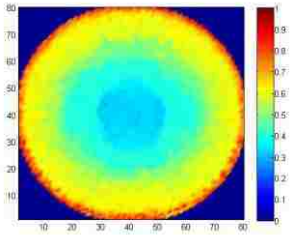

Solid holdup at Ug = 35 cm/s

Figure 4.3 Cross-section gas and solid holdup for glass beads at different superficial gas velocities

4.3 EFFECT OF GAS VELOCITY ON TIME-AVERAGE GAS AND SOLID HOLDUPS.

The effect of the superficial gas velocity on the time-average gas holdup radial profiles at different superficial gas velocities was investigated. The effect of increasing the superficial gas velocity at constant mass flux can be understood to decrease the solid

holdup due to the increase in the solid velocity. Since the gas injection is the only source of energy that drives the solids. Therefore, with an increase in the superficial gas velocity, the magnitude of the value of the gas holdup (void fraction or volumetric gas fraction) increased along the radial position (gas holdup + solid holdup = 1). The gas holdup (void fraction) data at specific axial position (H/D = 1.7) were averaged over the cross-section by numerical integration based on the trapezoidal rule:

$$\bar{\varepsilon} = \frac{2}{R}\int_0^R \varepsilon(r)\, dr \qquad (12)$$

These cross-sectional averaged value (void fraction) was about 0.32 at superficial gas velocity 20 cm/s and the magnitude of the gas holdup (void fraction) increased by 42% and 56% when the superficial gas velocity increased from 20 cm/s to 25 cm/s and from 20 cm/s to 35 cm/s, respectively. Figure 4.4 shows that the local gas holdup was greater near the center-line of the bed compared to that near the wall, Figure 4.4 shows the cross-sectional, time-averaged gas, and solid holdup distributions obtained using the gamma ray computed tomography technique for glass bead particles at various superficial gas velocities (25, 30, and 35 cm/s). The change in the gas holdup magnitude values was indicated by the color variation. It was observed that gas holdup increased as the superficial gas velocity increased; this was due to a higher volume of air passing through the bed, and confirms a trend identified by Mabrouk et al. [9]. In addition, increasing in superficial gas velocity enhances mixing throughout the bed, and also increases the bed expansion and the overall gas holdup in the system. An image of this cross-section is presented in Figure 4.3, for Ug = 25 cm/s, a high local gas holdup is concentrated in the

center of the bed and extended to the region near the bed wall. This behavior indicates that the air is flowing throughout the bed.

Increasing the superficial gas velocity to 30 cm/s enhances mixing throughout the bed, and higher gas holdup is located in the core of the bed, while lower solid holdup (solid concentration) are found along the bed walls, as can be seen in Figure 4.4. This behavior indicates that, the air is flowing mostly through the centre of the bed; the local gas holdup is more symmetrically distributed through the bed.

When the superficial gas velocity further increased, (Ug = 35cm/s), large bubbles erupted from the bed near the centre, throwing glass beads against the wall, which fell back into the bed; these hydrodynamics created a high gas holdup region in the centre of the bed, while lower gas holdup regions (higher solids concentration) were found along the bed walls.

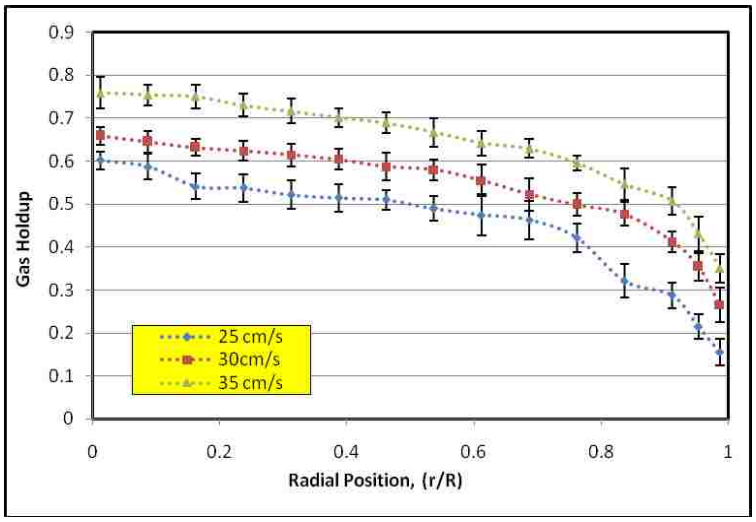

Figure 4.4 Effect of superficial gas velocity on radial profiles of gas holdup

To examine further the relationship between the changes of local gas concentration and changing of superficial gas velocity and spatial position, the representing probability density function (PDF). Figure.4.5 displays the probability density functions of the gas holdup distribution values in the pixel cells. PDF characterizes the gas holdup variation values along the pixel cells at different superficial gas velocities.

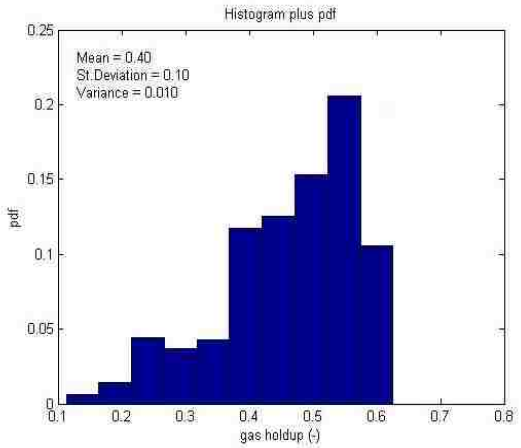

(a) Ug = 25 cm/s

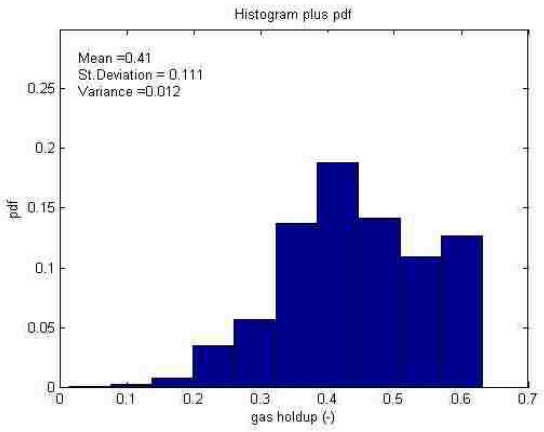

(b) Ug = 30 cm/s

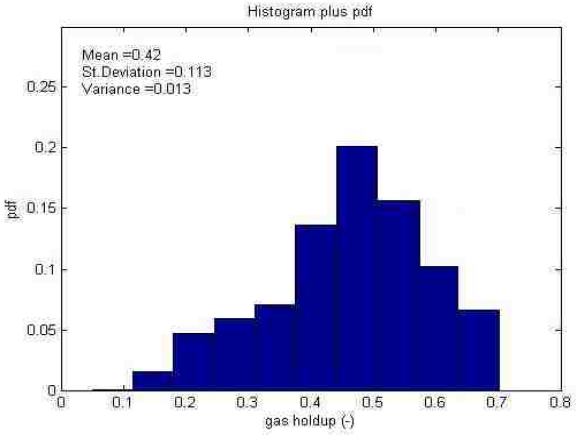

(c) Ug = 35 cm/

Figure 4.5 Probability Density Function of the values of gas Holdup in the Pixel cells

The variation in the corresponding mean, variance and standard deviation, which were directly calculated by MATLAB functions, increased with an increase in superficial gas velocity. The maximum variance of gas holdup was found to be less than 1.4%, while the standard deviation varied less than 12%.

4.4 EFFECT OF PARTICLE DENSITY ON TIME-AVERAGED GAS AND SOLID HOLDUPS.

The fluidization hydrodynamics of two bed materials (glass beads and copper particles) were compared in this study. Figures (4.6 and 4.7) show the reconstructed image for both glass beads-gas and copper particle-gas systems, respectively at 25 and 30 cm/s superficial gas velocity, respectively. Figure 4.8 (a, b) shows the time-averaged radial gas and solid holdup profiles obtained by averaging the data at H/D = 1.7 for both glass beads-gas and copper particle-gas systems, respectively at 25 cm/s superficial gas velocity. While Figure 4.9 (a, b) shows the time-averaged radial gas and solid holdup profiles obtained for both glass beads-gas and copper particle-gas systems, respectively, at 30cm/s, superficial gas velocity. It can be observed that the local time-averaged gas holdup is a function of the bed material density, as the material density decreased, gas holdup increased and solid holdup decreased (gas holdup + solid holdup = 1). The bed with copper particles was shown to have lower gas holdup than the glass bead bed, which exhibited a higher gas holdup. In addition Figures (4.8 and 4.9) show that the general fluidization behavior was similar for glass beads and copper particles, with a region of higher gas holdup in the center, and a region of low gas holdup (higher solids concentration) near the walls. Similar results were revealed by Franka et al. [16] for two different 3D beds and Escudero et al. [6]

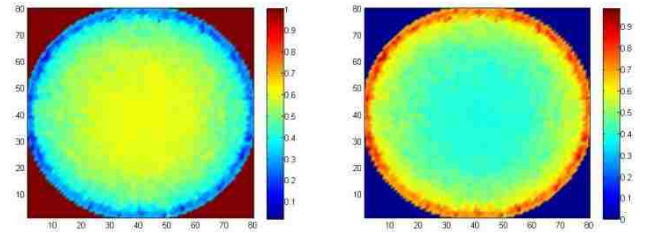

Gas holdup for glass beads at Ug = 25 cm/s

Solid holdup for glass beads at Ug = 25 cm/s

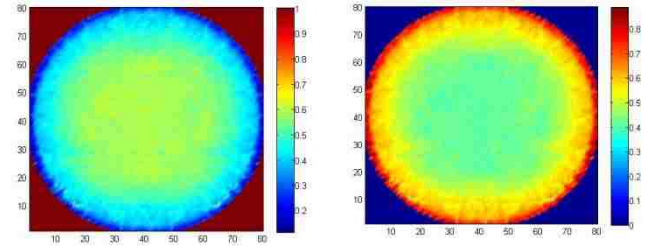

Gas holdup for copper at Ug = 25 cm/s

Solid holdup for copper at Ug = 25 cm/s

Figure 4.6 Time averaged cross-sectional gas and solid holdup distribution for glass bead-gas and copper particle- gas systems respectively at 25 cm/s.

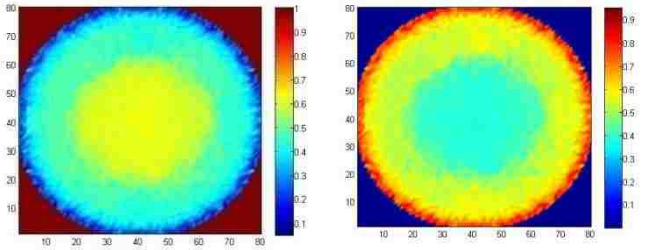

Gas holdup for glass beads at Ug = 30 cm/s

Solid holdup for glass beads at Ug = 30 cm/s

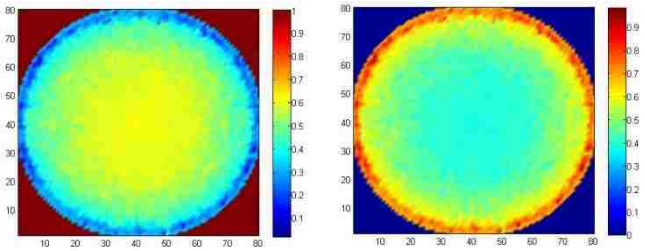

Gas holdup for copper at Ug = 30 cm/s

Solid holdup for copper at Ug = 30 cm/s

Figure 4.7 Time averaged cross-sectional gas and solid holdup distribution for glass bead-gas and copper particle- gas systems respectively at 30 cm/s.

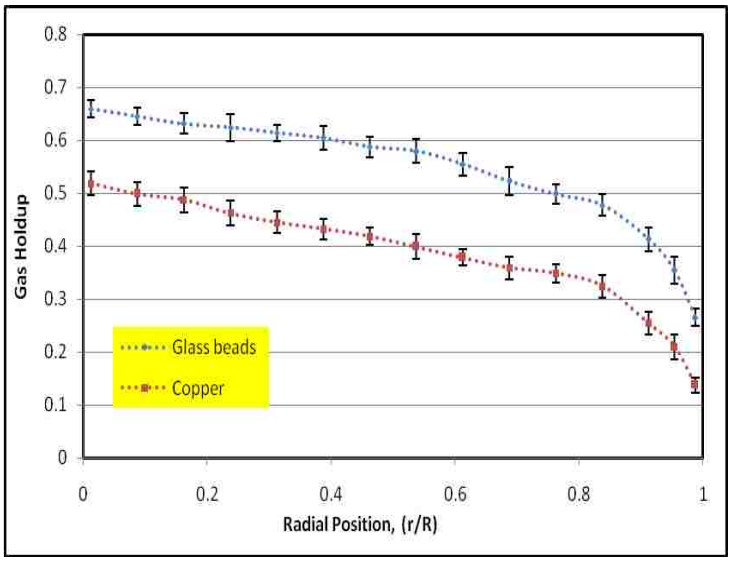

(a)

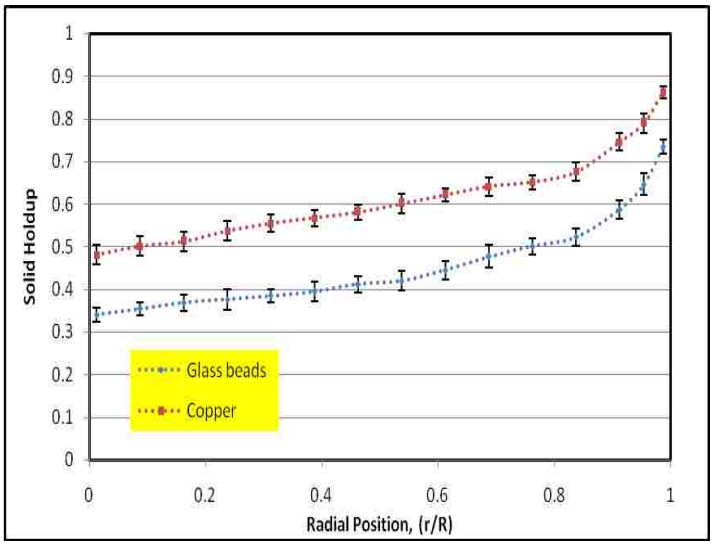

(b)

Figure 4.8 (a,b). Radial profiles of gas and solid holdups for glass beads and copper particle at Ug = 25 cm/s.

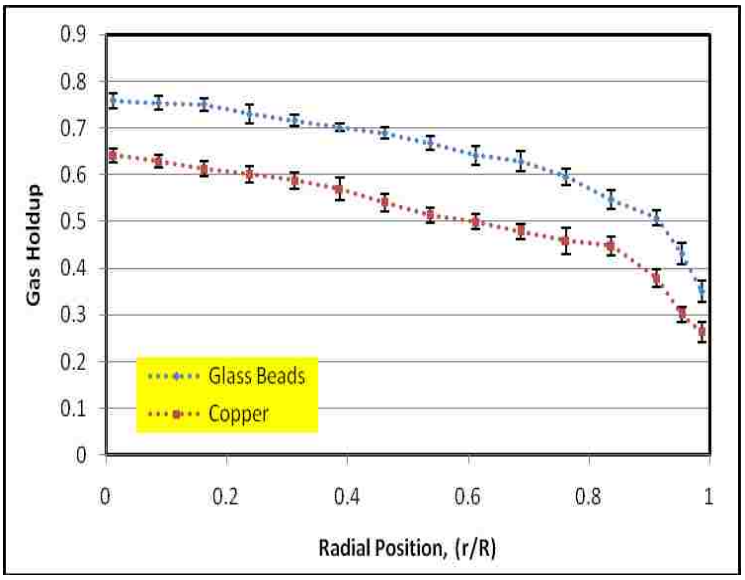

(a)

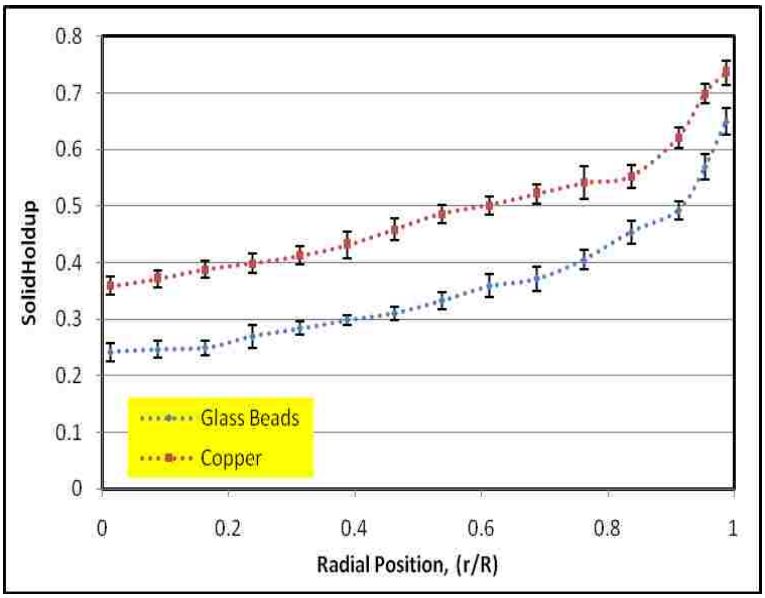

(b)

Figure 4.9 (a,b) Radial profiles of gas and solid holdups for glass beads and copper particle at Ug = 30 cm/s.

5. CONCLUSIONS

This study is part of a much more extensive investigation that includes many laboratory experiments. High resolution gamma-ray computed tomography was successfully applied for the determination of phases fraction distributions (gas holdup and solid holdup). The changes of local solids concentration reflect the interactions between gas and solids phase, which can influence the apparent reaction and mass and heat transfer in the fluidized beds, furthermore can influence the overall reaction rate in fluidized reactors. Gamma-ray CT is particularly useful in visualizing fluidized beds, and can provide a detailed 3-D time-averaged density map of the flow structure. Time-averaged gas and solid holdup distributions were measured in a 14 cm fluidized bed column using gamma rays instead x-rays (due to the height attenuation of copper particles) at different superficial gas velocities, (25, 30, and 35 cm/s), which cover the fluidization and bubbly flow regimes. To investigate the effect of superficial gas velocity and particle density on phase holdup distribution (gas holdup and solid holdup), glass beads and copper particles were used as the bed materials. It was observed that, the gas holdup increased with an increase in the superficial gas velocity. A rise in the superficial gas velocity was also found to affect the internal flow structure, enhancing mixing in the bed and producing a more homogenous bulk bed. In addition, while superficial gas velocity significantly affects fluidization hydrodynamics, it appears that changes in the superficial gas velocity do not significantly affect fluidization symmetry, as it can be seen in Figs (4.3, 4.6 and 4.7).

In addition, local time-averaged gas holdup is a function of bed material density. The two materials (glass beads and copper particles) exhibited a similar fluidization

structure, with a region of higher gas holdup in the centre and a region of low gas holdup (higher solids concentration) near the walls.

ACKNOWLEDGMENT

The authors wish to acknowledge the Libyan Ministry of Education for sponsoring the primary author's study within the Chemical and Biochemical Engineering Department at Missouri University of Science and Technology. The gamma ray facility and set-up used in this research were funded by Dr. Al-Dahhan.

REFERENCES

[1] McCabe W.E., J.C. Smith, and P. Harriott. Unit Operations of Chemical Engineering, McGraw Hill, New York, 2001.

[2] Fincke, J. R., Berggren, M. J. and Johnson, S. A. The application of reconstructive tomography to the measurement of density distribution in two-phase flow, in Proc. 26th Int. Instrumentation Symp., Seattle, pp. 235-243, 1980.

[3] Seville, J. P. K., Morgan, J. E. P, Clift, R. Tomographic determination of the voidage structure of gas fluidized beds in the jet region, in Fluidization V: Proceeding of 5th International. Conference Fluidization, Denmark, 1986.

[4] Banholzer, WF, Spiro, C. L., Kosky, P. G. and Maylotte, D.H. Direct imaging of time-averaged flow patterns in a fluidized reactor using X-ray computed tomography, Ind. Eng. Chem.Res. 26(4) pp. 763-767, 1987.

[5] Grassler, T., Wirth, K.E. X-ray computer tomography- potential and limitation for the measurement of local solids distribution in circulating fluidized beds. Chemical Engineering Journal 77 (1), pp.65-72, 2000.

[6] Escudero D, Theodore J. Heindel JT. Bed Height and Material Density Effects on Fluidized Bed Hydrodynamics.Chemical Engineering Science 66, pp.3648-3655, 2001.

[7] Zhu, H., Zhu,J., Li, G., Li, F. Detailed measurements of flow structure inside a dense gas-solid fluidized bed. Power Technology 180 (3), pp.339-349, 2008.

[8] Du B, Warsito W, Fan L-S. Bed nonhomogeneity in turbulent gas-solid fluidization. AICHE J 49(5): pp.1109-1126, 2003.

[9] Mabrouk R., Radmanesh R., Chaouki J., Guy C. Scale Effects on Fluidized Bed Hydrodynamics. Inter. J. Chem Reactor Eng 3:A18, 2005.

[10] Varma Characterization of anaerobic bioreactors for bioenergy generation using a novel tomography technique, Ph.D. Thesis, PhD, Washington University in St. Louis, Saint Louis, Mo, USA, 2008.

[11] Varma R, Al-Dahhan M. Effect of sparger design on hydrodynamics of a gas recirculation anaerobic bioreactor. Biotechnology and Bioengineering,Vol 98(6), pp.1146-1160, 2007.

[12] Varma R, Bhusarapu S, O'Sullivan JA, Al-Dahhan MH. A comparison of alternating minimization and expectation maximization algorithms for single source gamma ray tomography. Measurement Science & Technology, Vol 18, pp.1-13, 2007.

[13] Csiszár I (1991) Why least squares and maximum entropy? An axiomatic approach to inference for linear inverse problems. Annals of Statistics, Vol 19, pp. 2033-2066

[14] Bhusarapu S, Al-Dahhan MH, Dudukovic MP. Solids flow mapping in a gas-solid riser: mean holdup and velocity fields. Powder Technology, Vol 163, pp. 98-123, 2006.

[15] O'Sullivan, JA, Benac, J. Alternating minimization algorithms for transmission tomography. Medical Imaging, IEEE Transaction on 26(3), pp. 283-297, 2007.

[16] Franka N.P. Visualizing fluidized beds with X-rays, Master's Thesis, Iowa State University, Ames, IA, 2008.

IV. BED DIAMETER EFFECT ON THE HYDRODYNAMICS OF GAS-SOLID FLUIDIZED BEDS VIA RADIOACTIVE PARTICLE TRACKING (RPT) TECHNIQUE

Abdelsalam Efhaima and Muthanna H. Al Dahhan

Department of Chemical and Biochemical Engineering, Missouri University of Science and Technology, 1101 North State Street. 110 Bertelsmeyer Hall, Rolla, MO 65409,USA, ayed67@mst.edu

ABSTRACT

The hydrodynamics observed in large scale gas-solid fluidized bed reactors are different from those observed in smaller scale beds. In this work, the effect of bed diameter on the hydrodynamics of gas-solid fluidized bed reactors has been investigated in two bubbling fluidized beds of 0.44 m and 0.14 m in diameter using non-invasive radioactive particle tracking (RPT) technique. Compressed air at room temperature was used as the gas phase, and the solid was glass beads with the size particles of 210 μm and density of 2.5 gcm^{-3}. Particle velocity field, Reynolds stresses, normal stresses, turbulent kinetic energy, axial, and radial eddy diffusivities have been measured in two beds at superficial gas velocity of 1.5 U_{mf} , 2 U_{mf} and 3 U_{mf} . Experimental results showed that the bed scales had significant effect on these hydrodynamic parameters where the magnitude of solids velocity is much higher in larger bed and the solid mixing and diffusion of particles are increased by increasing the column diameter.

Keywords: Fluidized beds hydrodynamics, radioactive particle tracking, scale effects.

1. INTRODUCTION

Multiphase flow reactors are critically important in industrial applications across many sectors of the economy. Conventional industries as varied as petroleum refining, petrochemical, chemical, metallurgical, pharmaceutical, energy and power, as well as the new economy industries such as nanotechnology, all have multiphase reactors and contactors at the heart of their respective processes Rüdisüli et. al.[1].

Due to many advantages including high heat and mass transfer rates, approximately uniform temperature distributions, low pressure drops, intense solids mixing, good gas-solids contact and ability to fluidize many particle types of varying sizes (Geladart Groups), bubbling fluidized bed reactors (FBRs) are one of the best and widely used systems for handling multiphase chemical and physical processes, Dubrawski et al. [2]

In spite of these advantages, lack of understanding of the fundamentals of dense gas-solids flows, lack of reliable knowledge, design, scale-up, and effects of scale on the hydrodynamics, has affected their efficient applications. In addition, fluidized bed hydrodynamics behaviour is very complex, difficult to understand, and remains an active area of research, in particular for large scale fluidized beds, Laverman et al. [3]

The hydrodynamics behavior of gas-solid fluidized beds varies with scale therefore; it is difficult to predict the hydrodynamics of large industrial-scale reactors, based on the information of smaller scales. That is, if one parameter is changed (e.g. bed diameter) most of the other parameters (e.g. gas velocity) will not change concordantly. This discordance will ultimately result in significantly different hydrodynamics in the scaled fluidized bed.

The performance of these multiphase fluidized bed reactors greatly depends on their hydrodynamic properties. The hydrodynamics of a bubbling FBR is even more complex and known to change rapidly with change in bed diameter. One discouraging problem when a small scale reactor is scaled-up to a large scale reactor is the decrease in reactor performance. Such encountered problem could be related to poor solid mixing, undesirable gas flow patterns, physical operating problems, etc., Rüdisüli et al. [1]

The flow structures in large scale fluidized beds are quite different from those observed in small scale beds. Gas flow and gas-solids contacting patterns, and solids circulation in large reactors are different from those in small scales reactors. The bubbles are primarily responsible for improved gas-solids contact and consequently the chemical conversion in a fluidized bed. The bubble size, the bubble frequency, and the bubble rise velocity are all strongly influenced by the bed size. Primarily, this is caused by wall-effects which are more dominant in small scale reactors than in large scale reactors, Dubrawski et al. [2]

Therefore, any attempt for better understanding the fluidization phenomena would result in a more reliable design of fluidized reactors and efficient operation. In general, studies on the effects of diameter on the hydrodynamics of gas–solid systems are rare and most of the studies are carried out in circulating fluidized beds, Van der Meer. [4]; Xu et al. [5]. The problems of poor solids mixing, gas bypassing and poor contact with bed particles, and undesirable gas flow patterns were recognized as major considerations in the scale-up of fluidized beds, Rüdisüli et al. [1]

Several measurement techniques have been described and employed in the literature to characterize the flow behavior on different size gas-solid fluidized bed

systems to monitor or control the fluidization quality, and to detect the gas or solids phase properties. Basically, these techniques can be divided into two general categories: invasive and non-invasive. Invasive measurement techniques, such as optical fiber probes, extraction probes, pitot tubes, isokinetic probes, and non-invasive techniques, such as radioactive particle tracking (RPT) technique, gamma ray computed tomography (CT) technique, positron emission particle tracking (PEPT) technique, and others Al-Dahhan et al. [6]. Non-invasive techniques do not affect the gas–solid flow behavior inside the fluidized beds, which have been used in this work. The Radioactive particle tracking (RPT) technique provides detail gas–solid flow patterns in the fluidized beds.

Early experimental studies on fluidized bed scale-up based on dimensionless groups reported by Glicksman. [7]. Glicksman [7] recognized the influence of bed diameter on gas-solid fluidized bed hydrodynamics, such as conversion due to less efficient gas-solid contacting.

Frye et al. [8] used three beds of 0.0508, 0.2032 and 0.762 m ID fluidized beds to study the size effect on the reaction rate. It was observed that the reaction rate decreases by a factor of three between the 0.0508 m ID and 0.762 m ID beds.

Horio et al. [9] also observed that the yield of the reaction was decreasing by increasing the bed diameter; even though the conventional rules were respected. Horio et al. [9] in their work raised the problem of bubble distribution in different scales. New scale-up rules were suggested by Horio et al. [9] in addition to the conventional rules. These rules were developed by considering the bubble coalescence and bubble splitting in scaling-up the fluidized beds.

Mabrouk et al. [10] used optical probe and radioactive particle tracking (RPT) technique to study scale effects on fluidized bed hydrodynamics, and to address the smallest gas-solid fluidized bed diameter that can be used and investigated in the laboratory. Two radioactive tracers of 180 and 260 μm in diameter which made from scandium oxide with a half-life of 83.9 days were used to track the solids phase of sand (250 μm size) and alumina (150 μm size) particles. The experiments were carried out in three bubbling fluidized bed units of 0.050, 0.078, and 0.152 m ID, respectively. Air under ambient conditions was the fluidizing gas in all the experiments. Three superficial gas velocities (U = 0.3, 0.38, and 0.53 m/s) were used during these experiments. They observed that the radial solid hold-up profiles on the 0.1521 m ID and small bed diameters (0.078 and 0.050 m ID) are different, and the gas-solid behavior on scales is not similar even when the similarity of the geometry is respected and the experiments conditions are the same, on the very small scale 0.050 m ID, and small bed diameter 0.078 m ID, the radial solid hold-up profile at different levels above the distributor is high at the center region and low on region close to the wall, a phenomenon with which we are not familiar. They suggested that, there is a critical diameter below which the hydrodynamics are completely different from those above the critical diameter. In addition they concluded that, the scale-down of gas-sold hydrodynamics structures established from large scales to lab-scale lower than 0.078 m ID, leads to a misunderstanding of the exact phenomena involved.

Bashiri, et al. [11] experimentally studied effect of bed diameter on the hydrodynamics of gas-solid fluidized beds in two fluidized beds of 152 mm and 78 mm in diameter. Sand particle with two sizes, 385 and 250 μm were used as bed material. The

radioactive particle tracking (RPT) technique was employed to obtain the instantaneous positions of the particles at every 20 ms of the experiments. Two types of tracer particle were used in the experiments, the first one made of scandium oxide and the second made of mixture of gold powder and epoxy with a density and size close to those of the bed material in the experiments. The obtained RPT data was used to calculate hydrodynamic parameters, such as velocity of upward and downward-moving particles, jump frequency, cycle frequency and axial and radial diffusivities, which are representative of solids mixing and diffusion of particles in the bed. Although they used small bed size, 78 mm in diameter the results showed, that solids mixing and diffusivity of particles increase by increasing bed diameter.

Mostoufi and Chaouki [12] measured the diffusivity of the solids in a 152 mm bubbling gas-solid fluidized bed. The gas was air at room temperature and atmospheric pressure and the solids were 385 μm sand particles. By implementing radioactive particle tracking (RPT) technique. The tracer was made of a mixture of gold powder and epoxy. They showed that the solids diffusivities, both axial and radial, increases with increasing superficial gas velocity and that the diffusivities are correlated with the axial solids velocity gradient.

Mostoufi and Chaouki [13] also investigated the existence of clusters in 152 mm dense fluidized beds. The solids used in the experiments were sand with a size of 385 μm and density of 2.6 g/cm^3. They found that descending clusters were larger than ascending clusters and additionally that the size of the clusters increases with an increase in the superficial gas velocity.

Stein et al. [14] applied positron emission particle tracking (PEPT) experiments to investigate the solids flow pattern, solids velocity, and solids circulation frequency in two fluidized beds with inner diameters of 0.07 and 0.141 m. Stein et al. [14] found that, for relatively deep cylindrical beds loaded with Group B particles and an aspect ratio greater than 1, particles moves upwards in the central part of the bed, and downwards near the wall. This up-and-down movement is the main mechanism for vertical solids (convection) mixing. The average upward velocity of particles is measured to be about 50% of the bubble's rise velocity. In addition, lateral mixing occurs mainly at the top of the bed where bubbles burst and near the distributor where particles complete their old cycles and are carried away by bubbles to start new cycles. Furthermore, Stein et al. [14] performed an experimental verification of the scaling relationships that proposed by Glicksman [7] for bubbling gas-fluidized beds using beds with a diameter of 0.07, 0.141 and 0.240 m.

Bing Du et al. [15] studied the bed dynamics behavior in three gas-solid fluidized beds, 0.05, 0.1, and 0.3 m in diameters. The fluidized particles were FCC catalyst with a mean diameter of 60 μm and a particle density of 1.4 g/cm^3. The electrical capacitance tomography (ECT) and optical fiber probe were used in this study to measure the time-averaged cross-sectional solids holdup distributions. Bing Du et al. [15] found that, the 0.1 m ID fluidized bed exhibits the spiral motion of rising bubbles. However, for the 0.3 m ID fluidized bed, more than one spiral motion of bubble swarms is observed. The small fluidized bed exhibits the round nosed slug motion.

Bangyou et al. [16] used pressure fluctuations and X-ray computed tomography (CT) measurements to characterize the flow behavior of gas-solid fluidized beds using

polyethylene particles in three Plexiglas columns with diameters of 10, 20, and 30 cm, under ambient conditions. The time-averaged void distribution, bubble-phase area fraction, bubble diameter and bubble number distribution varying with the bed heights were characterized from statistical analysis of pressure fluctuation data and CT images. They conclude that the bed scales had significant effect on the hydrodynamics.

Efhaima and Al-Dahhan [33] used gamma ray computed tomography (CT) technique to investigate local time-averaged gas hold-up in fluidized bed reactor. Efhaima and Al-Dahhan [14] found that the gas holdup increased with an increase in the superficial gas velocity. In addition, local time-averaged gas holdup is a function of bed material density.

Vikrant et al. [17] presented two-fluid model simulations, based on the kinetic theory of granular flow of bubbling fluidization for Geldart B particles in a cylindrical fluidized bed with diameters of 0.10, 0.15, 0.30, 0.60 and 1.0 m, respectively. They showed the reliability of the model by comparing results for a 0.30 m bed with experimental measurement of Laverman et al. [3]. Also Vikrant et al. [17] measured the bubble size in the different size beds by utilizing the information on the gas volume fraction available for each computational cell in the domain of interest. In addition they quantified the effect of bed size on the bubble size, the bubble aspect ratio, the bubble rise velocity, porosity distribution and solids velocity and solids flow pattern. Vikrant et al. [17] concluded that the bubble size increases as the bed diameter is increased from 0.10 to 0.30 m. Concurrently, they observed an increase in bubble rise velocity, in the largest bed.

It seems studying the effect of bed diameter in beds less than 6 inch diameter is inadequate and could be misleading. Hence, in this work two sizes of gas-solid fluidized beds of 0.44 m (18 inch) and 0.14 m (6 inch) have been used where wall effects are strongly reduced in comparison to small scale fluidized beds to investigate the scale effect on the solids velocity and turbulent parameters using non-invasive radioactive particle tracking technique. Also the influence of the superficial gas velocity was investigated in this work.

2. EXPERIMENTAL SETUP

In this work, the effect of bed diameter on the hydrodynamic of gas-solid fluidized beds was investigated using two fluidized beds; 0.14 m and 0.44 m in diameter which were made of Plexiglas and consisted of two pieces: column and plenum. A schematic diagram of the setup used in this work is illustrated in Figure 2.1. The 0.14 m column was 1.68 m high connected from the top with an upper section that had a diameter of 0.42 m and was 0.84 m high; this upper section of the fluidized bed (the disengagement zone) had a larger diameter to reduce the superficial gas velocity of the gas phase to enhance the solids separation. The properties of solids, static bed height, and superficial gas velocity used in the experiments are listed in Table 2.1. The plenum was located at the bottom, which consisted of a sparger tube. The gas phase at ambient temperature was introduced through a distributor at the bottom after passing through the sparger. The gas distributor was made of a porous polyethylene sheet and had a pore size of 40 μm. The sparger was plugged at one end, and had 14 holes, all facing downward with respect to the column. The 0.44 m diameter fluidized bed very closely resembled the 0.14 m fluidized bed. The shape of the upper section was similar, but it had a diameter of 0.88 m and was 0.95 m high. The distributor design was similar to that used with the 0.14 m diameter fluidized bed. The plenum also consisted of a sparger tube, which had 20 holes, all facing downward with respect to the column. Both columns were electrically grounded to minimize electrostatic effects. Compressed air supplied from an industrial compressor, that can deliver compressed air of 735 CFM capacity at pressures up to 200 Psig, was used in this work. Two rotameters (Omega Engineering, Inc.) with different scales were connected in parallel to cover a wide range of flow rates (160 to 3200

SCFH). The static bed height above the distributor was at H/D = 2 for the two columns. The minimum fluidization velocity (U_{mf}) was measured by an absolute pressure transducer and the values are compared in this work with the empirical correlation of Miller and Logwinuk. [18]. It was found that the comparison of the values was in a good agreement (see Efhaima and Al-Dahhan, 2016). The values were 12 cm/s, and 10 cm/s, for the 0.14 m, and 0.44 m columns, respectively.

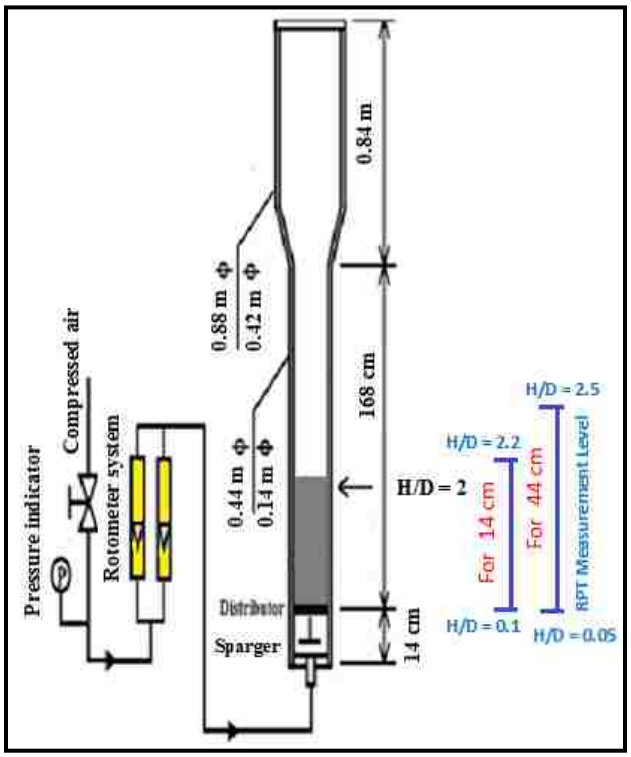

Figure 2.1 Schematic diagram of 0.44 and 0.14 m cold–flow fluidized beds used in this study

Table 2.1 Properties Of Solids Used In The Experiments

Properties	Glass Beads
Particle Diameter (μm)	210
Static Bed Height (H/D)	2
Superficial Gas Velocities (cm/s)	(1.5 - 3) $\mathbf{U_{mf}}$
Particle Density (g/cm^3)	2.5

3. MEASUREMENT TECHNIQUE

3.1. RADIOACTIVE PARTICLE TRACKING (RPT) TECHNIQUE

To obtain quantitative information about the solids motion in a full 3D bubbling gas-solid fluidized bed, radioactive particle tracking (RPT) technique was implemented. The radioactive particle tracking (RPT) technique is an advanced non-invasive measurement technique that is based on the principle of tracking the motion of a single tracer particle (gamma ray emitter) as a marker of the solids phase. The new RPT set-up was built in our Multiphase Reactors Engineering and Application Laboratory (m-Real) at the Chemical and Biochemical Engineering Department, Missouri University of Science and Technology (Missouri S&T). Details of the principle of RPT used in this study can be found elsewhere Bhusarapu. [19]; Bhusarapu et al. [20]; Shaikh, [21]; Shaikh and Al-Dahhan, [22]; Al-Mesfer, [23]; Efhaima and Al-Dahhan, [24]. This setup included a fully automatic calibration device that moves in all directions (r, z, and θ) and a signal processing and data acquisition system. Figure 3.1a shows the photograph of radioactive particle tracking (RPT) set-up. A single radioactive particle (cobalt-60) with an activity of approximately 500 μCi and a 600 μm diameter was used in a composite particle of 1 mm diameter as a tracer in this study. It was irradiated in the nuclear reactor at the University of Missouri Research Reactor Centre in Columbia, Missouri. Cobalt-60 has a half-life of 5.28 years and presents two photo-peaks, one at 1.18 MeV and one at 1.34 MeV. Cobalt-60 has a high density 8.9 gcm^{-3} and therefore it is difficult to make 210 μm radioactive particle with the same density of the glass beads 2.5 gcm^{-3}. Thus, the cobalt-60 particle was encapsulated with air in an aluminum ball with a 1 mm outer diameter to achieve the same density as the solids used (glass beads, 2.5 gcm^{-3}). Hence,

the particle density is the key parameter to match the used solid particles density in order to track the solids with fidelity. It is not necessary to use a tracer particle of size that matches the size of experimental particles. This is because the particles in the gas-solid fluidized bed usually do not move as single isolated particle but they do as a cluster. Tebianian et al. [25]; Mostoufi and Chaouki. [12,13] concluded that, the solid particles do not move individually. Each single particle is attached to a solid aggregate in the dense bed and moves with it until the solid aggregate breaks-up. The particle then enters another solid ensemble and continues its movement with the new ensemble. It is not necessary to match that of the experimental particle size. Mostoufi and Chaouki. [12] showed that all the parameters evaluated on their study changed only with superficial gas velocity, and were independent of the size of the tracer.

A total of 28 NaI scintillation detectors were positioned around each column. These detectors were held on four vertical supports at equal distances around the column. Each support had 7 detectors placed at different axial levels. A typical arrangement of the detectors around the fluidized bed is shown in Figure 3.1b. Each detector consisted of a cylindrical NaI crystal (2 in x 2 in), a photomultiplier and electronics. RPT experiments typically consist of the following two steps: 1) the RPT calibration (static placement of the radioactive tracer particle under experimental conditions), and 2) the RPT experiment (dynamic experiment). The counts data recorded in different detectors are collected continuously and used to reconstruct the instantaneous positions of tracer (its lagrangian trajectory).

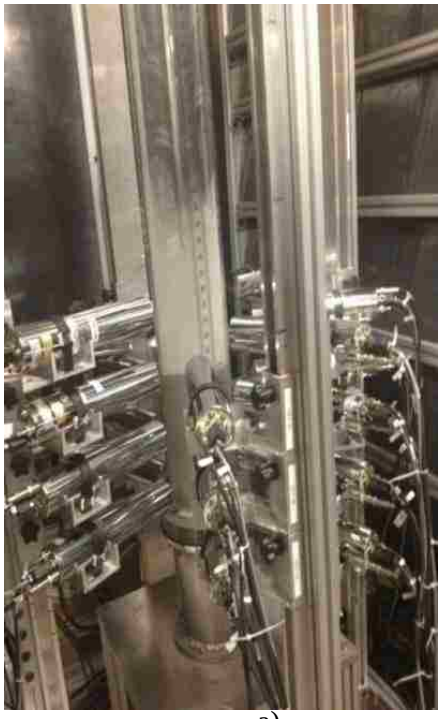

a)

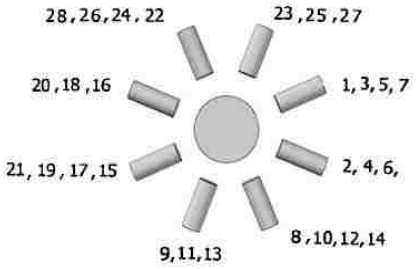

b)

Figure 3.1 a) - Photograph of radioactive particle tracking (RPT) set-up and b)- Side view of the detectors distribution around the bed.

From these instantaneous positions data, a rich database of flow quantities such as particle velocity field, various turbulent parameters, (shear stress, normal stresses, turbulent kinetic energy, turbulent eddy diffusivities), and other parameters that represent the flow characteristics can be determined. Table 3.1 summaries how these parameters are estimated (Efhaima and Al-Dahhan, [24]; Bhusarapu. [19]; Bhusarapu et al. [20]; Shaikh, [21]; Shaikh and Al-Dahhan, [22]; Bashirit et al. [11]; Laverman et al. [17]; Al-Mesfer, [23]; Dubrawski et al. [2]; Tebianian et al. [25]. The data are acquired at a frequency of 50 Hz and each experiment lasted for 8 hr. This duration is necessary to establish sufficient statistics in the experiments.

Table 3.1 hydrodynamic parameters estimated for each compartment (i,j,k) from rpt reconstruction lagrangian trajectory.

Instantaneous Velocity (cm/s)	$u_{z,i-1/2} = \frac{z_i - z_{i-1}}{\Delta t}$ $u_{r,i-1/2} = \frac{r_i - r_{i-1}}{\Delta t}$ $u_{\theta,i-1/2} = \frac{(\theta_i - \theta_{i-1})}{\Delta t} \ \frac{(r_i + r_{i+1})}{\Delta t}$
Time-averaged velocities (cm/s)	$\overline{u}_{p(i,j,k)} = \frac{1}{N_v} \sum_{i=1}^{N_v} u_{p(i,j,k),i} \quad p = z, r, \theta$
fluctuating velocity (cm/s)	$u'_{p(i,j,k)} = u_{p(i,j,k)} - \overline{u}_{p(i,j,k)}$
Azimuthally averaged velocity (cm/s)	$\overline{u}_{(i,k)} = \frac{1}{N_\theta \breve{N}_{v(i,k)}} \sum_{j=1}^{N_\theta} \overline{u}_{(i,j,k)} \quad N_{v(i,j,k)}$
Stresses (cm^2/s^2)	$\tau_{pq} = \overline{u'_p u'_q}(i,j,k) = \frac{1}{N_v} \sum_{n=1}^{N_v} u'_p(i,j,k),n \, u'_q(i,j,k),n$
Turbulent Kinetic Energy (cm^2/s^2)	$K = \frac{1}{2}(\overline{u'^2_r} + \overline{u'^2_z} + \overline{u'^2_\theta})$
Normal radial eddy diffusivity (cm^2/s^2)	$D_{rr}(t) = \frac{1}{2}\frac{d}{dt}\overline{Y_r^2(t)} = \int_0^t u'_r(t) \, . \, u'_r(t') \, . dt'$
Normal axial eddy diffusivity (cm^2/s^2)	$D_{zz}(t) = \frac{1}{2}\frac{d}{dt}\overline{Y_z^2(t)} = \int_0^t \left[\left[\overline{u'_z(t) \, . \, u'_z(t')} + \left.\overline{\frac{du_z}{dr}}\right|_{Y_{r(t')}} . \left(\int_0^{t'} u'_z(t) \, . \, u'_r(t'') \, dt'' \right) \right] . dt' \right]$

3.2 CALIBRATION OF DETECTORS (STATIC EXPERIMENTS)

Before performing the RPT actual experiments, calibration of all detectors used must be performed in-situ, preferably at the same operating conditions as used in the actual experiment, to obtain the calibration curve (the relationship between intensity of radiation (count) and the position of the radioactive tracer particle) for each detector. A

new version of RPT technique with advanced electronic has been used in this study (Al-Mesfer, [23]**.** This setup included a fully automatic calibration device to place the radioactive particle at known locations in all directions (r, z, and θ). The device can automatically move the calibration rod with a composite particle attached to its tip to several hundred or thousand known locations inside the column. Each NaI scintillation detector recorders intensity counts, which depend upon the distance between the radioactive tracer particle and the detector for each calibration location and the media between them. The three available rods, each with a length of 3 ft, can be connected as needed to create a long calibration rod. The movements of the motors are computerized and integrated with the data acquisition program. Thus, the counts received by each detector are recorded automatically. From the calibration step, a count-distance map can be obtained, which is used in a subsequent steps to obtain the locations of the tracer particle (lagrangian trajectory) which through post processing then instantaneous velociyies, time averaged velocities, fluctuation velocities, and turbulent parameters can be estimated (see Efhaima and Al-Dahhan, [24]; Bhusarapu et al. [20]; Roy, [31]; Upadhyay, [32]. Al-mesfer [23] provided a description of this type of automated calibration device.

3.3 REPRODUCIBILITY OF THE RPT DATA

The reproducibility of the experiments is one of the most important factors to consider before taking any measurements. To check the reproducibility, the RPT experiments were repeated two times under identical operating conditions (glass beads 210 μm, superficial gas velocity $U_g = 2U_{mf}$). Figure 3.2 shows the azimuthally and

axially averaged axial particle velocity and turbulence parameters radial profiles obtained by RPT measurements technique. The error bars represent the standard deviation from that average of each run. As shown in Figure 3.2 it can be concluded that the reproducibility of the RPT experiments is quite satisfactory for the particle velocity profiles and also for the turbulent parameters profiles. For example the maximum deviation between run 1 and run 2 for the particle velocity had a value of ±4%.

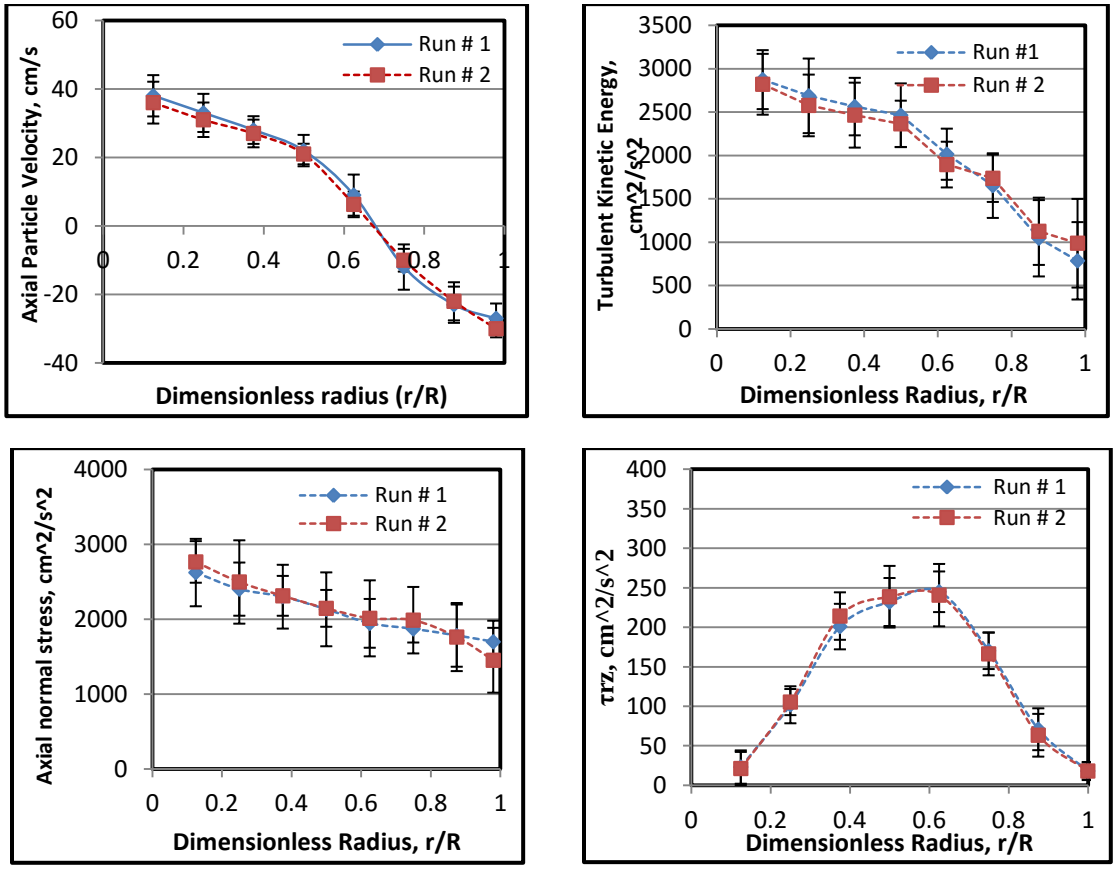

Figure 3.2 Time and aximuthally averaged axial particle velocity and turbulent parameters radial profiles for 210 μm glass beads and gas system at $U_g = 2U_{mf}$ in 14 cm column (dot lines represent the trend).

4. RESULTS AND DISCUSSION

In this section, the results of the RPT measurements are presented and discussed. First the influence of superficial gas velocity on particle velocity field on two different size fluidized beds is assessed, followed by a description and discussion of the RPT results for turbulente parameters at different superficial gas velocities on two different bed sizes. The superficial gas velocity was varied between 1.5 and 3 U_{mf} . The Minimum fluidization velocity **(**U_{mf} **)** was measured experimentally as mentioned earlier from the profiles of pressure drop versus superficial gas velocity **(**U_g**)** and the values are compared with the empirical correlation of Miller and Logwinuk. [18]. It was found that the comparison of the values were in a good agreement (see Efhaima and Al-Dahhan, [24]). The values were 12 cm/s, and 10 cm/s, for the 14 cm, and 44 cm columns, respectively. The minimum fluidization velocity decreases with increasing diameter of fluidized beds, Bashiri, et al. [11]. This may result from the higher friction forces in the small scale bed. It should be emphasized that the tracer particle (1 mm composite particle) used in this study does not meet the size of 210 μm glass beads used, but they have the same density which is 2.5 g/cm^3 where matching the density is the key to follow the bed particles used as discussed previously.

4.1 PARTICLE VELOCITY FIELD

The resultant velocity vectors plots for glass beads in two different bed sizes are presented in this study. Figure 4.1 shows the velocity vector plots for 0.14 m column, while Figure 4.2 shows the velocity vector plot for large column 0.44 m at different superficial gas velocities. It can be seen from these figures that, one-cell recirculation

pattern was observed for the glass beads in small size column. It has been known since the earliest studies of fluidization that even if the gas distribution is initially good and bubbles observed to form uniformly above the distributor, the bubbles near the walls tend to move away from the walls, due to coalescence with their neighbours. In these experiments, at a superficial gas velocity corresponding to 1.5 U_{mf} the outermost bubbles generated at the distributor were able to reach the center of the bed, therefore, there was a concentration of bubbles close to the centre of the bed giving rise to high upward solids velocities in that region, (positive axial velocity) in the central region of the column. While at the positions close to the wall, where the bubbles are absent, the solids move toward the distributor resulting in downward solids velocities in that region, down-flow (negative axial velocity) in the annular region near the column wall.

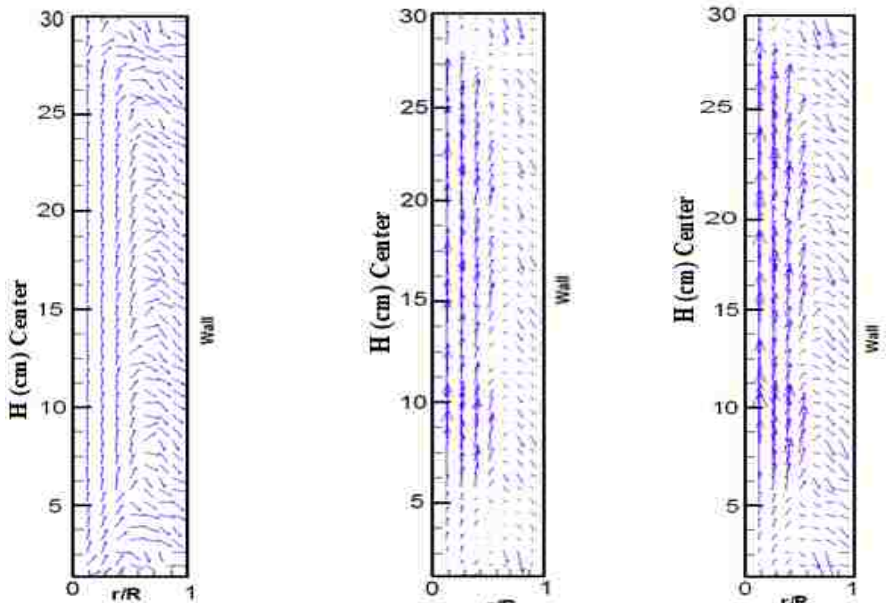

Ug = 1.5 U_{mf} **Ug = 2 U_{mf}** **Ug = 3 U_{mf}**

Figure 4.1 Time averaged velocity vector plot in the r-z plane at different superficial gas velocities for 0.14 m fluidized bed column, the arrows represent the direction of the velocity and the length represents the magnitude.

When the superficial gas velocity is increased to 2 U_{mf} , more bubbles are formed and the bubbles are large, which results in a faster coalescence and thus a large lateral velocity toward the centre of the column. For 3 U_{mf} this lateral bubble movement is even more pronounced, resulting in large upward particle velocity in the centre of the column. In larger bed the solids are mostly carried through the wakes of the bubble. As the bed diameter is increased from 14 to 44 m, the solids move with higher velocity due to the increase in bubble size and bubble rise velocity. From Figure 4.2 it is seen that, at low superficial gas velocities, two distinct counter-rotating vortexes appear above each other. When the superficial gas velocity is increased, the lower vortex decreases in size and at a higher superficial gas velocity U_g= 3 U_{mf} , the lower vortex somehow disappears while the top vortex spans the entire height of the fluidized bed.

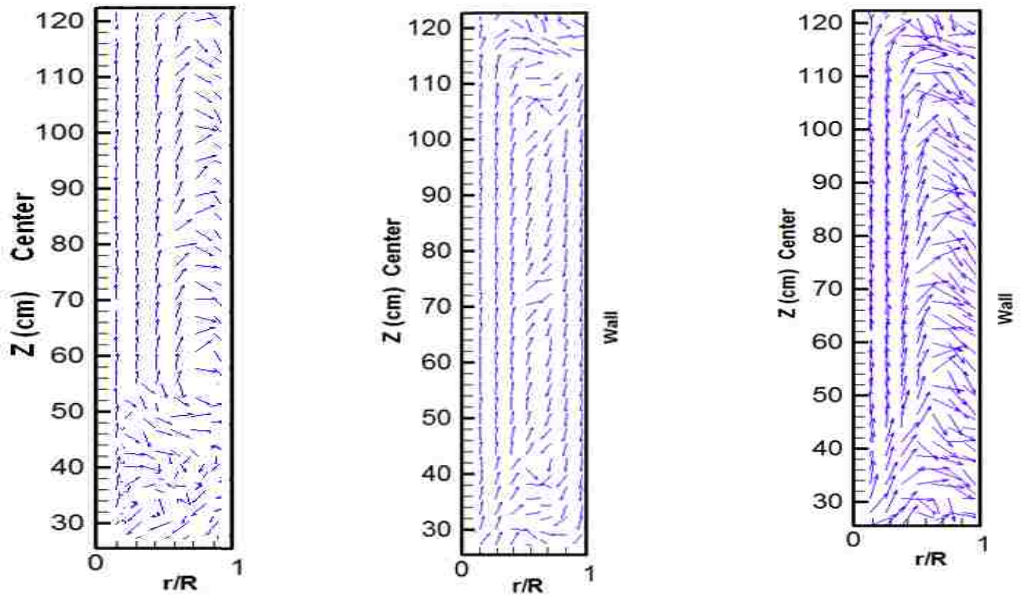

Ug = 1.5 U_{mf} **Ug = 2 U_{mf}** **Ug = 3 U_{mf}**

Figure 4.2 Time averaged velocity vector plot in the r-z plane at different superficial gas velocities for 0.44 m fluidized bed column, the arrows represent the direction of the velocity and the length represents the magnitude.

The behavior of the solids and bubbles displayed in these measurements agrees well with the literature, Bashiri et al. [11]; Laverman et al. [3]; Tebianian et al. [25]

4.1.1. Axial Particle Velocity. The particles in the gas-solid fluidized bed usually do not move as single isolated particles but they do as cluster, Tebianian et al. [25]; Mostoufi and Chaouki, [12]. The Instantaneous particle velocities components (axial, radial and azimuthal) were computed from the time differencing of the subsequent particle positions and assigned to the compartment in which the middle point of the two positions fell.

Figure 4.3 depicts the radial profiles of the azimuthally and axially averages axial solids velocity as a function of dimensionless radius for the two different sizes of 0.14 m and 0.44 m at different superficial gas velocities. From Figure 4.3, it is seen that, the axial velocity of glass beads particles in both sizes is positive at the center region of the bed and negative near the wall, which shows that the solids are going up from the center region of the column ($r/R = 0 – 0.62$) while coming down near the wall region ($r/R \geq 0.63$). This is consistent with the data reported in the literature, Moslemian et al. [28] used RPT to investigate the circulation patterns in two different sizes bubbling fluidized beds 0.19 m and 0.292 m, where glass beads with 700 μm diameter used as bed material. They found that, the transition from up- to down- flow was at approximately ($r/R = 0.63$). In addition, Stein et al.[14] also used positron emission particle tracking (PEPT) to investigate the macroscopic circulation patterns in a 141 mm diameter bubbling fluidized bed, resin beads with 65 μm diameter and a density of 1.1 g/cm^3 were used as bed material. They plotted the up flow and down flow of particle separately and found that

the up flow in a bubbling fluidized bed occurred at (r/R = 0 – 0.61) and the down flow was mainly achieved at (r/R = 0.63 – 1), where r is the radial position and R is the radius of the fluidized bed. The RPT measurements presented here also agree well with the findings of Tebianian et al. [25]

The magnitude of solids velocity is much higher in larger bed; the upward solids velocity of glass beads in large column is significantly higher than the upward axial velocity of glass beads particles in small column. In larger bed the solids are mostly carried through the wakes of the bubble and the effect of slugging behavior reduces depending on how large the bed is. As the bed diameter is increased, the solids move with higher velocity due to the increase in bubble size and bubble rise velocity. The bubbles in a large diameter column are large and tend to rise faster than bubbles in a smaller diameter column due to the restraining effects of the column walls and also due to the strong slugging effect in the small diameter column. The particle velocities are also increased by an increase in the gas velocity. This finding is consistent with the previous studies of Zhu et al. [29]; Wang et al. [30]; Tebianian et al. [25]; Laverman et al. [3]; Bhusarapu et al. [20]; Mostoufi and Chaouki. [12]. There are several earlier studies of solids motion in fluidized beds using different measurement techniques. Tebianian et al.[25] experimentally investigated particle velocity in FCC gas-solid fluidized beds based on four different experimental techniques (Radioactive Particle Tracking, positron emission particle tracking, optical fiber probes and borescopic high-speed particle image velocimetry). They used in RPT experiments scandium as tracer particle with size and density different from that solid particles used where the tracer particle diameter was 400 μm, which was 4-times larger than the bed particles size (107 μm). They conclude that,

radial profiles provided by each of the four techniques show upward solids velocity at the center region of the column due to the solid movement induced by the wakes and drift caused by rising voids, accompanied by corresponding downward velocities near the wall.

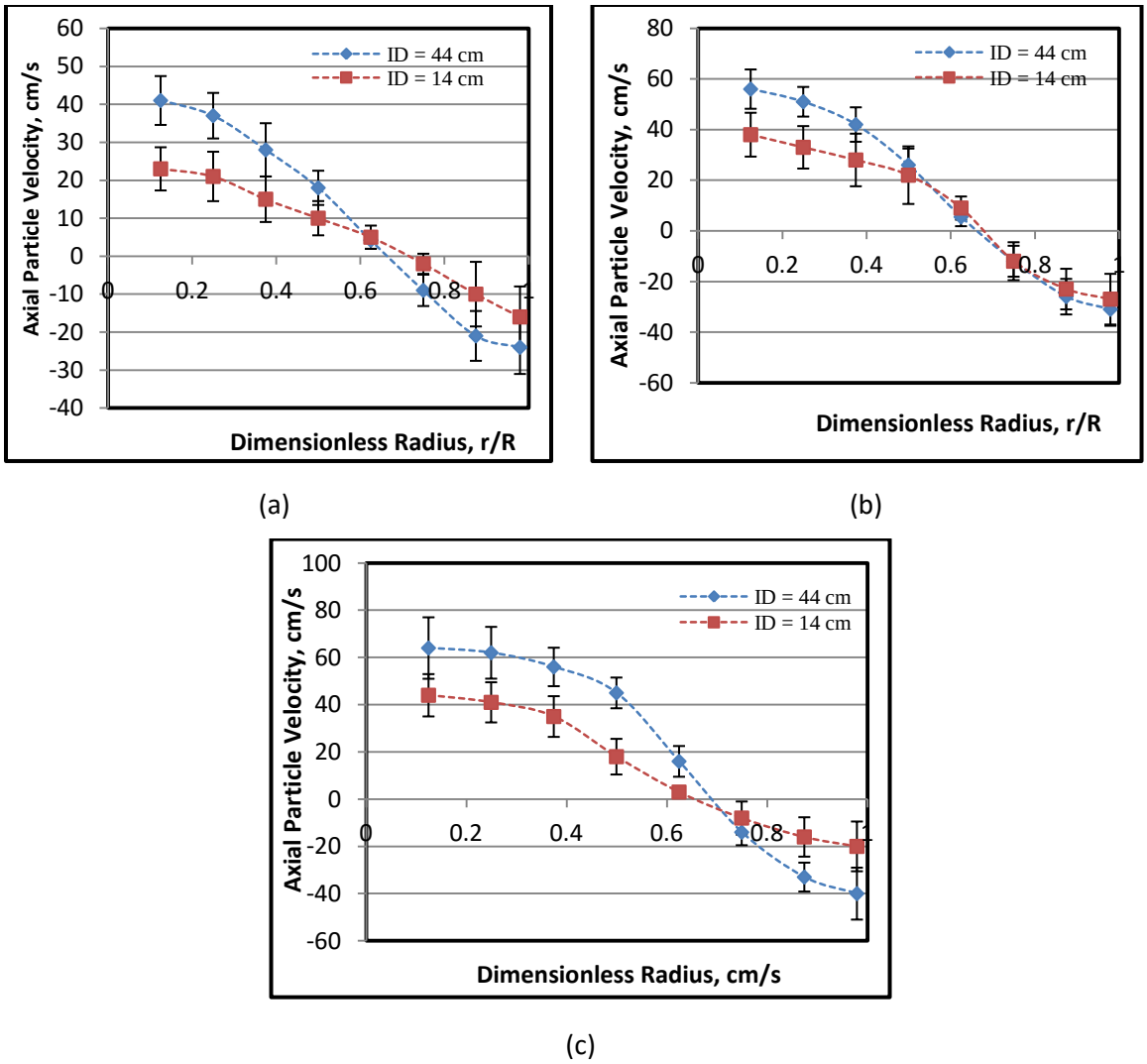

Figure 4.3 Axial particle velocity profiles for two different bed sizes 44 cm and 14 cm at different gas velocities, (a) at Ug = 1.5 U_{mf} , (b) at Ug = 2 U_{mf} , (c) at 3 U_{mf} (dot lines represent the trend)

4.1.2 Radial Particle Velocity. Figure 4.4 demonstrates the effect of the bed diameter on the azimuthally and axially averaged radial velocity of glass bead particle in two different sizes at different gas velocities (Ug = 1.5, 2, and $3U_{mf}$). The radial velocity profiles of glass beads particles with size of 210 μm are found to be below 3 cm/s, and increased with an increase in the superficial gas velocity.

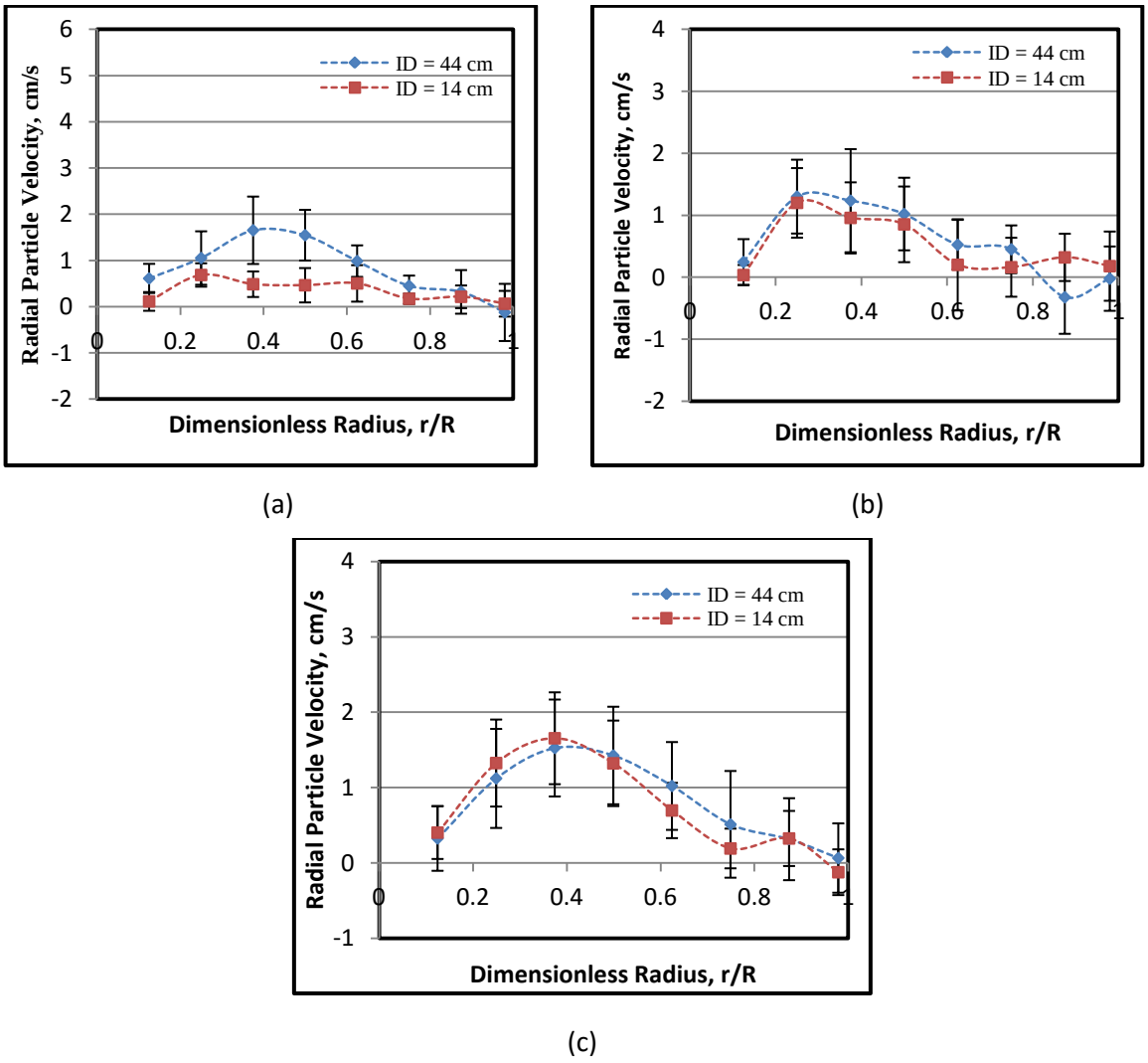

Figure 4.4 Radial particle velocity profiles for two different bed sizes 44 cm and 14 cm at different gas velocities, (a) at Ug = 1.5 U_{mf} , (b) at Ug = 2 U_{mf} , (c) at 3 U_{mf} (dot lines represent the trend)

The positive and negative values of radial velocity correspond to outward and inward motion of solids respectively. In general, for two different column sizes, radial velocities of solids are very small compared to the corresponding axial particle velocity.

4.1.3 Azimuthal Velocity. Figure 4.5 shows the azimuthally and axially averaged azimuthal velocity radial profiles. The azimuthal velocities are close to zero everywhere in the column. They do not show much sensitivity with the increase in superficial gas velocity.

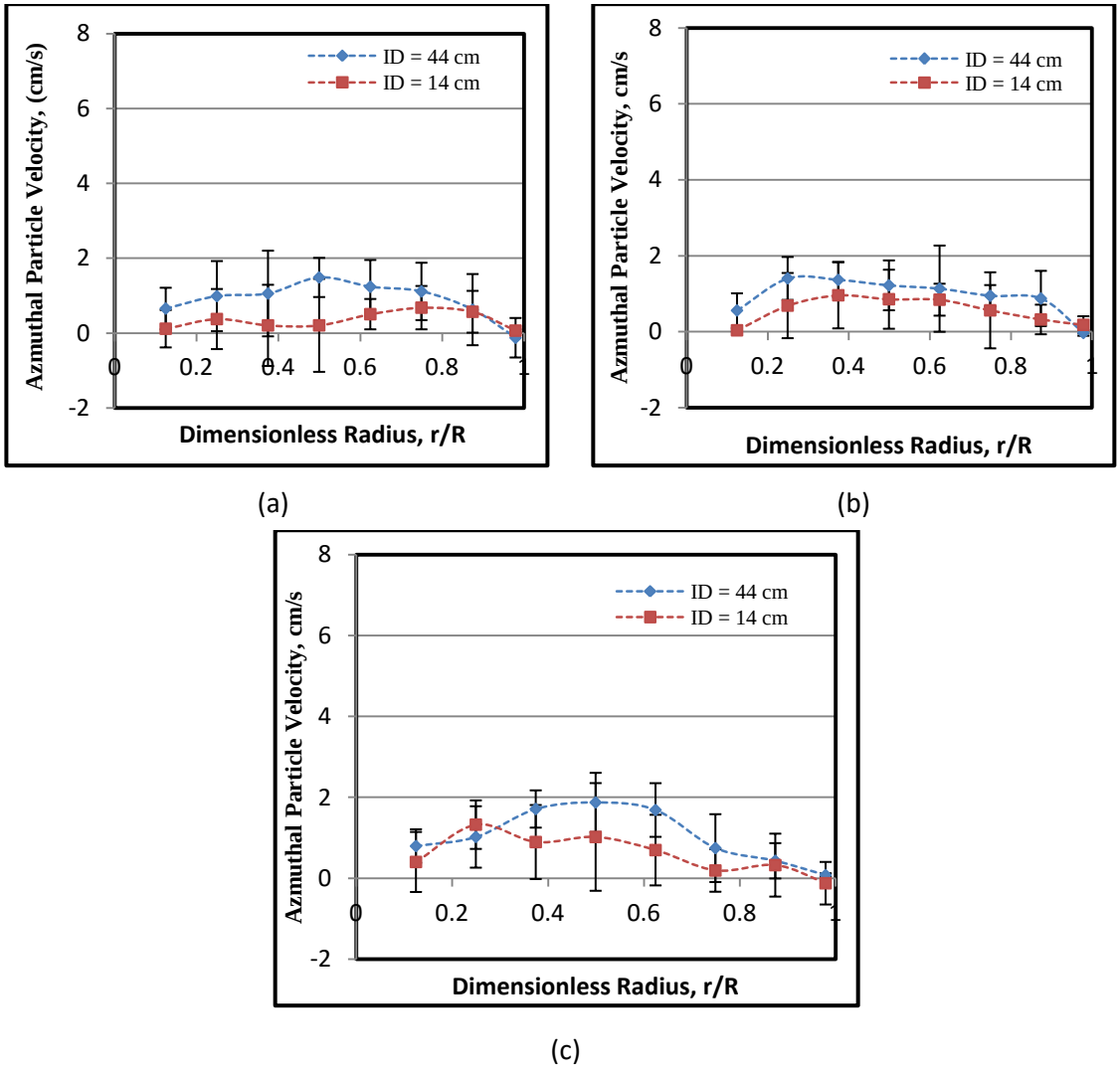

Figure 4.5 Azmuthal particle velocity profiles for two different bed sizes 44 cm and 14 cm at different gas velocities, (a) at Ug = 1.5 U_{mf} , (b) at Ug = 2 U_{mf} , (c) at 3 U_{mf} (dot lines represent the trend)

This is because the net motion for air bubble is in axial direction. Therefore, increase in superficial gas velocity does not affect the tangential direction movement.

4.2. TURBULENCE PARAMETERS

4.2.1 Reynolds Stresses. Both normal and shear stresses have been computed. Only shear stress and axial normal stresses are presented in this paper for brevity. Figure 4.6 shows the variation of the solids shear stress profiles with radial position at different fluidization velocities for 44 and 14 cm fluidized beds.

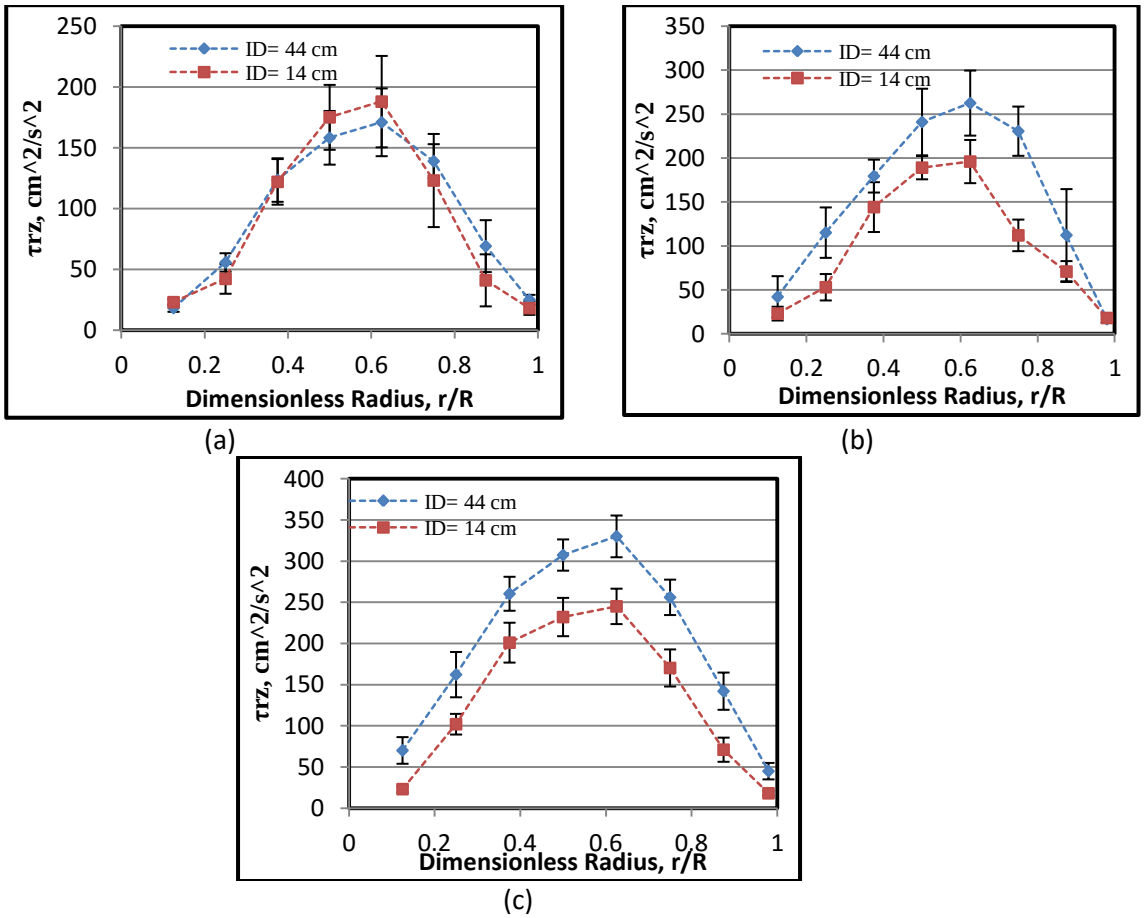

Figure 4.6 Reynolds shear stress profiles for two different bed sizes 44 cm and 14 cm at different gas velocities, (a) at Ug = 1.5 U_{mf} , (b) at Ug = 2 U_{mf} , (c) at 3 U_{mf} , (dots represent the trend)

The Reynolds's shear stress profiles show the same trend for both different sizes but their magnitudes were different, shear stress in larger column is greater than in small size, with the maximum in the shear stress values occurs at non-dimentional radius of about 0.61, which is about or close to the axial velocity inversion points (zero axial particle velocity), while the minimum value for both different sizes occurred at the center and the wall of the columns.

Solid shear stress is directly proportional to the radial gradient of solids axial velocity, therefore, the shear stress increases with increasing superficial gas velocity at each radial location for two different bed sizes, which results in higher solids shear stress at higher superficial gas velocity, as shown in Figure 4.6. The difference of the shear stress magnitude for small column when the gas velocity increased from 1.5 U_{mf} to 2 U_{mf} was 13%; while the magnitude increased by approximately 30% when the superficial gas velocity increased from 1.5 U_{mf} to 3 U_{mf} .

The measurements have shown that in both column sizes, 44 and 14 cm the solid axial normal stress as shown in Figure 4.7 is much higher than the corresponding Reynolds shear stresses. The solid axial normal stress profiles show the same trend for both sizes, with the maximum values close to the center region of the column and low values close to the wall.

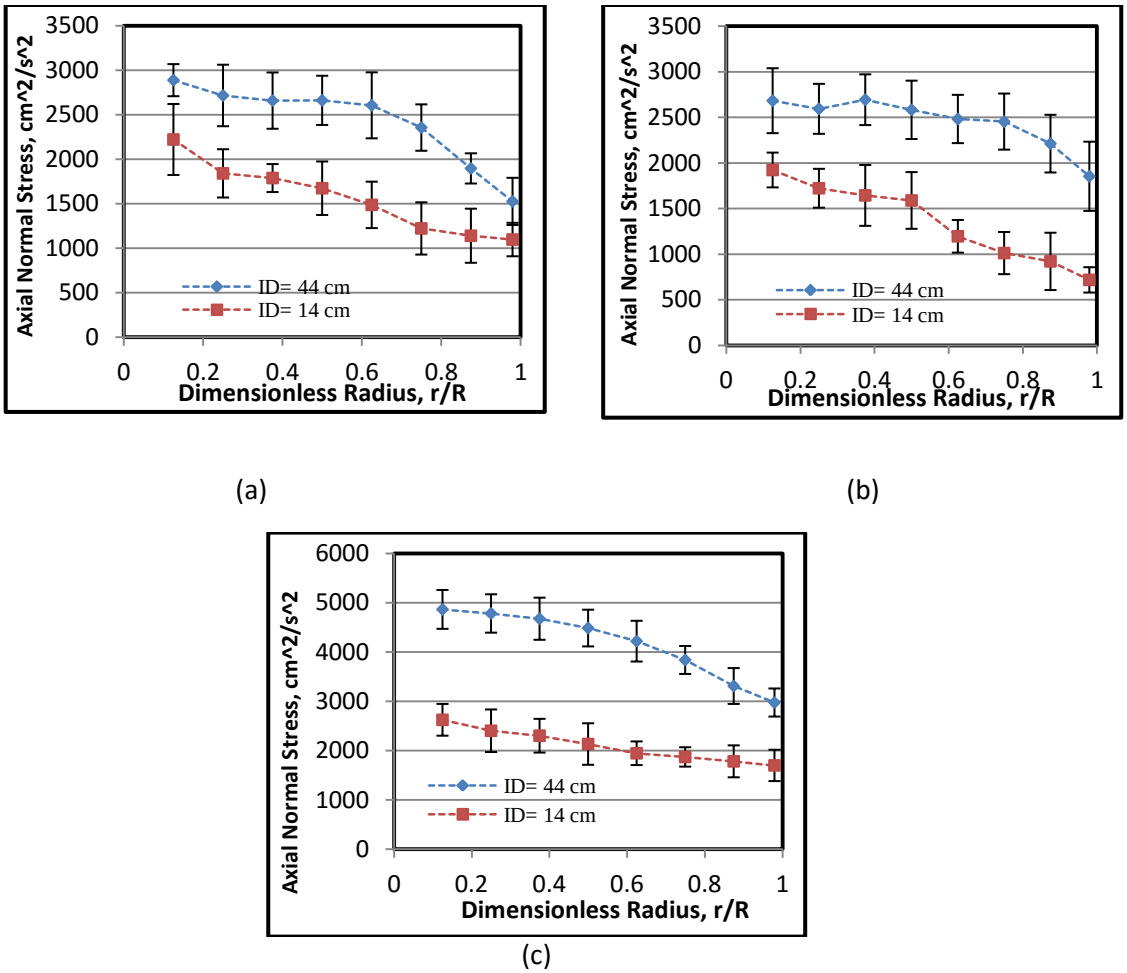

Figure 4.7 Axial normal stress profiles for two different bed sizes 44 cm and 14 cm at different gas velocities, (a) at Ug = 1.5 U_{mf} , (b) at Ug = 2 U_{mf} , (c) at 3 U_{mf} , (dot lines represent the trend)

In both sizes columns axial normal stress increases with superficial gas velocity at each radial location. It is evident that the shear stresses are less than the normal stresses. This is consistent with the data reported by Mostoufi and Chaouki. [12, 13].

4.2.2 Turbulent Kinetic Energy (TKE). An increase in superficial gas velocity makes the system increasingly more turbulent which is reflected in an increased turbulent kinetic energy. Turbulent kinetic energy (TKE) profiles as shown in Figure 4.8 exhibit maximum values in the center of the column and decrease towards the column wall.

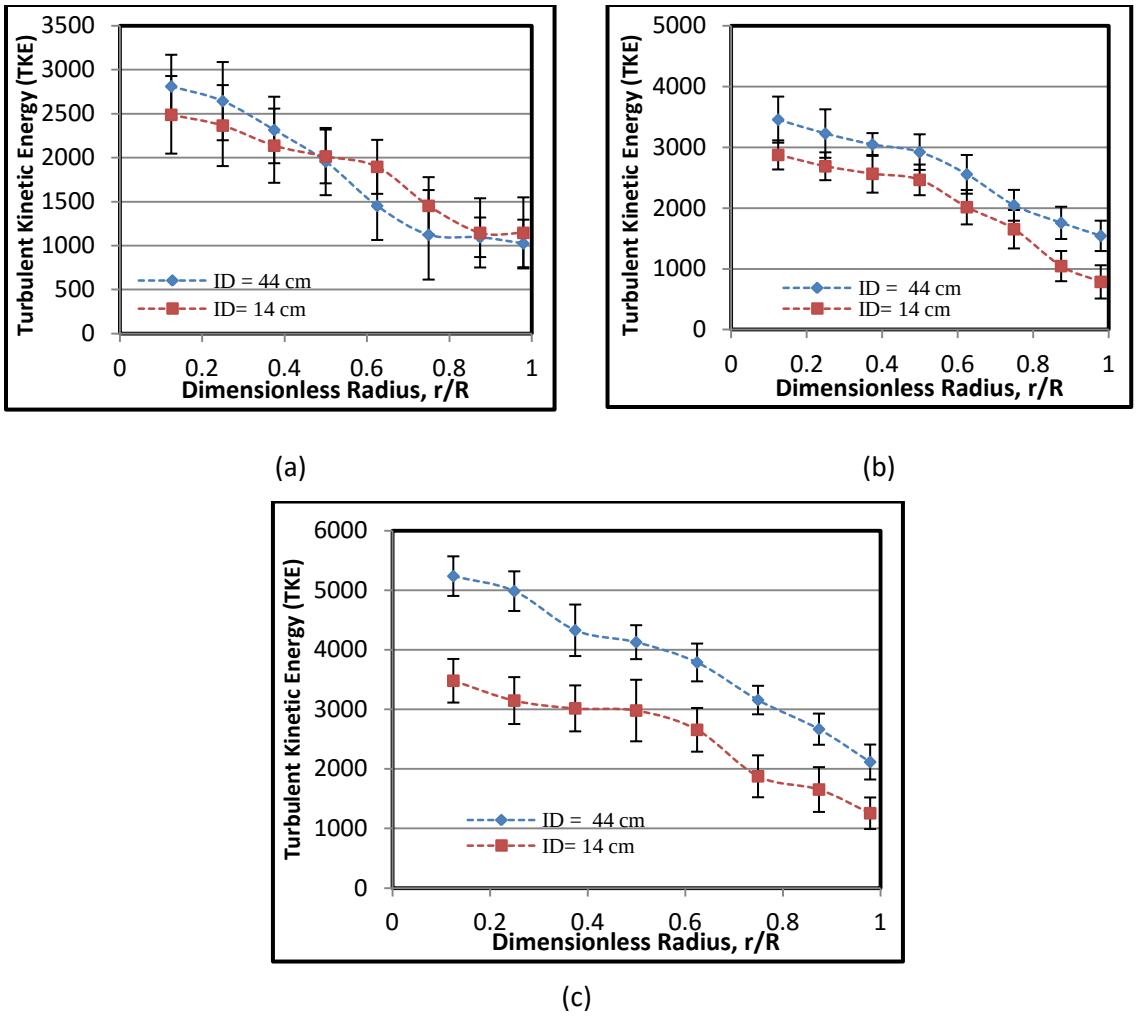

Figure 4.8 Turbulent Kinetic Energy profiles for two different bed sizes 44 cm and 14 cm at different gas velocities, (a) at Ug = 1.5 U_{mf} , (b) at Ug = 2 U_{mf} , (c) at 3 U_{mf} , (dot lines represent the trend)

The kinetic energy of glass beads particles is enhanced with an increase in superficial gas velocity. This is to be expected since with increase in superficial gas velocity there is more energy input to the system, hence a large fraction of input energy contributes to enhance the fluctuations in the solids phase. It observed that the radial profile of the solids turbulent kinetic energy follows the behavior of the solids axial normal stress.

4.2.3 Particle Diffusivity. Solids mixing are generally believed to be driven by two principal mechanisms: 1) convective mixing due to the gross circulation of solids, 2) dispersive mixing due to solids turbulent motion, Mostoufi and Chaouki. [12, 13]. The former mechanism governs the global solids mixing process in the bed while the latter controls the local solids mixing, Mostoufi and Chaouki. [12]. Axial and radial diffusivities are representative of solid mixing and diffusion of particles in the bed. The good solid mixing, high mass and heat transfer rate caused by rapid mixing of solids and solid diffusion.

In this section, axial and radial diffusivities for two different fluidized beds have been measured using the measured fluctuation velocities and formula reported by Efhaima and Al-Dahhan, [24]; Roy, [31]; Upadhyay, [32]). The results are presented as function of dimensionless radial position. The radial profiles of the axial and radial particles diffusivities for two different sizes 44 cm and 14 cm at different gas velocities (Ug = 1.5, 2, and $3U_{mf}$) are illustrated in Figures 4.9 and 4.10 respectively. It is apparent from these figures that, diffusivities in both directions (axial and radial) are higher in the large column. Lower particles diffusivity in smaller column can be attributed to the wall effect where restraining forces caused by the wall of the bed can be considered as an obstacle for circulating of particles. Therefore, in the smaller column, in which wall effect is more significant, particles would not be able to diffuse through the bed easily. Hence, the value of the diffusivity is lower near the column wall and increases by moving toward the column center in both sizes.

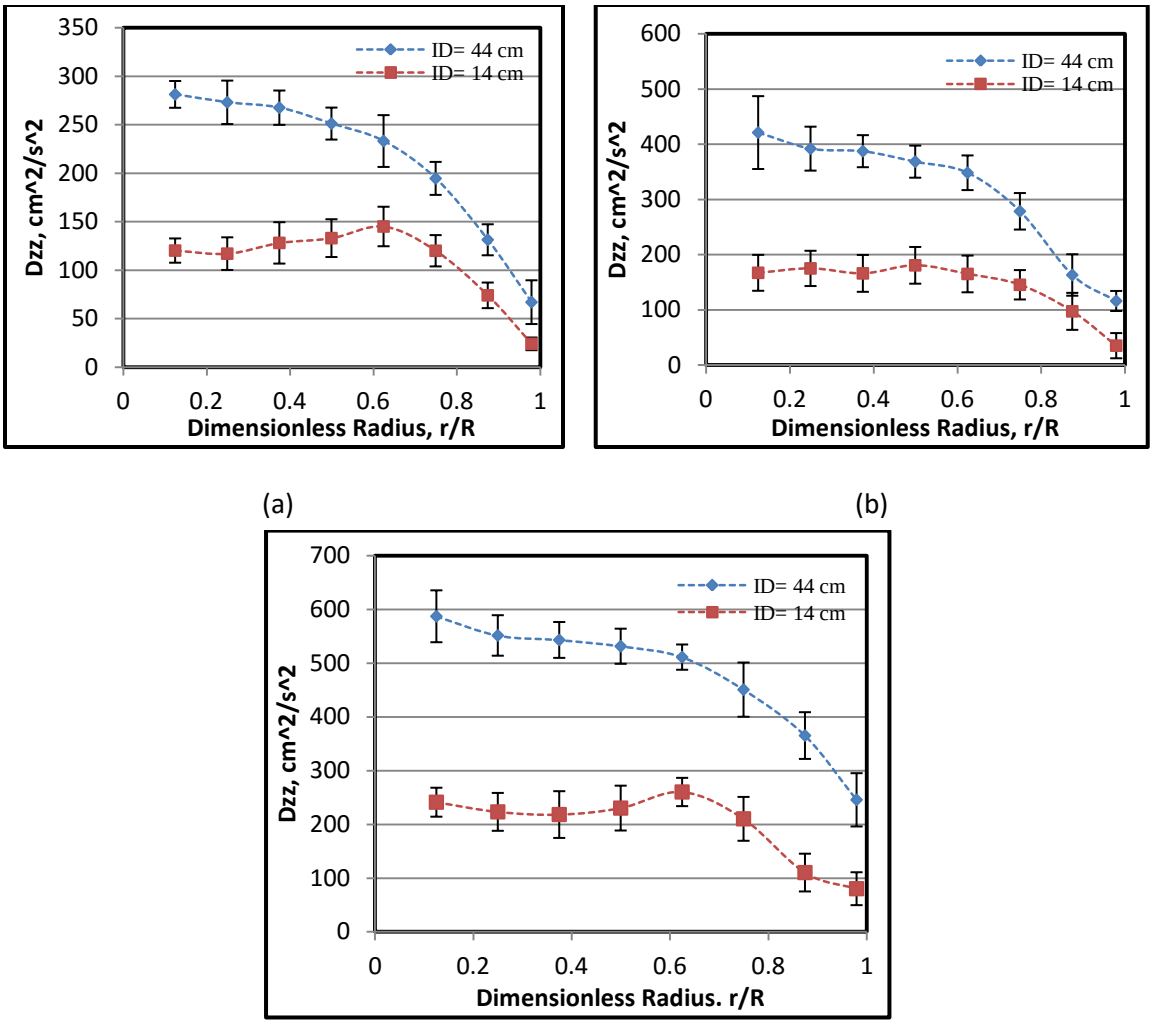

Figure 4.9 Axial eddy diffusivity profiles for two different bed sizes 44 cm and 14 cm at different gas velocities, (a) at Ug = 1.5 U_{mf} , (b) at Ug = 2 U_{mf} , (c) at 3 U_{mf} , (dot lines represent the trend)

Since it is evident that the bubbles/voids exist mainly close to the center of the bed and are absent near the wall (see Figure 4.1), therefore, value of the diffusivity is a direct function of the motion of the particles and the bubbles/voids. This is consistent with the data reported by Mostoufi and Chaouki.[27]. Mostoufi and Chaouki [27] proposed that the axial solids diffusivity is a linear function of the velocity gradient as follows:

$$D_z = \alpha\, \gamma_z + D_{z,0}$$

Where α is the slope, γ_z is the axial velocity gradient, and $D_{z,0}$ is the solids diffusivity at the zero gradient condition, (i.e., solids diffusivity in a constant velocity field). According to their experimental results, the slope was principally a function of the particle diameter in a dense gas solid fluidized bed. From Figure 4.9, 4.10, it is seen that diffusivities in both directions and in both sizes columns increased with the superficial gas velocity. It could be attributed to a higher turbulent activity of bubbles at higher gas velocities in the bubbling regime.

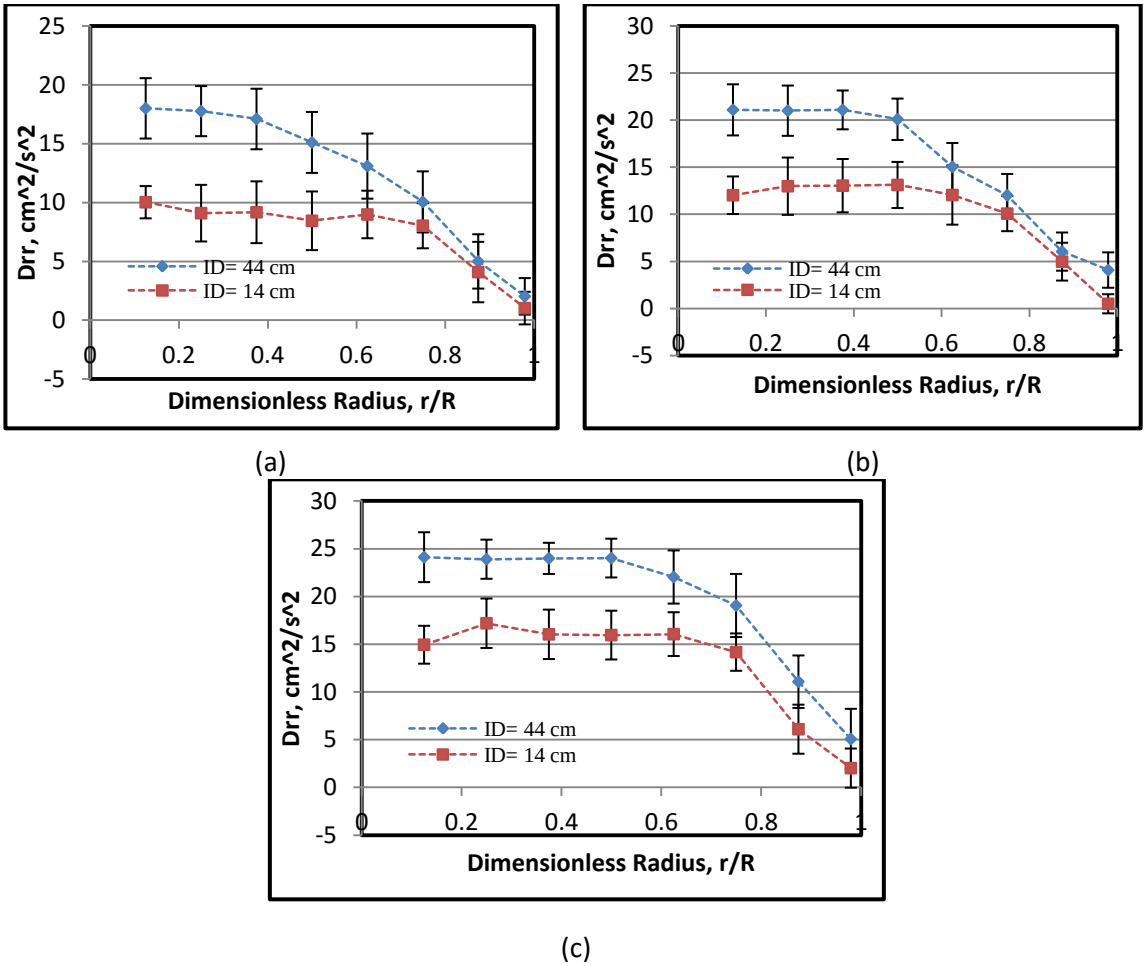

Figure 4.10 Radial eddy diffusivity profiles for two different bed sizes 44 cm and 14 cm at different gas velocities, (a) at Ug = 1.5 U_{mf} , (b) at Ug = 2 U_{mf} , (c) at 3 U_{mf} , (dot lines represent the trend)

Bubbles and voids are the main reason of particles circulation in fluidized beds. Shape and size of the bubbles influence the diffusivity of the particles. An increase in the superficial gas velocity increases the bubble rising velocity. Therefore, both axial and radial diffusivities are increased accordingly. Mostoufi and Chaouki. [27] concluded that the particle axial and radial diffusivities are not affected by the size of the radioactive tracer particle and changes only with the superficial gas velocity, and they also emphasis that the dispersion of solids in a fluidized bed is governed by the interaction between the ensemble of solids such as bubble wakes and clusters rather than random movement of individual particles.

5. REMARKS

Experimental results are reported on the solids motion in 3-D gas-solid fluidized beds operated in the bubbling mode and at atmospheric pressure. A non-invasive technique radioactive particle tracking (RPT) was employed in this work, which allowed the determination of solids velocity field and turbulente parameters. Comparison of the results obtained in two different beds show that, bed scales were found to greatly affect the hydrodynamics in fluidized bed systems. It is necessary then to establish a reliable mechanistic method for scaling up gas-solid fluidized bed to maintain hydrodynamics similarity of the key parameters in dimensionless form or magnitude.

The magnitude of solids velocity is much higher in larger bed; the upward solids velocity of glass beads in large column is significantly higher than the upward axial velocity of glass beads particles in small column due to the variation of the intensity of carrying solids by the wakes of the bubble and the variation of the effect of slugging behavior.

The solid mixing and diffusion of particles are increased by increasing the column diameter, this due to wall effects which are more dominant in small scale column than in large scale column. The axial velocity gradient, has a significant effect on the solid diffusivity, the radial velocity gradient, is found to be at least an order of magnitude smaller than the axial velocity gradient and therefore has no significant effect on the solid diffusivity. It is important to note that diffusivity is a linear function of the solids shear stress.

Mostly bubbles are initiated near the wall and move toward the center of the bed. The bubble size and the bubble rise velocity are all strongly influenced by the bed size. In

small bed bubbles move in the form of slugs, particularly at higher superficial gas velocities, whereas in larger beds bubbles grow in size due to coalescence. Due to decrease wall effect in large scale. These differences in the bubble behavior directly affect the contacting between gas and solids, and hence affect the chemical conversion.

In addition all the quantities studied in this work were increasing constantly without a sharp change in their trend by increasing the superficial gas velocity in two different bed sizes. These observations are in line with conclusions by Mostoufi and Chaouki, [27]. Further experimental work is highly recommended in this area by using more different bed diameters.

The tracer particle used in this study does not meet the size of glass beds used, but they have the same density which is 2.5 g/cm^3. It has been shown by Mostoufi and Chaouki.[12,13,27] that the matching the density of the tracer particle with that of particles of the bed used is the key in obtaining reliable data since the particles in a gas-solid fluidized bed do not move as single and isolated particles. In fact, they found that the solids mixing properties (such as diffusivity and dispersion coefficient) in the fluidized beds are the same for different particle sizes and vary only with superficial gas velocity.

ACKNOWLEDGMENT

The authors wish to acknowledge the Libyan Ministry of Education for sponsoring the primary author's study within the Chemical and Biochemical Engineering Department at Missouri University of Science and Technology. The radioactive particle tracking (RPT) technique and set-up used in this work were funded by professor Al-Dahhan's research fund.

REFERENCES

[1] Martin Rüdisüli, Tilman J. Schildhauer, Serge M.A. Biollaz J. Ruud van Ommen, Scale-up of bubbling fluidized bed reactors - A review. Powder Technology Volume 217, Pages 21–38 (2012).

[2] Dubrawski,K.,Tebianian,S.,Bi,H.T.,Chaouki,J.,Ellis,N.,Gerspacher,R.,Jafari,R., Kantzas, A.,Lim,C.,Patience,G.S.,Pugsley,T.,Qi,M.Z.,Zhu,J.X.,Grace,J.R.,2012. Traveling column for comparison of invasive and non-invasive fluidization voidage measurement techniques.PowderTechnol.224 (2012),p, (203–220).

[3] Laverman JA , Fan X, Ingram A van Sint Annaland, M, Parker DJ, Seville JPK, Kuipers JAM. Expermental study on the influence of bed material on the scaling of solids circulation patterns in 3D bubbling gas-solid fluidized beds of glass and polyethylene using positron emission particle tracking . Power Technol. 2012; 224:297-305

[4] Van der Meer, E.H., Thorpe, R.B., Davidson, J.F., Dimensionless groups for practicable similarity of circulating fluidized beds, Chem. Eng.Sc., Vol.54, No. 22,5369-5376 (1999).

[5] Xu, G., Nomura, K., Nakagawa, N., Kato, K., Hydrodynamic dependence on rise diameter for different particles in circulating fluidized beds. Powder Technology, Vol. 113, No. 1-2, 80-87 (2000)

[6] M. Al-Dahhan, S. Aradhya, F. Zaid, N. Ali, T. Aljuwaya., Scale-up and on-line monitoring of gas-solid system using advanced and non-invasive measurement techniques, Symphos 2013, 2nd International Symposium on Innovation and Technology in the Phosphate Industry, (2014)

[7] L. R. Glicksman. Scaling Relationships for Fluidised Beds. Chemical Engineering Science, 43, 1419-1421 (1988)

[8] Frye, C.G., Lake, W.C., Eckstrom, H.C., Gas-solid contacting with ozone decomposition reaction. AICHE J., Vol.4, No. 4,403-408 (1958)

[9] M. Horio, A. Nonaka, Y. Sawa and L. Muchi, A New Similarity Rule for Fluidized Bed Scale-up.AIChE Journal,32, pp. 1466-1482 (1986).

[10] R. Mabrouk, R. Radmanesh, J. Chaouki, C. Guy, Scale Effects on Fluidized Bed Hydrodynamics. Inter. J. of Chemical Reactor Eng (2005).

[11] Bashiri H., Ramin R., Rahmat S., Chaouki J., Effect of Bed Diameter on the Hydrodynamics of Gas-solid Fludized beds, Iran. J. Chem.Eng. Vol.29, No.3 (2010)

[12] Mosfoufi N., Chaouki J., Local solid mixing in gas–solid fluidized beds, Powder Technology 114 , pp. 23–31(2001)

[13] Mosfoufi N., Chaouki J., Flow Structure of Solids in Gas-Solid Fluidized Bed, Chem. Eng. Sci., 59, p. 4217 (2004).

[14] Stein M., Y.L. Ding, J.P.K. Seville, D.J. Parker, Solids motion in bubbling gas fluidized beds, Chemical Engineering Science 55 (2000) 5291–5300.

[15] Bing Du, W. Warsito, and Liang-Shih Fan, ECT Studies of Gas-Solid Fluidized Beds of Different Diameters. Ind. Eng. Chem. (2005), 44, pp-5020-5030

[16] Bangyou W., Guang Yu., Bellehumeur C., Kantzas A., Dynamic flow behavior measurements in gas-solid fluidized beds using different non-intrusive techniques and polyethylene powder. Flow measurement and instrumentation, 18 pp. 197-203 (2007)

[17] Vikrant V., Padding JT., Deen NG., Kuipers JAM,. Effect of Bed Size on Hydrodynamics in 3-D Gas–Solid Fluidized Beds. . AIChE J. 2015; vol. 61: N0.5 1632–1644.(2015).

[18] Miller, C.O.. Logwinuk, A. K., Ind. Eng. Chem., 43, 1220 (1951)

[19] Bhusarapu, SB. Solids flow mapping in gas-solids risers. D.Sc. Thesis. Department of Chemical Engineering, Washington University, St. Louis, 2005.

[20] Bhusarapu, S., H. Al-Dahhan., Dudukovic M. Solids flow mapping in a gas-solids risers: Mean holdup and velocity fields . Power Technolo 163, pp 98-123. (2006)

[21] Shaikh, A. Bubble and slurry bubble column reactors for syngas to liquid fuel conversion: Mixing, flow regime transition, and scale-up, PhD, Thesis, Washington University in St. Louis, Saint Louis, MO, USA, (2007).

[22] Shaikh, A. H. A-Dahhan A new methodology for hydrodynamic similarity in bubble columns, The Canadian journal of chemical eng. Vol 88, (2010)

[23] M. Almesfer, Effect of dense heat exchanging internals on the hydrodynamics of bubble column reactors using non-invasive measurement techniques, PhD, thesis, Missouri University of Science & Technology, Rolla, (2013)

[24] Efhaima. A., H. A-Dahhan, Assessment of Scale-up Dimensionless Groups Methodology of Gas-Solid Fluidized beds using Advanced Non-Invasive Measurement Technique (CT and RPT)

[25] Tebianian S., Dubrawski K., Ellis N., Cocco R., D.J. Parker., Chaouki J., Investigation of particle velocity in FCC gas-fluidized beds based on different measurement techniques, Chemical Engineering Science 127(2015) 310–322

[26] Luo, X.; Lee, DJ; Lau, R.; Yang, G.; Fan, L-S. Maximum stable bubble size and gas holdup in high-pressure slurry bubble columns. *AIChE J.*, 45(4), 655. 1999.

[27] Mosfoufi N., Chaouki J., On the Axial Movement of Solids in Gas-Solid Fluidized Beds. I ChemE, Vol 78, Part A, (2000).

[28] D. Moslemian, M.M. Chen, B.T. Chao, Experimental and numerical investigation of solids mixing in a gas fluidized bed, Part. Sci. Technol. 7 (1989) 335-355.

[29] Haiyan Zhu, Jesses Zhu, Guozheng Li, Fengyun Li, Detailed measurements of flow structure inside a densde gas-solids fluidized bed, Power Technology 180 ,pp 339-349, (2008)

[30] Wang Q., Zhnag K., Yang K., Jiang J., Particle velocity in a Dense Gas-Solid Fluidized Bed. Inter. J. of Chemical Reactor Eng (2008).

[31] Roy, S., Quantification of Two-phase Flow in Liquid-solid Risers, PhD, Thesis, Washington University in St. Louis, Saint Louis, MO, USA, (2000).

[32] Upadhyay. R., Roy. S, Investigation of hydrodynamics of binary fluidized beds via radioactive particle tracking and dual-source densitometry, The Canadian journal of chemical Eng. Vol. 88, 2010.

[33] Efhaima A., A-Dahhan Muthanna, Local time-averaged gas holdup in fluidized bed reactor using gamma ray computed tomography technique (CT), Int J Ind Chem. Vol.6, pp. 143-152 (2015)

SECTION

2. SUMMARY AND RECOMMENDATIONS

The main objectives of this work is to assess the scale-up methodologies based on detailed local hydrodynamics of gas-solid fluidized bed reactors (FBRs) by employing advanced non-invasive measurement technique which are gamma ray computed tomography (CT) technique to measure the time averaged cross-sectional distributions and radial profiles of gas and solids holdups along the height of the bed, and radioactive particle tracking (RPT) technique to measure 3-D particle velocities field and turbulent parameters (Reynolds stress, normal stresses, turbulent kinetic energy, turbulent eddy diffusivities, eddy diffusivity, etc).

2.1. SUMARY AND CONCLUSION

The key findings of this work are briefly summarized as follows:

1- By using CT and RPT techniques for local hydrodynamics measurements we have successfully validated the new mechanistic scale-up methodology for hydrodynamics similarity of gas-solid fluidized beds that has been proposed in our laboratory which is based on maintaining similar or close time averaged radial profiles of gas holdups in two different gas-solid fluidized beds to achieve local and global similarity of dimensionless hydrodynamic parameters. This is because the gas dynamic dictates the hydrodynamics in these beds.

2- The scale-up methodology that is based on matching dimensionless groups of the simplified set of Glicksman et al., (1993) has found to provide non-similar local

hydrodynamic parameters in terms of solids and gas holdups measured by CT technique and dimensionless solids velocities and turbulent parameters measured by RPT technique. With the variation shown in the local parameters, this confirms that global parameters should not be used primarily to assess scale-up methodologies. The assessment of the conditions for matching dimensionless groups suggests that current dimensionless groups are not sufficient to explain the complete hydrodynamics of the fluidized bed system. However, adding more dimensionless groups to match it wil only complicate the scale-up methodology since it is hard to practically match a large number of dimensionless groups. Therefore, our new mechanistic scale-up methodology mentioned above could be a reliable alternative to the matching dimensionless groups based methodology for fluidized bed reactors.

3- The increase in the superficial gas velocity causes increase in the bed expansion, overall and radial profiles of the gas holdup and the local and radial profiles of the solids velocities and turbulent parameters.

4- Two different Geldart type-B particle were used in this work glass beads of size 70 μm and 210 μm with a density of 2500 Kg/m^3, and copper particle of size approximately 200 μm with density of 5300 Kg/m^3 , solid holdup (gas holdup +solid holdup = 1) was determined by using computed tomography (CT) technique. As the density of the particles increases the values of the solids holdup increases. Also, an increase in the particle diameter the values of the solids holdup radial profiles also increase.

5- The shear stresses radial profiles showed the same trend for both different bed sizes but their magnitudes are different, with the maximum values of the shear stress occurs

within the range of r/R = 0.4- 0.63 and lower values at the centre and wall regions of the bed. The trend of the radial profiles of the shear stresses reflects the trend obtained for the radial profiles of the radial particles velocity. The radial profiles of shear stresses showed that it increases with the increase height of the bed in two different size fluidized beds.

6- The radial profiles of the normal solid stresses increases with the increase height of the bed in two different size fluidized beds. The normal stresses in the axial direction were larger than those in the radial and tangential directions.

7- The turbulent kinetic energy (TKE) radial profiles showed the same trend for the studied small and large columns with higher magnitude in the large column. The profiles follow the trend of the axial particle velocity where the fluctuations in the axial particle velocity dominate the estimation of the turbulent kinetic energy. The turbulent kinetic energy is larger in the centre region of the column and decrease towards the column wall for the two studied columns. Also the turbulent kinetic energy increases with the increase height of the bed.

8- The obtained data and knowledge are valuable as benchmarking data for validating computational fluid dynamics (CFD) simulations and closures which is essential for utilizing CFD as enabling tool to facilitate the implementation of the new mechanistic scale-up methodology and for simulating fluidized bed reactors in general.

2.2. FUTURE WORK

Although this work provided important knowledge and data to improve understanding the scale-up and hydrodynamics of the fluidized bed reactors, the following are some suggestions for possible future work:

1. The new mechanistic scale-up methodology which has been proposed and validated in our laboratory needs to be further studied using validated CFD including for hot and reactive fluidized beds.
2. The new mechanistic scale-up methodology needs to be implemented and validated on fluidized beds with internals by developing a mechanism of maintaining geometrical similarity. Industrial reactors often consist of internals such as sieve trays and heat exchanging tubes.
3. The RPT technique data need to be further processed to provide more insight on the hydrodynamics and the new scale-up method validation such as local residence time distribution, attractor, trajectory length distribution, solids holdup and its comparison with CT technique results, etc.
4. The present work was conducted at ambient temperature. More research needs to be conducted on fluidized beds at elevated temperatures and pressures that represent the actual manufacturing processes.
5. Industrial reactors often operate at the turbulent flow regime; hence, the applicability of the proposed methodology needs to be checked under such operating conditions for large size fluidized beds.
6. The effect of reactor diameter and operating parameters on the hydrodynamic of fluidized beds operated in turbulent flow regime needs to beinvestigated.

7. The effect of the design parameters of fluidized bed reactors such as the distributor types, the internals configurations and dimensions, etc, on the hydrodynamics of the fluidized beds also need to be studied.
8. Integrating the results and the findings of this work and the CT and RPT results with studies related to the bubble size, velocity and frequency distribution, heat and mass transfer coefficient and how these are matched during scale-up need to be considered for further studies.
9. Future experiments should be performed using particles of different sizes materials and morphology to evaluate the fluidization and hydrodynamics dependency on the particles properties.

APPENDIX A

EXPERIMENTAL SET-UP

A. EXPEREMENTAL SET-UP

In this work, two fluidized beds were used of 6-inch (0.14 m) and 18-inch (0.44 m) in diameter. The fluidized bed columns were constructed from Plexiglas and consisted of column and plenum. A schematic diagram of the beds used in this work is illustrated in Figures A-1 and A-2. The 0.14 m column was 1.68 m high connected from the top with an upper section that had a larger diameter of 0.42 m and was 0.84 m high to disengage the solid particles from the flowing gas by reducing the superficial gas velocity of the gas phase. The plenum was located at the bottom, which consisted of a sparger tube. The gas phase was introduced through a distributor at the bottom after passing through the sparger. The gas distributor was made of a porous polyethylene sheet and had a pore size of 40 μm. The sparger was plugged at one end, and had 14 holes, all facing downward with respect to the column. The 0.44 m diameter fluidized bed very closely resembled the 0.14 m fluidized bed. The shape of the upper section was similar, but it had a diameter of 0.88 m and was 0.95 m high. The distributor design was similar to that used with the 0.14 m diameter fluidized bed. The plenum also consisted of a sparger tube, which had 20 holes, all facing downward with respect to the column. Both columns were electrically grounded to minimize electrostatic effects. Compressed air supplied from an industrial compressor, that can deliver compressed air of 735 CFM capacity at pressures up to 200 Psig, was used in this work. Two rotameters (Omega® Engineering, Inc.) with different scales were connected in parallel to cover a wide range of flow rates (160 to 3200 SCFH). The gamma ray computed tomography (CT) scans were acquired at H/D = 0.286, 0.64 and 1.7 above the gas distributor for the 0.14 m diameter column, and at about equivalent or close levels, which are at H/D = 0.286, 0.88 and 1.6 above the gas distributor for 0.44 m diameter bed. Radioactive particle tracking (RPR) technique was

implemented on the bed height of H/D = 0.1 - 2.2 above the gas distributor for the 0.14 m diameter column and of H/D = 0.05 - 2.5 above the gas distributor for 0.44 cm diameter column as illustrated in Figures A-1 and A-2

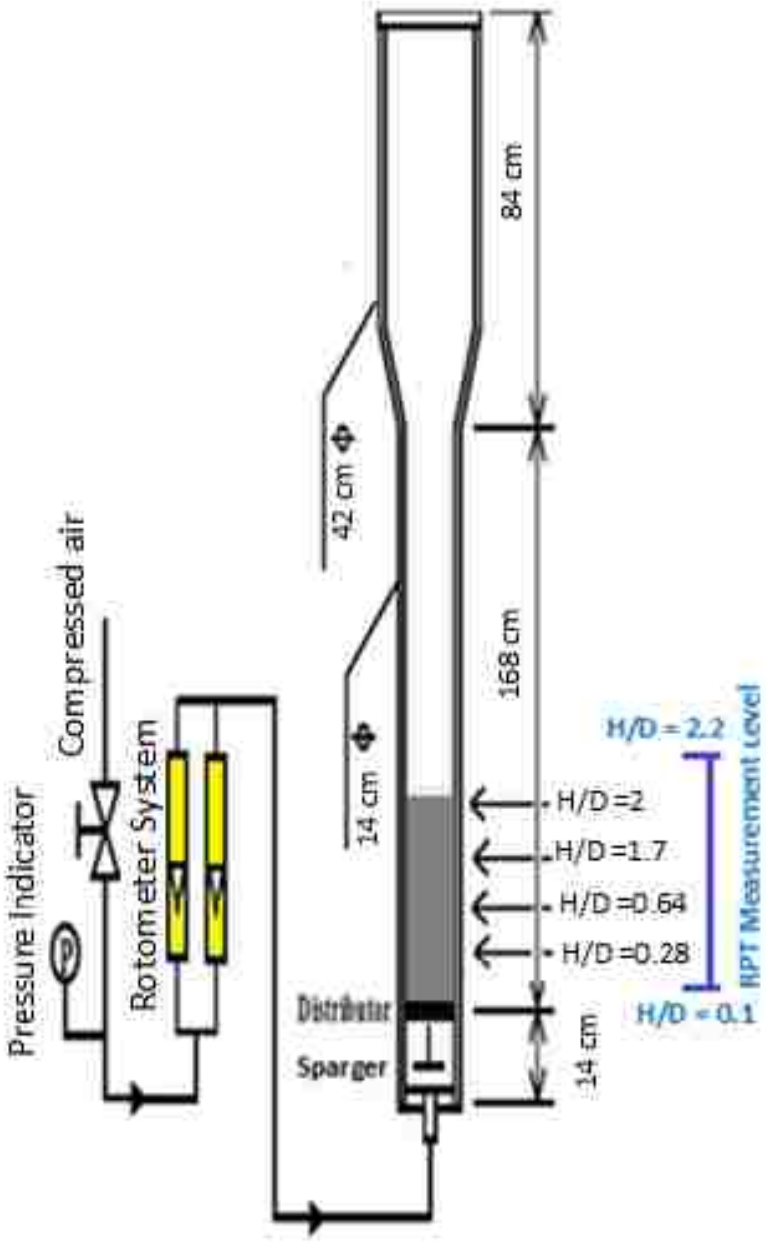

Figure A.1. Schematic diagram of 0.14 m cold–flow fluidized bed reactors with measurement levels for CT and RPT techniques

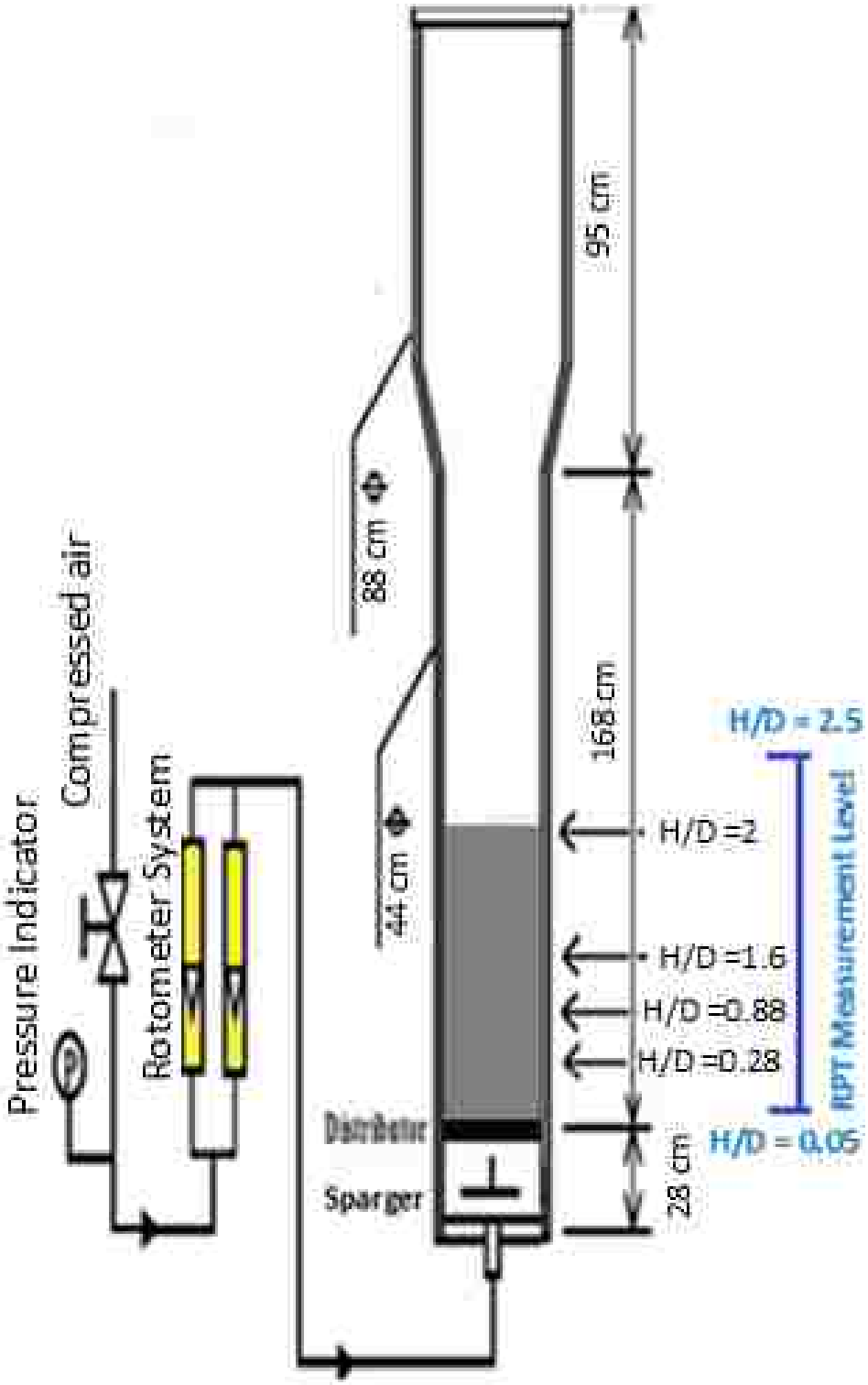

Figure A.2. Schematic diagram of 0.44 m cold–flow fluidized bed reactors with measurement levels for CT and RPT techniques

APPENDIX B

GAMMA RAY COMPUTED TOMOGRAPHY (CT) TECHNIQUE

B. GAMMA RAY COMPUTED TOMOGRAPHY (CT) TECHNIQUE

The gamma ray computed tomography (CT) technique that has been used in this work comprises of Cs-137 sealed source and a set of 15 NaI scintillation detectors. This technique is a part of our dual source and energy (Cs-137 and Cobalt Co-60) gamma ray computed tomography (CT) technique, which was developed by Varma (2008) with the help of the team from the Oak Ridge National Laboratory (ORNL) sponsored by the Department of Energy (DOE). It is currently available in the professor Al-Dahhan's multiphase reactors engineering and application laboratory (mReal) at the Missouri University of Science and Technology (Missouri S&T). In this work, CT experiments were performed under two-phase conditions, gas and solids, and hence a single sealed source (Cs-137) and its related 15 NaI scintillation detectors located opposite to the (Cs-137) sealed source has been used to measure in a non-invasive manner the time-averaged cross-sectional phase holdups distributions and their radial profiles. As shown in Figure B-1 the sources and detectors are built on a rotary plate to move together in 360° around the studied bed, providing 197 views in each scan and 21 projections in each view. The entire assembly could be moved up and down by stepper motor along the bed height to scan the bed at different axial positions. Each detector consists of a 2-inch cylindrical NaI crystal, a photomultiplier and electronics. Each of these detectors was collimated with a lead collimator with an open aperture. Two sizes of collimators were used in this work. Collimators that have approximately an open aperture of 2 mm × 2 mm were used with 0.14 m diameter column, while those that have approximately an open aperture of 2 mm × 5 mm were used with 0.44 m diameter column. Since in 0.44 m diameter bed high attenuation was encountered, large aperture size was used in order to collect enough

counts. However, in this case the spatial resolution was reduced to the size of 2 mm × 5 mm

Figure B.1. The photo of the dual source CT Setup with a 0.14 m fluidized bed reactor

The CT scan sampling rate was 60 samples at 10 Hz, which took approximately 7.2 seconds to finish a 50 projection and 8.25 hours to complete a full scan by 360° rotation of the Cesium (CS-137) source and detectors around the column.

B.1 STEPS OF SCANNING

In this work, CT experiments were performed under a two-phase condition, (gas and solid). The Cesium (Cs-137) source was used to measure time averaged cross-sectional distributions and radial profiles of gas and solids holdups at different axial levels. The set of scans performed consisted of: 1) Scanning the column empty as a

reference CT scan, 2) Scanning the column filled with solids (glass beads) as a packed bed to estimate the attenuation coefficient of the solids phase in each pixel, and 3) Scanning the column at the desired conditions of gas-solid fluidization. The CT scans were acquired at H/D = 0.28, 0.64 and 1.7 above the gas distributor for the 0.14 m diameter column, and at equivalent levels, which were at H/D = 0.28, 0.88 and 1.6 above the gas distributor for 0.44 m diameter bed as shown in Figure A-1 and A-2.

B.2. AVERAGING THE RAW DATA

The first step of data processing is averaging the data points of each projection for each sampling period and for all scans performed to reduce the effect of noise and uncertainty in the data and to get a better quality of the images. The mean value of the counts based on multiple samples or readings for a given projection is often used for processing the data.

B.3.TRANSMISSION RATIO CALCULATION (*I/Io*)

The averaged data files for packed bed desired condition and empty column (reference scan) scans are used to calculate the transmission ratio (I/I_o) of the scanned section. The transmission ratio is the ratio of counts obtained while scanning the object to that obtained when column is empty (I/I_o).

B.4. CALCULATING THE LENGTH OF THE CHORDS FOR EACH PROJECTION

The data obtained during scans are interpreted in terms of Beer-Lambert's law:

$$T = \frac{I}{I_0} = \exp(-\mu\rho l) \qquad \text{(B-1)}$$

Where, *Io* is the incident radiation (in our work we consider it that of the empty column) and *I* is the detected radiation intensity after passing through length *l* [cm] of object whose linear gamma-ray attenuation coefficient is μ [cm^{-1}], ρ is the medium density [$g.cm^{-3}$]. This equation is used to obtain the mass attenuation coefficient values($\rho\mu$) from the transmission ratio. In this case we also need to know the chord lengths *l*. The value of *l* is calculated based on the geometry of CT scanner and the dimension of the scanned bed. The first step is to decide on the pixel size or the dimensions of the elements of the matrix used for the discretization of the reconstruction domain. The circular section of the column was divided into n × m square pixels. The cross-section of the bed is divided into 80 × 80 square pixels. The size of the pixel depends on the achievable spatial resolution, or the width of the detector collimator. An even number of pixels is required on each side of the matrix. In this work, the linear attenuation coefficient in each pixel was verified for gas and solids phases.

B.5. ASSIGNING INITIAL GUES VALUES.

Since the AM reconstruction algorithm that is used in this work is an iterative process, we need to provide the initial guess values for the attenuation coefficient in each pixel. The initial guess values are generated by assigning 0.08 (unit in 1/cm) to all the pixels in the square matrix which falls within or on the boundary of the test section as shown in Figure B-2. The choice of the magnitude is arbitrary and only affects the required number of iterations in the reconstruction process. For the pixels that are fully outside the test domain, 0 is assigned.

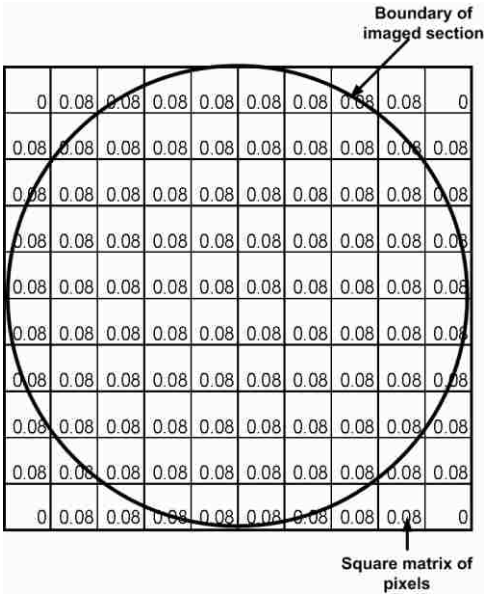

Figure B.2. Discretization of Domain Cross-Section

B.6. CT IMAGE RECONSTRUCTION

Image reconstruction is a key part of the tomography process. The transmission data of gamma ray photons, representing the line integrals of the attenuation along a path between the source and the detectors across the domain as shown in Figure B-3. The image is a collection of pixels such that each pixel represents a small spatial segment of the domain. The liner attenuation coefficients values of each pixel in the domain when view collectively represents the attenuation image of the domain. The goal of reconstruction step is to obtain attenuation coefficients values on the domain. The reconstruction algorithm developed and used by Varma et al., (2007) and Varma et al., (2008) was implemented in this work to reconstruct the cross-sectional distribution of relative attenuation in a two-phase system. Proposed an alternating minimization (AM) algorithm based on turning a maximum likelihood problem into a double minimization of

I-divergence introduced by Csiszar et al., (1991). I-divergence is a measure of inconsistency between two functions, a(y) and b(y), which is given as:

$$I(a\backslash\backslash b) = [\sum_{y\epsilon Y} a(y) \ln\left[\frac{a(y)}{b(y)}\right]] - \sum_{y\epsilon Y}[a(y) - b(y)] \quad \text{(B-2)}$$

where Y is a finite dimensional space. The function a(y) is taken to be the measured data, while b(y) is taken to be a nonlinear model (Bhusarapu, 2005). Let q(y:μ) be defined based on Beer Lamert's law for the transmission of photons Varma et al., (2008), as follows:

$$q(y{:}\,\mu) = I_0(y) \exp[-\sum_{x\epsilon X} b(y/x)\mu(x)]] \quad \text{(B-3)}$$

Where I_0(y) is the incident intensity, $b(y/x)$ is the length of projection y in pixel x, $q(y{:}\,\mu)$ represents the transmission of photons and is a function of the attenuation and b(y) represents a Poisson random number d(y). Equation (B-3) can be rewritten as

$$I(d\backslash\backslash q(y{:}\,\mu) = \sum_{y\epsilon Y} \left\{\mathrm{d(y)} \ln\left[\frac{d(y)}{q(y{:}\mu)}\right] - [d(y) - q(y{:}\,\mu)]\right\} \quad \text{(B-4)}$$

The algorithm minimizes the left term in Eq. (B-4) with respect to the attenuation (μ). More details and mathematical proofs regarding the AM algorithm are available elsewhere (O'Sullivan and Benace, 2001; Bhusarapu, 2005; O'Sullivan and Benace, 2007; Varma et al., (2007); Varma et al., (2008). In this work, the AM algorithm was used to reconstruct images that represent attenuation of the gas-solid system. For local holdup/attenuation measurements using computed tomography (CT). More detailed on both the hardware and the software used in this technique and the related post-data processing have been described by (Varma et al., 2007; Varma, 2008; Bhusarapu, 2005; Bhusarapu et al., (2006); Fadah, 2014).

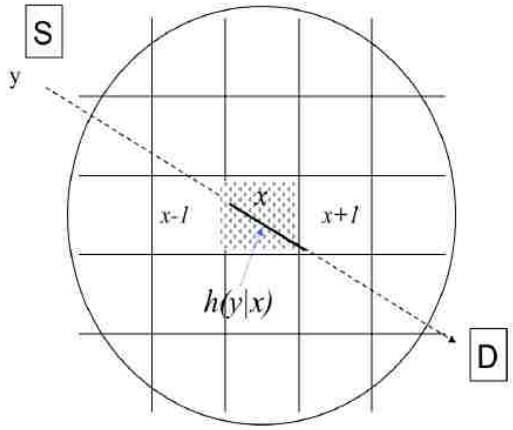

Figure B.3. Schematic of the representation of a transmission tomography domain

B.7. PHASE HOLDUP CALCULATION

The attenuations were measured along a number of beams paths through the column from different angles. Based on Beer Lambert's Law, the attenuation through the materials along the beam path is expressed as follows:

$$T = \frac{I}{I_0} = \exp(-\mu\rho l) \qquad \text{(B-5)}$$

Where (T) is the transmission ratio, (I_0) is the incident radiation, (I) is the detected radiation, (μ) is the mass attenuation coefficient, (ρ) is the medium density,(l) is the path length through the medium. The measured quantity ln (I/I_0) (called A, for simplicity) is equal to the integral sum of the attenuation through the material along the beam path. the attenuation values are measured from reconstruction step then they can be directly used.

$$ln\frac{I}{I_0} = -\mu\rho l, \qquad A = ln\frac{I_0}{I} = \mu\rho l \qquad \text{(B-6)}$$

To obtain statistically significant results and to reduce the effect of position, the CT scans were obtained by scanning 360 degrees around the column for a total scanning time of about eight hours, if the scanned cross-section is divided into pixels or cells

and the medium is comprised of two materials (gas and solid), (μ_s) is mass attenuation coefficient for solid, (μ_g) is mass attenuation coefficient for gas, ρ is the medium density, (ρ_s) solid density, (ρ_g) gas density, and thickness (l_g), (l_s) for gas and solid phases respectively.

When scanning the column as packed bed the total attenuation in each pixel is

$$A_{s,ij} = \rho_s \mu_s l_{s,ij} + \rho_g \mu_g l_{g,ij} \quad \text{(B-7)}$$

Where $L_{ij} = l_{s,ij} + l_{g,ij}$, $l_{s,ij} = \mathcal{E}_{s,ij} L_{ij}$ and $l_{g,ij} = \mathcal{E}_{g,ij} L_{ij}$

Where, L_{ij} is the total length between the pixel along the gamma ray beam, $\mathcal{E}_{g,ij}$, $\mathcal{E}_{s,ij}$ are the holdups (volume fractions) for the gas and solid phases.

$$A_{s,ij} = \rho_s \mu_s \mathcal{E}_{s,ij} L_{ij} \quad \text{(B-8)}$$

When scanning the column at the desired conditions of gas-solid fluidization the total attenuation in each pixel is

$$A_{s-g,ij} = \rho_s \mu_s l_{s,ij} + \rho_g \mu_g l_{g,ij} \quad \text{(B-9)}$$

$$A_{s-g,ij} = \left[\rho_s \mu_s \mathcal{E}_{s,ij} + \rho_g \mu_g \mathcal{E}_{g,ij}\right] . L_{ij} \quad \text{(B-10)}$$

$$A_{s-g,ij} = \hat{\mu}_{s-g,ij} . L_{ij} \quad \text{(B-11)}$$

Where $\hat{\mu}_{s-g,ij}$ is obtained from the AM reconstruction program for each pixel which represents the effective linear attenuation (1/cm) of the pixel.

The summation of the holdups is equal to unity (i.e. $\mathcal{E}_{g,ij} = 1 - \mathcal{E}_{s,ij}$)

Therefore, Equation (B-10) becomes:

$$A_{s-g,ij} = \left[\rho_s \mu_s \mathcal{E}_{s,ij} + \rho_g \mu_g (1 - \mathcal{E}_{s,ij})\right] . L_{ij} \qquad \text{(B-12)}$$

Since $\rho_g << \rho_s$, the attenuation caused by the gas phase is negligible compared to the solids, and *L* is common for all *A*s. Hence, solids holdup in pixel ij can be written as follows:

$$A_{s-g,ij} = \rho_s \mu_s \mathcal{E}_{s,ij}\, L_{ij} \qquad \text{(B-13)}$$

$$\mathcal{E}_{s,ij} = \left(\frac{A_{s-g,ij}}{\rho_s \mu_s\, L_{ij}}\right) \qquad \text{(B-14)}$$

By using Equation (B-11) the solids holdup in each pixel can be calculated as follows:

$$\mathcal{E}_{s,ij} = \left(\frac{\hat{\mu}_{s-g,ij}\ L_{ij}}{\rho_s \mu_s\, L_{ij}}\right) = \left(\frac{\hat{\mu}_{s-g,ij}}{\rho_s \mu_s}\right) \qquad \text{(B-15)}$$

From Alternating minimization reconstruction algorithm (AM) we obtained $\hat{\mu}_{s-g,ij}$ for the desired operation, μ_s is the mass attenuation coefficient (cm^2/g) of the particles (glass beads) which can be either obtained from the CT measurements of packed bed or determined from the standard tables such as (NIST Physical Data) if the material of the particles is well known, and ρ_s is the medium density ($g.cm^{-3}$)

Finally, the gas holdup was determined using the expression

$$\mathcal{E}_{g,ij} = 1 - \mathcal{E}_{s,ij} \qquad \text{(B-16)}$$

APPENDIX C

RADIOACTIVE PARTICLE TRACKING (RPT) TECHNIQUE

C. RADIOACTIVE PARTICLE TRACKING (RPT) TECHNIQUE

The radioactive particle tracking (RPT) technique is an advanced non-invasive measurement technique that is based on the principle of tracking the motion of a single tracer radioactive particle as a marker of the solids phase. The new RPT setup was built in our Multiphase Reactors Engineering and Applications Laboratory (mReal) at the Chemical and Biochemical Engineering Department, Missouri University of Science and Technology (Missouri S&T). Details of the principle of the RPT used in this study can be found elsewhere (Bhusarapu, 2005; Bhusarapu et al., 2006; Al-Mesfer, 2013). This setup included a fully automatic calibration device (r, z, and θ) and a processing and data acquisition system. For the gas-solid fluidized bed study the high velocities and high attenuation, gave rise to many implementation issues. These include the following: 1) selecting the radioactive particle, 2) devising a method for the detector calibration, 3) selecting a safe procedure for the introduction and recovery of the radioactive tracer, and 4) selecting a post-processing method for the data.

C.1. TYPICAL SET-UP OF RPT TECHNIQUE

In a typical implementation of RPT technique around complex multiphase system an array of 16 to 32 scintillation detectors surrounds the system. These detectors are arranged strategically around the system in order to improve the resolution and the accuracy, which are main performance indicators of RPT technique. In our experiment a total of 28 NaI scintillation detectors were positioned around the column. These detectors were held on four vertical supports at equal distances around the column. Each support had 7 detectors placed at different axial levels. Each level has 2 detectors that are staggered with the other levels by 45^0. Figure C.1 shows a photograph of the

configuration. Table C.1 and Table C.2 illustrate the position and configuration of the detectors around both 0.14 m and 0.44 m diameter columns respectively. Each detector consisted of a cylindrical NaI crystal (2 in x 2 in), a photomultiplier and electronics. RPT experiments typically consist of the following two steps: 1) the RPT calibration (static tracer particle location experiment under experimental conditions), and 2) the RPT experiment (dynamic experiment).

a)

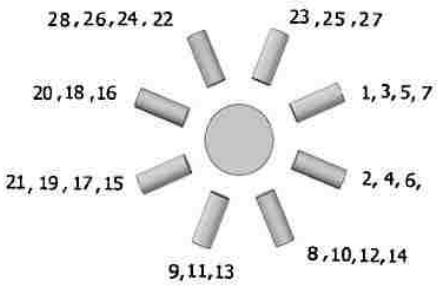

b)

Figure C.1. a) Photograph of radioactive particle tracking (RPT) set-up and b) Top view of the detectors distribution for RPT Technique.

Table C.1 Coordinates Of The Rpt Detectors For 6 Inch Fluidized Bed

Detector #	r, cm	θ ^{0}	Z, cm	Detector #	r, cm	θ ^{0}	Z, cm
1	12.7	115	0	15	12.7	295	0
2	12.7	70	5	16	12.7	250	5
3	12.7	115	10	17	12.7	295	10
4	12.7	70	15	18	12.7	250	15
5	12.7	115	20	19	12.7	295	20
6	12.7	70	25	20	12.7	250	25
7	12.7	115	30	21	12.7	295	30
8	12.7	25	2.5	22	12.7	205	2.5
9	12.7	340	7.5	23	12.7	160	7.5
10	12.7	25	12.5	24	12.7	205	12.5
11	12.7	340	17.5	25	12.7	160	17.5
12	12.7	25	22.5	26	12.7	205	22.5
13	12.7	340	27.5	27	12.7	160	27.5
14	12.7	25	32.5	28	12.7	205	32.5

Table C.2 Coordinates of the RPT detectors for 18 inch fluidized bed

Detector #	r, cm	θ ^{0}	Z, cm	Detector #	r, cm	θ ^{0}	Z, cm
1	12.7	115	0	15	12.7	295	0
2	12.7	70	16	16	12.7	250	16
3	12.7	115	32	17	12.7	295	32
4	12.7	70	48	18	12.7	250	48
5	12.7	115	64	19	12.7	295	64
6	12.7	70	80	20	12.7	250	80
7	12.7	115	96	21	12.7	295	96
8	12.7	25	8	22	12.7	205	8
9	12.7	340	24	23	12.7	160	24
10	12.7	25	40	24	12.7	205	40
11	12.7	340	54	25	12.7	160	54
12	12.7	25	72	26	12.7	205	72
13	12.7	340	88	27	12.7	160	88
14	12.7	25	104	28	12.7	205	104

C.2. RADIOACTIVE PARTICLE PREPARATION

Preparation of tracer particle involves selection of suitable radioisotope, activity selection, particle size selection and fabrication, sealing of particles inside vials, irradiation of sealed vials in high flux nuclear reactor, preparation of radioactive tracer particle inside hot glove box, sealing radioactive particle inside tracer particle, density matching and initial testing of the tracer particle for contamination in tumbler.

C.3. FABRICATION OF RADIOACTIVE TRACER

To perform safe handling of radioactive particles received after irradiation in nuclear reactor. A glove box (Figure C.2) was necessary. The glove box suitable for RPT tracer preparation houses optical Microscope with LCD screen. Arrangement for safe cutting of irradiated vials, and subsequent tracer preparation related activities which must be performed inside the sealed glove box. These activities include:

1. Opening of irradiated vials inside glove box with the help of glass-cutters and vial holder and retrieving radioactive cobalt particles safely.
2. Washing of particles inside a container filled with water and drying them, testing of washed water in liquid scintillation counting system for loose contamination, if any
3. Particle integrity inspection under microscope
4. Procuring of 1 mm Aluminum particle balls and central hole drilling with the help from Pat Harkins (St. Louis, MO, Harkins Specialties, L.L.C).
5. Putting radioactive Cobalt particle inside tracer particle with the help of tweezers
6. Sealing of tracer particle using glow to secure radioactive particle

7. Testing of tracer inside tumbler for contamination, if any a number of dry runs were carried out on dummy vials containing cobalt particles to demonstrate vial handling and opening procedure. The vial containing actual radioactive particle was opened after number of dry runs and tracer particle suitable for this study was prepared by following step- by-step procedure mentioned above.

The activity of a radioactive source is reduces by 50% in time equal to its half-life. Half-life of selected radionuclide should be an order of magnitude higher than that of total duration of given set of experiments. This will ensure that there is no significant reduction in the activity of source during experiment.

Figure C.2. RPT Glove box

A strong source of radioactivity is required for study of gas-solid system in a fluidized bed reactor (FBR) due to presence of highly attenuating glass beads. In this study a single radioactive particle (cobalt-60) with an activity of approximately 500 μCi and a 600 μm diameter was irradiated in the nuclear reactor at the University of Missouri Research Reactor Center in Columbia, Missouri. Cobalt-60 has a half-life of 5.28 years and presents two photo-peaks, one at 1.18 MeV and one at 1.34 MeV. Cobalt-60 has a high density 8.9 gcm^{-3}. The 600 μm diameter irradiated cobalt-60 particle was encapsulated with a gap of air in an aluminum ball with a 1 mm outer diameter to achieve the same density as the solids used (glass beads of 2.5 gcm^{-3} density) as shown in Figure C-3. This composite single radioactive tracer particle was used to track the solids of 210 and 70 μm in the studied fluidized beds. It is noteworthy that larger tracer particle with similar density of the solid particles of the fluidized bed should be able to track with confidence the smaller particles sizes in fluidized bed. This is because the particles in the gas-solid fluidized bed usually do not move as single isolated particles but they do as a cluster (Tebianian et al., 2015; Mostoufi et al., 2001; Mostoufi et al., 2004). Each single particle is attached to a solid aggregate in the dense bed and moves with it until the solid aggregate breaks-up. The particle then enters another solid ensemble and continues its movement with the new ensemble. It is not necessary then to use a tracer particle of size that matches the size of experimental particles. Mostoufi et al., 2001; Mostoufi et al., 2004 showed that all studied parameters were affected by the superficial gas velocity, and were independent of the size of the tracer. Tebianian et al. (2015) used in RPT experiments scandium as tracer particle with size and density different from that solid

particles used, tracer diameter was 400 µm, which was 4-times greater than the particle size (107 µm) but with the same density.

a)- Microscopic Picture of the Cobalt Particle (600 micron diameter)

b) Picture of an Aluminum Ball (1 mm)

c) Picture of a hollow an aluminum ball

d) Picture of the cobalt particle into a aluminum

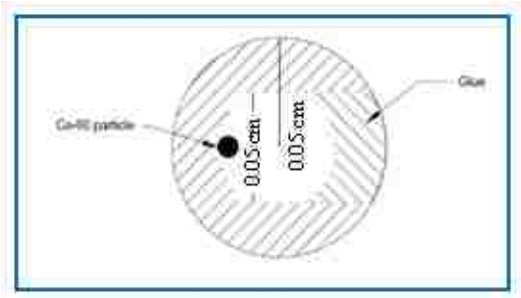

e)

Figure C.3. Cobalt particle and an aluminum ball

C.4. CALIBRATION OF DETECTORS (STATIC EXPERIMENTS)

Before performing the RPT experiment, calibration of all detectors used must be performed in-situ, preferably at the same operating conditions as used in the actual

experiment. During in-situ calibration, the detectors were calibrated by placing the tracer particle manually by the automated calibration device and moving it through the bed, at several hundred known locations. A fully automated calibration device was developed and implemented, as shown in Figure C-4. Each NaI scintillation detector records intensity counts, which depend upon the distance between the radioactive tracer particle and the detector for each calibration location and the materials in between. From the calibration step, a count-distance map can be obtained, which will be used in a subsequent step to obtain the location of the tracer particle

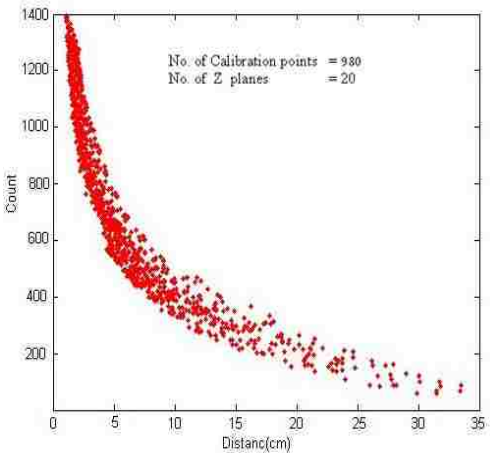

a) Calibration Curve for 0.14 m (6 inch) fluidized bed column

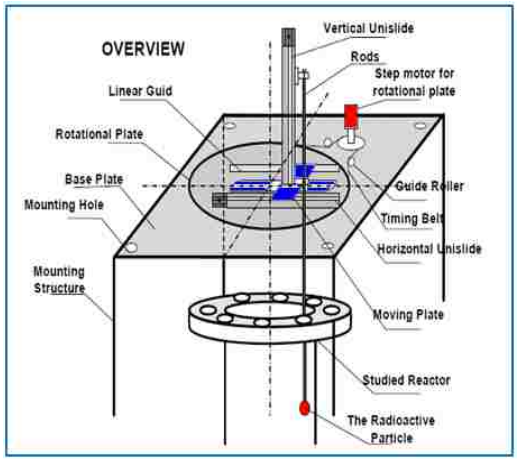

b) Schematic Diagram of the Calibration Device (Source: Luo, 2007)

Figure C.4. Calibration Device

As previously noted, the calibration experiment is performed in-situ, i.e. with the column operated at the same conditions as during the dynamic regular experiment. For the (6 inch) fluidized column the calibration was performed for 980 known locations, which were selected to cover all the dynamic bed. The locations were distributed

uniformly among 20 axial calibration levels, with increments of $\Delta z = 2$ cm apart with the lowest level at about 2 cm above the distributor. The 49 locations at each calibration level are grouped at four radial locations (Figure C-5)

- Ring 0: r = 0.00 cm , single central location
- Ring 1: r = 2.10 cm , 8 azimuthal locations 45.0^o apart
- Ring 2: r = 4.20cm , 16 azimuthal locations 22.5^o apart
- Ring 3: r = 6.30 cm , 24 azimuthal locations 15.0^o apart

Hence, the relationship between the intensity of radiation (counts) and the location of the particle was obtained for all detectors. During the regular experiment the particle was allowed to move freely into the column, acquiring data at a sample frequency of 50 Hz over 8 hours for 0.14 m (6 inch) column to assure that it visited each compartment of column and enough number of visits that the time and ensemble averaged particle velocity reaches plateau.

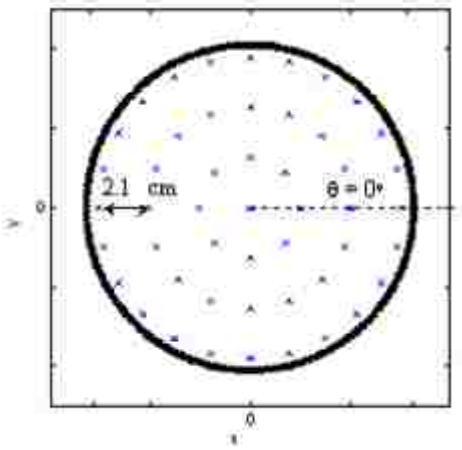

Z_0 = 2 cm (above the distributor)

N_z = 20 level

Δz = 2 cm

Z_{max} = 40 cm

Figure C.5. RPT Calibration Tracer Particle Locations for 6 inch column.

For the 18 inch fluidized column the calibration was performed for 6534 known locations, which were selected to cover all the dynamic bed. The locations were distributed uniformly among 54 axial calibration levels, with increments of $\Delta z = 2$ cm

apart with the lowest level at about 1 cm above the distributor. The 121 locations at each calibration level are grouped at seven radial locations (Figure C-6)

- Ring 0: r = 0.00 cm , single central location
- Ring 1: r = 3 cm , 8 azimuthal locations 45.0^o apart
- Ring 2: r = 6 cm , 16 azimuthal locations 22.5^o apart
- Ring 3: r = 9 cm , 24 azimuthal locations 15.0^o apart
- Ring 4: r = 12 cm , 24 azimuthal locations 15.0^o apart
- Ring 5: r = 15 cm , 24 azimuthal locations 15.0^o apart
- Ring 6: r = 18 cm , 24 azimuthal locations 15.0^o apart

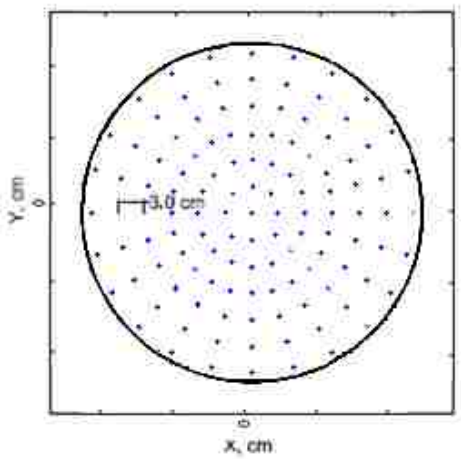

Z_0 = 1 cm (above the distributor)

N_z = 54 level

Δz = 2 cm

Z_{max} = 110 cm

Figure C.6. RPT Calibration Tracer Particle Locations for 18 inch column.

Hence, the relationship between the intensity of radiation (counts) and the location of the particle was obtained for all detectors. The particle was allowed to move freely into the column, acquiring data at a sample frequency of 50 Hz over 10 hours to assure that it visited each compartment of column and enough number of visits that the time and ensemble averaged particle velocity reaches plateau.

.

C.5. TRACER PARTICLE LOCATION RECONSTRUCTION

The data obtained from the calibration and actual experiments can be used to reconstruct the lagrangian trajectory of the tracer radioactive particle. A cross correlation based search method (Bhusarapu, 2005; Bhusarapu et al., 2006) was used to reconstruct the tracer particle position. This method is a two steps approach in which cross-correlation based search algorithm utilizing the calibration data is used to approximately locate the tracer particle position and a semi-empirical mechanistic model is fitted to the calibration data to relate the counts recorded to the position of emitting tracer particle. This semi-empirical model is a mechanistic model takes into account the effect of geometry as well as the attenuating medium in between the tracer particle and the detector. It has been found to work satisfactorily in gas-solid flows (Bhusarapu et al., 2006). In this study, calibration experiments suggested that counts received at the detectors are not only a function of distance between the tracer and the detector but also of the attenuation characteristics of a medium in between the tracer and the detector. Hence, a cross-correlation based position reconstruction algorithm was used in this study.

C.5.1. IMPLEMENTATION OF THE CROSS-CORRELATION BASED POSITION RECONSTRUCTION ALGORITHM FOR FBR STUDY (BHUSARAPU, 2005)

The calibration curves generated for each detector indicate that there is a spread in counts readings for same tracer-detector distance see (C-7). This suggests that counts received at the detectors are not only function of tracer-detector distance but also function of the attenuation characteristics of a medium in between the tracer and the detector. Each calibration position is mapped to a unique series of counts recorded on N_d detectors. Conversely, an inverse mapping should exist relating a series of counts at N_d detectors to

a unique position. Such an inverse mapping will exist if and only if the mapping is one-to-one. To solve the inverse problem of position reconstruction for the RPT experiment which results from exist another tracer position that yield in exactly the same series of counts for all the detectors, a cross correlation based search (Bhusarapu, 2005) for locating the tracer particle position and a semi-empirical model relating the counts recorded (*C)* to the position of the emitting tracer particle was used in this study

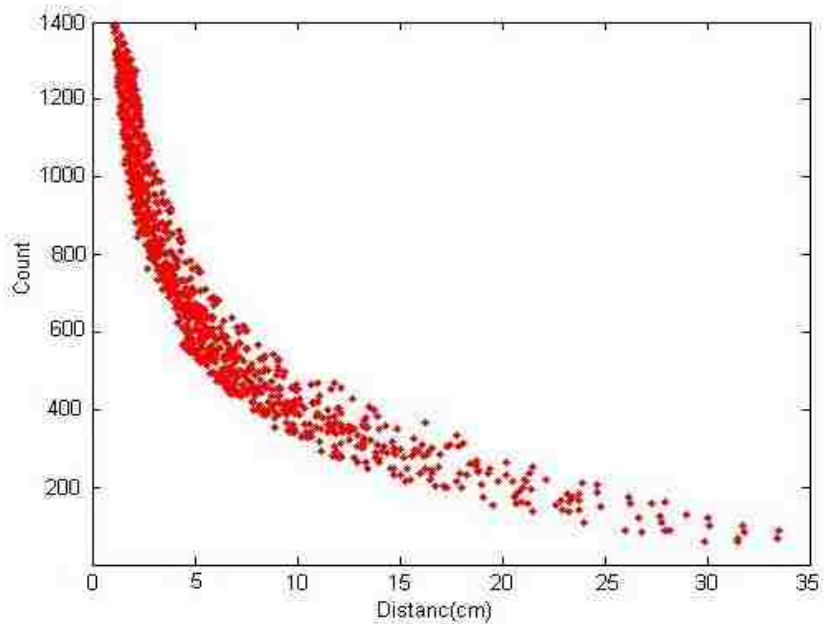

Figure C.7. Calibration map relating counts versus distance for a detector

Cross-correlation based method (Bhusarapu, 2005) is a two step approach in which cross-correlation based search is used to locate tracer particle position and a semi-empirical model is used to relate counts recorded to the position of emitting tracer particle. This semi-empirical model is a mechanistic simplification of actual complex mathematical model (Equation C-2) relating the counts (C) recorded in the detector to the position of tracer particle (Bhusarapu, 2005). This mechanistic model takes into account

geometry as well as the attenuating medium in between the particle and the detector. It provided satisfactory results in gas-solid flows (Bhusarapu, 2005) and hence, was chosen in this study.

Step I. Identification of peak in the zero lag of the cross-correlation function (finding cross-correlation coefficient): In this step The series of counts obtained on all the detectors at a given tracer particle position during a calibration (*Ccalib(i)* : $i = 1, N_d$) and similar series of counts obtained during an actual experiment (*Crun(j)* : $j = 1, N_d$) at a given instant of time can be analyzed to provide an estimate of match between the two counts series. This is quantified in terms of a cross-correlation coefficient (R) (Equation C-1). The zero lag of the cross-correlation between the two normalized series corresponding to each calibration location is found and the function variation is illustrated in Figure (C-8). The values of the function at different calibration positions (N_{calib} = 980 for 6 inch column) is shown. The position corresponding to the maximum in this function is the nearest known location which then provides the best initial estimate of the tracer location.

The zero lag of a cross-correlation function is an auto-correlation function, which has maximum value of 1. In other words, when the zero lag of the normalized cross-correlation function equals one, the two series: *Ccalib(i)* and *Crun(j)* are exactly the same. Hence, the unknown tracer position during the run (actual experiment) at that instant is the same as that of a known calibration position. Therefore, the approach to finding an unknown tracer position is reduced to matching the counts series from that position received by detectors to the counts received from known calibration positions.

The position of the tracer particle during an actual experiment should be the nearest to that known position in the calibration data set which has a maximum in the zero lag of the cross-correlation between the two normalized series given by Equation (C-1)

$$R_{run,calib\ k}(0) = \sum_{i=1}^{N_d} \frac{C_{calib}(i)}{\sqrt{\sum_{j=1}^{N_d} C^2_{calib}(j)}} \cdot \frac{C_{run}(i)}{\sqrt{\sum_{j=1}^{N_d} C^2_{run}(j)}} \qquad \text{(C-1)}$$

where $C_{calib(i)}$, series of counts obtained in detector i = 1 to N_d at a given tracer position during a calibration experiment and $C_{run(j)}$ series of counts obtained in detector j =1 to N_d, where N_d is the total number of detectors. The values for the cross-correlation function, $R_{run,calib\ k}(0)$, are found for the k calibration positions. Hence, the nearest known location is identified to be the calibration position where the series $\{ R_{run,calib\ k}(0) : k = 1, Ncalib\}$ peaks. This gives us the best estimate of the closest known position

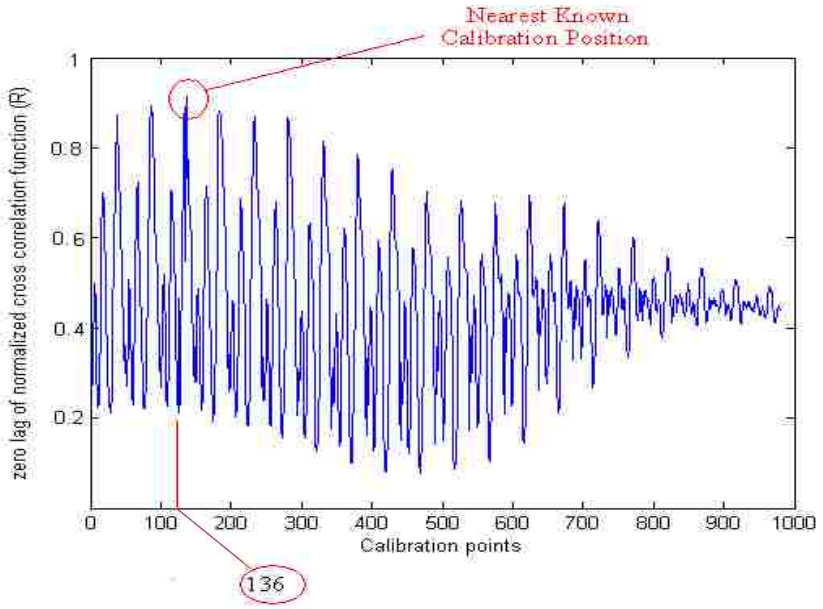

Figure C.8. Zero lag of the normalized cross-correlation function variation at the calibration points for an unknown location for 6 inch column.

Step II – Establishing additional calibration datasets at refined level by using semi-empirical model. Step II is fitting of simplified mathematical model over region of interest (ROI) to refine the experimental calibration grid and establishing additional calibration datasets. During actual RPT experiments, the tracer particle follows the dynamics of tracking phase and visits locations in the systems which are usually different than experimental calibration positions. Hence, there is a need to derive additional calibration datasets using RPT calibration experiments and a suitable mathematical model. This newly established calibration datasets at refined mesh level along with in-situ experimental calibration datasets can then solve the problem of identifying unknown tracer position based on the counts recorded in the detectors. A semi-empirical model (Equation C-2) is used to derive additional calibration datasets which was proposed and developed by (Bhusarapu, 2005). This semi-empirical model is a mechanistic simplification of an actual complex mathematical model relating the counts intensity (C) to the position of tracer particle emitting γ-radiation (given by Equation C-2).

$$C = \underbrace{\frac{k_1}{d^2}}_{1} \cdot \underbrace{exp\left(-k_2 d_x - k_3 d_y - k_4 d_z\right)}_{2} \underbrace{1 - exp(-\mu_d k_5)}_{3} \qquad \text{C-2}$$

Where,

C – Counts recorded in the detector

K_1 – Model fitted parameter proportional to the solid angle subtended by the detector at the tracer location (cm^2)

$K_{2,3,4}$ – Effective mass attenuation coefficients of the medium in between the tracer and the detector in x, y and z directions respectively (1/cm)

d – distance of the tracer from the center of the detector crystal (cm)

d_x, d_y, d_z – x, y and z components of the distance of the tracer from the center of detector crystal, (cm)

μ_d - Mass attenuation coefficient of the detector material (1/cm)

K_5 –Length of travel of the photon in the detector crystal (cm)

This model takes into account the geometry (thru model parameter K_1) as well as the attenuating medium effects in between the tracer and the detector (thru model parameters $K_{2,3,4,5}$). Term 1 of Equation (C-2) is corresponding to an inverse square law and K_1 is a parameter representing the solid angle subtended by the detector at the tracer location. According to inverse square law, counts intensity is inversely proportional to the square of the tracer-detector distance. Term 2 is corresponding to the attenuation characteristics of a heterogeneous medium in between the tracer and the detector. $K_{2,3,4}$ are effective mass attenuation coefficients in x, y and z directions, respectively. Term 3 is corresponding to the detector efficiency. k_5 is a parameter corresponding to the travel length of the photon in the detector material. In this manner, this semi-empirical model takes into account geometry as well as the attenuation characteristics of a medium in between the tracer and the detector and the detector efficiency.

Step I of cross-correlation based position reconstruction algorithm finds cross-correlation coefficient (R (0)) using Equation C-1 for each experimental calibration data point (N_{calib} = 980) and finds region of interest (ROI) from the whole domain. It involves finding initial best estimate (IBE) point with the maximum value of cross-correlation coefficient (R (0)) and then finding neighboring points around it to form ROI.

Step II implements a semi-empirical model which is a mechanistic simplification of actual complex mathematical model. In step II. After establishing additional calibration data sets, step I is repeated and a point with maximum value of R(0) is found out. This two step process is repeated until convergence criterion of 1- R(0) $\leq$0.005 is achieved. This is done by choosing a point with the second maximum value of cross-correlation coefficient as initial best estimate (IBE) point (C-9 and C-10) and forming ROI around it and repeating two-step process.

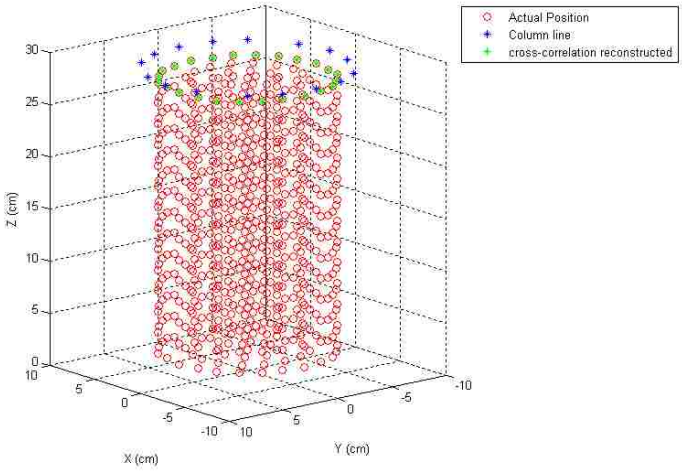

(a)

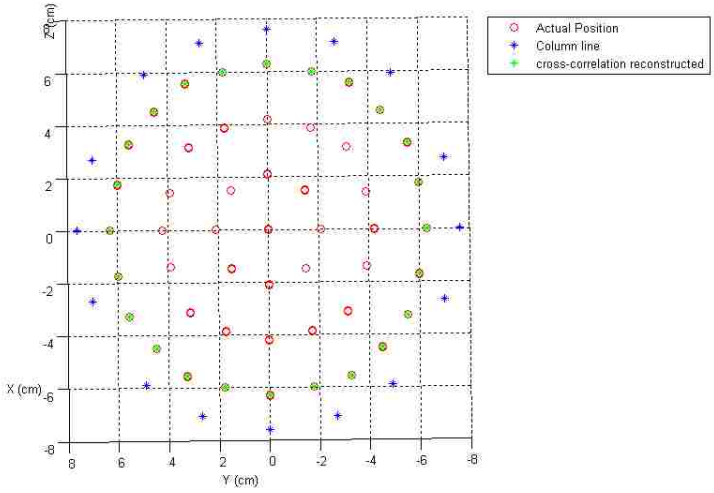

(b)

Figure C.9.The reconstructed position from cross correlation search with the actual positions for the calibration, b) top view of a) 3-D view

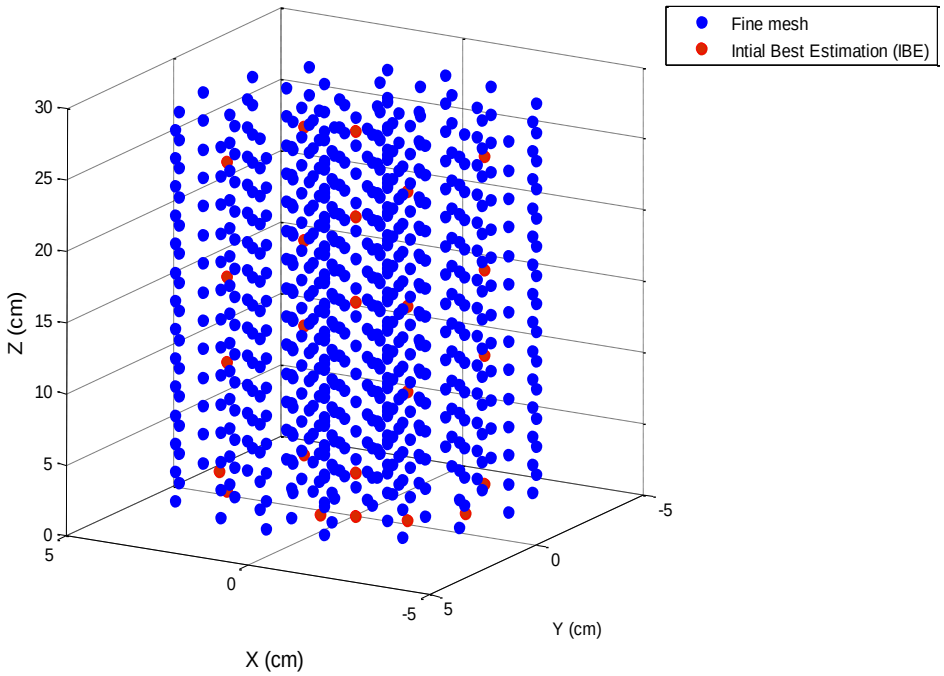

(a)

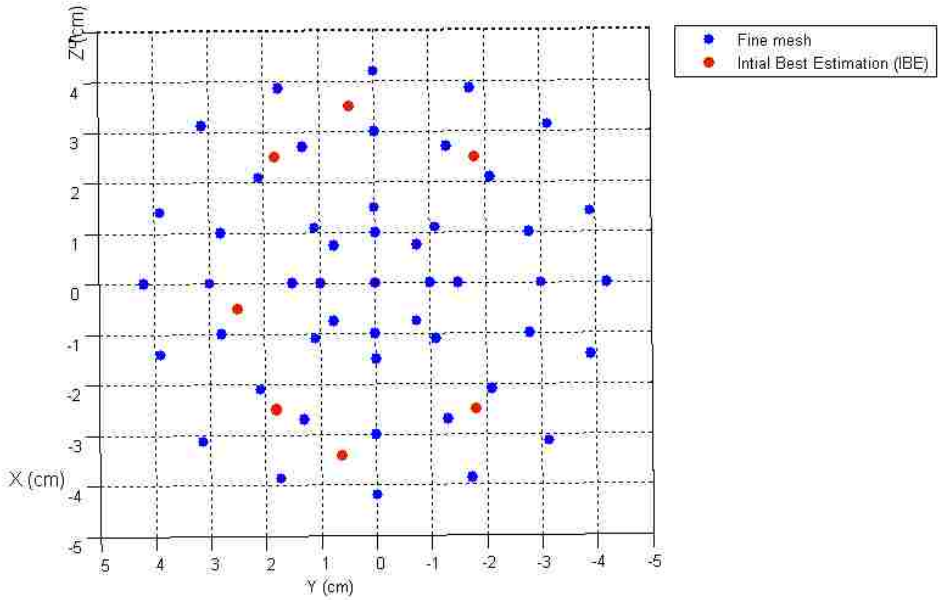

(b)

Figure C.10. Relative locations of initial best estimation (IBE) points, b) top view of a) 3-D view

C.6. COMPUTATION OF VELOCITY AND TURBULENCE PARAMETERS

C.6.1 SELECTION OF SAMPLING COMPARTMENTS

In order to obtain the time-averaged hydrodynamic parameters as a function of the position, the columns 0.14 m (6 inch) and 0.44 m (18 inch) were first divided into sampling compartments with the same volum depending on the column diameter and the height of expanded solid when is in operation. Degaleesan (1997) discussed several ways to discretize the column; based on her recommendation, the columns (6 inch and 18 inch) were divided into sampling compartments as shown in Figure C.11

$N_r = 8$

$\Delta r = 0.952$ cm

$N_z = 20$

$\Delta z = 2$ cm

$N_\theta = 2,4,4,6,6,8,10,12$

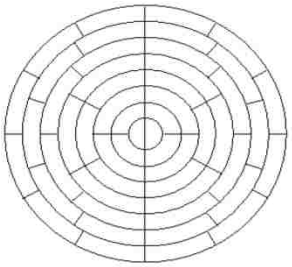

6 inch column cross- section

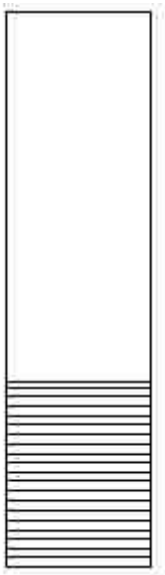

Axial

$N_r = 12$

$\Delta r = 1.905$ cm

$N_z = 45$

$\Delta z = 2$ cm

$N_\theta = 2,4,6,8,10,10,12,$

$14,16,18,20,24$

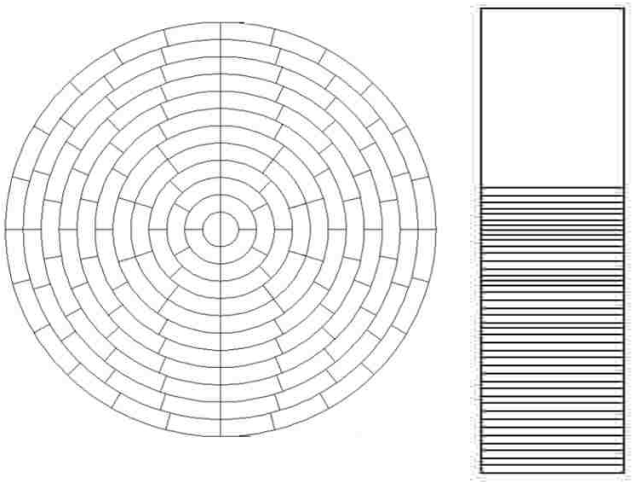

18 inch column cross- section

Axial

Figure C.11 RPT Processing Compartment Discretization for 6 and 18 inch Fluidized columns

Where: N_r, N_z and N_θ represent the number of divisions in the radial, axial and azimuthal directions, respectively.

As evident from Figure C.11, the radial and axial divisions were kept constant, while the azimuthal (angular) divisions were varied with the radial position in the column. This discretization is used to maintain a reasonable, uniform number of occurrences of the particle (statistic) in each compartment. In total, the (6 inch) column was divided into 1040 fictitious with 52 cross-sectional compartments at each of the 20 axial levels as shown in Figure C.11. While the (18 inch) column divided into 7776 fictitious with 144 cross-sectional compartments at each of the 54 axial levels as shown in Figure C.11.

C.6.2. VELOCITY FIELD

Radioactive particle tracking technique is the most accurate technique for velocity measurement in opaque systems that is available and is also is more sensitive at low fluid

velocities than other techniques such as hot wire anemometry, which is a more widely used technique . RPT detectors are strategically placed around the bed region of the column from the distributor level to 30 cm of height above the distributor for 0.14 m (6 inch) and from the distributor level to 104 cm of height above the distributor for 0.44 m (18 inch). This axial span of the detectors is sufficiently to cover the horizontal cross-sectional planes of the column where the CT scans are taken (H/D = 0.286, 0.64 and 1.7) for 0.14 m (6 inch) and (H/D = 0.286, 0.88 and 1.6) for 0.44 m (18 inch). Experimentally observed flow patterns are reported as the axial, radial, azimuthal solids velocities and time-averaged velocity vector plot. Also, reported the velocity field at three axial heights where the CT scans are performed. RPT results at the three CT scans are time and azimuthally averaged and the overall axially averaged are measured.

The Instantaneous velocities (axial, radial and azimuthal) velocities were computed from the time differencing of the subsequent particle positions and assigned to the compartment in which the middle point of the two positions fell, as shown in the following equations:

$$u_{z,i-1/2} = \frac{z_i - z_{i-1}}{\Delta t} \qquad \text{(C-3)}$$

$$u_{r,i-1/2} = \frac{r_i - r_{i-1}}{\Delta t} \qquad \text{(C-4)}$$

$$u_{\theta,i-1/2} = \frac{(\theta_i - \theta_{i-1})}{\Delta t} \quad \frac{(r_i + r_{i+1})}{\Delta t} \qquad \text{(C-5)}$$

Where (i- 1⁄2) is the midpoint of two successive particle positions.

Time-averaged (mean) velocities were calculated by averaging the instantaneous ensemble particle velocities for a given compartment (i, j, k).

$$u_{p(i,j,k)} = \frac{1}{N_v} \sum_{i=1}^{N_v} u_{p(i,j,k),i} \qquad p = z, r, \theta \qquad \text{(C-6)}$$

N_v is the number of velocity occurrences assigned to the midpoint of two successive particle positions for a given compartment (i, j, k).

The fluctuating velocity was computed by subtracting the time-averaged (mean) velocities from the instantaneous velocities.

$$u'_{p(i,j,k)} = u_{p(i,j,k)} - \overline{u}_{p(i,j,k)} \quad \text{(C-7)}$$

The azimuthally averaged velocity was used if the flow is symmetry due to the difficulty of representing three-dimensional velocities as a function of position in the domain.

$$\overline{u}_{(i,k)} = \frac{1}{N_\theta \, \breve{N}_{v(i,k)}} \sum_{j=1}^{N_\theta} \overline{u}_{(i,j,k)} \quad N_{v(i,j,k)} \quad \text{(C-8)}$$

$$\breve{N}_{v(i,k)} = \frac{1}{N_\theta} \sum_{j=1}^{N_\theta} N_{(i,j,k)} \quad \text{(C-9)}$$

Where $\overline{u}_{(i,k)}$ is the time-averaged and azimuthally averaged either axial or radial component of the two-dimensional velocity for compartment (i, k); N_θ is the number of divisions in the azimuthal direction, as shown in Figure C-11, and $\breve{N}_{v(i,k)}$ is the average number of velocity occurrences for a given two-dimensional compartment (i, k).

C.6.3. TURBULENCE STRESSES AND KINETIC ENERGY

Turbulence parameters are very important in modeling multiphase flows. In fluidized bed columns, the interactions between turbulent eddies in the solid phase can be characterized by Reynolds stresses. The RPT technique makes it possible to evaluate Reynolds stresses and other parameters. Once the fluctuating velocity was calculated, the turbulence parameters (Reynolds stresses and turbulent kinetic energy) were able to be

evaluated. The turbulent stress tensor in cylindrical coordinates can be defined as shown in Equation C-10):

$$\tau = \rho_l \begin{pmatrix} \overline{u_r' u_r'} & \overline{u_r' u_\theta'} & \overline{u_r' u_z'} \\ \overline{u_\theta' u_r'} & \overline{u_\theta' u_\theta'} & \overline{u_\theta' u_z'} \\ \overline{u_z' u_r'} & \overline{u_z' u_\theta'} & \overline{u_z' u_z'} \end{pmatrix} \quad \text{(C-10)}$$

The nine unknown components in equation (C-10) reduced to six components because of the symmetry of the stress tensor, namely:

Shear stresses $\rho_s \overline{u'_\theta u'_r}$, $\rho_s \overline{u'_\theta u'_z}$, $\rho_s \overline{u'_z u'_r}$ (C-11)

Where $\overline{u'_\theta u'_r} = \overline{u'_r u'_\theta}$, $\overline{u'_z u'_r} = \overline{u'_r u'_z}$ and $\overline{u'_\theta u'_z} = \overline{u'_z u'_\theta}$

Normal stresses $\rho_s \overline{u'_r u'_r}$, $\rho_s \overline{u'_\theta u'_\theta}$, $\rho_s \overline{u'_z u'_z}$ (C-12)

The turbulent stress components are calculated as

$$\tau_{pq} = \overline{u'_p u'_q}(i,j,k) = \frac{1}{N_v} \sum_{n=1}^{N_v} u'_p(i,j,k),n \; u'_q(i,j,k),n \quad \text{(C-13)}$$

where pq denotes the component of the stress tensor in the cylindrical coordinates system.

The turbulent kinetic energy (TKE) per unit mass is defined as follows:

$$K = \frac{1}{2}\left(\overline{u'^2_r} + \overline{u'^2_z} + \overline{u'^2_\theta}\right) \quad \text{(C-14)}$$

C.6.4.EDDY DIFFUSIVITY

Turbulent eddy diffusivities are important parameters for modeling and quantifying solid mixing and transport in fluidized bed columns. The eddy diffusivity,

which is mixing caused by eddies that can vary in size, can be obtained directly from RPT-measured Lagrangian autocorrelation. The procedure for obtaining eddy diffusivities is discussed in detail elsewhere (Degaleesan, 1997), so only a brief outline of the governing equations for calculating the eddy diffusivities is provided in this section.

The particle location displacements Y_r, Y_θ and Y_z caused by the corresponding fluctuation velocity components were evaluated according to the following equations:

$$Y_r(t) = \int_0^t u'_r\,(t')dt' \qquad \text{(C-15)}$$

$$Y_\theta(t) = \int_0^t u'_\theta\,(t')dt' \qquad \text{(C-16)}$$

$$Y_z(t) = \int_0^t u'_z\,(t')dt' + \left.\overline{\frac{du_z}{dr}}\right|_{Y_{r(t')}} .\, Y_r\,(\text{t'})) \,.\, \text{dt'} \,. \qquad \text{(C-17)}$$

(Degaleesan, 1997). Degaleesan (1997) defined eddy diffusivities as follows:

The normal radial eddy diffusivity is:

$$D_{rr}(t) = \frac{1}{2}\,\frac{d}{dt}\overline{Y_r^2(t)} \;= \int_0^t u'_r\,(t)\,.\;u'_r(t')\,.dt' \qquad \text{(C-18)}$$

The normal axial eddy diffusivity is:

$$D_{zz}(t) = \frac{1}{2}\,\frac{d}{dt}\overline{Y_z^2\,(t)} \;=$$

$$= \int_0^t \left[\left[\overline{u'_z(t)\,.\,u'_z(t')} + \left.\overline{\frac{du_z}{dr}}\right|_{Y_{r(t')}} .\,(\int_0^{t'} u'_z(t)\,.\,u'_r(t'')\,dt''\right].dt'\right] \qquad \text{(C-19)}$$

Equations (C-15) through (C-20), which govern the eddy diffusivities, all are related to the lagrangian autocorrelation coefficient, which is given by:

$$R_{IJ}(\tau) = \overline{u'_t(t)\,u'_j(t+\tau)} \qquad \text{i, j = z ,r , } \theta \qquad \text{(C-20)}$$

Where i=j for the autocorrelation coefficient.

C.7. DATA FILTRATION

To obtain reliable estimates of the turbulence parameter, the instantaneous particle position data obtained from RPT experiments must be filtered in order to extract only the coherent part of the signal by eliminating the white noise, as discussed by Degaleesan (1997) and Degaleesan et al. (2002). The discrete wavelet transformation threshold denoising filtration analysis proposed by Degaleesan (1997) was used in this work. Filtering can be implemented either directly to the radiation intensity count signal obtained by each detector or to the instantaneous particle position signal; the two methods yield the same results (Degaleesan, 1997). To achieve wavelet filtering, the original instantaneous position data should be split into sets of data with lengths of N=2L, L=10 and N=1024. A signal threshold for the wavelet packet coefficient, *st*, is selected to eliminate the incoherent part of the decomposed signal, and its value depends on the extent of noise in the data, x(t), y(t) and z(t). More details about the wavelet filtering analysis and the filtration algorithm have been provided elsewhere (Degaleesan, 1997; Degaleesan et al., 2002). By choosing the estimates of the *st* values, the filtered and unfiltered instantaneous position data were processed to obtain the Lagrangian autocorrelation coefficients for comparing these correlations. Figure C-12 illustrates the comparison of filtered and unfiltered axial particle velocity and turbulent parameters at different *st* values at a superficial gas velocity of 20 cm/s and. The plots in Figure C-12 illustrate that no much difference can be observed in the axial particle velocity and turbulent parameters before and after filtering.

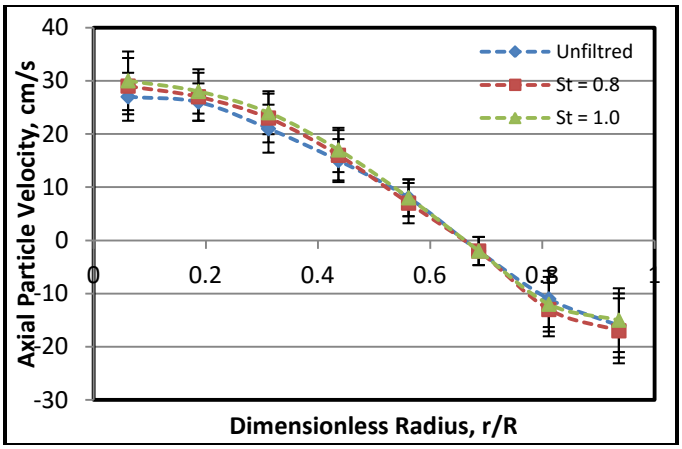

(a)- Time and azimuthally averaged axial particle velocity radial profile

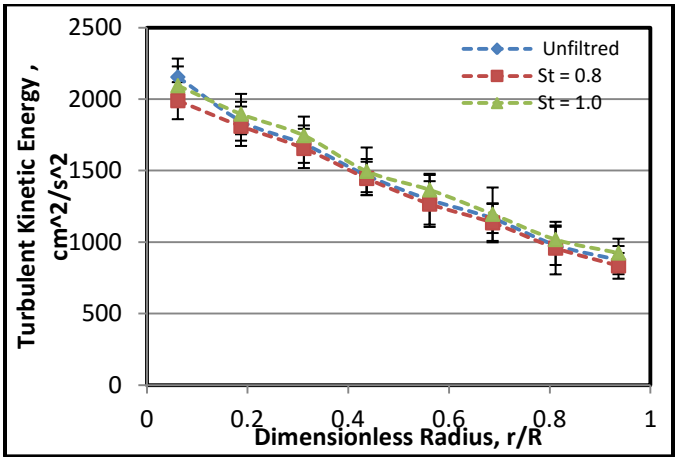

(b)-Time and azimuthally averaged turbulent kinetic energy radial profile

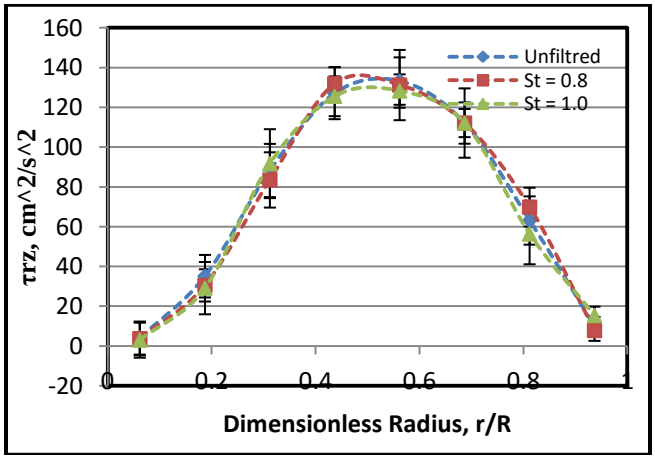

(c)-Time and azimuthally averaged turbulent kinetic energy radial profile

C-12 Time and azimuthally averaged axial particle velocity and turbulent parameters radial profiles

C.8. CHECKING THE RELIABILITY OF THE RPT MESUREMENTS

It is necessary to ensure that statistically sufficient information has been collected during RPT experiments so that the presented profiles of velocity at 10 hours and at combine of two runs at 20 hours are close to each other. Figure 9 shows a typical result for the time and azimuthally averaged axial particle velocity profiles obtained at 10 and 20 hours of RPT measurement duration. It is apparent from these Figures that the results do not vary with the increasing the time of the experiments, and hence, 10 hours duration of RPT measurements to collect enough ensembled data to represent the system statistically.

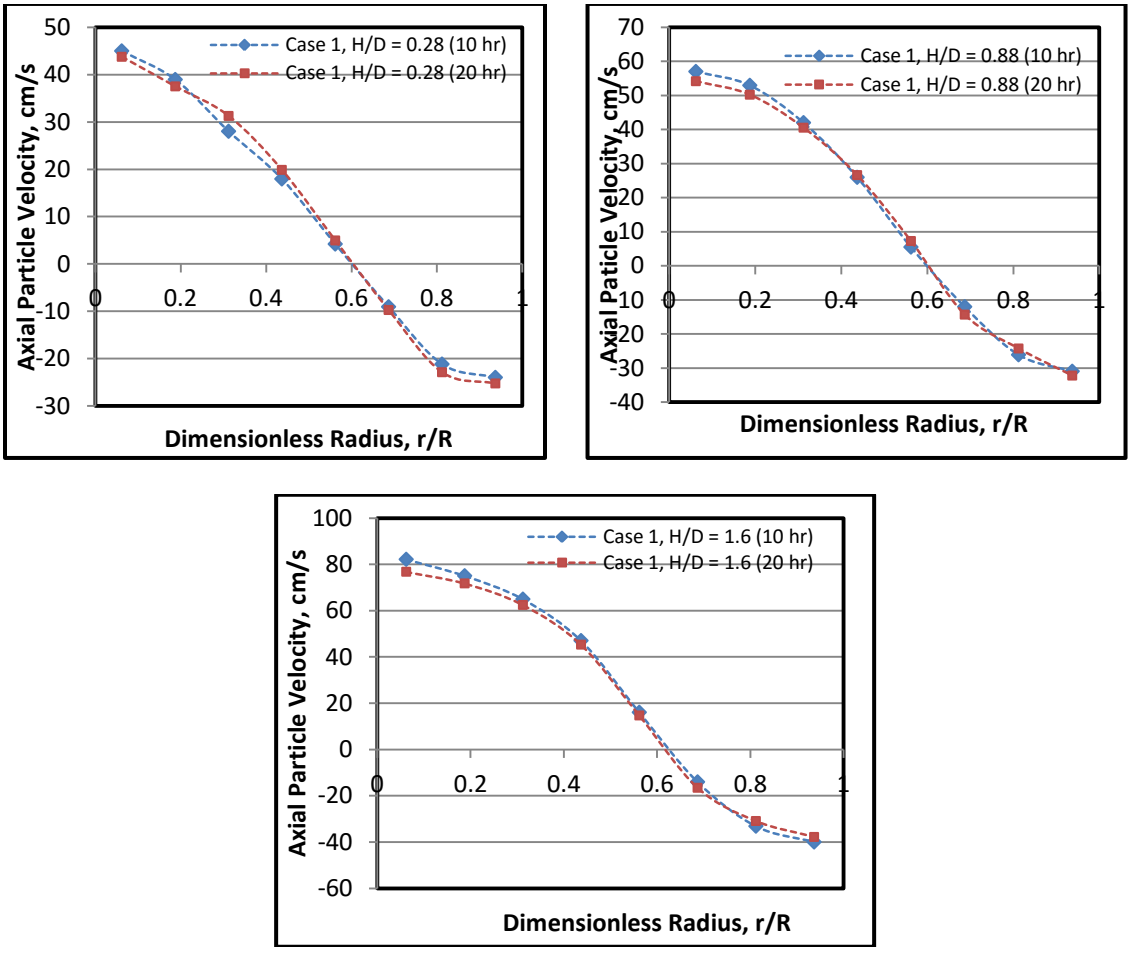

Figure C-13 Time and azimuthally averaged particle velocity radial profiles for Ca (18 inch) illustrating the effect of statistics

APPENDIX D

MINIMUM FLUIDIZATION VELOCITY

D. MINIMUM FLUIDIZATION VELOCITY (U_{mf})

The minimum fluidization velocity is one of the important parameters when characterizing fluidized bed conditions. It is important variable in the design of fluidized bed, which is proportional to the drag force needed to attain solid suspension in the gas phase. At the onset of fluidization, the drag force created by upward moving gas on the entire system of particles must be equal to the weight of the bed's particles, which can be expressed by flowing relationships.

$$\Delta p_b = (1 - \varepsilon_{mf})(\rho_s - \rho_g)\, g H_{mf} \qquad \text{(D-1)}$$

$$\mathrm{Ar} = \frac{1.75}{\emptyset^3 \varepsilon_{mf}^3} Re_{mf}^2 + \frac{150(1-\varepsilon_{mf})}{\emptyset^3 \varepsilon_{mf}^3} \qquad \text{(D-2)}$$

Here, the Reynolds number at a minimum fluidization state, is $\mathrm{Re_{mf}} = \frac{d_p\, U_{mf}\, \rho g}{\mu}$ and the Archimedes number is $\mathrm{Ar} = \frac{d_p^3 (\rho p - \rho g)\, g}{\mu^2}$.

Equation (D-2) can be simplified for incredibly small particles:

$$\mathrm{U_{mf}} = \frac{d_p^3 (\rho_p - \rho_g)\, g}{150\, \mu} \frac{\varepsilon_{mf}^3 \emptyset^2}{(1-\varepsilon_{mf})} \mathrm{Re_{mf}} \quad < 20 \qquad \text{(D-3)}$$

For very large particles

$$U_{mf}^2 = \frac{d_p (\rho_p - \rho_g)\, g}{1.75\, \rho\, g} \varepsilon_{mf}^3\, \emptyset \mathrm{Re_{mf}} \quad < 1000 \qquad \text{(D-4)}$$

The minimum fluidization velocity is typically obtained experimentally. However, there are many correlations reported in the literature to predict U_{mf} with fidelity. There are several methods than can be implemented to find the minimum fluidization velocity in fluidized flow systems. Gupta and Sathiyamoorthy (1990) described three different methods to measure U_{mf} which are (1) the pressure drop

method, (2) the voidage method, and (3) the heat transfer method. The first method measures the pressure drop across the bed as a function of the superficial gas velocity. The point of transition between a fixed bed regime and a bubbling regime is denoted by a constant pressure line in a plot of pressure vs. superficial gas velocity. This point marks the minimum fluidization velocity. The minimum fluidization velocity in the voidage method is determined when the voidage inside the bed begins to increase as the bed expands and the superficial gas velocity increases. This method, however, typically is not used because the point at which bed expansion begins is quite difficult to locate. Finally, the variation of the wall heat transfer coefficient in the heat transfer method is measured as the gas velocity increases. The point at which the heat transfer coefficient increases drastically is the onset of fluidization or (the minimum fluidization velocity point). This method, however, is too expensive and requires a reliable experimental setup to measure the heat transfer data under steady-state conditions. The minimum fluidization velocity (U_{mf}) is a function of the particle properties, fluid properties, distributor types, and bed geometry (Sau et al. 2007).

Gunn and Hilal (1997) studied the effects of bed's height on the minimum fluidization velocity. They used glass beads as bed materials in gas-solid fluidized beds with beds that had 89 and 290 mm ID. The glass bead's diameters were 100 and 500 μm. Four different bed heights were also used: 20, 30, 40 and 50 cm. The results for minimum fluidization velocity showed that for all the materials and experimental conditions used in this study, there was no significant change in the minimum fluidization velocity when the bed's height was increased. Therefore, U_{mf} was independent of bed height.

Sau et al. (2007), studied the fluidization characteristics of large alkalized alumina particles (1000-2000μm) in a fluidized bed at different bed heights (5, 10, 15, 20, 25 and 30 cm). They found that the minimum fluidization velocity remained constant regardless of the bed's height used in the experiments.

Sanchez-Delgado et al., 2011, also studied the effects of bed's height on the minimum fluidization velocity for a 2D fluidized bed. They concluded that negligible differences in U_{mf} occurred as bed's height changed.

David and Theodore (2011) studied the effects of bed height and material density on the minimum fluidization velocity for 10.2 cm diameter cylindrical fluidized bed, three different Geldart type-B particles were tested: glass beads, ground walnut shell, and ground corncob, with material densities of 1000, 1300 and 2600 Kg/m^3 respectively. The particle size's range was the same for all three materials and corresponded to (500-600) μm with five different bed height-to-diameter ratios were investigated: H/D=0.5,1, 1.5, 2, and 3. Pressure drop measurements were used to determine the minimum fluidization velocity for each H/D ratio. They noted that the minimum fluidization velocity was unaffected by a change in bed height. The minimum fluidization velocity did increase, however, as the material density increased. Numerous correlations have been made predicting the minimum fluidization velocity. A list of these correlations along with their applicability is presented in Table D.1. Miller and Logwinuk (1992) correlation was used in this work.

Table D.1.Correlations for Minimum Fluidization Velocity

No	Authors	Correlations
1	Wen and Yu (1966)	$U_{mf} = \frac{\mu_g}{\rho_g d_p}(\sqrt{1135.7 + 0.048\ \mathrm{Ar}} - 33.7)$
2	Baeyens and Geldart (1986)	$\mathrm{Ar} = 1823\ Re_{mf}^{1.07} + 21.27\ Re_{mf}^{2}$
3	Levsa et al.(1992)	$U_{mf} = \frac{7.39\ d_p^{1.82}(\rho_p - \rho_g)^{0.94}}{\rho_g^{0.06}}$
4	Goroshko et al.(1989)	$U_{mf} = \frac{\mu_g}{\rho_g d_p}\left(\frac{\mathrm{Ar}}{1400 + 5.2\sqrt{\mathrm{Ar}}}\right)$
5	Leva et al.(1949)	$U_{mf} = \frac{7.169 * 10^{-4}\ d_p^{1.82}(\rho_p - \rho_g)^{0.94}\ g}{\rho_g^{0.006}\ \mu_g^{0.88}}$
6	Bena et al.(1971)	$U_{mf} = \frac{\mu_g}{\rho_g d_p}\left(\frac{1.38 * 10^{-3}\ \mathrm{Ar}}{(\mathrm{Ar} + 19)^{0.11}}\right)$
7	Rowe and Henwood (1961)	$U_{mf} = \frac{8.1 * 10^{-3}\ d_p^2\ (\rho_p - \rho_g)\ g}{\mu_g}$
8	Miller and Logwinuk (1992)	$U_{mf} = \frac{0.00418\ d_p^2\ (\rho_p - \rho_g)^{0.9}\ \rho_g^{0.1}\ g}{\mu_g}$
9	Frantz et al.(1974)	$U_{mf} = \frac{1.065 * 10^{-3}\ d_p^2\ (\rho_p - \rho_g)\ g}{\mu_g}$
10	Davies and Richardson (1996)	$U_{mf} = \frac{1.948 * 10^{-3}\ d_p^2\ (\rho_p - \rho_g)\ g}{\mu_g}$

VITA

Abdelsalam Efhaima was born in Sirte in Libya. He received his Bachelor of Engineering degree in Chemical Engineering from Sirte University, Libya in July 1998 and his MSc form UKM University, Malaysia, in July 2007. He worked in Eni Oil Company, Libya form September 1999 to January 2005 and joined the department of chemical engineering at Sirte University, Sirte, Libya as Teaching Assistant from January 2008 to June 2010.

Abdelsalam Efhaima enrolled in the PhD program of the Department of Chemical and Biochemical Engineering at Missouri University of Science and Technology in the spring of 2011. His main research area is the design and scale-up of fluidized bed reactor. He received his Ph.D in chemical and biochemical engineering in May 2016 from Missouri University of Science and Technology.